SUPERINTENDENCIA DE INDUSTRIA Y COMERCIO

RAD: 11-9466- -9 **FECHA**: 2014-03-14 18:21:27
DEP: 2020 DIRECCION DE NUEVAS CREACIONES **EVE:** 378 FASE NACIONAL INCLUIDO CAPITULO I
TRA: 11 PCT-PATENTE DE INVENCION CAPITULOS I Y II **FOLIOS**: 11
ACT: 519 PRESENTACION

DIRECCIÓN DE NUEVAS CREACIONES

2020
Bogotá, D.C.,

Abogado(a)/Señor(a)
MAURICIO JARAMILLO CAMPUZANO

Asunto: Radicación: 11-9466- -9
Trámite: 11
Evento: 378
Actuación: 519
Oficio: 3407
Folios: 11

Patente de Invención	X			Patente de Modelo de Utilidad	
Vía Nacional					
Vía PCT (Fase Nacional)	X	Capítulo I	X	Capítulo II	
No. Solicitud Internacional	PCT/US2009/043830				
Fecha de Presentación Internacional	13/05/2009				

Como resultado del Examen de Fondo realizado, con fundamento en el Artículo 45 de la Decisión 486 de la Comisión de la Comunidad Andina, se comunica:

1. Documentos estudiados

Descripción:	Rad. N° 11-009466-00000-0000	28/Enero/2011
Reivindicaciones:	Rad. N° 11-009466-00000-0000	28/Enero/2011
Prioridades	US 61/076,873	30/Junio/2008

2. Análisis de la Prioridad

Se acepta la reivindicación de Prioridad porque esta solicitud fue presentada dentro del plazo establecido (Art. 9 D 486) y su contenido técnico corresponde con el de la prioridad reivindicada.

3. Objeto de la invención

De acuerdo con lo establecido en el numeral 1.2.2.2 del Capítulo Primero del Título X de la Circular Única para efectos del examen de patentabilidad, se tendrá en cuenta la tasa pagada por el solicitante al momento de comenzar el examen para las reivindicaciones adicionales; esto es que cuando la solicitud contenga más de diez (10) reivindicaciones y no se haya pagado la tasa complementaria, sólo se estudiarán las cubiertas por la tasa pagada. Por lo tanto se estudiaran las reivindicaciones 1 a 22.

Título de la solicitud: “Reactor Electrobioquímico” (Pág. 1, radicado N° 11-009466-00000-0000).

El problema planteado en esta solicitud consiste en la necesidad de remover semi-metales e iones inorgánicos/orgánicos de líquidos.

Para resolver este problema técnico, la solicitud en estudio proporciona un método y sistemas para la remoción de selenio, mercurio, arsénico y nitratos de un líquido, basados en la aplicación de una corriente eléctrica entre electrodos que permiten la viabilidad de microorganismos.

El objeto de la presente Solicitud se relaciona con la Clasificación Internacional de Patentes (CIP) C12M 1/33, 1/42.

4. De la Solicitud de Patente

Descripción

La descripción aunque es clara no contiene la totalidad de figuras presentes en la solicitud internacional, se sugiere anexarlas a la solicitud nacional.

Reivindicaciones (Art 30 D 486, Art 22 PCT)

Las reivindicaciones 1, 2, 5, 6, 8, 14 y 18 no son claras porque las expresiones *“una distancia”*, *“concentrados”, “compuesto objetivo”, “dirigiéndose dicha población de microorganismos al compuesto objetivo”, “múltiples compuesto objetivo”, “sustancialmente”, “conectadas de manera operativa”, “suficiente”, “superficies activas”* son generales, por lo cual no permite distinguir la invención del estado de la técnica. Se sugiere sustituirlas por un término preciso o un rango concreto.

Las reivindicaciones 6, 8, 18 y 19 no son claras porque las expresiones *“aproximadamente”* y *“al menos”* son imprecisas, ya que en este caso el alcance de la protección de las reivindicaciones deja de ser precisa y no permite distinguir la invención del estado de la técnica. Se sugiere sustituirlas por un término preciso o un rango concreto.

Las reivindicaciones 1, 3 a 6, 11 y 18 a 20, no son claras porque las expresiones “*en donde los microorganismos y la diferencia de potencial son suficientes…y mantener la población de microorganismos, siendo las superficies capaces de soportar una carga eléctrica y soportar el crecimiento biológico*”, “*la diferencia de potencial es suficiente para reducir la población de microorganismos”,* “*retirar un segundo compuesto objetivo*”, “*suficiente para dirigir la mayor parte del líquido…de cada reactor electrobioquímico*”, “*en donde el sistema retira al menos dos compuestos objetivo*” y “*retira un primer compuesto objetivo, retira un segundo compuesto objetivo*” son resultados a alcanzar, lo que no está permitido, no define al producto y/o método porque la invención no queda definida por el resultado a alcanzar, puesto que la reivindicación incluiría no sólo la solución propuesta por el solicitante, sino todas las alternativas presentes o futuras que lleguen a ese resultado. Adicionalmente se reitera que la remoción de selenio, arsénico, mercurio y otros compuestos objetivos son también resultados a alcanzar que dependen de las bacterias presentes y de los parámetros como voltaje, corriente y área superficial presente y/o aplicada al sistema. Se sugiere remplazarlas por las características esenciales estructurales que contribuyen a la obtención de ese efecto.

La reivindicación dependiente 2 no es clara porque hace referencia a que se recupera, mientras que la reivindicación 1 independiente hace referencia es a una remoción. Se sugiere realizar la aclaración y/o corrección necesaria.

La reivindicación 8 no es clara porque el voltaje aplicado es un parámetro propio de cada sistema/método y depende del volumen de trabajo del reactor, entre otras.

Las reivindicaciones 12 y 13 no son claras porque mencionan que los microorganismos son enzimas o proteínas, lo que es falso. Los organismos están compuestos de enzimas, de proteínas y otras macromoléculas y compuestos, y no tienen la posibilidad de un autodesarrollo por lo que la expresión "*en donde la etapa de desarrollar una población es subsequente a la etapa de aplicar una diferencia de potencial*" no tiene validez biológica si la población son enzimas o proteínas. Se sugiere realizar la aclaración y/o corrección necesaria.

Las reivindicaciones 14 y 18 en su parte (d) no son claras porque la trayectoria de flujo mencionada es una característica funcional que no le pueden brindar novedad ni nivel inventivo a tal reivindicación. Se sugiere remplazarlas por las características esenciales estructurales que contribuyen a la obtención de ese efecto.

Las reivindicaciones 15 a 17 no son claras porque la disposición del sistema en situ y las trayectorias de flujo son características funcionales que no le pueden brindar novedad ni nivel inventivo a la reivindicación 14 de la cual dependen. Se sugiere remplazarlas por las características esenciales estructurales que contribuyen a la obtención de ese efecto.

5. Determinación del Estado de la Técnica

El estado de la técnica se determinó con base en la fecha de presentación de la solicitud de prioridad invocada, es decir, el 30 de junio de 2008.

Consultadas las fuentes de información con que se cuenta, se encontraron los siguientes documentos que anticipan el objeto de esta solicitud.

Item	Documento	Título	Fecha de Publicación
D1	DE 10245408	"Reactor for separating and removing organic compounds from sewage/waste water, uses chemical and biological reactions together with a catalyst reaction from immersed electrodes"	8/Abril/2004
D2	Art 1[1]	"Towards practical implementation of bioelectrochemical wastewater treatment"	26/Junio/2008
D3	Art 2[2]	"Electrochemical studies of the interaction between a modified activated carbon surface and heavy metal ions"	2005
D4	Art 3[3]	"Advanced Carbon Electrode Materials for Molecular Electrochemistry"	17/Junio/2008
D5	Art 4[4]	"An introduction to anaerobic digestion of organic wastes"	Noviembre/2003

El documento D1[5] divulga un reactor electrobioquímico para la remoción de compuestos orgánicos de aguas residuales (Pág. 2, Párr. 9).

El documento D2 divulga bioelectrorreactores (BER) del tipo celda electrolítica microbiana (MEC) para la remoción de compuestos orgánicos de aguas residuales (Pág. 451, Fig. 1b).

[1]Rozendal et al. Trends in Biotechnology. Vol.26 (8). 2008. Págs. 450 a 459.
[2] Walczyk et al. Journal of Applied Electrochemistry. 2005. Vol 35. Pág. 128. Col. 2. Tabla 2. Fig. 9.
[3] McCreery. R. Chemical Reviews. Vol. 108 (7).2008.Pág. 2672. Fig. 30. Pág. 2673. Tabla 4.
[4]Monnet F. Final Report. Remade Scotland. 2003
[5]http://www.freepatentsonline.com/DE10245408A1.html

El documento D3 divulga electrodos de carbón activado que promueven la adsorción de metales como el mercurio (Pág. 128. Col. 2. Tabla 2. Fig. 9).

El documento D4 divulga electrodos de grafito que presentan diversas proteínas y/o enzimas (Pág. 2672. Fig. 30. Pág. 2673. Tabla 4).

El documento D5 divulga que se tienen sistemas multi-etapas donde hay microorganismos con actividad metabólica diferente en cada etapa (Pág 13. Párr. 5 a Pág. 14, Párr. 9).

6. Examen de Patentabilidad (Art 14 D486)

Novedad (Art 16 D486)

La reivindicación 1 consiste en "*Un método para retirar un compuesto objetivo de un líquido que comprende:…*" (Ver Pág. 45 del Rad. N° 11-009466-00000-0000).

Comparación de las características técnicas **esenciales**, con las del Estado de la Técnica:

Características **esenciales**	**D1**	**D2**
Un método para retirar un compuesto objetivo de un líquido que comprende:	Método para retirar compuestos orgánicos de aguas residuales (reivindicación 1, Pág. 4).	Método para retirar compuestos orgánicos de aguas residuales (Pág. 450, Pág. 451, Párr. 1 y Párr. 2, Fig. 1b).
Disponer dos superficies activas separadas por una distancia y colocarlas dentro de un flujo del líquido	Se emplean un cátodo y un ánodo ubicados dentro de la solución a ser limpiada, los electrodos están separados (reivindicación 1, Pág. 4, Fig. 1)	Se emplean un cátodo y un ánodo ubicados dentro de la solución a ser limpiada, los electrodos están separados (Pág. 451, Fig. 1b).
Desarrollar una población de microorganismos concentrados sobre las superficies activas;	Se tienen microorganismos sobre los electrodos (reivindicación 6, Pág. 4).	Se tienen microorganismos sobre los electrodos, llamados bio-ánodo y bio-cátodo (Pág. 451, Fig. 1b, Pág. 453, Párr. 2).
Y aplicar una diferencia de potencial entre las dos superficies activas.	Se aplica una diferencia de potencial entre los electrodos (reivindicación 1, Pág. 4).	Se aplica una diferencia de potencial entre los electrodos (Pág. 451, Fig. 1b).

De acuerdo con la tabla anterior, las características esenciales del método de la reivindicación 1 habían sido divulgadas previamente en los documentos D1 y D2, por lo tanto, la materia reivindicada no es nueva.

Asimismo, el documento D1 divulga las características de las reivindicaciones dependientes así:

> Reivindicación 2: remoción de compuestos orgánicos de un líquido como lo es el agua residual (reivindicación 1, Pág. 4)

Asimismo, el documento D2 divulga las características de las reivindicaciones dependientes así:

> Reivindicación 9: el empleo de bacterias sobre electrodos sin necesidad de aplicación de un potencial (Pág. 451, Fig. 1a, Pág. 453, Párr. 2).
>
> Reivindicación 10: la etapa de desarrollar una población de microorganismos es subsecuente al de aplicar una diferencia de potencial, ya que hay crecimiento de los microorganismos durante la aplicación de potencial, específicamente en los bioelectrorreactores MEC que requieren un potencial eléctrico (Fig. 1b).

Las reivindicaciones dependientes 2, 9 y 10 no mencionan alguna característica técnica que hagan nuevo el método de la reivindicación 1, por lo tanto no se consideran nuevas.

La reivindicación 14 consiste en "*Un sistema para retirar un compuesto objetivo de un líquido que comprende:…*" (Ver Pág. 47 del Rad. N° 11-009466-00000-0000).

Comparación de las características técnicas **esenciales**, con las del Estado de la Técnica:

Características **esenciales**	**D1**	**D2**
Un sistema para retirar un compuesto objetivo de un líquido que comprende:	Sistema para retirar compuestos orgánicos de aguas residuales (reivindicación 1, Pág. 4, Pág. 3, Párr. 20, Fig. 1).	Sistema para retirar compuestos orgánicos de aguas residuales (Pág. 450, Pág. 451, Párr. 1 y Párr. 2, Fig. 1b).
Dos superficies activas dispuestas a una distancia de separación y dispuestas paralelas entre sí;	Se emplean un cátodo y un ánodo ubicados dentro de la solución a ser limpiada, los electrodos están separados (reivindicación 1, Pág. 4, Fig. 1)	Se emplean un cátodo y un ánodo ubicados dentro de la solución a ser limpiada, los electrodos están separados (Pág. 451, Fig. 1b).
Una fuente eléctrica conectada de manera operativa a cada una de las superficies activas para proporcionar una diferencia de potencial entre las dos superficies activas;	Se tiene una fuente para aplicar una diferencia de potencial entre los electrodos (reivindicación 1, Pág. 4, Fig. 1, letra P).	Se tiene una fuente para aplicar una diferencia de potencial entre los electrodos (Pág. 451, Fig. 1b).
Una población de microorganismos sobre cada una de las dos superficies activas; y	Se tienen microorganismos sobre los electrodos (reivindicación 6, Pág. 4)	Se tienen microorganismos sobre los electrodos, llamados bio-ánodo y bio-cátodo (Pág. 451, Fig. 1b, Pág. 453, Párr. 2).

De acuerdo con la tabla anterior, las características esenciales del sistema de la reivindicación 14 habían sido divulgadas previamente en los documentos D1 y D2, por lo tanto, la materia reivindicada no es nueva.

Las reivindicaciones dependientes 15 a 17 no mencionan alguna característica tangible que hagan nuevo el sistema de la reivindicación 14, por cuanto se mencionó anteriormente son características funcionales del sistema.

La reivindicación 18 consiste en "*El sistema para retirar un compuesto objetivo de un líquido que comprende:…*" (Ver Págs. 47 y 48 del Rad. N° 11-009466-00000-0000).

Comparación de las características técnicas **esenciales**, con las del Estado de la Técnica:

Características **esenciales**	**D2**
El sistema para retirar un compuesto objetivo de un líquido que comprende:	Sistema para retirar compuestos orgánicos de aguas residuales (Pág. 450, Pág. 451, Párr. 1 y Párr. 2, Fig. 1b).
a) Un primer reactor electrobioquímico, que comprende:	Se tienen en serie los bioelectoreactores, siendo implícito que existe un primer reactor (Pág. 454. Col. 2, Párr. 2).
Dos superficies activas dispuestas a una distancia de separación y dispuestas paralelas entre sí;	Se emplean un cátodo y un ánodo ubicados dentro de la solución a ser limpiada, los electrodos están separados (Pág. 451, Fig. 1b).

Una fuente eléctrica conectada de manera operativa a cada una de las superficies activas para proporcionar una diferencia de potencial entre las dos superficies activas;	Se aplica una diferencia de potencial entre los electrodos (Pág. 451, Fig. 1b).
Una población de microorganismos sobre cada una de las dos superficies activas; y	Se tienen microorganismos sobre los electrodos, llamados bio-ánodo y bio-cátodo (Pág. 451, Fig. 1b, Pág. 453, Párr. 2).
b) Un segundo reactor electrobioquímico, que comprende:	Se tienen en serie los bioelectroreactores, siendo implícito que existe un segundo reactor (Pág. 454. Col. 2, Párr. 2).
Dos superficies activas dispuestas a una distancia de separación y dispuestas paralelas entre sí;	Se emplean un cátodo y un ánodo ubicados dentro de la solución a ser limpiada, los electrodos están separados (Pág. 451, Fig. 1b).
Una fuente eléctrica conectada de manera operativa a cada una de las superficies activas para proporcionar una diferencia de potencial entre las dos superficies activas;	Se aplica una diferencia de potencial entre los electrodos (Pág. 451, Fig. 1b).
Una población de microorganismos sobre cada una de las dos superficies activas;	Se tienen microorganismos sobre los electrodos, llamados bio-ánodo y bio-cátodo (Pág. 451, Fig. 1b, Pág. 453, Párr. 2).
c) Un tubo que conecta el primer reactor electrobioqíumico al segundo reactor electrobioquímico de tal manera que el líquido que sale del primer reactor eletrobioquímico entra en el segundo reactor electrobioquímico;	Se tienen en serie los bioelectoreactores, por lo que los dos equipos se conectan por una tubería que une la salida de uno con la entrada del otro (Pág. 454. Col. 2, Párr. 2).

De acuerdo con la tabla anterior, las características esenciales del sistema de la reivindicación 18 habían sido divulgadas previamente en el documento D2, por lo tanto, la materia reivindicada no es nueva.

Las reivindicación dependiente 22 no mencionan alguna característica tangible que haga nuevo el sistema de la reivindicación 18, por cuanto se mencionó anteriormente son características funcionales del sistema.

Nivel inventivo (Art 18 D486)

La reivindicación 7 consiste en "*El método de la reivindicación 1, en donde las dos superficies activas comprenden carbón activado*" (Ver Pág. 45 del Rad. N° 11-009466-00000-0000).

Comparación de las características técnicas **esenciales**, con las del Estado de la Técnica:

Características **esenciales**	**D1**	**D3**
El método de la reivindicación 1,	Método para retirar compuestos orgánicos de aguas residuales en donde se tiene microorganismos sobre electrodos y se aplica un potencial eléctrico (reivindicación 1, reivindicación 6, Pág. 4).	No se menciona
En donde las dos superficies activas comprenden carbón activado.	No se menciona	Se tienen electrodos de carbón activado que remueven mercurio (Pág. 128. Col. 2. Tabla 2. Fig. 9).

Los documentos D1 y D3 se consideran el estado de la técnica más cercano a la invención definida en la reivindicación 7, porque divulgan métodos y sistemas para

remover compuestos de aguas contaminadas.

La diferencia entre la invención, definida en la reivindicación 7 y el método del documento D1 consiste en que D1 no menciona las dos superficies activas que comprenden carbón activado.

La diferencia entre la invención, definida en la reivindicación 7 y el método del documento D2 consiste en que en D2 no se menciona la presencia de poblaciones de microorganismos sobre los electrodos.

El efecto que logra el incluir las dos superficies activas que comprenden carbón activado es que permiten una mayor área de contacto entre los microorganismos, la corriente eléctrica proporcionada y el material a remover, absorber y/o transformar de forma más eficiente.

Por lo tanto, el problema técnico objetivo que pretende resolver esta invención se puede formular así "¿cómo modificar el método de D1 para que se lleve a cabo la remoción del compuesto objetivo por parte de los microorganismos y las superficies activas de forma más eficiente?".

Sin embargo, el empleo de electrodos de carbón activado, ya está divulgado en el documento D3 que se refiere a la interacción de electrodos de carbón activado con metales para la transformación electroquímica de esos metales (Pág. 128. Col. 2. Tabla 2. Fig. 9).

En consecuencia, una persona normalmente versada en la materia incluiría los electrodos de carbón activado de D3 como las superficies activas en el procedimiento de la anterioridad D1, esperando con certeza lograr el método, como el de la reivindicación 7 de la solicitud, lo cual es considerado obvio y, por lo tanto, sin altura inventiva. Adicionalmente se indica que es conocido por la persona versada en la materia que el carbón activado favorece la adsorción y por lo tanto la actividad de los microorganismos sobre su superficie[6].

La reivindicación 12 consiste en "*El método de la reivindicación 1, en donde la etapa de desarrollar una población es subsecuente a la etapa de aplicar*…" (Ver Págs. 46 del Rad. N° 11-009466-00000-0000).

Comparación de las características técnicas **esenciales**, con las del Estado de la Técnica:

Características **esenciales**	**D1**	**D4**
El método de la reivindicación 1,	Método para retirar compuestos orgánicos de aguas residuales en donde se tiene microorganismos sobre electrodos y se aplica un potencial eléctrico (reivindicación 1, reivindicación 6, Pág. 4).	No se menciona
En donde los microorganismos son enzimas	No se menciona	Se presentan electrodos de grafito que presentan diversas proteínas y/o enzimas (Pág. 2672. Fig. 30. Pág. 2673. Tabla 4).

Los documentos D1 y D4 se consideran el estado de la técnica más cercano a la invención definida en la reivindicación 12, porque divulgan métodos y sistemas que emplean material biológico sobre superficies activas como electrodos.

[6]Rivera-Utrilla et al. Activated carbon surface modifications by adsorption of bacteria and their effect on aqueous lead adsorption. Journal of Chemical Technology and Biotechnology. 2001. Vol 76. Abstract.

La diferencia entre la invención, definida en la reivindicación 12 y el método del documento D1 consiste en que D1 no menciona las superficies activas con enzimas.

La diferencia entre la invención, definida en la reivindicación 12 y el documento D4 consiste en que en D4 no se menciona la remoción de un compuesto objetivo de un líquido.

El efecto que logra el incluir las enzimas sobre las superficies activas es que permiten mantener una cierta actividad biológica de remoción, absorción y/o transformación sobre las superficies activas subsecuente a la aplicación de un potencial eléctrico de forma más eficiente.

Por lo tanto, el problema técnico objetivo que pretende resolver esta invención se puede formular así "¿cómo modificar el método de D1 para que se lleve a cabo la remoción del compuesto objetivo por parte de las superficies activas y que mantengan actividad biológica subsecuente a la aplicación del potencial eléctrico de forma más eficiente?".

> Sin embargo, el empleo de electrodos de grafito que presentan diversas proteínas y/o enzimas sobre su superficie y que son activas en la presencia de un potencial eléctrico, ya está divulgado en el documento D4 que se refiere a electrodos que contienen material biológico y su interacción con diversos compuestos (Pág. 2672. Fig. 30. Pág. 2673. Tabla 4).

En consecuencia, una persona normalmente versada en la materia incluiría los electrodos con proteínas y/o enzimas de D4 como las superficies activas en el procedimiento de la anterioridad D1, esperando con certeza lograr el método, como el de la reivindicación 12 de la solicitud, lo cual es considerado obvio y, por lo tanto, sin altura inventiva.

Asimismo, el documento D4 divulga las características de las reivindicaciones dependientes así:

> Reivindicación 13: Se presentan proteínas sobre electrodos que interactúan con diversos compuestos (Pág. 2672. Fig. 30. Pág. 2673. Tabla 4).

Puesto que la reivindicación dependiente 13 no menciona características adicionales que hagan inventiva la solicitud, se considera que tal reivindicación tampoco tiene nivel inventivo.

La reivindicación 21 consiste en *"El sistema de la reivindicación 19, en donde los microorganismos del primer reactor electrobioquímico son diferentes a los microorganismos del segundo reactor electrobioquímico"* (Ver Pág. 49 del Rad. N° 11-009466-00000-0000).

Comparación de las características técnicas **esenciales**, con las del Estado de la Técnica:

Características **esenciales**	**D2**	**D5**
El sistema de la reivindicación 19,	Sistema para retirar compuestos orgánicos de aguas residuales, donde se tienen en serie los bioelectorreactores (Pág. 454. Col. 2, Párr. 2, Pág. 450, Pág. 451, Párr. 1 y Párr. 2, Fig. 1b).	No se menciona
En donde los microorganismos del primer		Se tiene un sistema multi-etapas donde hay

reactor electrobioquímico son diferentes a los microorganismos del segundo reactor electrobioquímico.	No se menciona	microorganismos con actividad metabólica diferente en cada reactor (Pág 13. Párr. 5 a Pág. 14, Párr. 9).

Los documentos D2 y D5 se consideran el estado de la técnica más cercano a la invención definida en la reivindicación 21, porque divulgan sistemas para remover compuestos de aguas residuales.

La diferencia entre la invención, definida en la reivindicación 21 y el sistema del documento D2 consiste en que D2 no menciona que en cada reactor electrobioquímico se presenten diferentes microorganismos.

La diferencia entre la invención, definida en la reivindicación 21 y el sistema del documento D5 consiste en que en D5 no se menciona los equipos en serie.

El efecto que logra el incluir diferentes microorganismos en cada reactor electrobioquímico es el de remover de forma independiente compuestos objetivo diferentes de forma más eficiente.

Por lo tanto, el problema técnico objetivo que pretende resolver esta invención se puede formular así "¿cómo modificar el sistema de D2 para que se lleve a cabo la remoción de diferentes compuestos objetivo de forma independiente de forma más eficiente?".

> Sin embargo, el empleo de un sistema multi-etapas donde hay microorganismos con actividad metabólica diferente en cada reactor con el fin de mejorar la degradación de diversos compuestos en cada etapa, ya está divulgado en el documento D5 que se refiere a métodos y sistemas de digestión anaerobia (Pág 13. Párr. 5 a Pág. 14, Párr. 9).

En consecuencia, una persona normalmente versada en la materia incluiría microorganismos con actividad metabólica diferente en cada reactor según lo sugiere D5 en el sistema de la anterioridad D2, esperando con certeza lograr el aparato, como la de la reivindicación 21 de la solicitud, lo cual es considerado obvio y, por lo tanto, sin altura inventiva, es decir que si deseo degradar o reducir metales por separado podría emplear bacterias con diferentes actividades para la reducción específica de metales[7] en cada reactor.

Puesto que las reivindicaciones dependientes 10, 12 y 13 no mencionan características adicionales que hagan inventiva la solicitud, se considera que tales reivindicaciones tampoco tienen nivel inventivo,

De igual manera, las reivindicaciones dependientes 3 a 6 y 11 no mencionan características técnicas y/o características tangibles adicionales que puedan brindarle novedad al objeto de la reivindicación 1, puesto que se encuentran redactadas en términos de resultados a alcanzar y/o efectos. Es oportuno reiterar que la posibilidad de remover selenio, arsénico, mercurio y otros compuestos depende de las bacterias presentes[4,7] y de los parámetros como voltaje, corriente y área superficial presente y/o aplicada al sistema[8] por lo que son considerados resultados a alcanzar.

---

[7] Carpentier et al. Microbial Reduction and Precipitation of Vanadium by Shewanella oneidensis. Applied and environmental microbiology. 2003. Vol 69 (6). Pág 3636. Párr. 1 y Párr. 2.

[8] Gardner K. Electrochemical Remediation and Stabilization of Contaminated Sediments. A Final Report Submitted to The NOAA/UNH Cooperative Institute for Coastal and Estuarine Environmental Technology (CICEET). 2005. Págs. 17 y 18. Fig. 6 y Tabla 2.

Adicionalmente, las reivindicaciones 19 y 20 no mencionan características técnicas y/o características tangibles adicionales que puedan brindarle novedad al objeto de la reivindicación 18, puesto que se encuentran redactadas en términos de resultados a alcanzar y/o efectos.

Por otro lado, la reivindicación dependiente 8 no menciona características técnicas y/o características tangibles adicionales que puedan brindarle novedad al objeto de la reivindicación 1, ya que hace referencia a voltaje el cual es un parámetro propio de cada sistema y cambia de magnitud dependiendo del volumen del equipo y la distancia entre las superficies activas, entre otros. Para fines de comparación los parámetros más conocidos en el campo técnico de la invención son corriente eléctrica por unidad de volumen o corriente eléctrica por unidad de área de las superficies activas.

7. Conclusión

Los requisitos de Patentabilidad de la presente Solicitud están afectados así:

Item	Documento	Reivindicaciones afectadas	Requisito que afecta
D1	DE 10245408	1,2, 9, 10 y 14 a 17	Novedad/Nivel inventivo
		7, 12 y 13	Nivel inventivo
D2	Art 1	1, 2, 9, 10, 14 a 18 y 22	Novedad/Nivel inventivo
		21	Nivel inventivo
D3	Art 2	7	Nivel inventivo
D4	Art 3	12 y 13	Nivel inventivo
D5	Art 4	21	Nivel inventivo

En cumplimiento del artículo 45 de la Decisión 486 de la Comisión de la Comunidad Andina, se le indica que debe dar respuesta dentro del término de sesenta (60) días contados a partir del día siguiente de la fecha de notificación de la presente comunicación. En caso de no dar respuesta al presente requerimiento, o si a pesar de la respuesta subsistieran los impedimentos para la concesión, se denegará la patente.

Se invita al solicitante se sirva indicar, si así lo considera, su renuncia al término faltante de sesenta (60) días para dar respuesta a este requerimiento y presentarla por escrito.

Finalmente, se le recuerda al solicitante que si como respuesta a este requerimiento llegara a modificar el capítulo reivindicatorio y éste contenga más de diez (10) reivindicaciones, no pagará la tasa de modificación voluntaria pero sí la correspondiente al pago por reivindicación adicional.

Notifíquese el presente oficio conforme a lo dispuesto en el numeral 5.2, literal e), del capítulo quinto del título primero de la Circular Única No. 10 de 2001.

JOSÉ LUIS SALAZAR LÓPEZ
Director de Nuevas Creaciones (c)

El anterior requerimiento fue notificado por fijación en lista, de fecha 2014-03-18

Elaboró: Jorge Eduardo Cortazar Gomez
Revisó: Olga Ximena Benavides Salazar

Review

Towards practical implementation of bioelectrochemical wastewater treatment

René A. Rozendal[1,2,3], Hubertus V.M. Hamelers[2], Korneel Rabaey[1], Jurg Keller[1] and Cees J.N. Buisman[2,3]

[1] Advanced Water Management Centre, The University of Queensland, St. Lucia, QLD 4072, Australia
[2] Sub-department of Environmental Technology, Wageningen University, Bomenweg 2, P.O. Box 8129, 6700 EV Wageningen, The Netherlands
[3] Wetsus, Centre for Sustainable Water Technology, Agora 1, P.O. Box 1113, 8900 CC Leeuwarden, The Netherlands

Bioelectrochemical systems (BESs), such as microbial fuel cells (MFCs) and microbial electrolysis cells (MECs), are generally regarded as a promising future technology for the production of energy from organic material present in wastewaters. The current densities that can be generated with laboratory BESs now approach levels that come close to the requirements for practical applications. However, full-scale implementation of bioelectrochemical wastewater treatment is not straightforward because certain microbiological, technological and economic challenges need to be resolved that have not previously been encountered in any other wastewater treatment system. Here, we identify these challenges, provide an overview of their implications for the feasibility of bioelectrochemical wastewater treatment and explore the opportunities for future BESs.

Introduction

Industrial, agricultural, and domestic wastewaters contain dissolved organics that require removal before discharge into the environment [1]. Traditionally, these organic pollutants are removed by aerobic treatment, which consumes large amounts of electrical energy for aeration. However, wastewaters are increasingly being recognized as a renewable resource for the production of electricity, fuels and chemicals. To date, the only technology that has proven capable of extracting this energy from wastewaters on a commercial scale is anaerobic digestion [2–4].

Recently, bioelectrochemical wastewater treatment has emerged as a potentially interesting technology for the production of energy from wastewaters. Bioelectrochemical wastewater treatment is based on the use of electrochemically active microorganisms [5–7]. Electrochemically

Glossary

Activated sludge treatment: aerobic treatment of wastewater based on suspended flocs of bacteria that oxidize organic material to carbon dioxide.
Anaerobic digestion: anaerobic treatment of wastewater based on microorganisms that convert organic material to methane.
Anion exchange membrane: type of membrane that is selectively permeable to anions.
Anode: electrode of an electrochemical device that accepts electrons from an electrochemical reaction.
Bioelectrochemical system (BES): an electrochemical system in which electrochemically active microorganisms catalyse the anode and/or the cathode reaction.
Bioelectrochemical wastewater treatment: wastewater treatment with a bioelectrochemical system.
Biofilm: multilayered aggregation of microorganisms.
Bipolar membrane: type of membrane that consists of a cation and an anion exchange layer. When current flows in an electrochemical cell that contains a bipolar membrane, water continuously diffuses to the interface between these two layers and is split into protons and hydroxyl ions. The produced protons migrate through the cation exchange layer towards the cathode and the hydroxyl ions migrate through the anion exchange layer towards the anode.
Bipolar plate: a conductive plate used in bipolar plate stack designs that connects the anode of one cell on one side of the bipolar plate to the cathode of the next cell on the other side of the bipolar plate.
Bipolar plate stack design: configuration of multiple electrochemical cells in series connected to each other with bipolar plates.
Cation exchange membrane: type of membrane that is selectively permeable to cations.
Cathode: electrode of an electrochemical device that donates electrons to an electrochemical reaction.
Cell reversal: when an electrochemical cell in an MFC stack cannot deliver the current that is demanded from the system, the cell can reverse polarity, that is, the cell voltage of the specific cell becomes negative and the cell turns into an electrolysis cell.
Charge mosaic membrane: type of membrane that is permeable to cations and anions but not to uncharged molecules.
Chemical oxygen demand (COD): measure used to indicate the amount of organic material in wastewater. It is expressed in mg O_2/l, which is the amount of oxygen needed to oxidize the entire organic material to carbon dioxide.
Electrochemically active microorganisms: microorganisms that are capable of either donating electrons to or accepting electrons from an electrode.
Electrolyte ohmic loss: voltage loss caused by the movement of ions through an electrolyte.
Electrode ohmic loss: voltage loss caused by the movement of electrons through electrodes, electrical contacts and electrical wiring of an electrical system.
Extracellular electron transfer (EET): mechanism by which electrochemically active microorganisms donate electrons to or accept electrons from an electrode.
Food web: network that describes the feeding relationships within a microbial community. The excreted products of one type of microorganism are the feed for the next type of microorganism.
Gibbs free energy: maximum amount of useful work that can be obtained from a reaction (expressed in J/mol).
Methanogenesis: microbial production of methane.
Microbial fuel cell (MFC): bioelectrochemical system that is capable of converting the chemical energy of dissolved organic materials directly into electrical energy.
Microbial electrolysis cell (MEC): bioelectrochemical system that is capable of generating a product (e.g. hydrogen) from dissolved organic materials and that drives the reactions with an electrical energy input.
Polymer electrolyte membrane (PEM) fuel cells: chemical fuel cells that are used for the production of electricity from hydrogen.
Single cell design: an electrochemical cell that is operated in a stand-alone manner.
Ultrafiltration membrane: type of membrane that is permeable to molecules of small molecular weight (as well as ions) but that retains suspended solids and molecules of higher molecular weight.

Corresponding author: Rozendal, R.A. (r.rozendal@uq.edu.au).

0167-7799/$ – see front matter doi:10.1016/j.tibtech.2008.04.008 Available online 26 June 2008

Box 1. Extracellular electron transfer (EET)

BESs rely on the capability of certain species of microorganisms to transfer electrons from the inside of the cell to an electrode. This is referred to as extracellular electron transfer (EET). Two EET mechanisms can be distinguished. The first mechanism is indirect and relies on the redox cycling of electron shuttling compounds between the microorganisms and the electrode. These electron shuttling compounds can either be naturally present redox-active organic or inorganic compounds, such as humic acids and sulfur species [8], or are in some cases produced by the microorganisms, such as quinones [11] or phenazines [12]. The second EET mechanism is direct and relies on direct contact between the electrochemically active microorganisms and the electrode. To establish this contact, some microorganisms utilize a connected series of inner-membrane, periplasmic and outer-membrane redox proteins (i.e. cytochromes) that conduct the electrons from the inside of the cell all the way to the electrode [6]. In addition, many electrochemically active species also appear to be capable of producing electrically conductive pili [9,10] or nanowires on the outside of their cells that can stretch over tens of microns. Nanowires allow microorganisms to be further away from the electrode and also make it possible for multilayered biofilms of these microorganisms, which rely on direct electron transfer through contact, to grow on electrode surfaces [7].

active microorganisms are capable of extracellular electron transfer (EET; Box 1) [8–12] and can use this mechanism to transfer electrons to an electrode (anode) while they are oxidizing (and thus removing) the organic materials in wastewaters (Figure 1). The microorganisms function as a catalyst for the electrochemical oxidation of the organic material [13–15], and the electrode is therefore referred to as a microbial bioanode. Bioelectrochemical wastewater treatment can be accomplished by electrically coupling a microbial bioanode to a counter electrode (cathode) that performs a reduction reaction. As a result of this electrical connection between the anode and cathode, the electrode reactions can occur and the electrons can flow from anode to cathode (i.e. electrical current can flow). The Gibbs

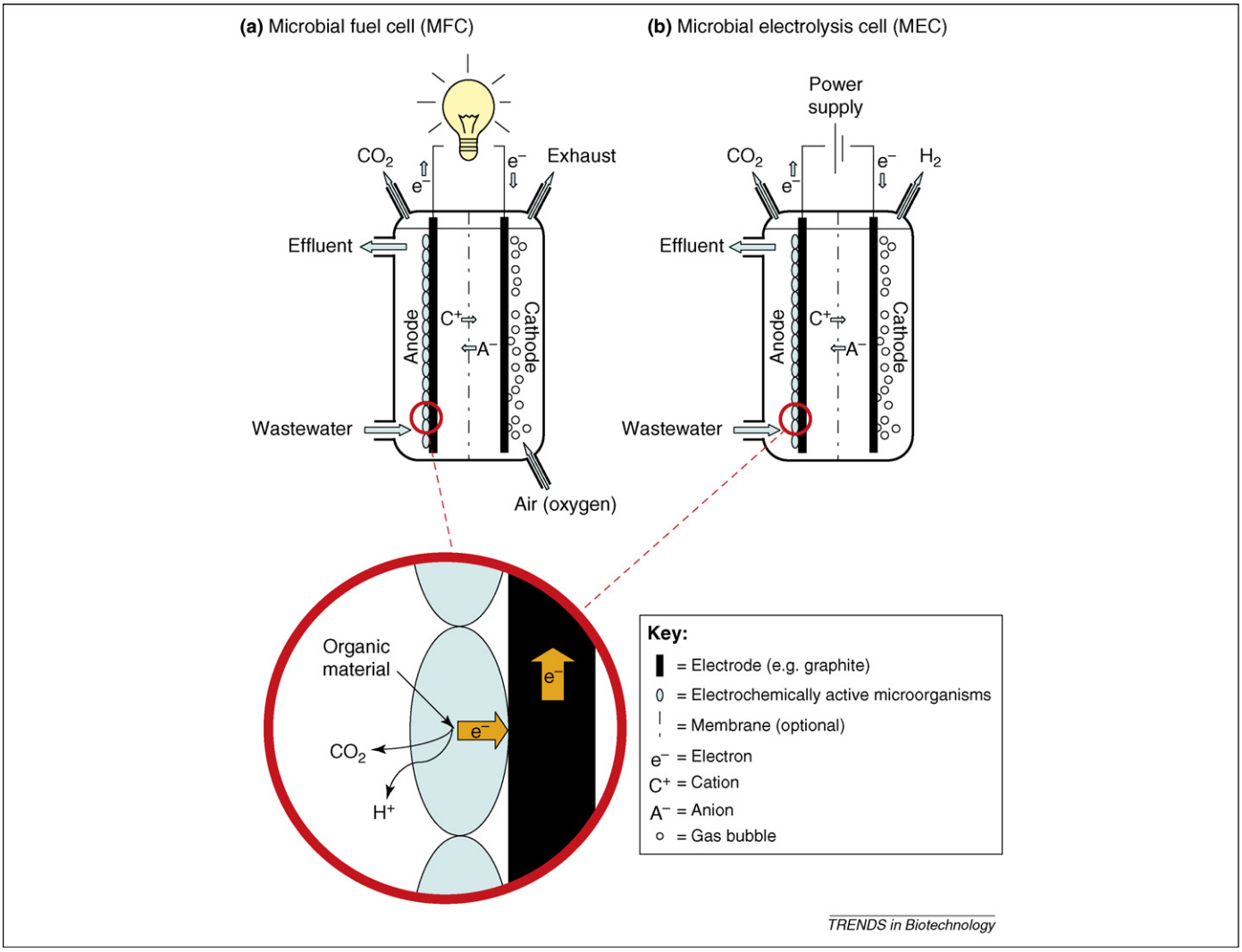

Figure 1. Bioelectrochemical wastewater treatment. Schematic representation of a typical configuration of the two most common bioelectrochemical wastewater treatment systems: the microbial fuel cell (MFC) (**a**) and the microbial electrolysis cell (MEC) for hydrogen production (**b**). At the anode, organic material from the wastewater is oxidized by electrochemically active microorganisms. Subsequently, the microorganisms transfer the electrons resulting from this oxidation reaction to the anode via extracellular electron transfer (EET). Via an electrical circuit, the electrons are transported to the cathode, where they are consumed for oxygen reduction (in the case of MFCs) or product formation (in the case of MECs). Both cathodic reactions can occur either through direct chemical catalysis (e.g. with platinum) or through biocatalysis (in the case of a microbial biocathode). Electroneutrality is maintained in the system by the transport of ions in between the electrodes (optionally through a membrane). In an MFC, electrical energy can be extracted from the electrical circuit. In an MEC, however, electrical energy needs to be supplied to the electrical circuit by means of a power supply.

Box 2. Working principle of BESs

The theoretical cell voltage or electromotive force (*emf*) of the overall reaction occurring in a BES determines whether electricity is produced or has to be invested to drive the reaction. The electromotive force can be calculated from the Gibbs free energy of the overall reaction occurring in the BES, according to:

$$emf = -\frac{\Delta G}{nF} \qquad \text{[Equation I]}$$

with *emf* being the electromotive force (in V), ΔG the Gibbs free energy of the reaction (in J/mol), *n* the amount of electrons involved in the reaction (in mol), and *F* Faraday's constant (96485.3 C/mol). The Gibbs free energy of a reaction gives the maximum amount of useful work that can be obtained from a reaction and can be calculated from tabulated values (e.g. in [16]).

In an MFC, the Gibbs free energy of the reaction is negative and the *emf* is positive, implying that electricity can be produced from the reaction. For example, for acetate as the organic substrate ($[CH_3COO^-]=[HCO_3^-]=10$ mM, pH 7, 298.15 K, $pO_2 = 0.2$ bar):

$$\text{Anode}: CH_3COO^- + 4H_2O \rightarrow 2HCO_3^- + 9H^+ + 8e^-$$

$$\text{Cathode}: 2O_2 + 8H^+ + 8e^- \rightarrow 4H_2O$$

$$\text{Overall}: CH_3COO^- + 2O_2 \rightarrow 2HCO_3^- + H^+$$

($\Delta G = -847.60$ kJ/mol; $emf = 1.10$ V)

In an MEC, however, the Gibbs free energy of the reaction is positive and the *emf* is negative and hence electricity needs to be invested. If acetate is used as the organic substrate and hydrogen is produced ($[CH_3COO^-]=[HCO_3^-]=10$ mM, pH 7, 298.15 K, $pH_2 = 1$ bar):

$$\text{Anode}: CH_3COO^- + 4H_2O \rightarrow 2HCO_3^- + 9H^+ + 8e^-$$

$$\text{Cathode}: 8H^+ + 8e^- \rightarrow 4H_2$$

$$\text{Overall}: CH_3COO^- + 4H_2O \rightarrow 2HCO_3^- + H^+ + 4H_2$$

($\Delta G = 93.14$ kJ/mol; $emf = -0.12$ V)

The value of the *emf* denotes the best possible cell voltage in a given system, that is, the maximum cell voltage that can be generated in an MFC and the minimum required voltage that is necessary to drive an MEC. Under practical working conditions, however, the actual performance is decreased because of various electrochemical losses, such as electrode potential losses (i.e. electrode overpotentials) and ohmic losses [17]. For an MFC this means that the resulting cell voltage will become less positive than the *emf*, and consequently less electrical energy is produced. In an MEC, the cell voltage will become more negative than the *emf*, hence more electrical energy is required. Efficient BES designs therefore need to focus on reducing electrochemical losses as much as possible.

free energy change of the overall reaction [16] determines how the bioelectrochemical system (BES) needs to be operated. When the Gibbs free energy change of the overall reaction is negative, electrical energy can be produced, and the BES is operated as a microbial fuel cell (MFC; Box 2; [17,18]). Conversely, when the Gibbs free energy change of the overall reaction is positive, electrical energy needs to be invested, and the BES is operated as a microbial electrolysis cell (MEC; Box 2; [19–26]).

Over the past few years the performance of BESs has improved almost exponentially [7]. In fact, the current densities of laboratory-scale BESs already approach values that would be suitable for practical implementation. Laboratory BESs have already achieved current densities of ~10 A/m^2 anode surface area [27,28]. Assuming a minimum cell thickness of ~1 cm to allow enough space for wastewater pumping, this means that full-scale BESs are expected to exhibit a volumetric current density in the order of 1000 A/m^3 reactor volume. This represents a volumetric wastewater treatment capacity of ~7.1 kg chemical oxygen demand (COD)/m^3 reactor volume/day, which is in the same range as conventional wastewater treatment systems, such as activated sludge systems (~0.5–2 kg COD/m^3 reactor volume/day) and high-rate anaerobic systems (~8–20 kg COD/m^3 reactor volume/day) [17].

However, thus far, BES experiments have typically been performed on a small scale, varying from just a few millilitres [22,27,29] to several litres at most [23,30,31]. To achieve practical implementation, BESs still need to be scaled-up by several orders of magnitude from the laboratory scale (10^{-6} to 10^{-3} m^3) to a scale suitable for wastewater treatment (1 to 10^3 m^3). Several researchers have aimed at developing scaleable designs [32–34], but so far no study has demonstrated that the respective designs can be operated satisfactorily beyond the litre-scale. The scaling-up and practical implementation of bioelectrochemical wastewater treatment is complicated and certainly not straightforward. In this review, we address this complexity from a microbiological, technological and economic perspective and assess the implications of this for practical implementation of bioelectrochemical wastewater treatment. Moreover, we aim to explore the opportunities for future BESs for wastewater treatment.

The microbiological challenge: taking control over microbial reactions

Metabolic diversity

Real wastewater contains a wide range of organic materials. Therefore, to create a BES that would be able to treat real wastewater, a large and versatile food web will be required that allows for the degradation of particulate and/or polymeric organic substances, such as cellulose [35,36]. Analysis of microbial communities in BESs have thus far revealed a high diversity of microbial species [7,37], but it remains to be investigated whether this microbial diversity also represents the much needed metabolic diversity. In tests with acetate, symbiotic relationships between Gram positive and Gram negative bacteria have been observed [38], which suggests that at least small food webs can be established. Nevertheless, most BES studies so far exhibited a decreased electrochemical performance when real wastewaters were used compared to synthetic media with easily biodegradable substrates (e.g. acetate). This could indicate that (i) the anodic microbial community could not degrade the more complex material at the same rates with which more simple substrates were degraded or (ii) competing processes, such as methanogenesis (see 'Methanogenic competition' below), consumed the substrates. For example, in a single-chamber MFC fed with synthetic acetate medium, Liu and Logan achieved a power density of 494 mW/m^2 anode surface area, whereas when the same MFC was fed with domestic wastewater, only 146 mW/m^2 anode surface area was generated [29].

Methanogenic competition

Methane is the natural end product in most anaerobic environments, and methanogenesis is therefore an import-

ant microbiological process that needs to be considered with respect to BES performance. Methanogens, that is, microorganisms that convert organic material to methane, compete with the electrochemically active microorganisms for the organic material in the wastewater. Hence, unless the formed methane can somehow be re-oxidized and thus reused for current generation, methanogenic activity reduces electron recovery. Recently, it was shown that although electrochemically active microorganisms at an anode can outcompete methanogens for acetate as an electron donor, the use of glucose leads to notable amounts of methane production [39,40]. Significant methane production was also observed for ethanol [28]. Whereas acetate is a nonfermentable substrate, glucose and ethanol are fermentable substrates that yield hydrogen gas when they are fermented. These observations suggest that the electrochemically active microorganisms are not able to completely outcompete methanogens for hydrogen [28,39,40]. A possible reason for this is that methanogens, in contrast to electrochemically active microorganisms, are not dependent on close, electrical contact with the electrode. Microorganisms can grow on the anode in multilayered aggregations that are referred to as biofilms. Methanogens can colonize the top of anodic biofilms, where they scavenge the hydrogen at the place it is formed in the fermentation process before it can reach the electrochemically active microorganisms deeper in the biofilm. From an operational perspective, this implies that when fermentable substrates are present in the wastewater, pre-fermentation might be required before bioelectrochemical wastewater treatment. Pre-fermentation will convert fermentable substrates to nonfermentable substrates (such as acetate) on which the electrochemically active microorganisms have a better chance of outcompeting the methanogens.

Besides the fact that methanogenesis can reduce electron recovery in anode compartments of all types of BESs, it can also reduce hydrogen recovery in cathode compartments of MECs. The hydrogen produced in the cathode of MECs is an ideal substrate for methanogens, therefore hydrogen loss can occur in any circumstance that brings hydrogen into contact with methanogens. Such a situation could arise, for example, when a microbial biocathode is used (see 'Electrode potential losses' below) [25], when a membrane-less MEC system is used (see 'Membrane pH gradients' below) [19] or when a nonsterilized cathode is used [41]. Operating the system in such a way that the availability of bicarbonate, which is needed for methane production from hydrogen, is limited [25] or aerating the system periodically to kill methanogens [19] might be necessary to prevent this kind of methanogenic hydrogen loss.

Biofilm pH gradients

The anode reaction in BESs produces protons (see Box 2), which can acidify the biofilm and negatively affect BES performance. Torres *et al.* suggested that at low buffer strengths an electrochemically active biofilm can be limited by the transport rate of these protons out of the biofilm [42]. It was shown that when the phosphate buffer concentration was increased from 12.5 to 100 mM, the current density more than quadrupled and approached 10 A/m^2 anode surface area. This effect was not caused by the increase of conductivity that resulted from the adding of buffer because when the conductivity was increased by adding similar amounts of sodium chloride, the current density only increased by 15%. Typical domestic wastewaters and many industrial wastewaters have an alkalinity in the order of 50 to 200 mg/l as $CaCO_3$ [43], which is equivalent to 1 to 4 mM of phosphate buffer. Consequently, these low buffer strengths are likely to limit the performance of the microbial bioanode and hence of the complete BES. A possible solution is to design BESs in a way that also encourages flow of wastewater through the electrode in addition to flowing past the electrode [44]. This will increase the supply of buffer to electrochemically active microorganisms and stabilizes pH in the biofilm. The addition of extra buffers to wastewater has been also proposed [45], but it is unlikely that this will be cost-effective for large-scale application.

The technological challenge: eliminating electrochemical losses

Electrode potential losses

Full-scale BESs are expected to exhibit volumetric current densities exceeding 1000 A/m^3 (see 'Introduction'). Potential losses at the electrodes (i.e. overpotentials) can significantly limit the attainable current densities, and it is therefore vital that electrode potential losses are minimized to achieve high current densities. Surprisingly, the potential losses of bioanodes in BESs have consistently been much lower than those observed for chemical cathodes, even when normally excellent (but expensive) electrocatalysts such as platinum were used at the cathode. MFCs, for example, can theoretically produce up to 1.1 V (Box 2). Under working conditions, less than 0.1 V of this theoretical voltage is typically lost at the bioanode, whereas the losses at the cathode typically exceed 0.5 V [17]. This leaves less than 0.6 V for electricity production and does not yet take into account any other losses, such as ohmic losses (see 'Ohmic losses' below) and losses caused by membrane pH gradients (see 'Membrane pH gradients' below). The high cathode overpotentials observed for electrochemical oxygen reactions are generally regarded as being caused by the slow kinetics of oxygen reduction [46]. However, high cathode overpotentials have also been encountered in MECs, in which hydrogen is created at the cathode, an electrochemical reaction that is generally regarded to be very fast and should therefore exhibit low potential losses [23]. The reasons for the low performance of platinum cathodes in BESs are not well understood. It could partly be explained by the relatively mild conditions, such as a wastewater pH of around 7. Conventional electrochemical systems that apply platinum catalysed cathodes (such as PEM fuel cells [47,48]) are able to sustain much higher current densities but are typically operated at a very low pH value (<1). Protons are a reactant in the cathode reaction (Box 2), and a low pH therefore guarantees that protons are available in high concentrations. Furthermore, these conventional systems typically also operate at much higher temperatures than BESs (e.g. ~50–100 °C for a PEM fuel cell), which also benefits reac-

tion kinetics and therefore reduces overpotentials. Finally, platinum in BESs might also be prone to irreversible poisoning, for example by H_2S that is present in the wastewater.

Therefore, to improve the performance and economic feasibility of BESs, platinum needs to be replaced by alternative catalysts. Up to now, three strategies have been explored in this perspective: the use of (i) materials that have a high specific surface area (e.g. granular graphite) [49], (ii) alternative inexpensive chemical electrocatalysts [50–52] and (iii) microbial biocathodes [25,53–55]. Of those three strategies, the development of biocathodes in particular has become a rapidly emerging research topic within the BES field. Similar to bioanodes, biocathodes utilize electrochemically active microorganisms, which have evolved to function optimally under the mild conditions present in BESs. In 2005, Bergel *et al.* demonstrated that an electrochemically active microbial consortium enriched in seawater was capable of catalysing oxygen reduction at a stainless steel cathode [55]. Subsequently, several groups demonstrated that such consortia that are able to catalyse oxygen reduction could also be enriched under freshwater conditions [53,54]. More recently, cathodic consortia were reported that were capable of catalysing hydrogen production at a graphite cathode [25]. Biocathodes have the important advantage that they can replace expensive precious metal electrocatalysts by providing a self-regenerating biocatalyst on an inexpensive electrode material, such as carbon or graphite. Because this can reduce the capital costs of BESs significantly (see 'Outlook'), the further development of biocathodes is likely to advance the field significantly.

Ohmic losses: wastewater conductivity and electrode resistivity

The ohmic resistance is the opposition that ions and electrons experience when they are moving through an electrochemical system. The higher the ohmic resistance and current density are, the higher will be the resulting ohmic loss in a system. The two most important types of ohmic losses relevant for BESs are: (i) electrolyte ohmic loss and (ii) electrode ohmic loss. The first refers to the voltage loss caused by the movement of ions through the electrolyte (including the wastewater and the membrane), and the latter refers to the movement of electrons through the electrodes, the electrical contacts and the electrical wiring of a BES.

Because of the low conductivity of many real wastewaters, the electrolyte ohmic losses can become considerable. Figure 2 shows calculations for electrolyte ohmic loss [56] at the typical current densities and wastewater conductivities expected for bioelectrochemical wastewater treatment in practice. In laboratory studies, conductivities are typically reasonably high because of the high salt concentrations and buffer strengths [57], but domestic and many industrial wastewaters typically exhibit low conductivities in the order of only 1 mS/cm [58]. At a typical expected current density for full-scale BESs of 10 A/m^2 anode surface area (see 'Introduction'), the electrolyte ohmic loss encountered at such low conductivity would be ~1 V for each cm of distance between anode and cathode

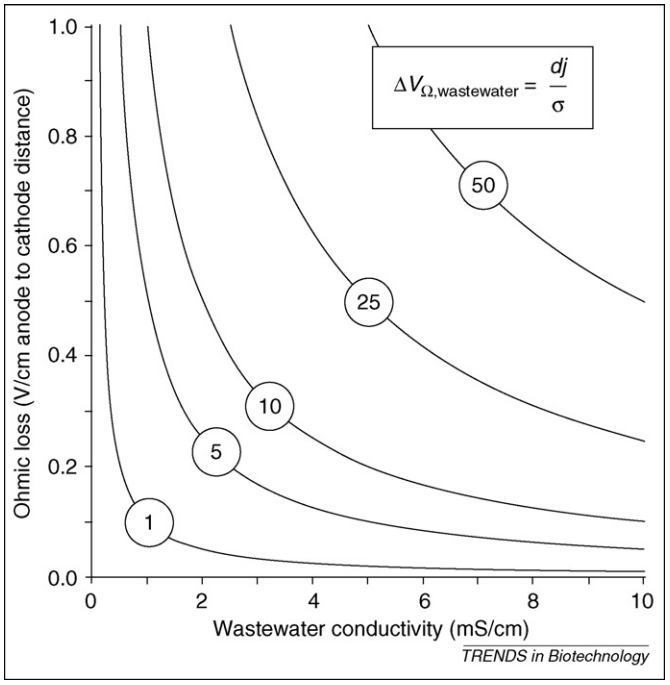

Figure 2. Electrolyte ohmic loss in bioelectrochemical systems (BESs). This graph illustrates the calculated electrolyte ohmic loss per cm of distance between anode to cathode in dependence of the wastewater conductivity at different current densities of 1, 5, 10, 25 and 50 A/m^2 anode surface area. Ohmic losses were calculated using the indicated equation [56], where $\Delta V_{\Omega,\text{wastewater}}$ is the ohmic loss in the wastewater (in V), d the distance between anode and cathode (in m), j the current density (in A/m^2) and σ the conductivity of the wastewater (in S/m).

(Figure 2). Because this is a significant loss compared to the theoretical cell voltages of BESs (Box 2), it is important to minimize the electrode spacing in a BES design [17]. Additionally, one could artificially increase the ionic strength of wastewater, for example by adding salts and buffers, but this is highly expensive and therefore not practical.

The choice of design of a BES can significantly affect the ohmic losses encountered in the process. Most BESs so far have been based on a single cell design, either in a standalone fashion or as several single cells connected in series [30] (Box 3). Single cell BES designs can minimize the electrolyte ohmic loss because the electrodes can be placed in close proximity to each other with only the membrane separating them. However, because of the large distance that electrons have to travel (an inherent feature of these designs), they are likely to suffer from high electrode ohmic losses instead (Box 3). Graphite and carbon are the most commonly used materials for bioanodes and biocathodes because of their compatibilty with the electrochemically active biofilm, their sufficiently low overpotentials and their low costs [17]. However, the electrical resistivity of graphite and carbon is very high (electrical resistivity of 1375 μΩcm for graphite versus 9.71 μΩcm for iron [59]), which causes high electrode ohmic losses in full-scale BESs. For example, two solid graphite electrodes with dimensions $10 \times 10 \times 0.3$ cm (laboratory scale) and $100 \times 100 \times 0.3$ cm (scale-up) will both have an ohmic resistance of ~4.6 mΩ. However, if granular (e.g. [33]) or fibrous materials (e.g. [60]) are used, which is typical for BESs, the ohmic resistance will be several times higher as

Box 3. Ohmic loss in a single cell design

The most straightforward BES design is a single cell design (Figure I), which has been used in almost all studies reported in the literature. Because the wastewater does not need to be pumped in between the anode and cathode, the electrodes can be placed in close proximity to each other with only the membrane separating them. Due to this small electrode spacing in a single cell design, the travel distance of ions through the electrolyte between the electrode compartments can be minimized, and this results in a low electrolyte ohmic loss. To optimally benefit from this advantage it is important to use porous or mesh electrodes instead of solid electrodes, so that ions can freely move through the electrolyte and do not have to go around the electrodes when migrating between the electrode compartments. An important disadvantage of single cell designs is the long travel distance of the electrons, which need to travel all the way through the anode, then through the electrical circuit and then all the way through the cathode to be consumed in the cathode reaction. This long travel distance can cause a high electrode ohmic loss if the electrode material that is used is not sufficiently conductive.

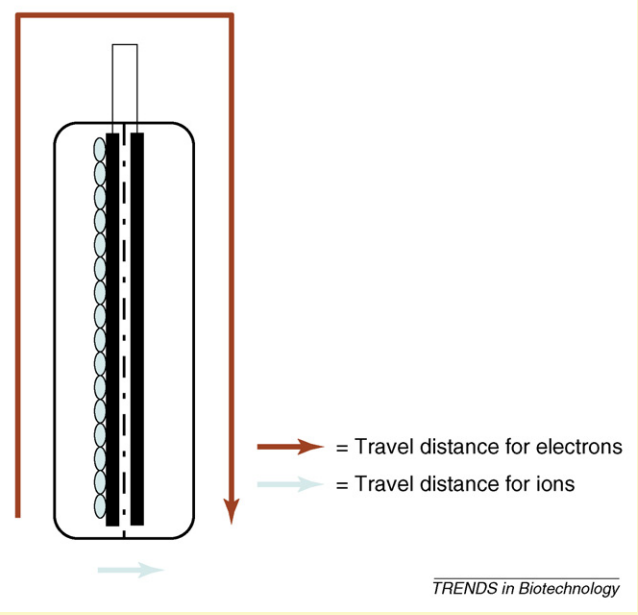

Figure I. Single cell design.

a result of the contact resistances between the granules or fibres. At laboratory scale these ohmic resistances will only cause a voltage loss of several millivolts, even at current densities exceeding 10 A/m^2 anode surface area, which is almost negligible compared to the theoretical voltage of BESs (Box 2). However, in a scaled-up system similar current densities will cause voltage losses that can amount to several hundreds of millivolts due to much higher absolute currents flowing true the electrode. These voltage losses are large compared to the theoretical voltage of BESs (Box 2). To reduce the electrode ohmic losses, graphite or carbon electrodes can be supported by a highly conductive metal current collector, such as stainless steel mesh, or integrated with a current collector, such as the graphite fibre brush anode integrated with a twisted core of titanium wires demonstrated in a study by Logan *et al.* [32]. However, because metals are generally more expensive than graphite, the inclusion of current collectors into the design of BESs can add significantly to their cost (see 'Outlook').

As an alternative to single cell designs, bipolar plate stack designs offer the possibility of eliminating current collectors. Bipolar plate stack designs are standard practice for PEM fuel cells [47,48], but they have not been investigated extensively for BESs. To the authors' knowledge, there has been only one BES study that uses a bipolar plate stack design [61]. Bipolar plate stack designs connect multiple single cells in series by using bipolar plates. These bipolar plates are typically made of graphite and connect the anode of one cell present on one side of the bipolar plate to the cathode of the next cell on the other side of the bipolar plate. By doing this, the travel distance of the electrons is significantly reduced compared to a single cell design because the electrons generated in the anode reaction only need to cross the bipolar plate to reach the cathode reaction. This can significantly reduce the electrode ohmic losses and can make current collectors redundant. One disadvantage that has been described for stacked MFC systems in general and that also applies to bipolar plate stacked systems is the phenomenon of cell reversal [30,62]. Cell reversal occurs when a cell in the stack cannot deliver the current that is demanded from the system (e.g. because of a limitation in the supply of organic material) and as a result it can reverse polarity, that is, the cell voltage of the specific cell becomes negative and the cell turns into an electrolysis cell. This can irreversibly damage the specific cell and consequently negatively affect the performance of the whole stack. Cell reversal in BESs is not well understood at this stage and needs to be further investigated.

Membrane pH gradients

The electrons that are flowing from the anode to cathode in a BES also represent a flow of negative charge from the anode to the cathode. To maintain electroneutrality, this flow of negative charges needs to be compensated by the transport of cations from anode to cathode or anions from cathode to anode (Figure 1). For this purpose, BES researchers typically utilize ion exchange membranes that enable the transport of ions across the membrane while keeping the anode and cathode reactions separated. In the first BES experiments, Nafion was most often used as the ion exchange membrane [31]. Nafion is well-known for its excellent cation conductivity, but it is relatively expensive compared to other ion-conducting membranes. Less expensive membranes, such as Ultrex^{TM} CMI-7000 (product of Membranes International Inc.) [33], have also been successfully implemented. Nevertheless, several researchers have noticed that there is a fundamental problem associated with the use of ion exchange membranes in BESs that run on wastewater [31,46,63] and that these problems also arise when membranes other than cation exchange membranes are used, such as anion exchange membranes, bipolar membranes, charge mosaic membranes and ultrafiltration membranes [24,26,64,65]. Under the conditions that are prevalent in wastewater, membranes predominantly transport ion species other than protons and hydroxyl ions to maintain electroneutrality. Because the anode reactions in BESs are proton producing and the cathode reactions in BESs are proton consuming (Box 2), this will cause a pH decrease in the

anode chamber and a pH increase in the cathode chamber. As shown by the Nernst equation, the resulting membrane pH gradient causes a potential loss of ~0.06 V per pH unit [24]. Laboratory experiments have shown that membrane pH gradients easily exceed 5 pH units, which causes a significant decrease of BES performance [24,26,46].

Membrane-less operation appears to be an obvious solution to the problem arising from membrane pH gradients [19,29] and would simultaneously offer a cost advantage by eliminating an expensive component from the BES. However, an important drawback of membrane-less operation of BESs is that it can lead to a reduced electron recovery. Membrane-less operation of MFCs can cause an increased contact between oxygen from the cathode chamber and organic material in the anode chamber, which will lead to direct aerobic conversion of the organic material [29]. This organic material is lost and cannot be used by the electrochemically active microorganisms for current generation. Membrane-less operation of MECs causes an increased diffusion of the hydrogen product from the cathode to the anode, where it can be consumed in the anode reaction. Furthermore, membrane-less operation of MECs brings the hydrogen into contact with the microbial community, which stimulates hydrogenotrophic methanogens to convert hydrogen to methane [19]. An alternative way of avoiding membrane pH gradients has been suggested that involves operating the BES in a loop configuration [54,66]. In a loop configuration, the effluent from the anode chamber does not leave the system, which is the case in a more traditional configuration (Figure 1): instead, it is directed to the cathode chamber (Figure 3). This largely solves the problem of the membrane pH gradient because the protons that are produced in the anode reaction (Box 2) are actively transported to the cathode chamber, where they compensate for the protons that are consumed in the cathode reaction (Box 2) and retain the pH in the cathode chamber at a lower value. Furthermore, because the membrane is maintained, the reduction in electron recovery that can occur in membrane-less systems is prevented.

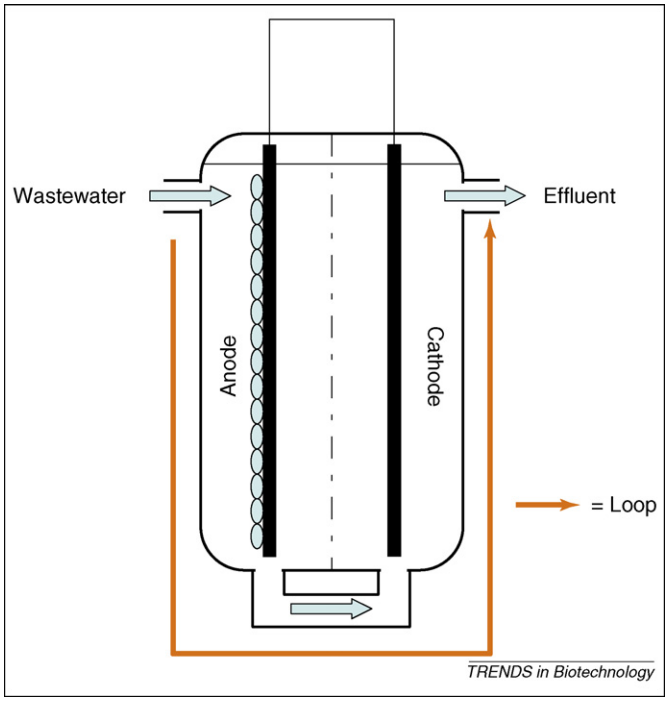

Figure 3. Loop configuration of a bioelectrochemical system, in which the effluent from the anode compartment is directed to the cathode compartment. This is in contrast to what occurs in a more conventional configuration, in which the effluent from the anode compartment directly leaves the system after it has passed the anode (Figure 1). The loop configuration can solve the problem of membrane pH gradients to a large extent because the protons that are produced in the anode reaction (Box 2) are actively transported to the cathode chamber, where they compensate for the protons that are consumed in the cathode reaction (Box 2) and retain the pH in the cathode chamber at a lower value.

Outlook: from an economic challenge to added value

Bioelectrochemical wastewater treatment is a novel and promising biotechnological approach for the production of renewable energy from wastewaters. However, if it is to achieve practical implementation as a wastewater treatment system, several important challenges need to be faced. More studies with real wastewaters are required so that strategies can be developed for (i) improving the degradation of complex materials and (ii) controlling the microbial reactions occurring in the system. New designs are needed for full-scale BESs that are able to minimize potential losses and optimize performance. Most of all, the capital costs of BESs have to be reduced so that the field of large-scale wastewater treatment can be targeted. The extent to which these challenges can be resolved will eventually determine how bioelectrochemical wastewater treatment can be practically implemented.

Figure 4 gives an overview of the estimated capital costs of BESs based on materials currently used in laboratory systems, as well as the predicted future capital costs based on inexpensive substitute materials. Table 1 compares their anticipated costs with the capital costs of the two most widely used conventional wastewater treatment systems, activated sludge treatment and anaerobic digestion. This comparison shows that, based on the materials currently used in the laboratory, the capital costs of a full-scale BES would be orders of magnitude higher than those of conventional wastewater treatment systems. Via improved designs and innovative materials, these capital costs might be reduced significantly, but because of the inherently complex design of BESs, it is expected that the capital cost will always remain several times that of conventional wastewater treatment systems. Therefore, bioelectrochemical wastewater treatment can only become economically interesting if these larger capital costs are compensated for by increased revenue from its products.

MFCs have the advantage that they can produce electricity directly from wastewater. Consequently, MFCs might at some point in the future become a cost-effective and energy-efficient alternative to activated sludge systems (Table 1). However, compared to anaerobic digestion, the revenue that might be raised from the production of electricity in MFCs is unlikely to offset their higher capital cost and to create a competitive advantage. Still, MFCs have some particular benefits over anaerobic digestion that could make them competitive under certain circumstances [3], such as operation on a small-scale, at low COD concentrations, at low temperatures and/or with integrated nitrogen removal [66,67].

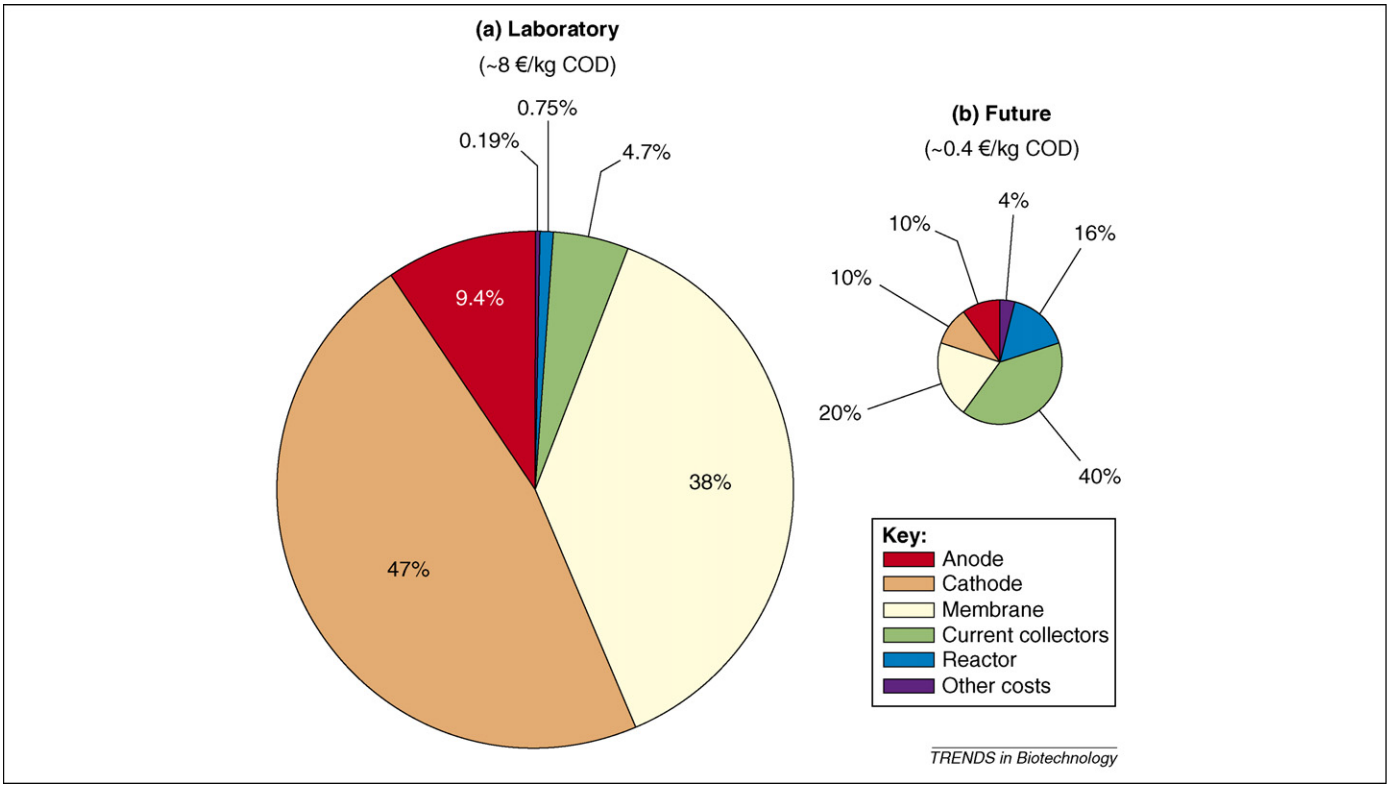

Figure 4. Estimated capital costs of BESs (single cell design; current density: 1000 A/m^3 reactor volume). The costs were either estimated based on materials currently used in laboratory systems (**a**) or on predicted future capital costs assuming less expensive substitute materials (**b**). The cost assumptions of the laboratory materials are based on the authors' experience and the cost assumptions of the future materials are estimated based on raw material costs. The following cost assumptions were used: laboratory anode (graphite felt), 100 €/m^2; laboratory platinum catalysed cathode, 500 €/m^2; laboratory membrane, 400 €/m^2; laboratory current collectors, 25 €/m^2; future substitute electrodes (graphite), 5 €/m^2; future substitute membrane, 10 €/m^2; future substitute current collectors, 10 €/m^2; reactor, 4000 €/m^3 reactor volume [18]; other costs, 1000 €/m^3 reactor volume. Lifetime assumptions: electrodes, membranes and current collectors, 5 yr; reactors and other materials, 25 yr.

Apart from electricity production, BESs can also offer other interesting opportunities for improving their economic feasibility. BESs present unequalled means to influence product outcome because they enable the decoupling of oxidation and reduction reactions. During the oxidation of organic materials in wastewater, electrochemically active microorganisms transfer electrons to the anode. These electrons, which contain most of the energy previously stored in the organic waste materials, subsequently flow to the cathode, where they can be used for the production of value added products. Hydrogen production in MECs is just the first example of this strategy, and it is expected that future innovations of BESs will proceed along this path. For example, the electrons generated at the anode might be used to reduce glycerol, a waste product from the biodiesel industry, into 1,3-propanediol, which is a valuable chemical, or to reduce acetate to ethanol for use as fuel (K.J.J. Steinbusch *et al.*, personal communication). The catalysis of these reactions could be achieved chemically, but in the authors' opinion, it is more likely that future innovations in the BES field will arise from the development of a completely new range of microbial biocathodes. The reactions occurring at these microbial biocathodes will be catalysed by enriched mixed populations of electrochemically active microorganisms or by carefully selected and/or genetically engineered pure cultures (such as *Sphingobacterium* [68] and *Geobacter* species [69]) that can either use cathodically produced hydrogen or electrons to perform the reducing reactions necessary for producing value added chemicals. The production of the valuable chemicals is expected to significantly contribute to offsetting the higher capital investments associated with BESs. Furthermore, the production of such value added chemicals will support the sustainable production of renewable materials, which is one of the most promising biotechnological approaches at the centre of current interests [70]. Hence, bioelectro-

Table 1. Comparison of estimated capital costs and product revenues among bioelectrochemical wastewater treatment, activated sludge treatment and anaerobic digestion

System	Product	Capital costs (€/kg COD)	Product revenue (€/kg COD)	Offset (product revenue minus capital costs) (€/kg COD)
AS	N/A	0.1[a]	−0.3[a,b]	−0.4
AD	CH_4	0.01[a]	0.1[a]	0.1
MFC	Electricity	8[c]/0.4[d]	0.2[e,f]	−0.2
MEC	H_2	8[c]/0.4[d]	0.6[e,g]	0.2

Abbreviations: AD, anaerobic digestion; AS, activated sludge; MEC, microbial electrolysis cell; MFC, microbial fuel cell.
[a]Data from [3,4] – assuming a reactor lifetime of 25 years.
[b]Electricity consumption and sludge disposal.
[c]Capital costs based on materials currently used in laboratory systems (Figure 4).
[d]Predicted future capital costs based on less expensive substitute materials (Figure 4).
[e]Assuming an electricity price of 0.1 €/kWh.
[f]Assuming an MFC voltage of 0.5 V.
[g]Assuming an electricity requirement of 1 kWh/m^3 H_2 and a hydrogen price of 0.5 €/Nm^3 H_2.

chemical wastewater treatment offers exciting future prospects.

Acknowledgements

J.K. and R.A.R. are supported by the Australian Research Council (DP 0666927). K.R. is supported by the Australian Research Council (DP0879245) and the University of Queensland (Postdoctoral Research Fellow scheme and Early Career Researcher scheme). J.K., K.R. and R.A.R. also thank the EPA Queensland (QSEIF) and Foster's Group. Part of this work was performed at Wetsus, Centre of Excellence for Sustainable Water Technology. Wetsus is funded by the city of Leeuwarden, the Province of Fryslân, the European Union European Regional Development Fund and by the EZ/KOMPAS program of the 'Samenwerkings-verband Noord-Nederland'.

References

1 Angenent, L.T. *et al.* (2004) Production of bioenergy and biochemicals from industrial and agricultural wastewater. *Trends Biotechnol.* 22, 477–485
2 Lettinga, G. *et al.* (1980) Use of the upflow sludge blanket (USB) reactor concept for biological wastewater-treatment, especially for anaerobic treatment. *Biotechnol. Bioeng.* 22, 699–734
3 Pham, T.H. *et al.* (2006) Microbial fuel cells in relation to conventional anaerobic digestion technology. *Eng. Life Sci.* 6, 285–292
4 Aiyuk, S. *et al.* (2006) Anaerobic and complementary treatment of domestic sewage in regions with hot climates – a review. *Bioresour. Technol.* 97, 2225–2241
5 Rabaey, K. *et al.* (2007) Microbial ecology meets electrochemistry: electricity-driven and driving communities. *ISME J.* 1, 9–18
6 Lovley, D.R. (2006) Bug juice: harvesting electricity with microorganisms. *Nat. Rev. Microbiol.* 4, 497–508
7 Logan, B.E. and Regan, J.M. (2006) Electricity-producing bacterial communities in microbial fuel cells. *Trends Microbiol.* 14, 512–518
8 Stams, A.J.M. *et al.* (2006) Exocellular electron transfer in anaerobic microbial communities. *Environ. Microbiol.* 8, 371–382
9 Gorby, Y.A. *et al.* (2006) Electrically conductive bacterial nanowires produced by *Shewanella oneidensis* strain MR-1 and other microorganisms. *Proc. Natl. Acad. Sci. U. S. A.* 103, 11358–11363
10 Reguera, G. *et al.* (2005) Extracellular electron transfer via microbial nanowires. *Nature* 435, 1098–1101
11 Newman, D.K. and Kolter, R. (2000) A role for excreted quinones in extracellular electron transfer. *Nature* 405, 94–97
12 Rabaey, K. *et al.* (2005) Microbial phenazine production enhances electron transfer in biofuel cells. *Environ. Sci. Technol.* 39, 3401–3408
13 Cohen, B. (1931) The bacterial culture as an electrical half-cell. *J. Bacteriol.* 21, 18–19
14 Potter, M.C. (1911) Electrical effects accompanying the decomposition of organic compounds. *Proc. Biol. Sci.* 84, 260–276
15 Kim, B.H. *et al.* (1999) Direct electrode reaction of Fe(III)-reducing bacterium, *Shewanella putrefaciens*. *J. Microbiol. Biotechnol.* 9, 127–131
16 Heijnen, J.J. (1999) Bioenergetics of microbial growth. In *Encyclopedia of Bioprocess Technology: Fermentation, Biocatalysis, and Bioseparation* (Flickinger, M.C. and Drew, S.D., eds), pp. 267–291, John Wiley & Sons
17 Logan, B.E. *et al.* (2006) Microbial fuel cells: methodology and technology. *Environ. Sci. Technol.* 40, 5181–5192
18 Rabaey, K. and Verstraete, W. (2005) Microbial fuel cells: novel biotechnology for energy generation. *Trends Biotechnol.* 23, 291–298
19 Call, D. and Logan, B.E. (2008) Hydrogen production in a single chamber microbial electrolysis cell lacking a membrane. *Environ. Sci. Technol.* 42, 3401–3406
20 Cheng, S. and Logan, B.E. (2007) Sustainable and efficient biohydrogen production via electrohydrogenesis. *Proc. Natl. Acad. Sci. U. S. A.* 104, 18871–18873
21 Ditzig, J. *et al.* (2007) Production of hydrogen from domestic wastewater using a bioelectrochemically assisted microbial reactor (BEAMR). *Int. J. Hydrogen Energy* 32, 2296–2304
22 Liu, H. *et al.* (2005) Electrochemically assisted microbial production of hydrogen from acetate. *Environ. Sci. Technol.* 39, 4317–4320
23 Rozendal, R.A. *et al.* (2006) Principle and perspectives of hydrogen production through biocatalyzed electrolysis. *Int. J. Hydrogen Energy* 31, 1632–1640
24 Rozendal, R.A. *et al.* (2007) Performance of single chamber biocatalyzed electrolysis with different types of ion exchange membranes. *Water Res.* 41, 1984–1994
25 Rozendal, R.A. *et al.* (2008) Hydrogen production with a microbial biocathode. *Environ. Sci. Technol.* 42, 629–634
26 Rozendal, R.A. *et al.* (2008) Effect of the type of ion exchange membrane on performance, ion transport, and pH in biocatalyzed electrolysis of wastewater. *Water Sci. Technol.* 57, 1757–1762
27 Fan, Y.Z. *et al.* (2007) Enhanced Coulombic efficiency and power density of air-cathode microbial fuel cells with an improved cell configuration. *J. Power Sources* 171, 348–354
28 Torres, C.I. *et al.* (2007) Kinetics of consumption of fermentation products by anode-respiring bacteria. *Appl. Microbiol. Biotechnol.* 77, 689–697
29 Liu, H. and Logan, B.E. (2004) Electricity generation using an air-cathode single chamber microbial fuel cell in the presence and absence of a proton exchange membrane. *Environ. Sci. Technol.* 38, 4040–4046
30 Aelterman, P. *et al.* (2006) Continuous electricity generation at high voltages and currents using stacked microbial fuel cells. *Environ. Sci. Technol.* 40, 3388–3394
31 Rozendal, R.A. *et al.* (2006) Effects of membrane cation transport on pH and microbial fuel cell performance. *Environ. Sci. Technol.* 40, 5206–5211
32 Logan, B. *et al.* (2007) Graphite fiber brush anodes for increased power production in air-cathode microbial fuel cells. *Environ. Sci. Technol.* 41, 3341–3346
33 Rabaey, K. *et al.* (2005) Tubular microbial fuel cells for efficient electricity generation. *Environ. Sci. Technol.* 39, 8077–8082
34 Liu, H. *et al.* (2008) Scale-up of membrane-free single-chamber microbial fuel cells. *J. Power Sources* 179, 274–279
35 Ren, Z. *et al.* (2007) Electricity production from cellulose in a microbial fuel cell using a defined binary culture. *Environ. Sci. Technol.* 41, 4781–4786
36 Rismani-Yazdi, H. *et al.* (2007) Electricity generation from cellulose by rumen microorganisms in microbial fuel cells. *Biotechnol. Bioeng.* 97, 1398–1407
37 Kim, G.T. *et al.* (2006) Bacterial community structure, compartmentalization and activity in a microbial fuel cell. *J. Appl. Microbiol.* 101, 698–710
38 Pham, T.H. *et al.* (2008) Metabolites produced by *Pseudomonas* sp enable a Gram-positive bacterium to achieve extracellular electron transfer. *Appl. Microbiol. Biotechnol.* 77, 1119–1129
39 Freguia, S. *et al.* (2007) Electron and carbon balances in microbial fuel cells reveal temporary bacterial storage behavior during electricity generation. *Environ. Sci. Technol.* 41, 2915–2921
40 Lee, H.S. *et al.* (2008) Evaluation of energy-conversion efficiencies in microbial fuel cells (MFCs) utilizing fermentable and non-fermentable substrates. *Water Res.* 42, 1501–1510
41 Clauwaert, P. *et al.* (2008) Combining biocatalyzed electrolysis with anaerobic digestion. *Water Sci. Technol.* 57, 575–579
42 Torres, C.I. *et al.* (2008) Proton transport inside the biofilm limits electrical current generation by anode-respiring bacteria. *Biotechnol. Bioeng.* DOI: 10.1002/bit.21821 (http://www3.interscience.wiley.com/journal/117933915/grouphome/home.html)
43 Tchobanoglous, G. *et al.* (2003) *Wastewater Engineering: Treatment and Reuse* (4th edn), McGraw-Hill, Metcalf & Eddy
44 Cheng, S. *et al.* (2006) Increased power generation in a continuous flow MFC with advective flow through the porous anode and reduced electrode spacing. *Environ. Sci. Technol.* 40, 2426–2432
45 Fan, Y. *et al.* (2007) Sustainable power generation in microbial fuel cells using bicarbonate buffer and proton transfer mechanisms. *Environ. Sci. Technol.* 41, 8154–8158
46 Zhao, F. *et al.* (2006) Challenges and constraints of using oxygen cathodes in microbial fuel cells. *Environ. Sci. Technol.* 40, 5193–5199
47 Hoogers, G., ed. (2003) *Fuel Cell Technology Handbook*, CRC Press
48 Larminie, J. and Dicks, A. (2000) *Fuel Cell Systems Explained,* John Wiley & Sons
49 Freguia, S. *et al.* (2007) Non-catalyzed cathodic oxygen reduction at graphite granules in microbial fuel cells. *Electrochim. Acta* 53, 598–603

50 Cheng, S. *et al.* (2006) Power densities using different cathode catalysts (Pt and CoTMPP) and polymer binders (Nafion and PTFE) in single chamber microbial fuel cells. *Environ. Sci. Technol.* 40, 364–369
51 Zhao, F. *et al.* (2005) Application of pyrolysed iron(II) phthalocyanine and CoTMPP based oxygen reduction catalysts as cathode materials in microbial fuel cells. *Electrochem. Commun.* 7, 1405–1410
52 Yu, E.H. *et al.* (2007) Microbial fuel cell performance with non-Pt cathode catalysts. *J. Power Sources* 171, 275–281
53 Clauwaert, P. *et al.* (2007) Open air biocathode enables effective electricity generation with microbial fuel cells. *Environ. Sci. Technol.* 41, 7564–7569
54 Freguia, S. *et al.* (2008) Sequential anode-cathode configuration improves cathodic oxygen reduction and effluent quality of microbial fuel cells. *Water Res.* 42, 1387–1396
55 Bergel, A. *et al.* (2005) Catalysis of oxygen reduction in PEM fuel cell by seawater biofilm. *Electrochem. Commun.* 7, 900–904
56 Ter Heijne, A. *et al.* (2006) A bipolar membrane combined with ferric iron reduction as an efficient cathode system in microbial fuel cells. *Environ. Sci. Technol.* 40, 5200–5205
57 Liu, H. *et al.* (2005) Power generation in fed-batch microbial fuel cells as a function of ionic strength, temperature, and reactor configuration. *Environ. Sci. Technol.* 39, 5488–5493
58 Taylor, B. and Gardner, T. (2007) Southeast Queensland recycled water aspects and soil impacts, In *Proceedings of the AWA Queensland 2007 Regional Conference: 9–11 November; Sunshine Coast, Australia*, Australian Water Association
59 Lide, R.L., ed. (2004) *CRC Handbook of Chemistry and Physics* (85th edn), CRC Press
60 Kim, H.J. *et al.* (2002) A mediator-less microbial fuel cell using a metal reducing bacterium, *Shewanella putrefaciens*. *Enzyme Microb. Technol.* 30, 145–152
61 Shin, S.H. *et al.* (2006) Development of bipolar plate stack type microbial fuel cells. *Bull. Korean Chem. Soc.* 27, 281–285
62 Oh, S.E. and Logan, B.E. (2007) Voltage reversal during microbial fuel cell stack operation. *J. Power Sources* 167, 11–17
63 Gil, G.C. *et al.* (2003) Operational parameters affecting the performance of a mediator-less microbial fuel cell. *Biosens. Bioelectron.* 18, 327–334
64 Harnisch, F. *et al.* (2008) The suitability of monopolar and bipolar ion exchange membranes as separators for biological fuel cells. *Environ. Sci. Technol.* 42, 1740–1746
65 Kim, J.R. *et al.* (2007) Power generation using different cation, anion, and ultrafiltration membranes in microbial fuel cells. *Environ. Sci. Technol.* 41, 1004–1009
66 Virdis, B. *et al.* (2008) Microbial fuel cells for simultaneous carbon and nitrogen removal. *Water Res.* DOI: 10.1016/j.watres.2008.03.017 (http://www.sciencedirect.com/science/journal/00431354)
67 Clauwaert, P. *et al.* (2007) Biological denitrification in microbial fuel cells. *Environ. Sci. Technol.* 41, 3354–3360
68 Rabaey, K. *et al.* (2008) Cathodic oxygen reduction catalyzed by bacteria in microbial fuel cells. *ISME J.* 2, 519–527
69 Gregory, K.B. *et al.* (2004) Graphite electrodes as electron donors for anaerobic respiration. *Environ. Microbiol.* 6, 596–604
70 Kamm, B. and Kamm, M. (2004) Principles of biorefineries. *Appl. Microbiol. Biotechnol.* 64, 137–145

Journal of Applied Electrochemistry (2005) 35:123–130
DOI 10.1007/s10800-004-2399-0

Electrochemical studies of the interaction between a modified activated carbon surface and heavy metal ions

M. WALCZYK[1], A. ŚWIĄTKOWSKI[2], M. PAKUŁA[3] and S BINIAK[1]*
[1]*Faculty of Chemistry, N. Copernicus University, ul. Gagarina 7, 87-100 Toruń, Poland*
[2]*Military Technical Academy, Institute of Chemistry, ul. Kaliska 2, 00-908 Warsaw, Poland*
[3]*Naval University of Gdynia, 81-103 Gdynia, Poland*
*(*author for correspondence, e-mail: sbiniak@chem.uni.torun.pl)*

Received 23 October 2003; accepted in revised form 27 July 2004

Key words: activated carbon, electrochemical properties, heavy metal cations, X-ray photoelectron spectroscopy

Abstract

Cyclic voltammetric studies of the influence of surface chemistry on the electrochemical behaviour of powdered activated carbon electrodes (PACE) in the presence of selected heavy metal ions (Pb^{2+}, Hg^{2+}, Cd^{2+}) in bulk solution and pre-adsorbed on carbon were carried out. The variety of surfaces was achieved via the modification of carbon samples by heat treatment under vacuum and in an oxygen/ammonia atmosphere, as well as oxidation with conc. nitric acid. The chemical structures of the modified carbon surfaces were characterised by XPS and standard pH-titration. The adsorption capacities of the modified carbon samples towards the heavy metal ions in question were estimated. The mechanisms of adsorption processes of metal species on carbon surfaces were analysed and described on the basis of their electrochemical behaviour. The nature of the interactions between the modified carbon surfaces and adsorbed cations is discussed.

1. Introduction

Although heavy metals are considered harmful to the environment, their concentrations in surface water have increased considerably in recent times. As they are among the most toxic of water pollutants, investigations concerning their removal or at least their minimisation are of considerable importance. A variety of techniques are now being applied in the treatment of surface water or waste water to reduced the levels of these pollutants to a minimum. Activated carbon has been an effective adsorbent for the removal of inorganic metal ions because of their highly developed surface area and microporosity, high chemical, thermal and ionising radiation stability, and their distinctive sorptive behaviour in solutions of electrolytes [1–3]. Although the selectivity and sorptive capacity of commercial carbon adsorbents towards metal ions is rather low, these parameters can be altered by the introduction of functional groups through surface modification [4–12]. The following phenomena may occur on a carbon surface during adsorption: (i) active proton/cation exchange, (ii) surface complex formation of metal ions, (iii) spontaneous reduction of metals with low standard redox potentials (charge-transfer processes), (iv) interaction of metal cations with the π electrons of the carbon network. Thus, modification of the activated carbon surface can affect adsorption mechanisms and the ways in which surface and sorbed cation interact.

In the present investigations, we studied the influence of surface oxygen and/or nitrogen groups on the adsorption of Pb^{2+}, Hg^{2+}, Cd^{2+} ions from aqueous solution on modified activated carbon. We further attempted to ascertain the real nature of the adsorbed ionic species – modified carbon surface interactions using X-ray photoelectron spectroscopy and cyclic voltammetric measurements.

2. Experimental

2.1. *Materials*

A commercial active carbon ROW 0.8 Supra (Norit, The Netherlands) was washed (demineralised) with concentrated HF and HCl acids (ash content 0.2 wt. %) and subsequently modified by:

(i) heating at 1173 K under vacuum (HTV),
(ii) heating in a stream of 1:1 oxygen–ammonia at 673 K (OPA),
(iii) oxidation with concentrated nitric acid at 355 K (ONA).

The physicochemical properties of the carbon samples obtained in these ways have been described elsewhere [13, 14].

2.2. *Surface chemistry*

2.2.1. *XPS measurements*

The XPS method was used to characterise the chemical properties of the modified carbon surface. XP spectra were obtained with an EscaLab 210 (V.G. Scientific Ltd.) photoelectron spectrometer using non-monochromatised Al K_α radiation (1486.6 eV), the source being operated at 15 kV and 34 mA. Prior to XPS measurement the powdered carbon samples were dried for 2 h at 100 °C (373 K). The vacuum in the analysis chamber was always better than 5×10^{-10} Pa. The high-resolution scans were performed over the 280–294, 395–407 and 527–540 eV ranges (C 1s , N 1s and O 1s spectra, respectively). In order to obtain an acceptable signal-to-noise ratio the spectral region was scanned 20 times. After subtraction of the base line (Shirley-type), curve fitting was performed using the non-linear least-squares algorithm and assuming a mixed Gaussian/Lorenzian peak shape of variable proportion (mainly 0.3). This peak-fitting was repeated until an acceptable fit was obtained (error – 5%). The positions of the deconvoluted peaks (binding energy – BE) were determined from both literature data [15–17] and empirically derived values.

2.2.2. *pH-metric titration*

The pH-metric titrations were carried out using the point-by-point method [18, 19]. Known portions of each carbon were added to the mixtures containing various quantities of NaCl, NaOH and HCl (pH = 1–13).The ionic strength was kept constant ($I = 0.1$).

2.3. *Adsorption studies*

The active carbon samples (ca. 0.2 g) were immersed in the metal (Pb, Hg, Cd) nitrate solution (10 cm^3) of concentration 0.01 M and pH = 1.33 adjusted by the addition of 0.1 M HNO_3. Each mixture was shaken in a dark bottle for 48 h, after which the cation concentration and the pH of the solutions were determined. The metal ion concentrations were determined as follows: Pb^{2+} by colorimetric analysis using PAR as complexing agent [20], Hg^{2+} by spectrophotometry according to the procedure described in the literature [21], and Cd^{2+} by atomic absorption spectroscopy (Philips PU9100 AAS).

2.4. *Cyclic voltammetry*

Electrochemical studies of all the activated carbon samples, both before and after metal cation adsorption, were performed as previously described [7, 10, 22]. Cyclic voltammetry measurements were carried out in blank electrolyte solutions (0.1 M $NaNO_3$ + 0.1 M HNO_3 (pH = 1.33)) using the powdered active carbon electrode (PACE) technique [10, 22]. After prior vacuum desorption (10^{-2} Pa), the powdered carbon (grain size 0.075–0.063 mm, mass 50 mg) was placed in an electrode container and drenched with a de-aerated solution to obtain a ~3 mm sedimentation layer. First, the potentiometric responses of the carbon electrodes were measured in an oxygen-free atmosphere once their values had stabilised (usually after 24 h). Next, cyclic voltammetry (CV) was performed using the typical three-electrode system and an Autolab (Eco Chemie) modular electrochemical system equipped with a PGSTAT 10 potentiostat, driven by GEPS3 software (Eco Chemie). All potentials were measured, and are reported against a potassium chloride saturated calomel electrode (SCE). A platinum gauze served as counter electrode. The cyclisations were started from zero to positive potentials and were carried out in potential ranges precluding the electrolysis of water. The cyclic voltammograms were recorded after curve shapes had stabilised. Although the electrode design ensures that the shape of the CV curves recorded is reproducible, the specific capacitance cannot now be estimated because the potential and current distribution in the electrode bed are unknown [23].

The electrochemical behaviour of prepared PACEs was compared with that of solid glassy carbon GC (3 mm disc diameter) and graphite RG (Radelkis, OP-C-711-C, 6 mm disc diameter) commercial electrodes [7, 10].

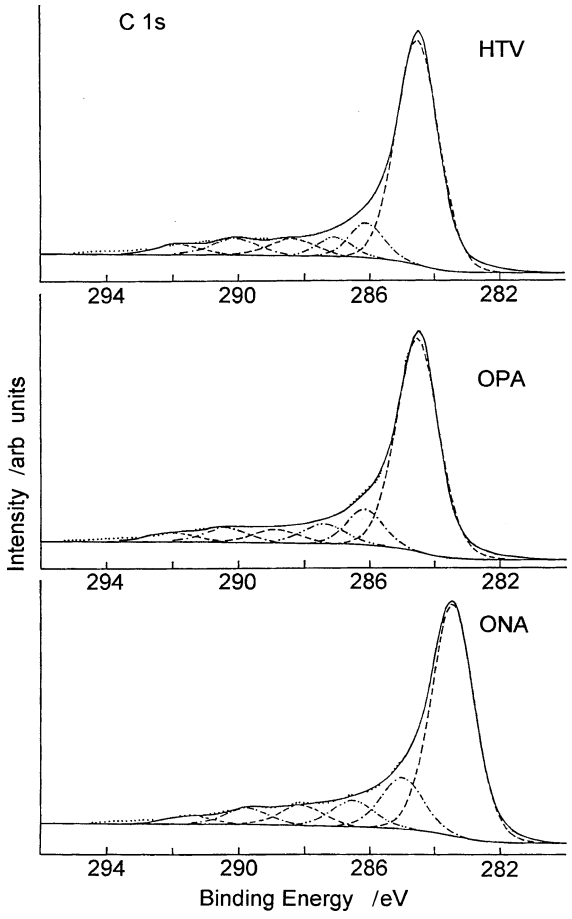

Fig. 1. High resolution XP spectra of C 1s for modified carbon samples.

3. Results and discussion

The surface properties of the activated carbon samples have in part already been described [13, 14]. The chemical structure of surface layer of the materials is highly diverse. Annealing under vacuum (HTV) gives basic properties on the carbon surface while the oxidised carbon sample (ONA) has acidic groups at different acidic strength. Amino-oxidative treatment (OPA) produces amphoteric characteristic with a slight excess of basic properties. The specific surface areas of the modified carbon samples obtained from nitrogen adsorption (at 77 K) were calculated by the BET method to be 1003, 1024 and 970 $m^2 g^{-1}$ for HTV, OPA and ONA, respectively. To facilitate the discussion of the later electrochemical studies performed in this work, the surface chemistry of the carbon samples was characterised by XPS and pH-metric titration.

The high-resolution XP spectra for the C 1s, N 1s and O 1s regions are presented in Figures 1–3, respectively: several peaks are present for each element. Deconvolution of the C 1s spectra (Figure 1) yields several peaks with different binding energies (BE), which probably represent: (i) graphitic carbon (284.5 eV), (ii) carbon atoms in phenolic, alcohol or ether groups (286.1 eV), (iii) carbonyl or quinone groups (287.4 eV), (iv) nitrogen-containing and/or ester groups (288.7 eV), (v) carboxylic acidic groups (289.3 eV), and (vi) carbon present in acid anhydride, carbonate groups and/or adsorbed carbon oxides (290.4 eV). These assignments agree very well with the extensive XPS studies done on the commercially available carbons used as catalyst supports [25–28]. Heat treatment under vacuum (HTV) or in an oxygen/ammonia atmosphere (OPA) enhanced the amount of total surface carbon and the relative concentration of graphitic carbon; oxidation with nitric acid (ONA) reduced these quantities.

Following the modification procedures used here, the N 1s peak shape undergoes considerable change (Figure 2). Four types of nitrogen can be distinguished in the modified material according to the schematic representation put forward by Kapteijn et al. [29]: N-6 (pyridinic), N-5 (pyrrolic and pyridonic), N–Q (nitrogen substitutes in aromatic graphene structures – quaternary nitrogen) and N-X (nitrogen oxides, pyridine-*N*-oxides) with binding energies of 398.6, 400.2, 401.3 and 404.5 eV, respectively. Heat treatment under vacuum retains a small amount of surface nitrogen (0.3%)

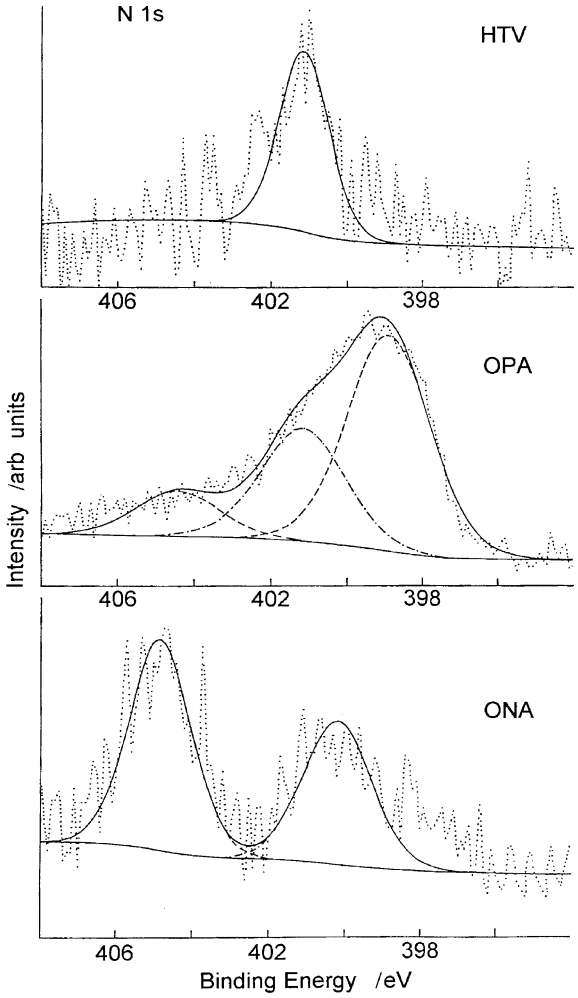

Fig. 2. High resolution XP spectra of N 1s for modified carbon samples.

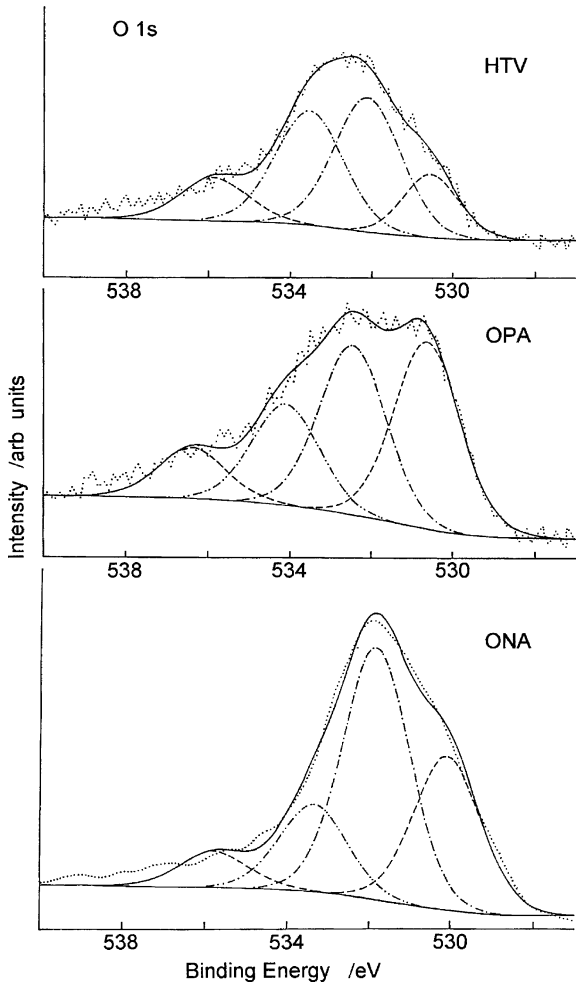

Fig. 3. High resolution XP spectra of O 1s for modified carbon samples.

Table 1. Physicochemical characteristic of modified carbon samples

Sample	S_{BET}/m g^{-1}	O/N (at.%/at.%)		pH[a]	H_3O^+ ads. /mM g^{-1}	OH^- ads. /mM g^{-1}	E_s[b]/mV	c_0[c] /mC g^{-1}
		Elemental	XPS					
HTV	1003	0.30/0.26	2.5/0.2	10.8	0.568	0.163	+380	74
OPA	1024	1.51/1.81	2.5/2.1	8.9	0.495	0.296	+298	68
ONA	970	3.87/0.62	7.0/0.7	4.5	0.348	1.125	+512	102

[a] pH of carbon slurry (1 g AC in 100 cm^{-3} of 0.1 M $NaNO_3^-$).
[b] For pH = 1.33.
[c] c_0 – cathodic peak capacity (see Figure 5).

bound as quaternary nitrogen (N–Q). After modification in an oxygen/ammonia atmosphere, the total nitrogen surface concentration increases to 2.1%. This is probably due to the partial replacement of surface oxygen atoms by nitrogen-containing species. After oxidative modification a new type of bonded nitrogen (like nitric oxides) appears.

The O 1s spectra (Figure 3) for the carbon samples display several peaks whose binding energies depend on the modification procedure. Three main peaks corresponding to C═O (530.6 eV), C—O (532.3 eV) and adsorbed water (536.3 eV) are present for all the samples studied. The other two peaks with binding energies 533.5 and 534.3 eV can be ascribed to C—O—C and C═N—O structures, respectively, in different surface oxygen-as well as oxygen- and nitrogen-containing functional groups [17]. The higher concentration of surface carbonyl groups on oxygen/ammonia treated carbons suggests their higher ability to chemisorb dioxygen with the formation of a superoxide species (in the first stage) and then carbonyl moieties (surface autocatalytic oxidation) [27].

The surface elemental composition was estimated on the basis of the XPS data. The surface oxygen and nitrogen atomic percentages are set out in Table 1.

The results of pH titration for the modified carbon samples are shown in Figure 4. Basic properties are dominant for HTV samples up to pH 11.5, for the OPA sample up to about pH 10. This stands in contrast to the acid–base behaviour of the nitric-acid-oxidised sample (ONA), which exhibits acidic properties above pH 3. These values are similar to the results obtained by mass titration (10.87, 7.36, 3.48) and the pH of a carbon slurry in 0.1 M $NaNO_3$ (10.8, 8.9, 4.5), respectively. Titration of the samples with 0.1 M hydrochloric acid and sodium hydroxide solutions yielded the capacities listed in Table 1.

The electrochemical behaviour of electrodes prepared from the tested carbons was investigated at potential ranges from −0.8 to +1.8 V (vs SCE) and for sweep

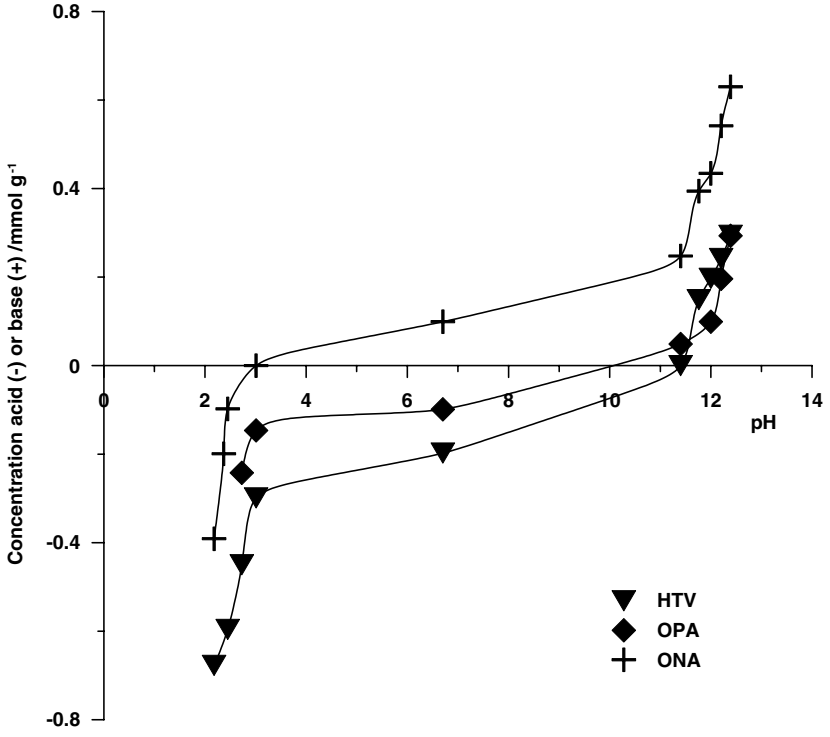

Fig. 4. pH-metric titration curves for modified carbon samples.

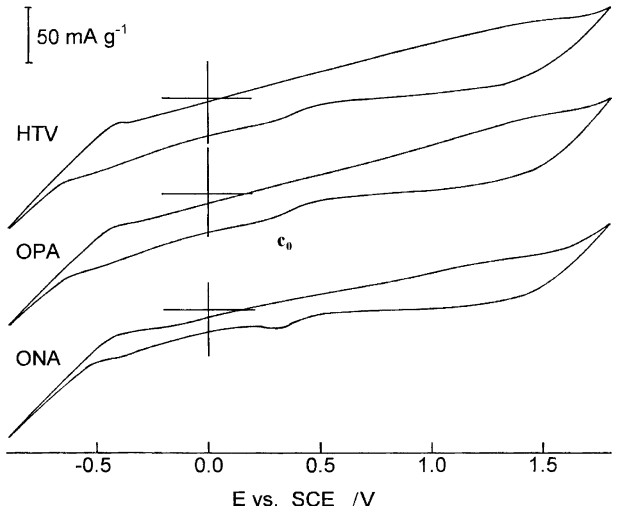

Fig. 5. Cyclic voltammograms for the PACEs prepared from tested carbons recorded in blank electrolyte solution (pH = 1.33, $v = 3 \times 10^{-3}$ V s^{-1}).

rates from 0.1 to 0.001 V s^{-1}. In acidic blank solutions (pH = 1.33) the presence of a cathodic peak (or wave) (c_o) was recorded for all samples (Figure 5). The shape

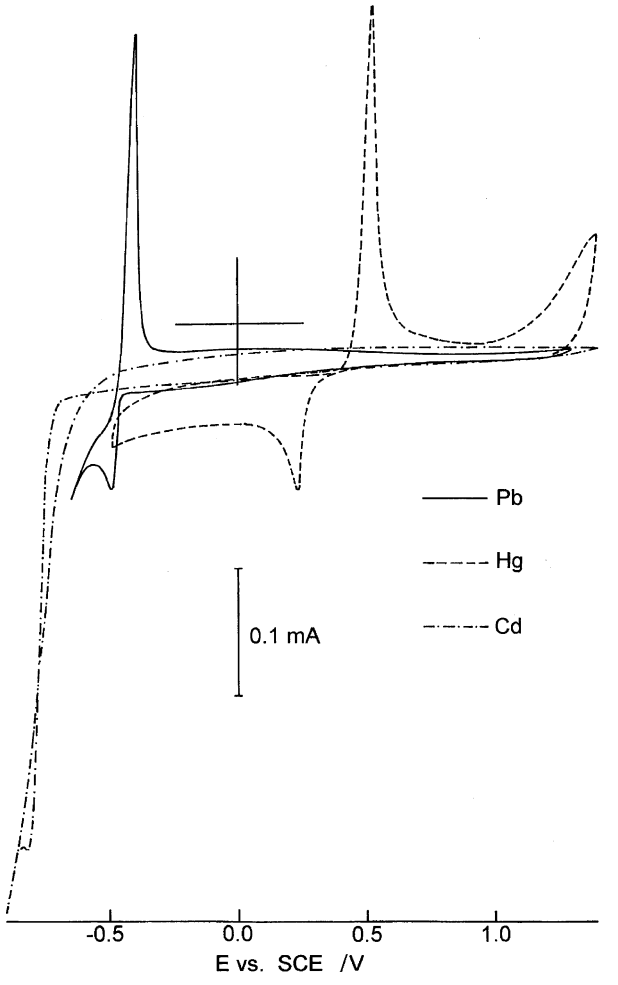

Fig. 6. Cyclic voltammograms for the glassy carbon electrode recorded in blank electrolyte solution containing 0.01 M metal (Pb, Hg, Cd) nitrate, (pH = 1.33, $v = 3 \times 10^{-3}$ V s^{-1}).

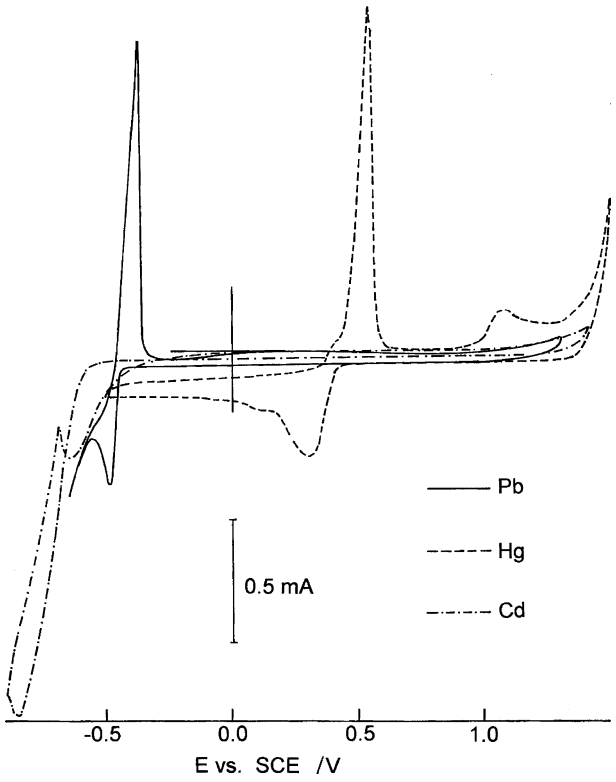

Fig. 7. Cyclic voltammograms for the graphite electrode recorded in blank electrolyte solution containing 0.01 M metal (Pb, Hg, Cd), nitrate (pH = 1.33, $v = 3 \times 10^{-3}$ V s^{-1}).

of the cyclic voltammograms (CVs) obtained may be indicative of the reduction of electrochemically active surface groups that were oxidised in the 1.2–1.3 V potential range. The charge transferred during reduction processes depends on the carbon modification procedure and is the highest for the ONA sample (Table 1).

The electrochemical properties of the oxidised/reduced forms of the couples to be tested were characterised using commercial glassy carbon (GC) and graphite (RG) electrodes. The cyclic voltammograms obtained in acidic blank solutions (pH = 1.33) containing the cations to be tested are presented in Figures 6 and 7. Both these CVs are similar and approach the literature data [30–33]. A two-electron cathodic reduction and anodic response according to the scheme: $Me^{2+} + 2e \Leftrightarrow Me^0$ may explain the peaks on the CV curves.

Next, the electrochemical behaviour of the couples to be tested was investigated using the powdered activated carbon electrode technique. The potential responses for the respective systems are given in Table 2.

The electrochemical behaviour of PACE–lead ion systems is illustrated in Figure 8. This shows cyclic voltammograms recorded in acidic electrolyte solution containing Pb^{2+} ions for modified activated carbon with pre-adsorbed lead. Generally, besides the c_0 of the cathodic peak, the presence of a second cathodic peak (c_1) and a broad anodic peak (a_1) is observed for all samples. For ONA carbon a distinctly shaped second anodic peak (a_2) is present. The following reactions may explain the observed cathodic peaks and waves [34–36]:

Table 2. Adsorption capacity, response potential and peaks potentials (for adsorbed cations) of modified carbon samples

Carbon sample	Lead				Mercury					Cadmium			
	A^a /mM g^{-1}	E_s^b /mV	$E_{p,c1}$ /mV	$E_{p,a2}$ /mV	A^a /mM g^{-1}	E_s^b /mV	$E_{p,c1}$ /mV	$E_{p,a2}$ /mV	$E_{p,a1}$ /mV	A^a /mM g^{-1}	E_s^b /mV	$E_{p,c1}$ /mV	$E_{p,a2}$ /mV
GC	–	–	−535	−390	–	–	+230	+530	–	–	–	−830	–
RG	–	–	−490	−380	–	–	+300	+550	+1100	–	–	−850	−690
HTV	0.053	+466	+980	–	0.155	+593	−300	+1300	+1550	0.010	+375	−660	−70
OPA	0.084	+486	+990	–	0.162	+605	+50	+1150	+1600	0.010	+486	−540	−70
ONA	0.071	+619	+930	−460	0.158	+618	–	+750	+1200	0.014	+505	−580	−100

[a] From 0.01 M. $Me(NO_3)_2$ (Me = Pb^{2+}, Hg^{2+}, Cd^{2+}) + 0.1 M HNO_3, pH = 1.33.
[b] In 0.01 M $Me(NO_3)_2$ + 0.1 M HNO_3 + 0.1 M $NaNO_3$, pH = 1.33.

$$(c_0) \quad >C{=}O + H^+ + e = >C{-}OH \qquad (E_{p,c_0} \cong +250\ \text{mV}) \quad (1)$$

$$(c_1) \quad Pb^{4+} + 2e = Pb^{2+} \qquad (E_{p,c_1} \cong +950\ \text{mV}) \quad (2)$$

The broad anodic peak (a_1) for HTV and OPA can be explained by the following processes:

$$Pb^{2+} - 2e = Pb^{4+} \quad (3)$$

$$O_2 - 2e = O_2^{2-} \qquad (E_{p,a_1} \cong +1600\ \text{mV}) \quad (4)$$

$$Pb^{2+} + O_2^{2-} + 4H^+ = Pb^{4+} + 2H_2O \quad (5)$$

and that for ONA carbon by the reaction:

$$Pb^{2+} - 2e = Pb^{4+} \quad (6)$$

$$>C{-}OH - e => C{=}O + H^+ \qquad (E_{p,a_1} \cong +1000\,\text{mV}) \quad (7)$$

$$2 > C{=}O + Pb^{2+} + 2H^+ = Pb^{4+} + 2 > C{-}OH \quad (8)$$

Figure 8 also shows that for the potential range used here (<−500 mV) a Pb^{2+} reduction wave is observed only for ONA carbon. The anodic response yields peak a_2 with a potential of −460 mV.

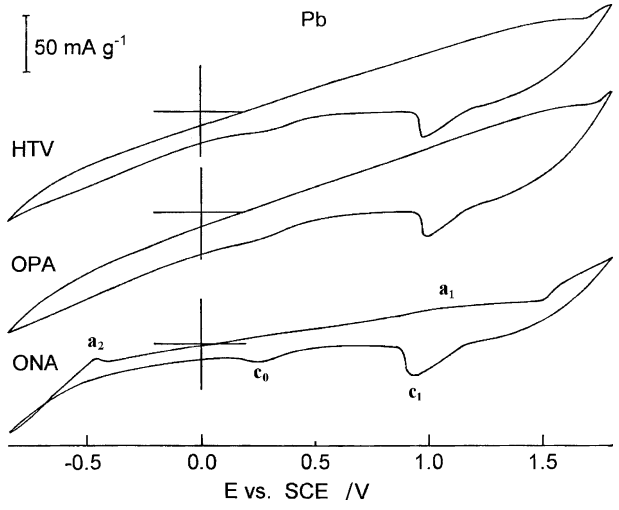

Fig. 8. Cyclic voltammograms for PACEs prepared from tested carbons with pre-adsorbed lead recorded in blank electrolyte solution containing 0.01 M lead nitrate (pH = 1.33, $v = 3 \times 10^{-3}$ V s^{-1}).

The electrochemical behaviour of PACE – mercury ion systems is shown in Figure 9: cyclic voltammograms recorded in acidic electrolyte solution containing Hg^{2+} ions for modified activated carbon with pre-adsorbed cations. Generally, besides the c_0 cathodic peak, a second cathodic peak/wave (c_1) and a broad, double anodic peak (a_1,a_2) is observed for all samples. The following reactions may explain the observed cathodic peaks and waves [31, 37, 38]:

$$(c_0) \quad >C{=}O + H^{++}e => C{-}OH \qquad (E_{p,c_0} \cong +250\text{mV}) \quad (9)$$

$$(c_1) \quad Hg^{2+} + 2e = Hg^0 \quad \text{(see Table 2)} \quad (10)$$

$$(a_2) \quad Hg^0 - e = Hg^+ \quad \text{(see Table 2)} \quad (11)$$

$$(a_1) \quad Hg^+ - e = Hg^{2+} \quad \text{(see Table 2)} \quad (12)$$

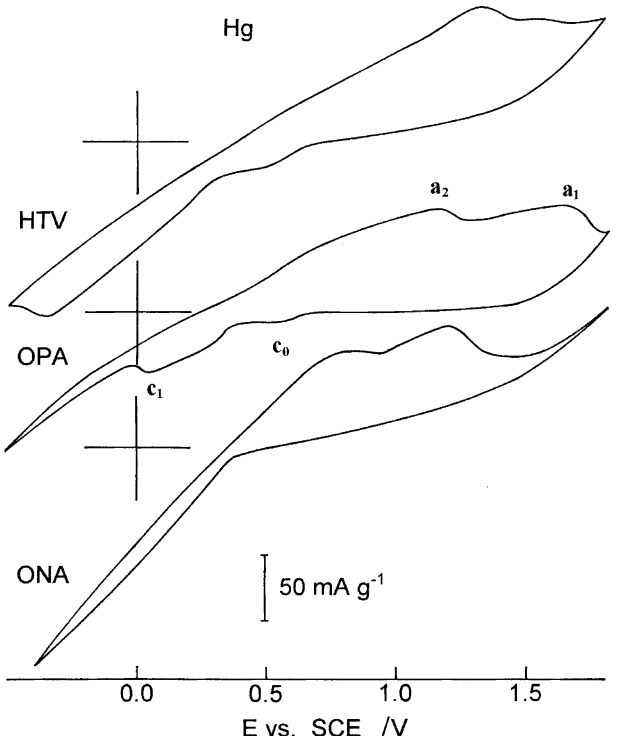

Fig. 9. Cyclic voltammograms for PACEs prepared from tested carbons with pre-adsorbed mercury recorded in blank electrolyte solution containing 0.01 M mercury nitrate (pH = 1.33, $v = 3 \times 10^{-3}$ V s^{-1}).

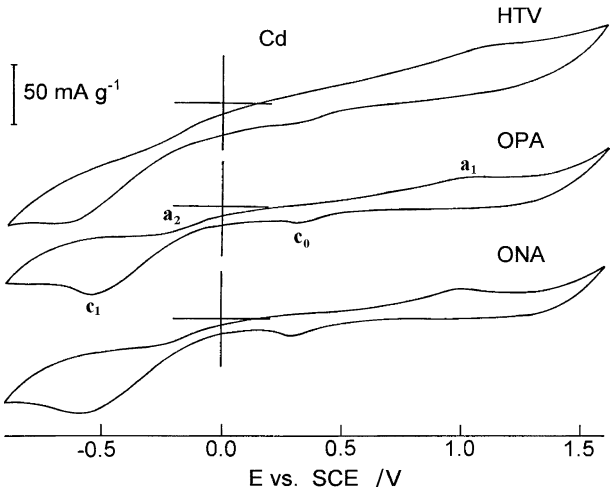

Fig. 10. Cyclic voltammograms for PACEs prepared from tested carbons with pre-adsorbed cadmium recorded in blank electrolyte solution containing 0.01 M. cadmium nitrate, (pH=1.33, $v=3\times10^{-3}$ V s^{-1}).

Anodic oxidative processes may be accompanied by the following reactions:

$$2Hg^{+} = Hg^{2+} + Hg^{0} \quad (13)$$

$$> C{=}O + Hg^{+} + H^{+} = Hg^{2+} + > C{-}OH \quad (14)$$

$$Hg^{+} + 4H^{+} = Hg^{2+} + 2H_2O \quad (15)$$

Figure 10 illustrates the electrochemical behaviour of PACE–cadmium ion systems: cyclic voltammograms recorded in acidic electrolyte solution containing Cd^{2+} ions for modified activated carbon with pre-adsorbed cadmium. In general, apart from a c_0 cathodic peak, a second cathodic peak (c_1) and a broad anodic peak (a_1) are present for all samples. Additionally, there is an anodic wave (a_2) in the potential range from −100 to −70 mV. The following reactions may explain the observed cathodic peaks and waves [32, 33]:

$$(c_0) \quad > C{=}O + H^{+} + e => C{-}OH \quad (E_{p,c_0} \cong +250\,\text{mV}) \quad (16)$$

$$(c_1) \quad Cd^{2+} + 2e = Cd^{0} \quad (E_{p,c_1} \cong -600\,\text{mV}) \quad (17)$$

$$(a_1) \quad > C{-}OH - e => C{=}O + H^{+} \quad (E_{p,a_1} \cong +1000\,\text{mV}) \quad (18)$$

$$(a_2) \quad Cd^{0} - 2e = Cd^{2+} \quad (E_{p,c_1} \cong -80\,\text{mV}) \quad (19)$$

The surface modification procedures applied to the carbons tested alter its surface area only slightly (see Table 1). The nearly 10% differences in apparent surface area (S_{BET}) could not explain the marked differences in adsorption capacity towards cations (Table 2). The contact of active carbon materials with an aqueous solution containing the tested cations may lead to the adsorption of cations and metal-containing species (i.e. $MeOH^{+}$), partial reduction of adsorbed cations and the formation of an imperfect metallic layer

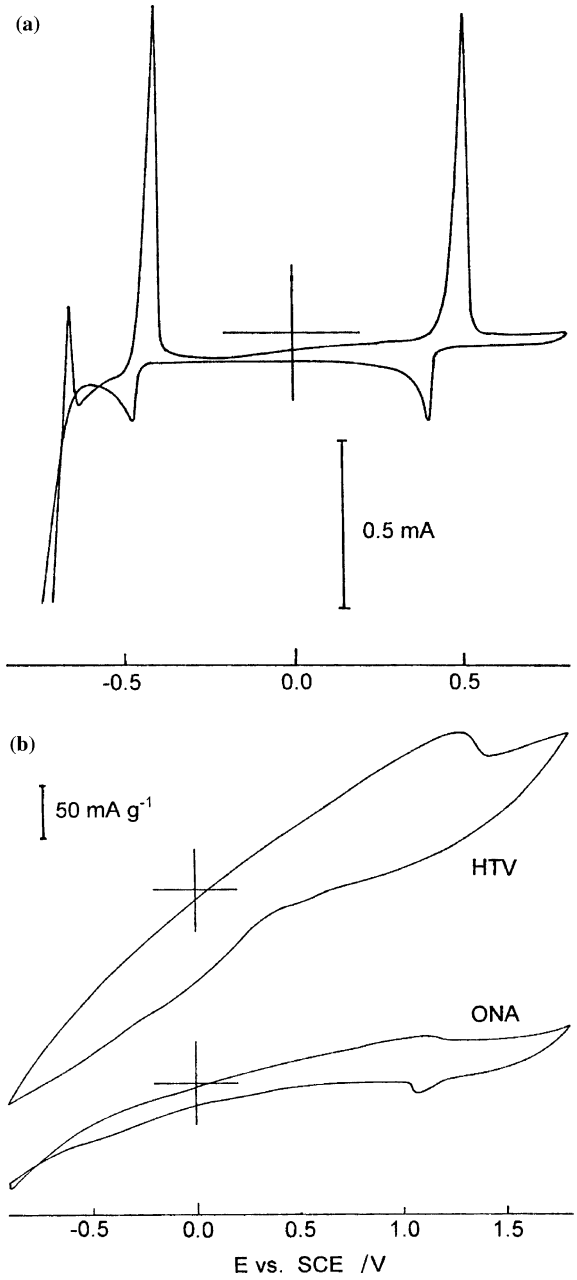

Fig. 11. Cyclic voltammograms for ternary system containing together Pb^{2+}, Hg^{2+} and Cd^{2+} nitrate solution ([Me^{2+}] = 0.0033 M) recorded for RG (a) as well as for PACE (b) electrodes (pH = 1.33, $v = 3\times10^{-3}$ V s^{-1}).

deposited on the carbon surface (especially for mercury) [37, 39]. Modification of the carbon surface chemistry strongly influences the extent and mechanisms of metal cation adsorption (Table 2) and the electrochemical activity of the cations present in the system studied here (Figures 8–10). However, knowledge of the acid–base properties of a carbon surface is insufficient to explain the adsorption capabilities of this system. Generally speaking, the electrochemical activity (magnitude of the metal oxidation–reduction peaks) of cation/activated carbon surface systems in nitrate solution depends on the ion uptake, as Figures 8–11 clearly show. The

electrochemical behaviour of a mixture of cations in solution on a commercial carbon electrode (GC) (Figure 11(a)) is close to the literature data [30–37], but for studied PACE depends on the surface chemistry of modified carbon samples and correlates with their adsorption ability. For this particular mixture of cations in solution the dominant electrochemical process is connected with mercury oxidation-reduction reactions (Figure 11(b)), which can be explained by the highest adsorption of this cation on the carbon surface (Table 2).

4. Conclusion

The various methods of chemically modifying the activated carbon surfaces investigated here led to a differentiation in the electrochemical properties of PACE in the aqueous solutions used. Mechanisms of electrode behaviour (oxidation–reduction) of the heavy metal ions investigated (Pb, Hg, Cd) with respect to the chemical properties of the PACE surface are put forward. In the case of a mixture of heavy metal ions, the extent of their adsorption (especially mercury) on the electrode processes was established.

Acknowledgement

This work was partially supported by Polish Committee for Scientific Research, Grant No. 7 T09B 091 21.

References

1. C.P. Huang, *in* 'Carbon Adsorption Handbook' (edited by P.N. Cheremisinoff and F. Ellerbush) (Ann Arbor Science, Ann Arbor, 1978) pp. 281–329.
2. R.C. Bansal, J.B. Donnet and F. Stoeckli, 'Active Carbon' (Marcel Dekker, New York, 1988).
3. L.R. Radovic, C. Moreno-Castilla and J. Rivera-Utrilla, *in* L.R. Radovic (Ed.), 'Chemistry and Physics of Carbon' Vol. 27 (Marcel Dekker, New York, 2001), p. 227.
4. B.M. Babic, S.K. Milonjic, M.J. Polovina, S. Cupic and B.V. Kaludierovic, *Carbon* **40** (2002) 1109.
5. A. Gierak, *Adsorption Sci. Technol.* **14** (1996) 47.
6. A.M. Youssef, A.M. El-Wakil, E.A. El-Sharkawy, A.B. Farag and K. Tollan, *Adsorption Sci. Technol.* **13** (1996) 115.
7. M. Pakuła, S. Biniak and A. Świątkowski, *Langmuir*. **14** (1998) 3082.
8. S. Biniak, M. Pakuła and A. Świątkowski, *J. Appl. Electrochem*. **29** (1999) 481.
9. S. Biniak, M. Pakuła, G.S. Szymański and A. Świątkowski, *Langmuir*. **15** (1999) 6117.
10. S. Biniak, A. Świątkowski and M. Pakuła, *in* L.R. Radovic (Ed.), 'Chemistry and Physics of Carbon' Vol. 27 (Marcel Dekker, new York, 2001) pp. 125–225.
11. L. Lakov, P. Vassileva and O. Peshev, *Carbon* **37** (1999) 1655.
12. V. Strelko Jr. and D.J. Malik, *J. Colloid Interface Sci.* **250** (2002) 213.
13. M. Walczyk, M. Pakuła, S. Biniak and A. Świątkowski, 'Influence of aminooxidative modification of activated carbon surface on electrochemical properties in electrolyte solution', Proceedings of an International Conference on Carbon, CARBON'03, Oviedo, Spain, 6–10 July (2003) No. 457.
14. A. Świątkowski, M. Pakuła, S. Biniak and M. Walczyk, *Carbon* (2004) (accepted for publication).
15. S. Biniak, G.Szymański, J. Siedlewski and A. Świątkowski, *Carbon* **35** (1997) 1799.
16. F. Kapteijn, J.A. Moulijn, S. Matzner and H.-P. Boehm, *Carbon* **37** (1999) 1143.
17. P. Burg, P. Fydrych, D. Cagniant, G. Nanse, J. Bimer and A. Jankowska, *Carbon*. **40** (2002) 1521.
18. J.P. Chen and M. Lin, *Carbon* **39** (2001) 1491.
19. J. Kazmierczak, S. Biniak, A. Świątkowski and K.-H. Radeke. *J. Chem. Soc. Faraday Trans*. **87** (1991) 3557.
20. R.M. Dagnal, T.S. West and P. Young, *Talanta* **1965** 583.
21. M. Struszyñski, *Analiza iloœciowa i techniczna*, PWN Warszawa (1957) T1: 362–365.
22. M. Pakuła, A. Świątkowski, and S. Biniak, *J. Appl. Electrochem*. **25** (1995) 1038.
23. J.C. Card, G. Valentin and A. Storck, *J. Electrochem. Soc*. **137** (1990) 2736.
24. A. Swiątkowski, M. Pakuła, and S. Biniak, 'Influence of the surface chemistry of modified active carbon on its electrochemical behavior in the presence of lead(II) ions', Proceedings of an International Conference on Carbon, CARBON'02, Beijing, China, 15–20 September (2002) No. E004.
25. P. Albers, K. Deller, B.M. Despeyroux, A. Schafer and K. Seibold, *J. Catalysis* **133** (1992) 467.
26. P. Albers, K. Deller, B.M. Despeyroux, G. Prescher, A. Schafer and K. Seibold, *J. Catalysis* **150** (1994) 368.
27. B. Stohr, H.P. Boehm and R. Schlogl, *Carbon* **29** (1991) 707.
28. L.R. Radovic, I.F. Silva, J.I. Ume, J.A. Menendez, C.A. Leon y Leon and A.W. Scaroni, *Carbon* **35** (1997) 1339.
29. F. Kaptejn, J.A. Moulijn, S. Matzner and H.P. Boehm. *Carbon* **37** (1999) 1143.
30. A. Zeng, E. Liu, S.N. Tan, S. Zhang and J. Gao, *Electroanalysis* **14** (2002) 1294.
31. M.E. Hyde and R.G. Compton, *J. Electroanal. Chem*. **531** (2002) 19.
32. D.R. Crow and P.J. Stronach, *Electroanal. Chem. Interfacial Electrochem*. **56** (1974) 209.
33. C. Neubold, K. Kalcher, W. Diewald, X. Cai and G. Raber, *Electroanalysis* **6** (1994) 227.
34. N. Zakharchuk, S. Meyer, B. Lange and F. Scholz, *Croat. Chem. Acta* **73** (2000) 667.
35. C. Ponce de Leon and D. Pletcher, *Electrochim. Acta* **41** (1996) 533.
36. V.S. Ijeri and A.K. Srivastava, *Anal. Sci.* **17** (2001) 605.
37. M.A. Nolan and S.P. Kounaves, *Electroanalysis* **12** (2000) 96.
38. H.E. Zittel and F.J. Miller, *Anal. Chem*. **37** (1965) 200.
39. R. Fu, H. Zeng and Y. Lu, *Carbon* **32** (1994) 593.

Advanced Carbon Electrode Materials for Molecular Electrochemistry

Richard L. McCreery*

National Institute for Nanotechnology, Department of Chemistry, University of Alberta, Edmonton, Alberta T6G 2M9, Canada

Received October 26, 2007

Contents

1. Introduction and Scope

Since the historical application by Sir Humphrey Davy of graphite electrodes for electrochemical production of alkali metals, carbon materials have been widely used in both analytical and industrial electrochemistry. The often-cited advantages of carbon electrodes include low cost, wide potential window, relatively inert electrochemistry, and electrocatalytic activity for a variety of redox reactions. Of particular relevance to the current review are oxidations and reductions of organic and biological molecules in both aqueous and nonaqueous media, for which the electrochemical properties of carbon electrodes are often superior to those of noble metals. In addition, the well-known applications of carbon electrodes to metals production, energy storage in batteries and supercapacitors, and catalyst supports has resulted in a rich literature on both carbon materials and their interactions with electrolytes and redox systems. Of general interest are several reviews and monographs on carbon electrode materials, notably the "classical" carbon materials based on graphite, glassy carbon, and carbon black.[1–4]

Despite extensive past investigations of carbon materials for electrochemistry, recent years have brought fundamental innovations that add significantly to the utility of this venerable material in organic and biological electrochemistry. Boron-doped diamond, fullerenes, vapor deposited carbon films, and microfabricated carbon structures offer distinct properties compared with the graphitic carbon electrodes in common use in the early 1990s and also enable novel applications in sensing, electrocatalysis, and electronics. The diversity of carbon as an electrode material stems largely from its structural polymorphism, chemical stability, rich surface chemistry, and strong carbon−carbon bonds present both internally and often between the carbon material and a surface modifier. A comprehensive review of all of the electrochemical properties and applications of carbon materials would require several volumes, even if limited to the past 15 years. Hence, the scope of the current review is limited to physical and analytical electrochemistry using carbon electrode materials, with an emphasis on the electronic and chemical properties of carbon that determine its electrochemical performance. Of particular interest are the relationships between carbon surface and bulk structure, which affect electrode kinetics and interactions with molecules in solution. While it is not practical to write a comprehensive review of all electrochemical applications of carbon electrodes, it is useful to consider those aspects of the materials chemistry of carbon that dictate its electrochemical utility. Borrowing an analogy from Richard Feynman, it is possible to understand the rules of a chess game without also knowing all possible outcomes that arise from those rules. As much as possible, this review will attempt to understand which aspects of bulk and surface chemistry of carbon electrode materials determine their utility for physical and analytical electrochemistry, particularly involving organic and biological redox systems.

* E-mail: mccreery@ualberta.ca.

10.1021/cr068076m CCC: $71.00
Published on Web 06/17/2008

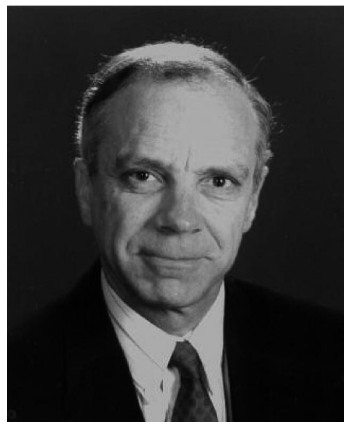

Richard L. McCreery is currently Professor of Chemistry at the University of Alberta, with a joint appointment as a Senior Research Officer at the National Institute for Nanotechnology. Until 2006, he was Dow Professor of Chemistry at The Ohio State University. He received his B.S. in chemistry from the University of California, Riverside, in 1970, and Ph.D. under Ralph Adams at the University of Kansas in 1974. His research involves spectroscopic probes of electrochemical processes, the electronic and electrochemical properties of carbon materials, and carbon-based molecular electronics. Much of the research involves collaborations with materials scientists and engineers, as well as surface scientists and electrochemists. He leads an effort at NINT and UofA to investigate hybrid devices for molecular electronics, which combine existing CMOS technology with new electronic and optoelectronic devices containing active molecular components.

This review will start with some of the "rules" associated with carbon electrodes, that is, the electronic and materials properties that partially determine electrochemical behavior. These include band structure, polymorphism, and optical properties. The next section deals with how these materials properties relate to electrochemical properties, including electrode kinetics, adsorption, and electrocatalysis. The third major section deals with the fabrication and novel aspects of new carbon materials developed in the past 15 years, including boron-doped diamond, carbon nanotubes, vapor-deposited carbon films, and various composite electrodes. Finally, the several approaches to surface modification of carbon electrodes are reviewed, emphasizing those developed since the early 1990s. Throughout the discussion of carbon electrode materials, examples related to organic and biological redox reactions are cited.

2. Materials Chemistry of Carbon Electrodes

It is convenient to broadly separate the materials properties of carbon electrodes into two subdivisions: bulk properties derived from the interior structure and surface effects such as termination and surface modification. Bulk properties include electronic conductivity, hardness, band structure, and optical absorption and will be discussed first, after an initial overview of carbon structures relevant to electrochemistry. Surface properties are of obvious importance to electrochemistry and are discussed together with carbon electrochemical properties in section 3.

2.1. Carbon Allotropes

Although carbon materials used in electrochemistry share some of the electronic properties of metals, their structures and chemistry differ dramatically from all metallic electrodes. The well-known allotropes of carbon include graphite, diamond, and fullerenes, each of which can exist in a variety of materials with differing electrochemical properties. The most common are based on the graphite structure, consisting of ideally infinite sheets of "graphene" stacked like parallel sheets of chicken wire. The carbon atoms in graphite are all sp^2 hybridized, with an intraplanar C−C bond length of 1.42 Å and interplanar spacing of 3.354 Å. Diamond is entirely sp^3 hybridized and tetrahedral, with a C−C bond length of 1.54 Å, and usually contains dopants to provide sufficient conductivity for electrochemistry, as described in sections 2.1.2 and 4.2. The most common fullerenes used as an electrode material are carbon nanotubes, which amount to single or multiple layers of graphite sheets "rolled up" to form tubes of varying diameter, length, and termination. The physical properties of these carbon materials relevant to electrochemistry are discussed below in turn.

2.1.1. Graphite and Related sp^2 Hybridized Carbon Materials

Several structural and electronic properties of graphitic carbon materials are summarized in Table 1. The simplest graphite material is a two-dimensional graphene sheet, which is essentially a very large polyaromatic hydrocarbon. The synthesis and properties of a wide variety of graphene structures were recently reviewed.[5] The most ordered three-dimensional graphite materials are relatively uncommon and comprise highly oriented pyrolytic graphite (HOPG) and natural crystalline graphite. HOPG is made by high-temperature decomposition of gaseous hydrocarbons, often acetylene, followed by hot pressing at high pressure and temperature.[3,6] Graphite materials are often characterized by the dimensions of the crystallites, L_a for the in-plane crystallite size and L_c perpendicular to the graphene planes. X-ray diffraction and Raman spectroscopy are commonly used to determine these parameters, as has been discussed elsewhere.[3,7−10] The interplanar spacing in graphitic materials is often labeled "d_{002}", in reference to an X-ray diffraction peak. HOPG and natural single crystal graphite have L_a and L_c values exceeding 1 μm, while polycrystalline graphite similar to pencil lead has values ranging from 10 to 100 nm, and carbon black has values in the range of 1−10 nm[3]. To provide some perspective, a single graphene square 1 μm on a side contains about 10^7 carbon atoms and thus represents a quite large "molecule". HOPG is "turbostratic", meaning that the crystallites have their *c*-axes aligned parallel but are rotationally disordered relative to adjacent crystallites. Natural single crystal graphite shares the ABAB layer ordering of HOPG but has longer range rotational order. However, natural graphite contains various inorganic impurities (e.g., "ash") and is rarely used for electrochemistry. The atomically ordered hexagonal plane containing the "*a*" axis is commonly known as the "basal plane", while the irregular surface parallel to the "*c*" axis is known as "edge plane". Edge plane graphite contains a variety of sites, often called "armchair" or "zig-zag", as well as various oxygen-containing functional groups. As will be discussed in detail later, the edge and basal planes differ greatly in chemical and electrochemical reactivity, and are fundamental to the behavior of graphitic electrodes.

Carbon fibers have been used extensively for electrochemistry, particularly in applications requiring a small "footprint" such as in vivo monitoring in living tissue.[11−13] They generally have diameters in the range of 5−50 μm and are made from small hydrocarbons or polymers or by catalytic chemical vapor deposition. Since the most common industrial application of carbon fibers is in structural materials, the

Table 1. Properties of Various Carbon Electrode Materials[3]

	apparent density (g/cm^3)	d_{002} (Å)	ρ (Ω·cm)	L_a (Å)	L_c (Å)
HOPG, *a*-axis	2.26	3.354	4×10^{-5}	>10000	
HOPG, *c*-axis			0.17		>100000
pyrolytic graphite	2.18	3.34		1000 (typ)[a]	1000 (typ)
randomly oriented graphite (ultracarbon UF-4s grade)	1.8	3.35	1×10^{-3}	300 (typ)	500 (typ)
Tokai GC-10[b]	1.5	3.49	4.5×10^{-3}	20 (typ)	−10
Tokai GC-20[b]	1.5	3.48	4.2×10^{-3}	25 (typ)	12
Tokai GC-30[b]	1.5	3.41	3.7×10^{-3}	55	70
carbon fiber (typ)	1.8	3.4	$(5-20) \times 10^{-4}$	>100	40
carbon black (spheron 6)	(1.3−2.0)[c]	3.55	0.05	20	13
evaporated a-C	−2.0	>3.4	$\sim 10^3$	~10	~10
a-C:H	1.4−1.8		$10^7 - 10^{16}$		
pyrolyzed photoresist film (PFF)			0.006[149]		
boron-doped diamond			0.05−0.5[d]		
N-doped amorphous tetrahedral carbon			10−1000[e]		

[a] Entries marked "typ" may vary significantly with sample or preparation procedures. [b] Number refers to heat treatment temperatures, for example, GC-20 was treated at 2000 °C. [c] Depends on technique used to measure density. [d] Depends strongly on doping level. See ref 30. [e] See ref 35.

fabrication process is designed to orient the graphitic *a*-axis along the length of the fiber to maximize tensile strength. Carbon fibers occur in a wide range of order and crystallite size and fall into three general types.[14] Radial fibers have graphene planes radiating out from the center of the fiber, "onion" fibers consist of concentric cylinders of graphene planes, and "random" fibers have a random orientation of graphitic planes. The degree of order and graphitization is often increased by heat treatment, and fiber manufacturers generally specify the thermal history in fiber specifications. The preparation and morphology of "onion" fibers is similar to those for carbon nanotubes (section 2.1.3), although nanotubes have much smaller diameters. The distinction between a small "onion" fiber and a multiwalled carbon nanotube is somewhat artificial, although as a practical matter carbon fibers are subject to manual manipulation while nanotubes are much less so.

An electrochemically important variant on the graphite structure is glassy carbon (GC), which is made by heat treating various polymers, often polyacrylonitrile. By heating the polymer under pressure in an inert atmosphere to 1000−3000 °C, the heteroatoms are evaporated until only carbon remains.[15] The C−C bonds in the polymer backbone do not break at these temperatures, so the carbon can form graphitic planes of only limited size, with L_a and L_c in the range of 30−70 Å. The interplanar spacing is larger than that of HOPG, about 3.6 Å, and the graphite structure cannot fully develop due to the unbroken C−C bonds. The structure is generally presented as randomly intertwined ribbons of graphitic planes, although the randomness results in significant uncertainty about the detailed microstructure.[16,17] It is known that GC is about 60% as dense as HOPG and must contain many voids, but its disordered nature makes structural characterization difficult at the atomic level. GC may also be made from a reactive polymeric precursor at relatively low temperature (~700 °C), which permits "doping" with various heteroatoms in the polymer, as well as the final product, including halogens, silicon, and metal catalysts.[18–21]

Glassy carbon should be distinguished from a variety of other disordered graphitic materials, such as "diamond-like carbon" (DLC),[22] amorphous carbon, polycrystalline graphite, and carbon black (see Table 1). While the properties of the materials vary greatly with preparation and pretreatment, some generalizations based on their origins are useful. As noted earlier, polycrystalline graphite has $d_{002} = 3.35$ Å but with randomly oriented crystallites much smaller than HOPG. It is made under conditions where the carbon is allowed to "graphitize", meaning allowed to form parallel planar sheets with the 3.35 Å layer spacing. Disordered carbon materials derived from polymers, such as GC and pyrolyzed photoresist, are unable to graphitize completely and have $d_{002} >$ 3.35 Å and $L_a <$ 10 nm (see Table 1). Amorphous carbon is made by vacuum deposition of carbon evaporated with an electron beam or by sputtering and is a very disordered combination of sp^2 and sp^3 hybridized carbon atoms and often small amounts of hydrogen.[23,24] Graphitization is prevented by the difficulty of breaking C−C bonds, and the ratio of sp^2 to sp^3 carbon atoms, as well as the hydrogen content, varies greatly with preparation conditions. DLC is a variant of amorphous carbon that is hard and wear resistant and is used widely for coating disk drive heads, while vapor-deposited amorphous carbon is used as a sample substrate for electron microscopy. Carbon black is made by several industrial processes, which result in materials of differing order and composition. "Graphitized" carbon black is used in electrochemistry and resembles polycrystalline graphite with quite small crystallites.[3] Although the list of graphitic materials is nearly endless and their properties range from soft, conductive lubricants to very hard, low conductivity solids, the parameters of crystallite size, long-range order, and anisotropy are critical factors toward determining electrochemical reactivity, as described in later sections.

Mesoporous carbon is a high surface area graphitic material made by "carbonization", or pyrolysis, of carbon-rich precursors such as sucrose, often using a silica template, which is later removed by etching.[25,26] Porosity is generally undesirable in electroanalytical applications; however mesoporous carbon has been used for the oxidation of cysteine,[25] as well as in supercapacitors[26] and electrocatalytic surfaces for methanol oxidation in fuel cells.[27] Mesoporous carbon supports for metal catalysts have been reported to be superior to more conventional carbon black materials, for example, Vulcan XC-72, in fuel cell applications.[28,29]

2.1.2. Diamond

The completely sp^3 hybridized, tetrahedral bonding of diamond results in both its hardness and low electrical conductivity, with the latter property making single- or polycrystalline diamond uninteresting as an electrode mate-

rial. However, intentional introduction of impurities, for example, boron or nitrogen, into diamond during deposition can increase the conductivity of diamond sufficiently to make electrodes with distinct electrochemical properties. The most common of these is microcrystalline boron-doped diamond (BDD),[30] which is made by vapor deposition from a H_2 plasma containing methane and a source of boron, often B_2H_6. Boron is electron-deficient relative to carbon and therefore a p-dopant, and the boron doping level is often quite high, often in the range of $10^{18}-10^{20}$ atoms/cm^3 or a B/C ratio of about 10^{-5} to 10^{-3}. Microcrystalline BDD has randomly oriented crystallites a few micrometers in size, with facets and grain boundaries characteristic of a polycrystalline material.

Nanocrystalline diamond is made from a CH_4/Ar plasma under conditions where nucleation is rapid, resulting in randomly oriented crystallites with dimensions of a few tens of nanometers.[31–34] Nitrogen gas or a boron source is often present during deposition, leading to nanocrystallites that are n-doped or p-doped, respectively. The crystallites have a much higher surface/volume ratio than microcrystalline diamond, and the surfaces have significant π-bonding and sp^2 hybridization. The result is much higher electrical conductivity than undoped bulk diamond, even when the nanocrystalline diamond is itself undoped. As discussed in section 4.2, BDD and nanocrystalline diamond have useful electrochemical properties compared with graphitic materials and are chemically much more inert.

A significant variation on diamond electrodes is nitrogen-incorporated tetrahedral amorphous carbon, taC:N, which is made by deposition from beams of ionized carbon and nitrogen.[35,36] Although the resistivity of this material is relatively high, $10-10^3$ Ω·cm, it is used in electrochemistry as thin films on conducting substrates so the ohmic potential losses are minimal. It has a high content of sp^3 bonded carbon and may be deposited on unheated substrates. As will be described later, taC:N has low background current and active electrocatalysis relative to BDD.

2.1.3. Carbon Nanotubes

Carbon nanotubes (CNTs) are generally categorized into single-walled carbon nantotubes (SWNTs), which consist of a single graphene sheet "rolled" into a tube, or multiwalled carbon nanotubes (MWNTs), which contain several concentric tubes sharing a common axis. In addition, MWNTs can occur in various morphologies such as "hollow tube", "bamboo" and "herringbone", depending on their mode of preparation.[37] A recent review of CNT utility in analytical science discusses the various unusual properties, which hold promise for new applications, such as high aspect ratio, conductivity, thermal stability, flexibility, and reactivity.[38] Nanotubes are made either by the arc-discharge method, which also produces fullerenes such as C_{60} and C_{70}, or by chemical vapor deposition on metal particles, often Fe or Ni. Thousands of papers have appeared on CNT properties and applications, including reviews on their use as electrode materials.[37,39] The carbons are arranged hexagonally, like basal plane graphite, along the walls of the nanotubes, but the tube ends are terminated with a fullerene structure incorporating pentagons, or by functional groups similar to those on edge plane graphite. Individual nanotubes have metallic or semiconducting electronic properties, depending on the number of hexagons around the circumference of the tube, and these differences strongly affect certain nanotube applications. However, the CNT materials used for electrochemistry are generally complex "ropes" consisting of bundles of nanotubes of various sizes. Some elegant experiments with single nanotube electrodes have been reported,[40–42] but the difficulty of isolating and mounting single nanotubes has impeded broad electrochemical application of individual SWNT or MWNT electrodes.

2.2. Electronic Properties of Carbon Electrode Materials

The resistivities of various carbon materials used in electrochemistry are listed in Table 1, with the caveat that some carbon materials show a wide range of resistivity depending on preparation conditions. Since the resistance for a carbon electrode equals the product of the resistivity and thickness divided by the cross sectional area of the carbon material, the observed resistance is a strong function of geometry. For example, a 1×1 cm^2, 100 nm thick carbon film with a resistivity of 0.15 Ω·cm has a resistance of 15 kΩ for current passing parallel to the plane of the film and 10^{-5} Ω for current passing perpendicular to the plane. In addition, some carbon materials are anisotropic, particularly pyrolytic graphite with its much lower resistance parallel than perpendicular to the graphene layers.

An important consideration regarding electrode materials is the density of electronic states (DOS), which varies greatly for different forms of carbon. The high conductivity of metals results from the combination of a large number of atomic orbitals to form bands with a high density of electronic states. Electrons move freely without changing energy, and metallic conduction follows Ohm's law. For example, gold has a DOS of 0.28 states atom^{-1} eV^{-1}, and this value is relatively constant with energy.[43] Conservation of energy dictates that electron transfer between an electrode and a redox system in solution or adsorbed on the electrode surface is fastest when the energy of the electron is equal in the metal and in the thermally activated redox system. A higher DOS in the electrode increases the likelihood that an electron of the correct energy is available for electron transfer to a redox system, so the heterogeneous electron transfer rate is expected to be dependent on the DOS of the electrode material.[44,45] Semiconductor electrodes represent the extreme opposite of a metallic DOS, in which there are no electronic states in the gap region, and electron transfer does not generally occur between a semiconductor electrode and redox systems with $E°$ values in the gap region.

Unlike the high and weakly energy-dependent DOS observed for metals, both the shape and magnitude of the DOS distribution for carbon materials vary greatly with carbon structure. The DOS distribution for HOPG is shown in Figure 1, with an expansion of the region near the Fermi energy as an inset.[46,47] The σ and π orbitals of the graphitic carbons combine to form the filled valence bands, which are shaded in the upper drawing, while antibonding orbitals comprise the conduction band. For an infinite graphene sheet and ideal crystalline graphite, there is a small overlap of the valence and conduction bands, leading to a low DOS at the Fermi level. Disorder in the graphite lattice results in many defect states with energies between the conduction and valence bands, effectively filling in the DOS near the Fermi level.[48] HOPG is considered a semimetal, while disordered graphite behaves electronically like a metal with a low DOS.

The minimum DOS for HOPG[49] is 0.0022 states atom^{-1} eV^{-1}, or about 0.8% that of Au. Even with disorder to

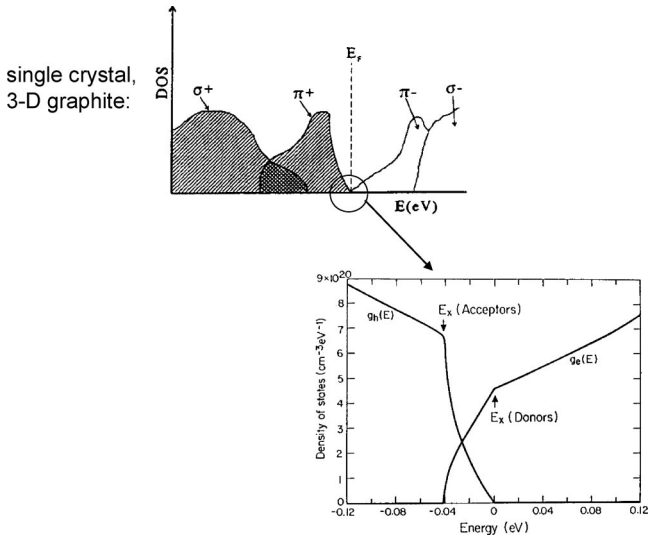

Figure 1. Calculated density of electronic states (DOS) for ideal single-crystal graphite. Reprinted with permission from refs 46 (http://link.aps.org/abstract/PRB/v15/p3180) and 47. Copyright 1977 American Physical Society and Copyright 1981 Marcel Dekker, respectively.

increase the DOS near the Fermi level, the lower conductivity of graphite materials compared with metals is at least partially a consequence of the low DOS. As will be noted in section 3.1, the low DOS of graphite also affects its electrochemical reactivity. An electrochemical manifestation of the unusual properties of ordered graphite is the low double layer capacitance of the basal plane of HOPG, <2 μF/cm^2 in aqueous electrolytes, compared with $\sim$60 μF/cm^2 for edge plane HOPG,[50] 24−36 μF/cm^2 for glassy carbon,[51] and 20 μF/cm^2 for typical metal electrodes.[52]

Crystalline diamond is a wide bandgap semiconductor, with a gap of >6 eV in a single crystal. However, the boron or nitrogen doping introduces a range of energy states in the gap region, as do defects present in microcrystalline and nanocrystalline diamond films. Nanocrystalline diamond has a sufficiently large number of defects that it is much more conductive than single crystal diamond even without doping. As discussed in section 3.1, the distribution of these energy levels is important to electron transfer to common redox systems at BDD electrodes,[53] although the details of the DOS will depend on electrode composition and preparation.

Carbon nanotubes have a variety of DOS distributions, which depend on tube diameter. Figure 2 shows an example,[41] plotted in the format developed by Gerischer for semiconductor electrochemistry.[52] The DOS of a semiconducting nanotube is shown in the left portion of Figure 2 and exhibits significantly more structure than that of graphite.[40,41] Semiconducting nanotubes have no electronic states in the gap region, while metallic nanotubes have a nonzero DOS both above and below the Fermi energy.

In the case shown in Figure 2, an oxidation occurs when the distribution of electron energies in the reduced material, W_{red}, overlaps with an unfilled level in the nanotube, as shown by the red arrow. As with semiconducting electrode materials, redox activity does not occur to redox levels of the molecule within the gap region.

To summarize the electronic properties of carbon materials relevant to electrochemistry, it is reasonably accurate to consider disordered sp^2 carbon materials such as polycrystalline graphite and glassy carbon and sp^3 carbon such as heavily boron-doped diamond to conduct electrons qualitatively similarly to metals. Although these materials do not exhibit gaps in the electronic DOS like semiconductors, the lower DOS leads to generally lower conductivity than metals. However, for ordered graphite, nanotubes, and lightly doped diamond, the generally lower and energy-dependent density of electronic states can have major effects on electron transfer behavior and cannot be ignored. Although many carbon materials used in electrochemistry are electronically similar to metals with no gaps in the DOS diagram, they differ greatly from metals in their surface chemistry, as will be discussed throughout this review, starting with section 3.

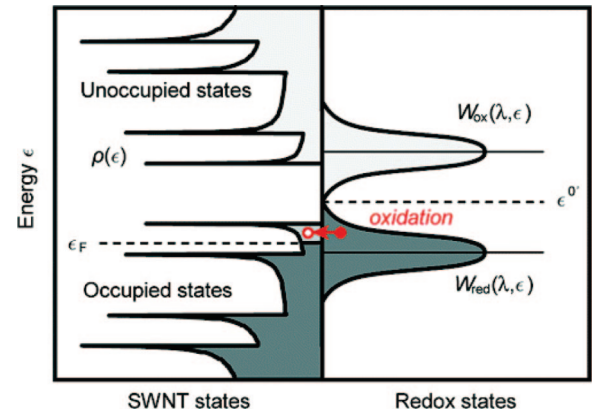

Figure 2. Density of electronic states for a semiconducting single-walled carbon nanotube plotted vs energy (left half) and the energy states of a redox system in solution (right half). Arrow indicates a favorable electron transfer from a reduced redox molecule to an empty level in the nanotube. Reprinted with permission from ref 41. Copyright 2006 American Chemical Society.

2.3. Spectroscopy and Optical Properties

Graphitic carbon materials such as graphite and GC absorb light over a wide energy range, at least from deep UV to radio frequencies.[54,55] Despite its black color as a bulk sample, thin films of disordered graphitic carbon are partially transparent in the visible wavelength range, with optically transparent carbon electrodes made from electron beam deposited carbon reported in 1975,[56] pyrolysis of an anhydride reagent from the gas phase in 1993,[57] and transparent thin films of pyrolyzed polymer on quartz in 2006.[58] Figure 3 shows the observed UV−vis spectrum of a $\sim$6 nm thick film of pyrolyzed photoresist on quartz, showing the broad absorption of the disordered graphitic structure.[59] Also included in Figure 3 are plots of the real and imaginary components of the refractive index, n and k, determined with spectroscopic ellipsometry. Crystalline diamond is optically transparent from its band gap at $\sim$220 nm into the infrared, but impurities and defects can result in weak absorption throughout the visible region.[60] Doping of diamond with boron decreases its optical transparency, but thin films of BDD have been used for both UV−vis and infrared spectroscopy.[61−63]

As one would expect for a technologically and scientifically important material, carbon has been examined with virtually all forms of analytical spectroscopy, for example, Raman and infrared spectroscopy, X-ray photoelectron spectroscopy (XPS), UV−vis, NMR, etc. Raman spectroscopy has proven particularly informative about all carbon materials used in electrochemistry and will be reviewed briefly here. Perfect graphite has two Raman active modes at 47 cm^{-1} ($E_{2g}^{(1)}$) and 1582 cm^{-1} ($E_{2g}^{(2)}$) plus two infrared active modes at 868 cm^{-1} (A_{2u}) and 1588 cm^{-1} (E_{1u}).[64,65]

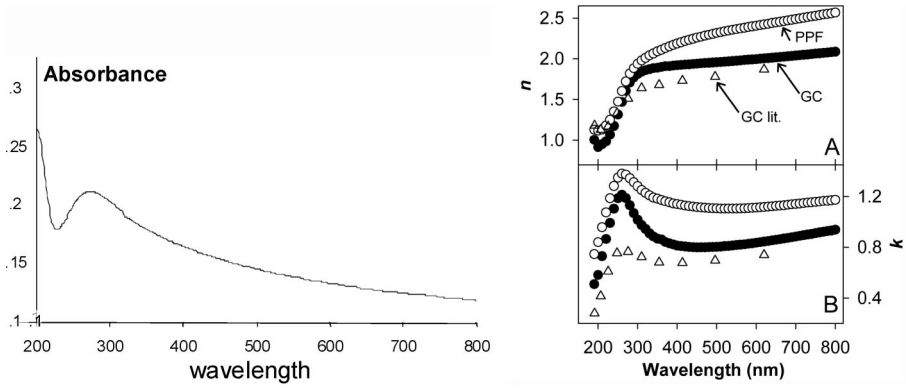

Figure 3. UV−vis absorption spectrum (left) of a 6 nm thick film of PPF on quartz and optical constants n and k (right) for GC (●) and PPF (○) determined by ellipsometry[59] and for GC from ref 10 (△). Right figure reprinted with permission from ref 59. Copyright 2007 American Chemical Society.

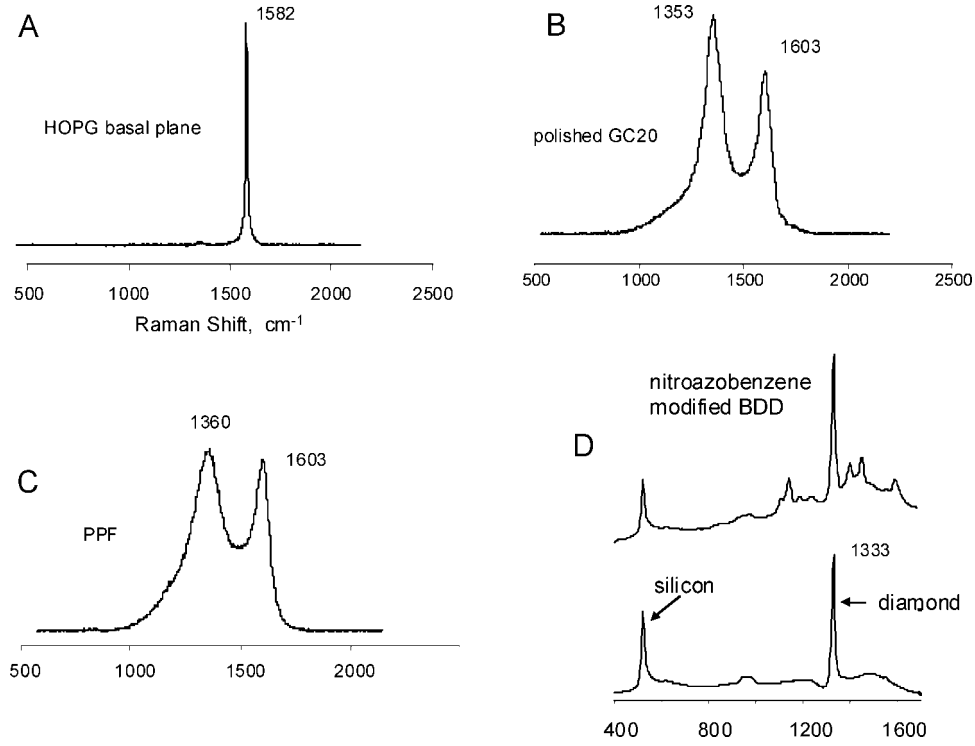

Figure 4. Raman spectra of carbon materials, obtained with 514.5 nm laser light. Intensity scales differ and are arbitrary: (A) HOPG basal plane; (B) polished GC; (C) pyrolyzed photoresist film; (D) boron-doped microcrystalline diamond, before (lower) and after (upper) modification with nitroazobenzene molecules. Panel D reproduced from ref 68 (Copyright 1999) by permission of The Electrochemical Society.

Since dipoles are weak or nonexistent in graphite, the IR modes are quite weak and have not been studied as extensively. However, graphite is very polarizable, and the Raman mode at 1582 cm^{-1} is a prominent feature of Raman spectra of graphitic materials.[7,10,66,67] Although the mode itself is quite strong, the penetration and escape depths of the laser and Raman scattered photons are short in graphite (~20 nm);[10] hence the Raman signal of graphite is weaker than that of diamond. Figure 4A shows a Raman spectrum of HOPG basal plane obtained with a 514.5 nm laser. The sharp E_{2g} phonon vibration at 1582 cm^{-1} is the only prominent feature in this region, although second-order transitions are observable above 2400 cm^{-1}. If the graphite is disordered, a new band appears near 1360 cm^{-1}, as shown for GC in Figure 4B. In addition, disorder causes broadening and slight upward frequency shifts of the 1582 cm^{-1} band, as well as changes in the higher order features.[10] The ~1360 and ~1582 cm^{-1} bands of disordered graphitic materials are generally referred to as the "D" (disorder), and "G" (graphite) bands, since their origins are less clear in disordered materials. The D band was initially mistakenly attributed to vibrations along the edges of graphitic crystallites, since a smaller L_a yielded a larger D/G intensity ratio.[64] However, the D band is observed in HOPG substitutionally doped with boron atoms;[10] hence it is more correct to conclude that the D band results from breakdown of symmetry in the graphite lattice and the resulting effect on Raman selection rules.[9,14,66] The D band shows an unusual shift in frequency with laser wavelength,[10] a property that was explained only relatively recently.[7] In the context of electrochemistry, the D band has been useful for observing changes in electrode surface structure with various pretreatments, such as laser activation[69,70] and electrochemical oxidation.[71–73] Raman spectroscopy is also a good probe of intercalation, a process that is relevant to battery applications of graphite as well as to the effects of electrochemical pretreatment.[14,74] As the graphite layers

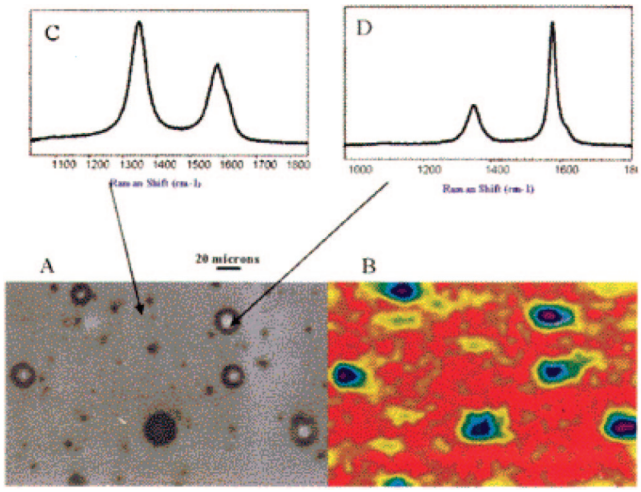

Figure 5. Raman imaging of polished glassy carbon (GC20): (A) 100× bright-field image; (B) Raman image of same area as panel A constructed by taking the ratio of the 1360/1580 peak area from 1200 points inside the sample area (red color indicates a high ratio; purple indicates a low ratio); (C) single spectrum acquired outside of pit; (D) single spectrum acquired inside of pit. Reprinted with permission from ref 76. Copyright 1997 American Chemical Society.

separate, the G band splits into two bands at 1582 and 1620 cm^{-1}, with the relative intensities depending on the degree of intercalation.[46] As ions penetrate between graphite layers, the graphene sheets can fragment, leading to formation of the D band.[74] Raman spectra of both graphite oxide and modified graphene sheets have been reported recently.[75]

For graphitic materials more disordered than GC, the D and G bands broaden further and begin to merge. An example is pyrolyzed photoresist (Figure 4C). Significant effort has been expended toward relating the Raman features to the ratio of sp^2 and sp^3 bonding in the carbon material, in part because of the technological importance of hard carbon materials in wear resistance, particularly on disk drive read/write heads. Although the shape and relative magnitudes of the D and G bands, as well as related features in the second-order region, depend on carbon microstructure, their broad linewidths and overlap make interpretation difficult. Carbon fibers, carbon black, and polycrystalline graphite exhibit D and G bands that reflect their degrees of disorder as well as thermal history. The correlation of the D/G intensity ratio with disorder is illustrated graphically in Figure 5, which includes a Raman image of polished glassy carbon. GC often has "pits" derived from gas bubbles formed during fabrication. Raman microspectroscopy inside a pit shows a lower D/G ratio, implying a more ordered material, while the polished surface shows a higher D/G ratio. The red color of the Raman image indicates a high D/G ratio and is observed wherever the surface was disturbed by polishing.[76]

Microcrystalline diamond exhibits a prominent 1332 cm^{-1} phonon band (Figure 4D and 6a), which occurs in single-crystal diamond. The line width of this band and changes in smaller features of the diamond Raman spectrum are good indicators of crystallinity and purity, providing a useful diagnostic for diamond film preparation.[30,53,68,77] Except for proximity, it bears no relation to the graphite D band, since it results from the first-order phonon associated with the sp^3 diamond lattice rather than disorder in the sp^2 structure of graphitic carbon. The 1332 cm^{-1} diamond band is used extensively to evaluate the relative amounts of sp^3 and sp^2 hybridized carbon in diamond samples. The Raman cross

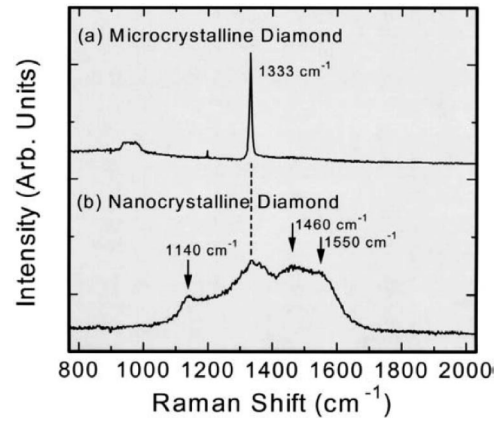

Figure 6. Raman spectra of microcrystalline and nanocrystalline boron-doped diamond, using visible laser light. Reprinted with permission from ref 30. Copyright 2004 Marcel Dekker.

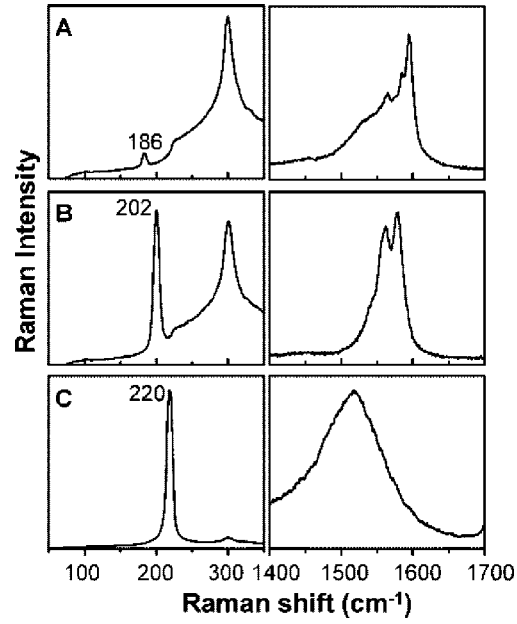

Figure 7. Raman spectra (632.8 nm laser) of metallic carbon nanotubes chosen from a mixture to indicate variations observed in the "G" band region (right) and "ring breathing mode" frequency region (left). Reprinted with permission from ref 85. Copyright 2007 American Chemical Society.

section for sp^2 carbon is approximately 50 times that of sp^3 carbon, so the 1360 cm^{-1} intensity relative to the 1332 cm^{-1} band is a sensitive indicator of sp^2 impurities in natural or synthetic diamond. The line width of the 1332 cm^{-1} band indicates the level defects,[30] with a single crystal having a line width of ~2 cm^{-1} and microcrystalline diamond ~10 cm^{-1}. Nanocrystalline diamond exhibits the severely broadened spectrum of Figure 6b, in which the 1332 cm^{-1} band is part of a broad set of bands spanning the range from 1100 to 1600 cm^{-1}. Boron doping at the high levels generally employed in electrochemically useful BDD results in observable changes in the symmetry of the 1332 cm^{-1} Raman band, which can be used to infer doping level.[53]

Carbon nanotubes have quite interesting Raman spectra, due to resonance effects and electron−phonon interactions.[78–81] An example is shown in Figure 7 for the case of Raman microscopy of selected nanotubes in a complex mixture of metallic and semiconducting nanotubes. The "G" band in the region of 1600 cm^{-1} has a similar origin to that observed in HOPG, but it obviously varies in position and shape for

different nanotubes. The low-frequency modes near 300 cm^{-1} are commonly referred to as "ring breathing modes" and arise from vibrations of the circular cross section of the tube. Since there is no analogous vibration in graphite, the low-frequency modes are particularly useful for distinguishing nanotubes from the disordered graphitic materials which often accompany nanotubes as impurities.[80,82–84] Other than this quality control application of Raman spectroscopy, CNT Raman is not commonly used in electrochemical applications and will not be discussed in any detail.

An intriguing optical effect was reported recently for carbon "nanocrystals" made by electrochemical treatment of nanotubes to break the tubes into smaller particles, presumably at defects.[86] The nanocrystals exhibited a well-defined UV−vis absorption band at 270 nm and blue photoluminescence with a maximum at 410 nm. Although the mechanism for photoemission is not clear, it is likely to involve quantum size effects such as those observed for semiconductor nanoparticles.

The optical properties of carbon materials are relevant both to spectroelectrochemical applications involving transmission or reflection of light from carbon surfaces and to characterization techniques such as ellipsometry and Raman spectroscopy. For example, the sampling depth of Raman and the transmission of carbon optically transparent electrodes are directly related to the real and imaginary components of the refractive index, usually stated as n and k. Attenuation of light in a carbon material may be determined from k as $\exp(-4\pi kz/\lambda)$, where z is the path length into the material and λ is the wavelength. The two transparent sp^2 hybridized carbon materials used in spectroelectrochemistry are thin films of disordered sp^2 carbon made from electron beam deposition[56,87,88] and pyrolyzed photoresist,[58,89] usually deposited on quartz. The n and k values for pyrolyzed photoresist and glassy carbon are shown in Figure 3.

Pure diamond is transparent to visible wavelengths, of course, with a refractive index of 2.418. Diamond thin films are appreciably transparent over a wide wavelength range of 225 nm to ~100 μm,[30] making them useful for a wide variety of spectroelectrochemical applications. Boron doping, defects, and microcrystallite scattering can significantly reduce the transmission of diamond optically transparent electrodes (OTEs), as does the substrate employed during diamond deposition. Quartz is generally used as the substrate for UV−vis spectroelectrochemistry, while undoped silicon serves as a transparent substrate for the infrared region. Figure 8 shows transmission spectra for various diamond OTEs in both the visible and infrared regions. With comparison to sp^2 carbon transmission shown in Figure 3, it is apparent that both BDD and graphitic thin films are sufficiently transparent in the visible region for spectroelectrochemical experiments. In addition, a recent report of a graphene−silica composite material demonstrates high transmission in the 400−1000 nm wavelength range as well as high electrical conductivity.[90]

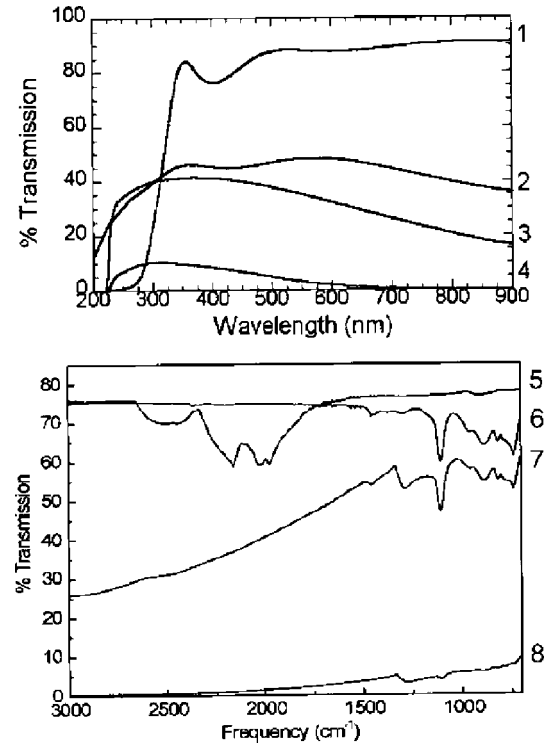

Figure 8. UV−vis (upper) and FTIR (lower) transmission spectra of several transparent electrode materials: (1) a thin film of indium−tin oxide on quartz, (2) boron-doped nanocrystalline diamond on quartz, (3) boron-doped diamond on a white diamond substrate, (4) a free-standing boron-doped polished diamond disk, (5) polished diamond disk, (6) undoped Si substrate, and (7, 8) moderately and heavily boron-doped microcrystalline diamond thin films on undoped Si. From: Stotter, J.; Haymond, S.; Zak, J. K.; Show, Y.; Cvackova, Z.; Swain, G. M. Interface 2003, 12, 33. Reproduced by permission of The Electrochemical Society.

3. Electrochemical Properties of Carbon Materials

In the context of the general review of carbon materials in section 2, we now turn to specific properties of carbon electrodes that affect electrochemical behavior. The choice of electrode material and surface preparation method are usually dictated by the suitability of the electrode for observing an electrochemical parameter, such as heterogeneous electron transfer rate, surface coverage, or redox potential. Carbon electrode properties that affect electrochemical behavior will be discussed in a series of sections on surface structure, electronic structure, adsorption, electrocatalysis, and surface preparation. Closing section 3 will be a brief discussion of how these properties can affect different redox systems to quite variable extents.

To aid comparison of various carbon electrodes for electron transfer reactivity to a simple outer-sphere redox system, the $Ru(NH_3)_6^{3+/2+}$ redox system serves as a useful benchmark. As described in section 3.5, $Ru(NH_3)_6^{3+/2+}$ is a nearly ideal outer-sphere redox system that is insensitive to most surface defects or impurities. Recent measurements of the electron transfer rate constant, $k°$, for $Ru(NH_3)_6^{3+/2+}$ in aqueous KCl electrolyte on a submicrometer diameter Pt ultramicroelectrode yielded a value of 17.0 ± 0.9 cm/s, based on the steady-state voltammogram.[91] While this high value may indeed be correct, more commonly reported values are in the range of 0.6−1.0 cm/s on metal electrodes, determined by fast scan voltammetry and impedance techniques.[44,92] Given the difficulty in measuring $k°$ values above 1 cm/s, suffice it to say that $Ru(NH_3)_6^{3+/2+}$ is a fast redox system with nearly ideal behavior ($k°$ above 1 cm/s and transfer coefficient near 0.5), which can serve as a benchmark for comparing carbon electrodes. A selection of reported $k°$ values for $Ru(NH_3)_6^{3+/2+}$ in aqueous KCl electrolyte is listed in Table 2, and the many entries for carbon electrodes will be used as examples in subsequent sections.

Table 2. Electrode Kinetics[a] of $Ru(NH_3)_6^{+3/+2}$ and $Fe(CN)_6^{3-/4-}$

electrode material	pretreatment	method	$k°$, $Ru(NH_3)_6^{+3/+2}$ cm/s	$k°$, $Fe(CN)_6^{3-/4-}$ cm/s	ref
Pt[b]		UME ss[c]	17.0 ± 0.9		91
Pt		UME fast CV[e]	0.8		408
Pt[d]	ultrasound	sampled voltammetry	0.6		92
Pt, Au, other metals			0.8−1.0		44
HOPG basal plane		CV	0.0014	$<10^{-7}$	50, 114
HOPG edge plane				0.06 - 0.1	50
GC 20[f]	fractured	CV		0.5 ± 0.2	51
GC20	conventional polish[g]	CV		0.005 ± 0.003	51
GC20	ultraclean polish	CV	0.51	0.14	144, 146
GC20	polish + laser	CV	>0.4	0.46	51
GC20	IPA/AC[h]	CV	0.11	0.090	146
carbon fiber, 60 um	polishing	UME CV	0.5 ± 0.06		166
carbon fiber, 60 um	laser activation	UME CV	0.96 ± 0.07		166
carbon fiber, 7 um	freshly cut	UME CV	1.22 ± 0.07		150
microcrystalline diamond, B-doped		CV	0.012−0.017	0.017−0.019	53
nanocrystalline diamond, B-doped		CV	*i*	*i*	225
nanocrystalline diamond, N-doped		CV	0.1		32
PPF	IPA/AC	CV	0.02		99
e-beam carbon	IPA/AC	CV	0.046		88
electron cyclotron resonance carbon film		CV	*i*	0.012	24

[a] 1 M KCl in water unless noted otherwise. [b] 0.5 M KCl. [c] Ultramicroelectrode, steady state current. [d] 0.1 M KCl. [e] Cyclic voltammetry. [f] Tokai glassy carbon, fabricated at 2000 °C. [g] Diamond followed by Al_2O_3 slurries in water. [h] Isopropyl alcohol, activated carbon, ultrasound. [i] Close to the reversible limit using cyclic voltammetry.

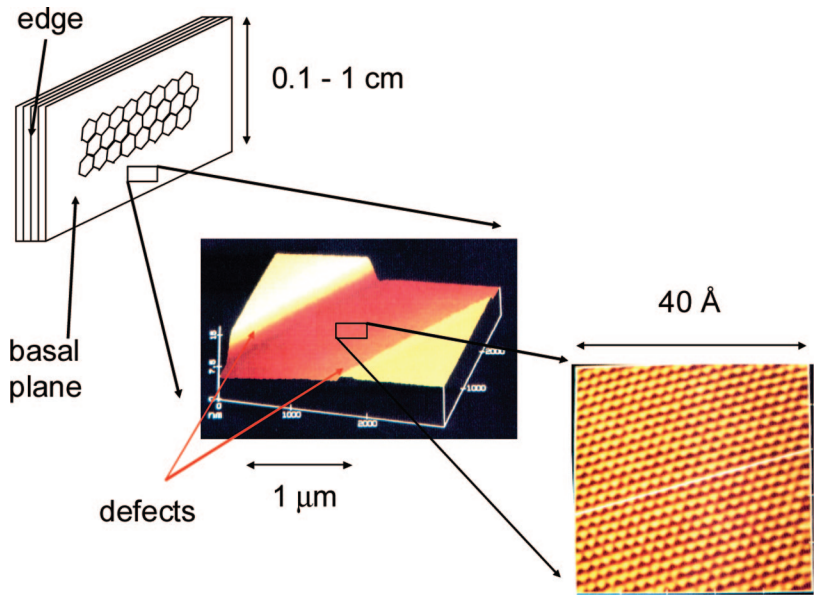

Figure 9. Scanning tunneling microscopy of HOPG basal plane, showing step edge defects (center) as well as an atomically smooth region between defects. Reprinted with permission from ref 16. Copyright 1993 American Chemical Society.

3.1. Surface Structure of Carbon Electrode Materials

Carbon materials have significantly more complex surface chemistry than metals, not only because the underlying microstructure varies with carbon type, but also because carbon forms a wider variety of surface bonds and functional groups. Since electrochemistry is based fundamentally on interfacial phenomena, the nature of the carbon electrode surface is of obvious importance. The discussion of carbon surface chemistry starts with the termination of the carbon electrode material at its surface, then continues with a brief discussion of a very common and electrochemically relevant termination, that is, surface oxides.

3.1.1. Termination

When the bulk carbon microstructure is interrupted at a surface, reactions generally occur with ambient gases or liquids to result in "termination", whether intentional or adventitious. Considering HOPG initially, the basal plane parallel to the *a*-axis is atomically ordered and does not react with air except at elevated temperatures. Figure 9 shows a schematic of a HOPG sample with magnified images obtained using scanning tunneling microscopy. Although the HOPG sample may be centimeters in size, the basal plane contains step edge defects whose density depends on history and preparation. As shown in the lower right image, HOPG is atomically smooth over dimensions of a few tens of nanometers, but defects are difficult to avoid for areas greater than a few micrometers.[16,93,94] Thus for the much larger areas useful in electrochemistry, a basal plane electrode will certainly contain defects at step edges and grain boundaries. The "edge plane" of HOPG is rough and "ragged", with features that cannot be imaged by STM due to multimicrometer variations in height. When the unsatisfied valences of the graphene edges are formed during cleavage or

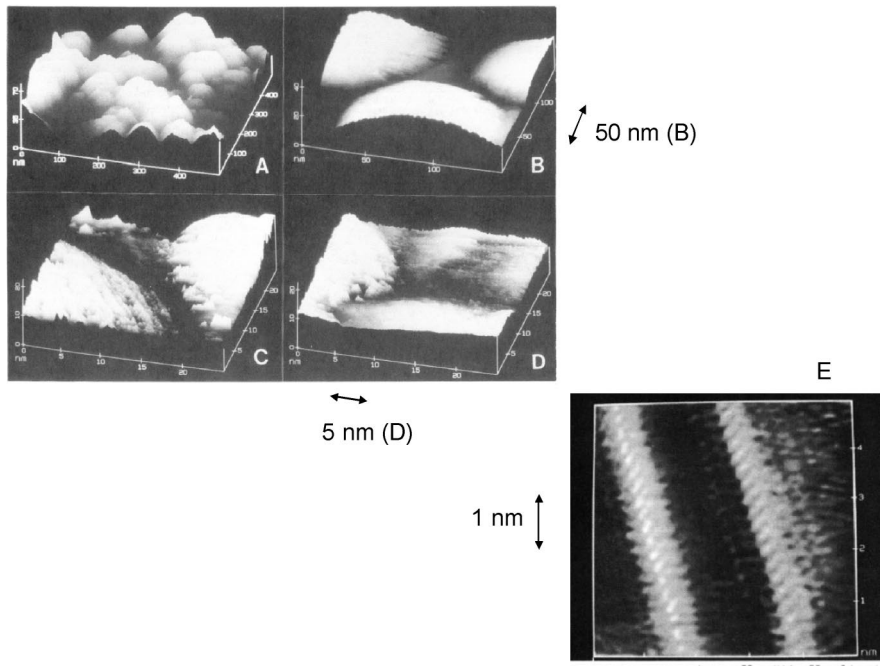

Figure 10. STM images of glassy carbon, after "fracturing" to avoid disturbance from polishing. Scale bars refer to the indicated panels. Reprinted with permission from refs 16 and 17. Copyright 1993 and 1994 American Chemical Society.

polishing, they react with oxygen and water to form various oxygen-containing functional groups, as discussed in the next section. The most common procedure for preparing carbon electrodes is polishing, usually with an abrasive such as diamond or alumina. Unfortunately, polishing results in a wide range of surface reactions with air and water, and the resulting surface is generally quite complex.[3] The hydrogen-terminated carbon surface is among the simplest structurally, but also one of the more difficult to prepare.[95] For now, suffice it to say that graphite basal and edge planes differ fundamentally in surface morphology and chemistry, and these differences are very apparent in electrochemical experiments, as described in section 3.5.

Given the origin of GC discussed in section 2.1.1, we expect that a GC surface would be a mixture of basal and edge plane, because the graphitic crystallites and "ribbons" are exposed at an electrode surface. A means to avoid disturbance of the GC structure induced by polishing involves "fracturing" a GC rod encased in epoxy such that the GC surface is exposed only to the electrolyte solution.[96,97] As noted in section 3.5, "fractured" GC surfaces show unusually high electrochemical reactivity, and relatively low oxide coverage. Figure 10 shows STM images of the fractured surface at various magnifications,[16] which reveals the nodules formed during heat treatment of the polymer precursor. At high magnification, the STM images show short-range order in the GC structure, presumably related to the edges of incompletely graphitized sheets.[17] Since most GC surfaces are polished, the edges will usually be terminated by surface oxides, but the oxide coverage and functional group identities can vary widely.

Hydrogen termination is widely used on silicon surfaces, since Si reacts quickly with aqueous HF to produce a Si−H surface stable in air for at least several hours.[98] H termination of carbon is more difficult, but also leads to a quite stable surface. A hydrogen plasma can terminate the surface of GC with C−H bonds, in addition to removing most of the surface oxides.[95] The surface is roughened somewhat by the reactive plasma, and the H-terminated surface has the lowest reported reactivity toward surface oxidation in air of any disordered carbon material. As shown in Figure 11, vacuum heat-treated and H-terminated GC both start with surface oxide coverage of less than 2 atom %, but the H-terminated surface gains only 1% additional surface oxygen after four days in air, while the vacuum-treated surface increases to over 8% O/C ratio in 5 h. Although H-termination is effective for stabilizing the GC surface as well as other forms of sp^2 carbon materials, it requires an expensive and cumbersome vacuum apparatus and is not widely used.

The H_2 plasma used to make BDD automatically results in a H-terminated diamond surface, which reacts slowly with oxygen.[30] Carbon nanotubes are formed with a variety of surface terminations, depending on preparation route. While the cylindrical walls of nanotubes resemble HOPG basal plane and are relatively unreactive, the tube ends are subject to oxidation and other reactions.[100–103] Termination with a fullerene cage containing pentagonal and hexagonal carbon atoms yields a low reactivity and relatively stable termination. The cylindrical walls are subject to both defects and oxidation.

3.1.2. Surface Oxides

As noted earlier, nearly all carbon surfaces are prone to reactions with oxygen and water, and oxygen-containing functional groups will be present on carbon electrodes unless special pretreatments are used. The nature and formation of oxygen-containing functional groups on carbon have been studied extensively, and the carbonyls, phenolic OH, lactones, ethers, and carboxylates on carbon surfaces will be referred to collectively as "surface oxides" or merely "oxides". Examples of surface oxides that form at a graphitic edge are shown schematically in Figure 12. Surface oxides on carbon electrodes have been studied by a variety of methods, notably XPS,[2,3,104] thermal desorption mass spectrometry,[105] and optical spectroscopy.[2,106,107] In the vast majority of electrochemical applications of carbon materials, there are oxides present whether intentional or not, and the

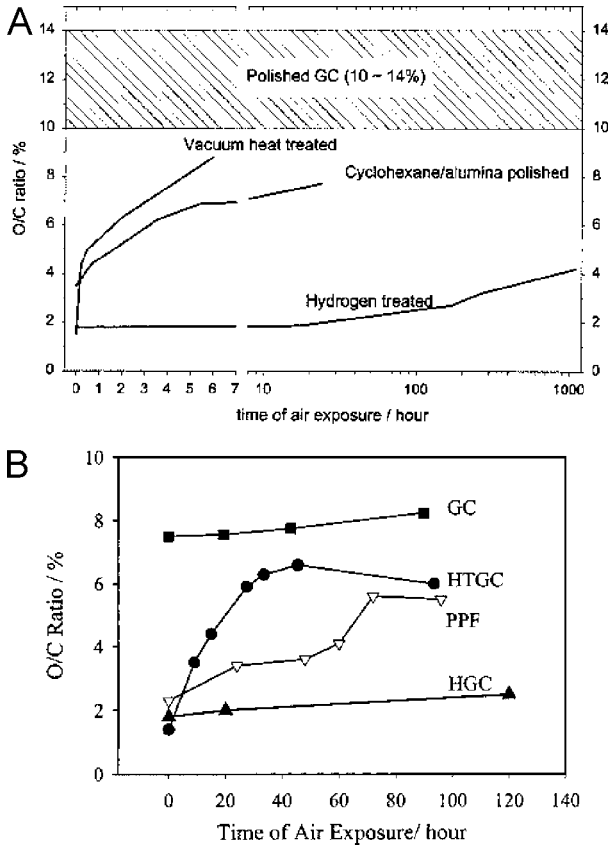

Figure 11. Comparisons of various carbon surfaces regarding stability toward surface oxidation in ambient air. Panel A shows the surface atomic O/C ratio determined from XPS for polished glassy carbon (GC) and GC prepared by vacuum heat treatment, polishing in cyclohexane, and a hydrogen plasma. Panel B compares H-plasma-treated GC (HGC) to pyrolyzed photoresist film (PPF) and GC heat-treated in a H_2/N_2 atmosphere (HTGC). Reprinted with permission from refs 95 and 99. Copyright 1999 and 2001 American Chemical Society.

user must be cognizant of possible effects of these oxides on adsorption, electron transfer kinetics, electrocatalysis, etc. While the presence of surface oxides is unavoidable without rigorous pretreatment and handling, the distribution of functional groups is subject to manipulation. Some examples are discussed in section 3.4, but for now, suffice it to say that surface oxides are a given and in some cases may be exploited for useful electrochemical performance.

The negative surface charge resulting from some surface oxides on carbon, notably carboxylates, can have significant electrochemical effects on adsorption and electron transfer rates. The well-known Frumkin correction modifies the observed electron transfer rate to charged redox systems,[52] and the extent of adsorption of ionic analytes can vary strongly with surface charge.[97] Extreme effects of surface electrostatic charge are observed in "electrochemically pretreated" carbon surfaces, following intentional anodization of the carbon surface to generate a variety of surface oxides, many of which are anionic.[3,108–110]

3.2. Electronic Structure and Conductivity

As noted in section 2.2, the conductivity of carbon materials has practical importance in designing electrode geometries to reduce ohmic potential losses. This issue is rarely a problem with common electrode materials such as bulk glassy carbon, but ohmic losses can be serious with

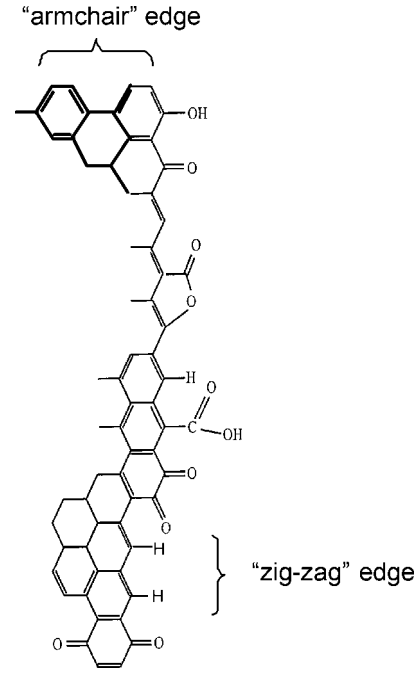

Figure 12. Examples of surface oxides that can occur at the edge plane surface of graphite or the graphene sheets in disordered sp^2 carbon materials.

thin films of disordered carbon, such as those in carbon OTEs. A more fundamental issue is the effect of electronic DOS on electron transfer. As noted earlier in section 2.2 and Figure 2, electron transfer is fastest when there is a high density of electronic states in the electrode at the $E°$ of the redox system involved. More precisely, there should be states in the electrode with energies within the range of donor or acceptor levels in the redox system, including the distribution in such energies caused by thermal fluctuations. Metals have a high DOS over a wide energy range, including the entire electrochemical potential scale. Randin and Yeager[111] recognized quite early that graphite had unusually low double layer capacitance, and Gerischer et al., investigated the relationship between the capacitance and the low DOS in HOPG.[49,112,113] Unlike metals, carbon materials exhibit extremes of DOS, ranging from undoped diamond with a large energy gap containing no states to HOPG with its low DOS at the Fermi level (Figure 1), nanotubes with significant structure in the DOS (Figure 2), and disordered graphitic materials with a relatively even DOS distribution.

Figure 13 shows a dramatic example of the effects of basal plane orientation on electrode kinetics, for the case of cobalt trisphenanthroline on HOPG. The slightly irregular shape of the edge plane voltammogram is due to difficulty in fabricating a smooth edge plane surface; however, it is clear that the electron transfer rate is much faster at the edge plane than at the basal plane.[114] To avoid uncertainties about edge plane roughness, a better comparison is between HOPG basal plane and laser-activated GC, which has a smoother, reactive, and nonporous surface. For eight quasireversible one-electron redox systems, the GC rates were 1−3 orders of magnitude higher than those for HOPG basal plane, an effect attributed to the low DOS of HOPG[49,113,114] and its semimetal character.[45] For the case of $Ru(NH_3)_6^{3+/2+}$, Table 2 indicates that various disordered carbon materials exhibit rates in the range of 0.5 to >1 cm/s, while HOPG basal plane is 0.0014 cm/s. Figure 14 summarizes $k°$ values for the eight redox systems on GC and HOPG, correlated with their self-

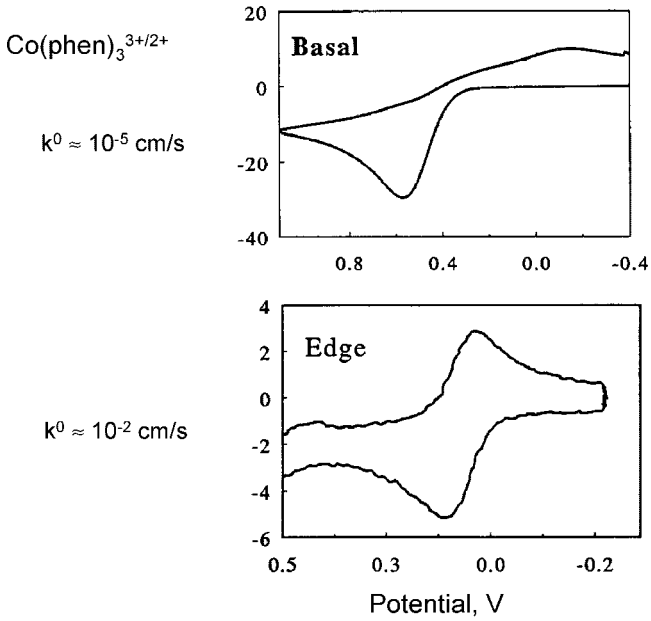

Figure 13. Voltammograms of $Co(phen)_3^{3+/2+}$ in 1 M KCl, 0.2 V/s, on HOPG basal plane (upper) and HOPG edge plane (lower). Approximate rate constants determined from the peak separation are indicated, and current axis is in microamps. Reprinted with permission from ref 114. Copyright 1992 American Chemical Society.

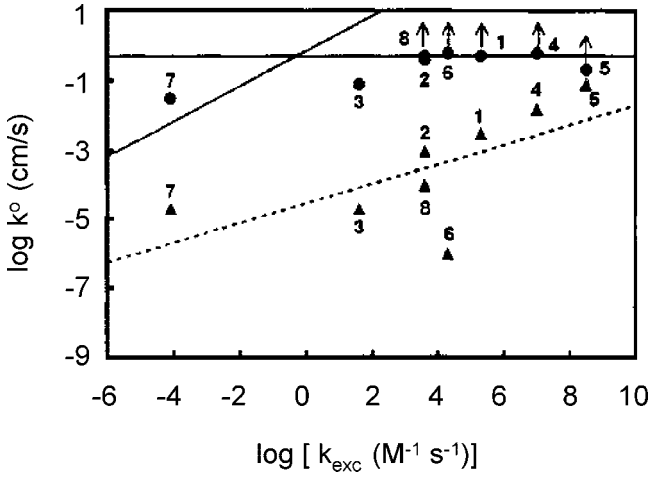

Figure 14. Observed rate constants on low defect HOPG basal plane (▲) and laser-activated glassy carbon (●). Horizontal line indicates instrumental limit for $k°$ determination, and dashed line is the least-squares fit to the HOPG data. Redox systems are (1) $IrCl_6^{2-/3-}$, (2) $Ru(NH_3)_6^{3+/2+}$, (3) $Co(phen)_3^{3+/2+}$, (4) methyl viologen, (5) $Fe(phen)_3^{3+/2+}$, (6) $Fe(CN)_6^{3-/4-}$, (7) $Co(en)_3^{3+/2+}$, and (8) $Ru(en)_3^{3+/2+}$, all in 1 M KCl. Reprinted with permission from ref 114. Copyright 1992 American Chemical Society.

exchange rates in homogeneous solution.[114] In addition to the consistently lower values observed on HOPG, there is a moderate correlation on HOPG with the square roots of the homogeneous rate constants, as predicted by Marcus/Levich kinetics (solid, slanted line in Figure 14). More recently, a detailed theoretical analysis of this effect was presented by Royea et al.[45] A natural consequence of the large reactivity difference between HOPG basal plane and the much more reactive edge plane is extreme sensitivity of the observed basal plane rates to defects. It is very easy to create step-edge defects on HOPG basal plane, and special treatment is required to reduce the defect density sufficiently to observe the true basal plane rate.[114] The kinetic contrast between edge and basal plane may be used to advantage, for "decoration" of adventitious step edge defects to result in metal and metal oxide "nanowires".[115–117]

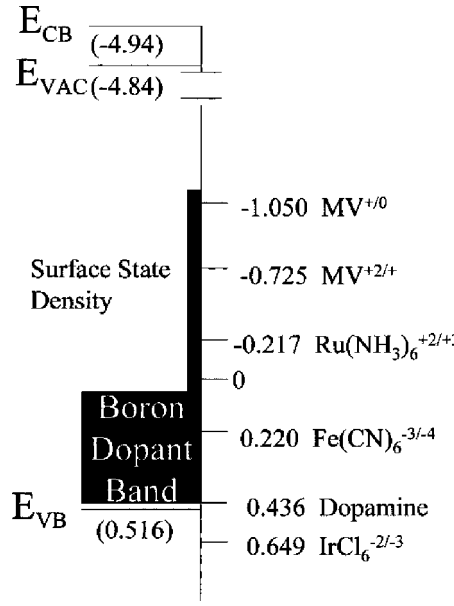

Figure 15. Energy states in BDD with the redox potentials of several common redox systems included. Reprinted with permission from ref 53. Copyright 2000 American Chemical Society.

Undoped diamond has no electronic states within its band gap, which covers most of the electrochemical potential scale. Boron doping, however, introduces "midgap" states, which increase both conductivity and electron transfer reactivity.[53] For the benchmark $Ru(NH_3)_6^{3+/2+}$ redox system, the $k°$ observed on BDD is 0.012 cm/s compared with 0.0014 on HOPG basal plane and 0.5−1 on sp^2 hybridized disordered carbon (Table 2). Both BDD and nanocrystalline diamond have many defect states on the crystallite surfaces, many of which are also in the midgap region. In many cases, these defects include hydrogen, which significantly perturbs the local energetics of the diamond lattice. Figure 15 summarizes these effects by showing the midgap states of diamond electrode materials relative to several aqueous redox systems.[53] A useful conclusion related to Figure 15 is that BDD and nanocrystalline diamond contain sufficient electronic states to support reasonable electron transfer rates to at least −1.1 V on the SCE potential scale,[53] whereas undoped diamond would not support electron transfer to any redox systems more positive than ∼0.45 V vs SCE.

As already noted in Figure 2, nanotubes have a DOS distribution related to but quite different from that of HOPG, and there should be a correlation between the DOS and electron transfer reactivity. However, the difficulty in isolating a given nanotube and characterizing its DOS makes observing such a correlation difficult. Practically speaking, most electrochemical applications of nanotubes involve ensembles of large numbers of tubes with different diameters and varying DOS distribution, so the effective DOS will be broadened by combination of many different profiles. Nevertheless, we can make a generalization about nanotubes as well as graphitic and diamond electrode materials: that the electronic DOS has magnitude and structure that is very different from that of metals and these differences can affect electrode kinetics.

3.3. Adsorption

Given the widespread use of sp^2 hybridized carbon materials as adsorbents, there is a large body of literature on the factors governing the adsorption of molecules to carbon surfaces. A review of same will not be attempted here, except to note the main factors relevant to electrochemistry. The forces that govern adsorption to carbon depend strongly on the type of carbon, its surface chemistry, and the structure of the adsorbate, among other factors. Whether adsorption is a problem or an asset of a given carbon electrode will obviously depend on the application.

The interactions between surface and adsorbate that control adsorption include dipole−dipole interactions, induced dipoles, hydrophobic effects, and electrostatic and covalent bonds, all of which depend on the history and preparation of the carbon material. Graphitic carbon materials commonly used as adsorbents have a high microscopic surface area and many oxygen-containing functional groups. The high polarizability of graphite leads to relatively strong induced dipoles, and the permanent dipoles associated with functional groups support dipole−dipole interaction with adsorbates. The ability of carbon to form strong covalent bonds with a variety of materials has been exploited extensively for surface modification (section 5). Each of these interactions varies in magnitude depending on the carbon allotrope, the exposure of basal or edge planes at the surface, and the distribution of surface oxides. For example, adsorption to the basal plane of HOPG is relatively weak, since there are no permanent dipoles, electrostatic charges, or unsatisfied valences. However, adsorption is generally strong on edge plane graphite and on step-edge defects on the basal plane.[17,94] The electronic disturbance near a graphitic edge can extend onto the basal plane, creating local dipoles, which enhance adsorption relative to perfect basal plane HOPG.[17] A detailed scanning force microscopy study of anthraquinone adsorption on HOPG showed that anthraquinone adsorbed with various geometries on HOPG basal plane but also implied that only the adsorbate present at defect sites was electroactive.[118] Figure 16 shows the results of Raman microspectroscopy used to investigate the adsorption of rhodamine 6G (R6G) on defects on HOPG basal plane.[76] The upper image is a photomicrograph of an intentional scratch on the basal plane surface, following adsorption of R6G from solution. Panel B is a Raman image of the same scratch, in which high intensity from the 1180 cm^{-1} band of R6G is shown as yellow and green, while low 1180 intensity is shown as dark red. Combined with the Raman spectra at various points on the image (panels C−E), the results indicate that R6G adsorption is significantly higher on the edge plane defects than on undisturbed basal plane.

Not surprisingly, carbon electrodes are subject to unintentional or unknown adsorption of impurities during electrode preparation. Intentional or not, these adsorbates can dramatically affect the electron transfer rates and electrocatalytic activity of carbon electrodes, possibly subverting their intended electrochemical applications. There is a long history of "activation" procedures for carbon electrodes, including polishing, heat treatment, solvent treatment, laser activation, ultrasonication, and others.[3,119] These procedures improve electrode performance in part by removing adventitious adsorbates from the electrode surface and are discussed in somewhat more detail in section 3.6. There are many examples of electrocatalytic effects of adsorbates on carbon surfaces for redox reactions of redox peptides, oxygen reduction, and organic molecules, a few of which are discussed in the next section.

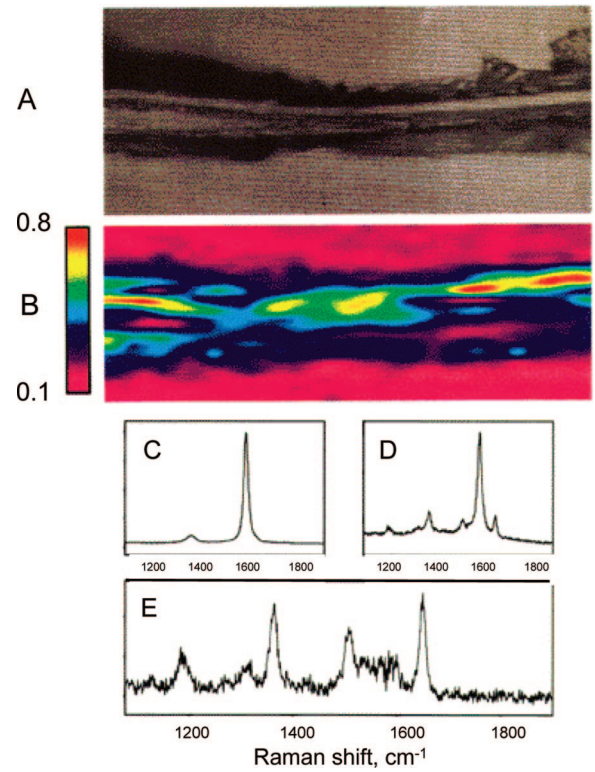

Figure 16. (A) Bright-field image of HOPG basal plane with an intentional defect, (B) Raman image of the same area as panel A after adsorption of R6G, constructed using the 1180/1580 peak area ratio from 1200 points, (C) spectrum acquired near the intentional defect before R6G exposure, (D) spectrum acquired near the intentional defect after exposure to R6G, and (E) resultant spectrum of spectrum C subtracted from spectrum D. Reprinted with permission from ref 76. Copyright 1997 American Chemical Society.

3.4. Electrocatalysis

The term "electrocatalysis" is used herein to designate a redox process that involves a specific chemical interaction with the electrode surface. Such interactions often accompany electron transfer reactions, particularly those involving organic and biological redox agents. The propensity of carbon to adsorb molecules from solution and the presence of surface oxides permit electrocatalytic reactions on carbon electrodes that are weaker or absent on metal electrodes. Furthermore, the history and preparation of carbon electrodes can have profound effects on the coverage and activity of catalytic sites; hence it is important to understand electrocatalytic effects. From the wide variety of reported electrocatalytic reactions on carbon electrodes, a few are considered here as illustrations.

As noted earlier, $Ru(NH_3)_6^{3+/2+}$ represents the simplest case of an outer-sphere electron transfer reactions with no known chemical interactions with the surface. It is nearly unaffected by a monolayer of uncharged adsorbates and serves as the null case for electrocatalysis. The observed k° depends on the DOS of the electrode material but in practice is uniformly high for clean electrodes with DOS similar to that of metals (Table 2). In contrast, the $Fe^{3+/2+}$ redox reaction depends strongly on the presence of surface oxides on carbon and is inhibited significantly if they are absent or

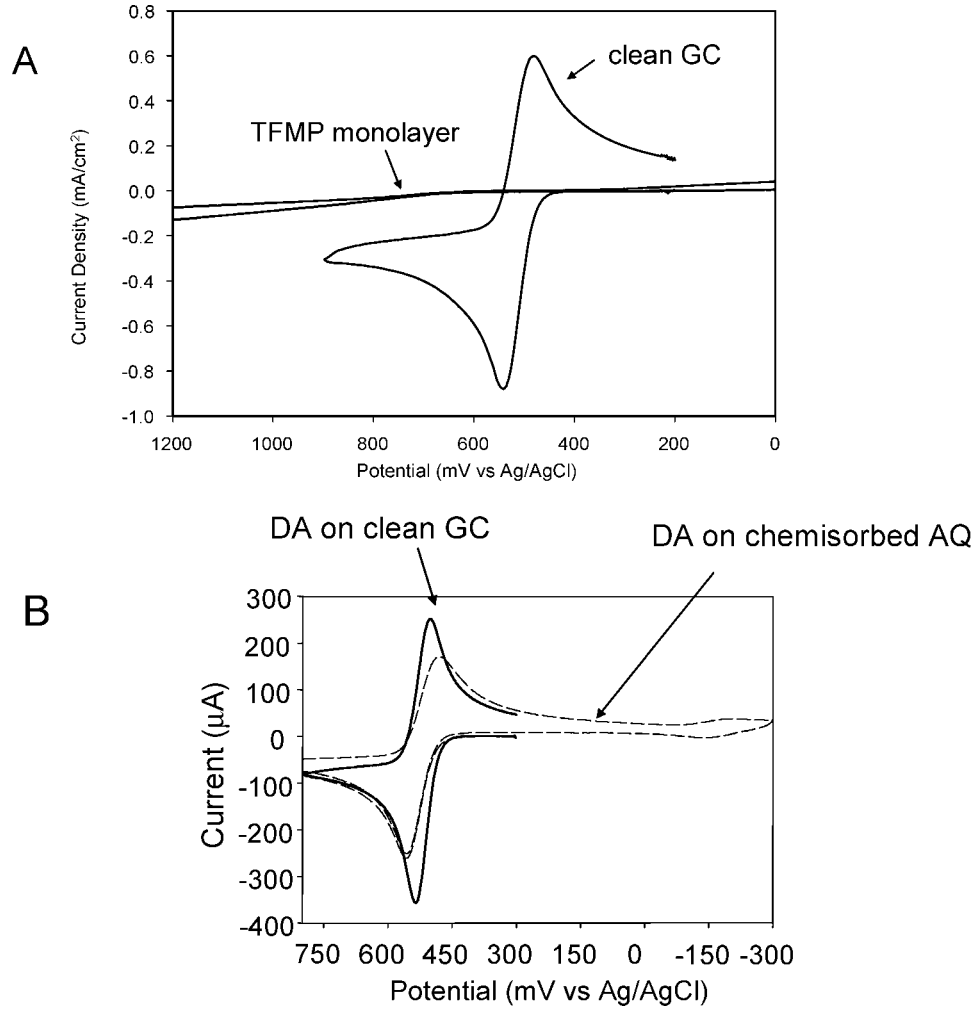

Figure 17. (A) Voltammetry of dopamine in 0.1 M H_2SO_4 on clean GC and on GC modified with a monolayer of trifluorophenyl groups and (B) comparison of dopamine voltammetry on clean GC (solid line) and on a GC surface modified with chemisorbed anthraquinone (dashed line). AQ = anthraquinone, DA = dopamine, TFMP = trifluoromethylphenyl. Reprinted with permission from ref 126. Copyright 2000 American Chemical Society.

obscured by adsorbates.[120–122] The Fe−O bond length in hydrated Fe^{3+} changes length upon reduction, and this process is facilitated by transient interactions with surface oxides. $Fe(CN)_6^{3-/4-}$ is also sensitive to the state of the carbon surface, although the nature of the catalytic interaction is not clear.[121,122] Unfortunately, $Fe(CN)_6^{3-/4-}$ is often used as an "ideal" outer-sphere redox reaction but in fact is quite complex and dependent both on the surface chemistry and interactions with cations in solution.[3,123,124] To use a phenomenological term, we might consider $Fe^{3+/2+}$ and to be "surface sensitive", with kinetics that are influenced by an electrocatalytic interaction, while $Ru(NH_3)_6^{3+/2+}$ is "surface insensitive", with the electrode merely serving as a source or sink of electrons. An observation that clearly distinguishes $Ru(NH_3)_6^{3+/2+}$ from $Fe(CN)_6^{3-/4-}$ in this respect was made with the aid of the diazonium reduction reaction described in section 5.1. A nitrophenyl modification of GC caused a significant decrease in the electron transfer rate to $Fe(CN)_6^{3-/4-}$ (ΔE_p increased from 91 to 229 mV), but had minor effects on $Ru(NH_3)_6^{3+/2+}$ (76 to 88 mV).[122]

The oxidation of catechol derivatives has been studied widely, due to the importance of catecholamine neurotransmitters and related compounds in biology. Dopamine (3,4-dihydroxy phenethylamine, DA) is an example of a catechol with heterogeneous electron transfer strongly dependent on electrocatalysis. As shown in Figure 17A, DA oxidation is completely inhibited by a monolayer of triphenylmethyl phenyl groups bonded to glassy carbon.[125,126] This surface treatment has minor effects on $Ru(NH_3)_6^{3+/2+}$, so electrons are capable of tunneling through the monolayer.[122] DA oxidation is fully restored if a monolayer of anthraquinone instead of trifluoromethylphenyl covers the electrode surface, as shown in Figure 17B. The catalytic effect was attributed to the presence of hydrogen bonding sites on the surface, which assisted DA oxidation by transient bonding to the catechol hydrogen to effect "proton-assisted electron transfer".[126] On a bare carbon surface lacking hydrogen bonding sites, the catechol itself can adsorb on the surface to permit "self-catalysis" by hydrogen bonding to catechols in solution undergoing oxidation.

Redox mediation is a widely studied example of electrocatalysis on carbon surfaces, in which a redox active adsorbate can act as an electron relay to molecules in solution. Of particular note is the widely used blood glucose analyzer, which is based on redox mediation between a carbon surface and NADH.[127–129] In some cases, a covalent chemisorption bond between the carbon surface and the electroactive species can catalyze electron transfer.[130] While carbon is not as broadly reactive toward chemisorption as catalytic metals such as Pt and Ru, its rich surface chemistry provides a route to build in such interactions by surface modification (section 5).

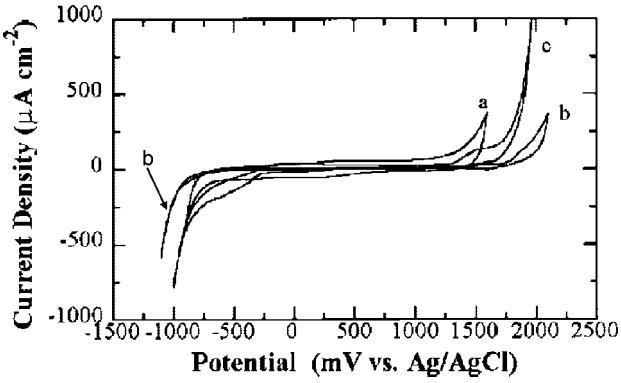

Figure 18. Background current for voltammetry (0.1 V/s) in 0.1 M $HClO_4$ for (a) glassy carbon, (b) moderately boron-doped microcrystalline diamond, and (c) heavily B-doped diamond. Reprinted with permission from ref 30. Copyright 2004 Marcel Dekker.

A practically important issue related to surface reactivity is the available potential range of carbon electrode materials over which background reactions contribute negligibly to the observed current. Such reactions depend strongly on the nature of the carbon electrode material as well as the preparation of the surface. The kinetics of surface oxidation and hydrogen evolution are significantly slower on carbon than on most commonly used metal electrodes, and the resulting wide potential window is one reason for the widespread use of carbon materials for electrodes. Since the onset of background current also depends strongly on solvent, pH, electrolyte composition, and current sensitivity, quantitative comparisons of different carbon materials are approximate. That said, diamond electrodes have electrochemical windows significantly wider than most graphitic materials, as demonstrated by an example shown in Figure 18. For single-crystal boron-doped diamond, positive potentials as high as +2.5 V vs NHE were accessible in water before large anodic currents occurred.[131] For polycrystalline diamond, a background oxidation was observed at +1.83 V on the first scan, and was attributed to irreversible oxidation of sp^2 impurities along grain boundaries.[131] Nitrogen-incorporated tetrahedral amorphous carbon and electron cyclotron deposited carbon[24,132] have higher potential limits than typical BDD or nanocrystalline diamond,[35] although this comparison will depend significantly on the origin of each sample.

Based on these examples and a host of others from the literature, it is clear that electrocatalytic reactions are very common on carbon electrodes, with the true outer-sphere redox reactions being in the minority. Obviously, the carbon electrode material and surface preparation will strongly affect the population of sites available for catalysis, and the underlying interactions are quite varied. As noted in section 3.5, the importance of identity and coverage of surface sites depends on the particular redox system involved, although some useful generalizations are available.

3.5. Classes of Redox Systems on Carbon Electrodes

The term "activation" has been used for several decades to describe procedures that modify the electron transfer kinetics at carbon electrodes, usually measured by the increase in $k°$ for a benchmark redox system. Three of the more common benchmark redox systems were $Fe(CN)_6^{3-}$, ascorbic acid, and dopamine, all in aqueous solution, but

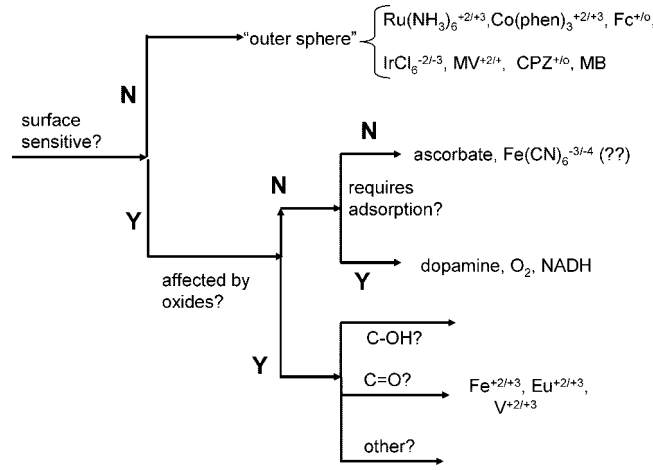

Figure 19. Classification of redox systems according to their kinetic sensitivity to particular surface modifications on carbon electrodes. See text and ref 121 for details. Reprinted with permission from ref 121. Copyright 1995 American Chemical Society.

others included ferrocene in acetonitrile, anthracene and anthraquinone, and dioxygen reduction. Unfortunately, the collection of activation procedures led to the inference that a "reactive" electrode will exhibit fast electron transfer kinetics for all redox systems considered, when in fact the sensitivity of $k°$ values to various activation procedures depends strongly on the redox system involved. This variation with electrode surface condition has been exploited to impart selectivity of carbon surfaces for particular analytes. For example, an anionic carbon surface is much more sensitive to dopamine at pH 7 (a cation) than to ascorbate (an anion) due to electrostatic repulsion of the ascorbate by the surface. Clearly any "activation" or modification of a carbon electrode surface must be considered in light of the particular redox system involved. The purpose of the present section is to classify redox systems according to the sensitivity of their electron transfer kinetics to the surface chemistry of a carbon electrode. Figure 19 presents a scheme for such a classification, based on experimental observations of a variety of carbon electrodes and mainly inorganic redox systems.[122] The next few sections explain the logic underlying the "tree" diagram of Figure 19, and its utility for classifying redox systems on carbon electrodes.

3.5.1. Outer-Sphere Redox Systems

The first breakpoint in the tree diagram is based on "surface sensitivity", that is, variations in $k°$ with the condition of the surface. Outer-sphere redox systems are generally considered to lack any electrocatalytic or adsorption step and often have low reorganization energies. Examples include $Ru(NH_3)_6^{3+/2+}$, ferrocene$^{+/0}$, and anthracene$^{0/-}$. Figure 19 is phenomenological, in that it discriminates on the basis of an experimental observation rather than a mechanism. The "test" for surface sensitivity is the absence of a significant change in $k°$ when the carbon surface is purposely modified with a physi- or chemisorbed monolayer, such as a covalently bonded layer of nitrophenyl groups. An example is shown in Figure 20a, for $Ru(NH_3)_6^{3+/2+}$ on GC. Adsorption of a monolayer of bis(methyl styryl)benzene has no effect on the observed peak separation or $k°$, indicating that the electron transfer may occur with equal efficacy on a bare GC surface or on a surface coated with an organic molecule.[121,122] Obviously a significant effect would be

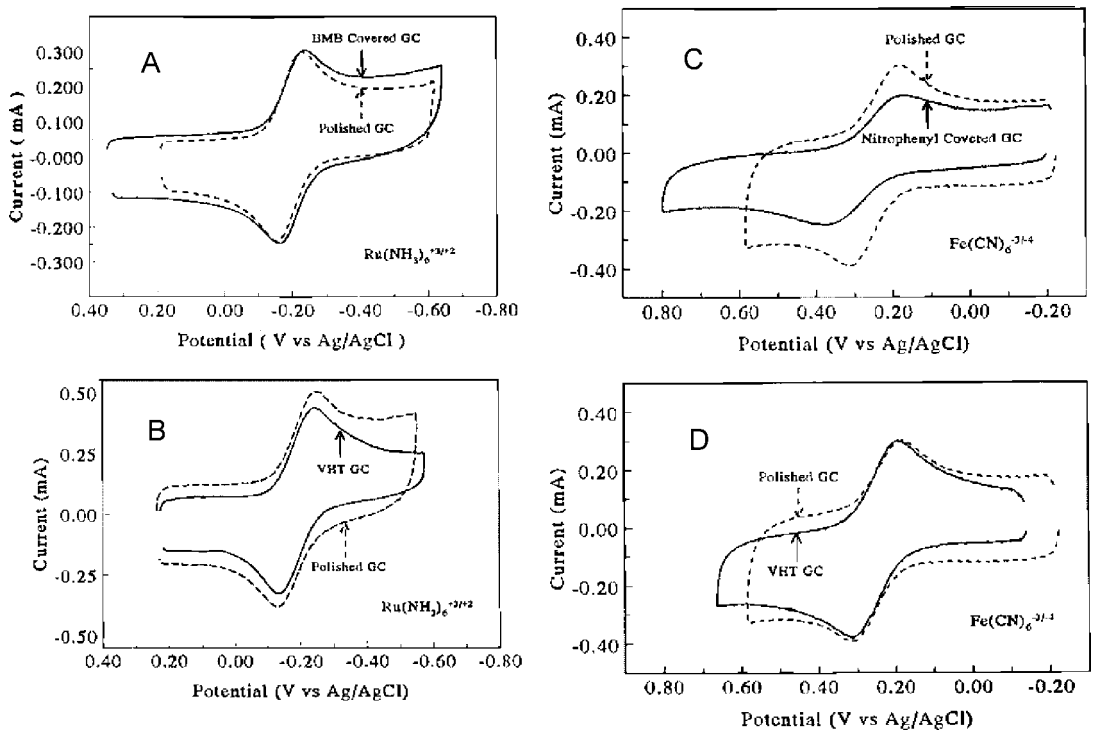

Figure 20. Voltammograms of $Ru(NH_3)_6^{3+/2+}$ and $Fe(CN)_6^{3-/4-}$ on various glassy carbon electrode surfaces: (A) $Ru(NH_3)_6^{3+/2+}$ on polished and bismethylstyrylbenzene coated GC; (B) $Ru(NH_3)_6^{3+/2+}$ on polished and vacuum heat-treated GC; (C) $Fe(CN)_6^{3-/4-}$ on polished and nitrophenyl-modified GC, and (D) $Fe(CN)_6^{3-/4-}$ on polished and vacuum heat-treated GC. Reprinted with permission from ref 122. Copyright 1996 American Chemical Society.

expected if the $Ru(NH_3)_6^{3+/2+}$ redox reaction depended on a surface interaction between the redox center and some site on the GC surface. It should be noted at this point that the lack of surface sensitivity, as defined here, does not rigorously establish a redox system as outer-sphere, but it does imply that significant changes in surface chemistry have no observable effect on electrode kinetics. It is also possible that the k° is too fast to measure on either bare or modified electrodes, so that "surface sensitivity" was not observed.

While specific surface interactions related to electrocatalysis are clearly examples of effects that underlie "surface sensitivity", a finer and more recent issue relates to electron tunneling. Even for outer-sphere redox reactions, a surface film will slow electron transfer because the electron must tunnel through the film between the reactant and the conducing electrode surface. The extreme case is a thick film, which totally prevents electron transfer. However, tunneling through monolayers of less than 1−2 nm thickness can be quite fast, and such monolayers are common on electrode surfaces, intentional or not. Numerous studies on electron transfer through self-assembled monolayers of alkanes and conjugated molecules have been reported, and it is well established that such monolayers slow but do not prevent electron transfer.[133–138] The observation that a monolayer of an organic molecule has little effect on $Ru(NH_3)_6^{3+/2+}$ kinetics on a carbon surface (Figure 20A) indicates that electron tunneling can easily occur through a monolayer on the time scale of typical cyclic voltammetry. In the context of the "tree" of Figure 19, the test of surface sensitivity uses a monolayer thin enough for electron tunneling to be efficient on the experimental time scale employed. The tunneling rate is strongly dependent on monolayer thickness,[139] as expected, and can even be manipulated electrochemically by structural changes in the monolayer.[140] In the current context, "surface sensitive" refers to reactions that show significantly more than the slight decrease in electron transfer kinetics expected from an organic monolayer with a thickness of less than ~1 nm.

3.5.2. "Surface-Sensitive" and Electrocatalytic Redox Systems

In addition to a test based on a nonspecific organic monolayer, Figure 20B,D illustrates a second breakpoint in the classification "tree", involving the effect of surface oxides. As will be discussed in section 3.6, polished GC carbon surfaces generally have 8−15% surface O/C ratio, while vacuum heat treatment reduces oxide coverage to a few percent. The example of dopamine oxidation cited in section 3.4 illustrates that certain redox processes have electron transfer rates that depend on the presence of surface oxides, in some cases on particular functional groups, such as carbonyl or carboxylate. Figure 20B,D shows that neither $Ru(NH_3)_6^{3+/2+}$ nor $Fe(CN)_6^{3-/4-}$ exhibit a dependence of peak separation on oxide coverage, implying that they are not "oxide-dependent". However, $Fe(CN)_6^{3-/4-}$ exhibits significantly slower kinetics on a surface modified with a monolayer of covalently bonded nitrophenyl groups (Figure 20C). These observations indicate that $Ru(NH_3)_6^{3+/2+}$ is neither "surface-sensitive" nor "oxide-sensitive", while $Fe(CN)_6^{3-/4-}$ is "surface-sensitive" but not "oxide-sensitive". Various explanations for the dependence of $Fe(CN)_6^{3-/4-}$ on the condition of the electrode surface have been discussed.[3,122–124,141]

In contrast to $Ru(NH_3)_6^{3+/2+}$ and $Fe(CN)_6^{3-/4}$, the $Fe(H_2O)_6^{3+/2+}$ redox system depends strongly on the presence of surface oxides on carbon electrodes.[120,121] The voltammetry of $Fe^{3+/2+}$ is shown in Figures 21 and 22 for glassy carbon electrodes, and a collection of ΔE_p values appears in Table 3. Note first that the ΔE_p for $Fe^{3+/2+}$ is large for carbon surfaces low in oxide coverage, notably

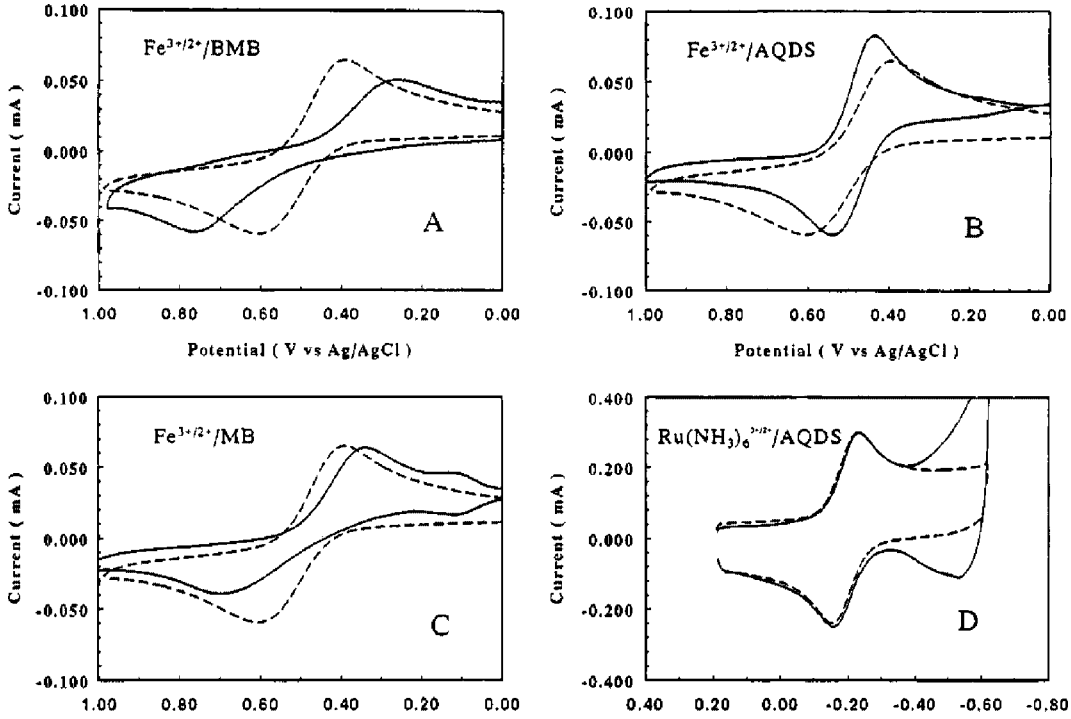

Figure 21. Voltammetry on polished GC before (dashed) and after (solid) adsorption of organic molecules. (A−C) $Fe^{3+/2+}$ with adsorption of bismethylstyrylbenzene (BMB), methylene blue (MB), and anthraquinone 2,6-disulfonate (AQDS); (D) $Ru(NH_3)_6^{3+/2+}$ with AQDS. Reprinted with permission from ref 121. Copyright 1995 American Chemical Society.

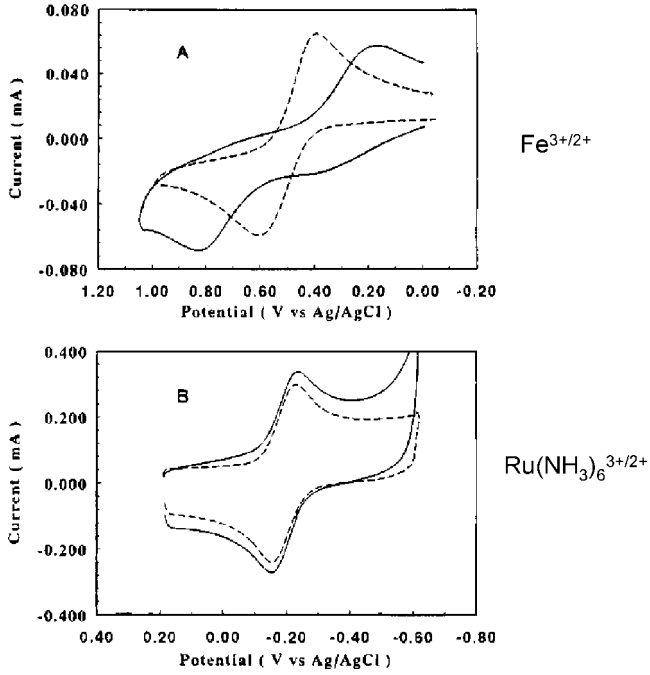

Figure 22. $Fe^{3+/2+}$ voltammetry in 0.1 M $HClO_4$ on polished GC before (dashed lines) and after (solid lines) reacting surface carbonyl groups with DNPH. Reprinted with permission from ref 121. Copyright 1995 American Chemical Society.

vacuum heat treated (ΔE_p =439 mV), and Ar^+ sputtered (900 mV). Electrochemical oxidation of the GC surface greatly decreases ΔE_p, for example, from 900 to 80 mV for the Ar^+-sputtered surface, indicating that surface oxides significantly accelerate electron transfer. Since a polished GC surface has significant surface oxides, it exhibits faster kinetics than the low oxide surfaces, even though it may not be as clean. However, as shown in Figure 21A,C, adsorption of a monolayer of an organic molecule on top of the polished surface significantly increases the peak separation, presumably by obscuring oxygen-containing catalytic sites. We conclude that $Fe^{3+/2+}$ and other aquated transition metals like $Eu^{3+/2+}$ and $V^{+3/+2}$ have electron transfer rates that depend strongly on surface oxide level, in contrast to $Ru(NH_3)_6^{3+/2+}$, ascorbic acid, and $Fe(CN)_6^{3-/4-}$.

The variation of electron transfer rates with surface oxide coverage implies an electrocatalytic mechanism for $Fe^{3+/2+}$, and its absence with $Ru(NH_3)_6^{3+/2+}$ indicates that it is more than an electrostatic effect of possible anodic functional groups. The catalysis may be probed further with reagents that react with particular oxygen-containing functional groups, and observation of the effect of these reagents on electron transfer kinetics. Two such reagents are dinitrophenylhydrazine (DNPH), which reacts with surface carbonyl groups, and dinitrobenzoylchloride (DNB), which bonds to surface hydroxyl groups. The products of the reactions of these materials with carbon surfaces are observable with Raman spectroscopy and XPS,[106,107] with the Raman scattering being enhanced by the resonance Raman activity of the surface adduct. As shown in Figure 22, the ΔE_p for $Fe^{3+/2+}$ on polished GC increases dramatically upon DNPH treatment, while DNB had little effect on $Fe^{3+/2+}$kinetics. Since DNPH binds specifically to surface carbonyl groups, the sensitivity of $Fe^{3+/2+}$ kinetics to DPNH treatment implies a specific surface interaction between carbonyl groups and $Fe^{3+/2+}$ as the electrocatalytic event. Observation of the DNPH adduct with Raman spectroscopy revealed a linear dependence of the $Fe^{3+/2+}$ rate with the coverage of surface carbonyl groups.[121] Furthermore, intentional adsorption of a molecule containing carbonyl groups accelerates $Fe^{3+/2+}$ electron transfer, as shown for anthraquinone in Figure 21B, but it has no effect on $Ru(NH_3)_6^{3+/2+}$ (Figure 21D). An inner sphere complex of $Fe^{3+/2+}$ has been proposed,[120,121] although hydrogen bonding between the water of hydration of $Fe^{3+/2+}$ and a surface carbonyl is also possible.[126] The effect of DNPH and DNB on the kinetics of a particular redox

Table 3. Electrode Kinetics for $Fe^{3+/2+}$ and for $Eu^{3+/2+}$ on Carbon Materials[a]

electrode	ΔE_p for $Fe^{3+/2+}$ (mV)	ΔE_p for $Eu^{3+/2+}$ (mV)	atomic O/C ratio	ref
HOPG	1062	936	≪0.01	120
HOPG/ECP[b]	162	372		120
GC, polished in H_2O	150	428	0.10−0.14	120, 122
GC, polished in cyclohexane	352		0.04	122
GC, fractured	186	509		120
GC, fractured + ECP	93	70		120
GC, polshed + Ar^+ sputtered	908		<0.01	122
GC, polished + Ar^+ + ECP	80			122
GC, polished + DPNH	670			122
GC, polished + BMB	506			122
GC, polished + anthraquinone	100			122
GC, vacuum heat treatment	439		0.016	122, 409
PPF, IPA/AC	647			99
electron cyclotron resonance carbon film	587			24
boron doped nanocrystalline diamond	679			30

[a] 0.2 M $HClO_4$, 0.2 V/s. [b] Electrochemical pretreatment by anodization.

reaction may be used as additional breakpoints in the "tree" of Figure 19.

To summarize the current section, it should come as no surprise that the extent to which surface chemistry affects electron transfer rates is a strong function of the redox reaction involved. While "activation" may be a useful term for treatments that increase electron transfer rates, it should not be assumed that all redox systems will be "activated" equally. Since electrochemical reactions are inherently heterogeneous, they will always depend to some degree on the nature of the electrode surface. If a specific surface interaction is identified as catalytic for an electrochemical reaction, then the electrode may be tailored to maximize the extent of the resulting catalysis.

3.6. Carbon Electrode Surface Preparation

Surface preparation is of obvious importance for any heterogeneous process like electrochemistry, and the literature on carbon electrodes is particularly rich. The three allotropes of carbon, the wide variation of surface structure and functional groups, and the propensity of carbon to adsorb adventitious impurities make the story complex, but in many cases surface preparation may be exploited to achieve selectivity or modify electrode kinetics. The extensive literature on electrode polishing, laser and electrochemical pretreatment, vacuum heat treatment, etc, was reviewed in some detail in the mid 1990s,[3,119,142] so the current discussion will briefly summarize the salient points from that period and emphasize recent procedures and materials. In many comparisons of preparation procedures, the $k°$ observed for $Fe(CN)_6^{3-/4-}$ in aqueous 1 M KCl is used as a benchmark of electrode "activity". As noted in section 3.4, $Fe(CN)_6^{3-/4-}$ is far from an "ideal" outer-sphere redox system, and in fact, its kinetics depend strongly on the state of the surface. However, this sensitivity makes it a useful monitor of variations in surfacecondition, and it has been used for over three decades as a benchmark redox system. Preparation methods will be presented in three groups: polishing and cleaning, vacuum treatments, and activation procedures, using both $Fe(CN)_6^{3-/4-}$ and $Ru(NH_3)_6^{3+/2+}$ kinetics as benchmarks of electrochemical reactivity.

3.6.1. Polishing and Cleaning

Polishing has a long history for carbon materials and remains the most common preparation for carbon electrodes used in electrochemistry. Perhaps the most commonly used carbon electrode material is glassy carbon, most often polished with silicon carbide paper followed by a series of alumina slurries with successively smaller particles size, typically finishing with 0.05 μm. Past reviews should be consulted for polishing details,[3,119,142] but a few lessons from the past deserve repetition. First, a "course" polish with silicon carbide sandpaper results in a relatively rough but reactive surface. In the case of carbon fiber microelectrodes, the "coarsely polished" surface is adequate for many purposes, and potential contamination from polishing compounds is minimized.[143] Second, many commercial diamond and alumina polishing slurries contain deagglomerating agents, which can seriously affect electrode reactivity due to adsorption on the carbon surface. Good practice dictates the use of pure, dry alumina powder slurried with ultrapure water (e.g., Barnstead "nanopure"). Third, the surface oxide level can be significantly modified by polishing and by the liquid used to make the abrasive slurry. As shown in Figure 11, a water/alumina slurry yields a surface O/C atomic ratio on GC of about 10−15%, while the same surface polished with cyclohexane/alumina has an O/C ratio below 4%.[95] Fourth, it is good practice to sonicate after polishing, but the purity of the sonication liquid is important. Sonication may remove particles, but it may also permit adsorption of impurities from the sonication bath.[144] Fifth, polishing generally results in a residue of both polishing material and carbon particles, which is difficult to remove and can adversely affect electrochemical reactivity.[3,144] As noted in section 3.6.3.3, an effective method to remove such debris is a short anodization pulse in basic media.[145] As indicated by several of the entries in Table 2, variations in polishing procedure result in reported $k°$ values for $Fe(CN)_6^{3-/4-}$ in 1 M KCl from <0.001 to 0.14 cm/s. Such variations are less pronounced for outer-sphere redox systems such as $Ru(NH_3)_6^{3+/2+}$, but the $Fe(CN)_6^{3-/4-}$ results indicate the importance of surface condition to reactivity.

A more recent preparation procedure is simpler than polishing and also amenable to electrodes of any shape and size. When a carbon electrode is treated with an organic solvent containing activated carbon (AC), the much higher surface area of the AC effectively "getters" the impurities

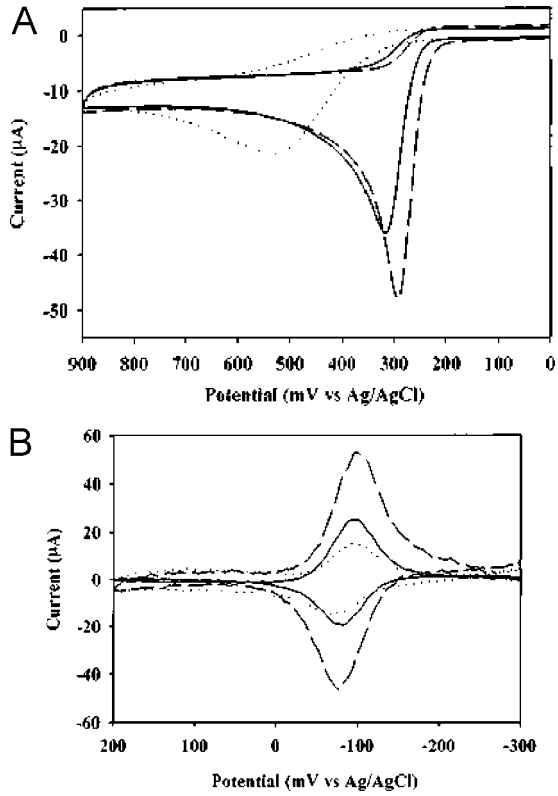

Figure 23. Voltammograms from GC electrodes pretreated by polishing (solid curve), isopropyl alcohol (dotted), and isopropyl alcohol in the presence of activated carbon (dashed): (A) 1 mM ascorbic acid in 0.1 M H_2SO_4; (B) 40 μM anthraquinone 2,6-disulfonate in 0.1 M $HClO_4$. Reprinted with permission from ref 146. Copyright 1999 American Chemical Society.

off the electrode surface.[146] Without activated carbon, organic solvents can significantly decrease the reactivity of a carbon electrode, due to adsorption of large trace organics from the solvent. A combination of AC and sonication produces a surprisingly large increase in electron transfer rates and adsorption of carbon electrodes. Figure 23A shows the effect of isopropanol/AC on the oxidation of ascorbic acid, with the solid curve being the voltammogram on a carefully polished GC electrode.

Treatment with reagent grade isopropanol (IPA) alone causes a large shift toward more positive potentials, reflecting a reduction in electron transfer rate presumably caused by adsorption of impurities in the isopropanol. Treatment with isopropanol/AC but no additional polishing shifts the peak potential to a value more negative than that on the polished surface.[146] A quantitative indication of the solvent/AC effect is shown in Figure 23B for the adsorption of anthraquinone 2,6-disulfonate (AQDS). The increase in AQDS adsorption after CH_3CN/AC treatment by a factor of 2 implies that about half of the polished surface was occupied by adventitious adsorbates, which prevented AQDS adsorption. For the case of dopamine oxidation in mild acid, the observed ΔE_p was smaller for the isopropanol/AC treated GC surface than for careful polishing, and IPA/AC treatment restored the small ΔE_p after deactivation with a surfactant solution or by exposure to ambient air for a week.[146] A particularly beneficial application of solvent/AC cleaning involves the exposed cylindrical sides of carbon fibers for in vivo monitoring of neurotransmitters.[11,13,147] Such electrodes cannot be polished and are quite fragile, but IPA/AC treatment enhances the adsorption and voltammetric response of catecholamine neurotransmitters such as dopamine and norepinephrine.

Boron-doped diamond adsorbs most chemical species more weakly than GC or carbon fibers, due to its low polarizability and relative lack of local dipoles. The relatively large, polar impurities often present in electrochemical solvents at trace levels are less prone to adsorb on BDD compared with graphitic carbon electrodes and hence are less likely to reduce electrochemical reactivity. BDD surfaces are usually microscopically rough and not readily amenable to conventional polishing. However, BDD electrodes exhibit fast electron transfer right out of the reactor in which they are made and may be exposed to ambient air for weeks without significant decrease in electrochemical reactivity.[30,53] Purified IPA has also been used for cleaning BDD surfaces before electrochemical measurements.[53]

3.6.2. Vacuum and Heat Treatments

The thermodynamic stability of carbon−oxygen bonds makes most carbon materials susceptible to air oxidation, leading to the surface oxides described in section 3.2. These oxides are hard to remove and in fact can be beneficial for certain redox reactions involving adsorption or hydrogen bonding to surface oxide functional groups. Conventional polishing generally increases the level of surface oxides, as well as disordering both the oxides and the carbon microstructure. Several vacuum procedures have been developed to remove oxides from carbon surfaces, in order to study the behavior of "oxide-free" carbon. An early example was that of Mazur et al., who heated carbon fibers to 1020 °C in a 10^{-5} Torr vacuum, then exposed the cooled fiber to O_2 or several organic gases.[148] The reactions of the "oxide-free" carbon surface with olefins implied that heat treatment resulted in unsatisfied valences or "dangling bonds" on the surface, which underwent free radical addition reactions to irreversibly adsorb molecules such as allene and vinyl bromide. Vacuum heat treatment (VHT) of GC at 725 °C and $<2 \times 10^{-6}$ Torr reduced the surface O/C ratio from 0.25 to 0.05 and resulted in a very electrochemically active surface with a $k°$ for the $Fe(CN)_6^{3-/4-}$ system of 0.14 cm/s.[144,146]

More recent vacuum treatments are derived from chemical vapor deposition (CVD) techniques developed for fabricating diamond films, including BDD. A hydrogen plasma formed from H_2 with a hot tungsten filament or microwave heating contains significant concentrations of H atoms, which react with surface oxides and etch the carbon surface. When applied to GC electrode surfaces, a hydrogen plasma roughens the surface slightly and decreases the surface O/C ratio to below 0.02.[95] As noted previously in section 3.1.2, the C−H termination of the GC structure resists surface oxidation by air much better than the VHT surface, with the oxide level remaining below 4% after a week in air. The unsatisfied valences on the carbon surface following VHT are more reactive to dioxygen and water than the C−H terminated surface, resulting in the behavior illustrated in Figure 5.

As described later in section 4.1, pyrolysis of an organic polymer photoresist material can be used to make an electrochemically interesting carbon surface, PPF (pyrolyzed photoresist film).[99,149] Heating to 1100 °C in a 5% H_2/N_2 atmosphere decreased the surface O/C ratio to <2%, which then increased to ~6% after 4 days in air. The rate of increase of the O/C ratio on PPF was significantly slower than that

on GC heat treated similarly in H_2/N_2, but faster than that on H-terminated GC made in a hydrogen plasma.[99] We infer that pyrolysis in a hydrogen atmosphere results in a partially H-terminated surface, but the more aggressive hydrogen plasma reacts with more of the unsatisfied valences on the carbon surface.

Sputtering with high-energy (>500 eV) Ar^+ is commonly used in surface science to remove surface layers from samples in UHV, most commonly on metals such as Pt, Ru, etc. Sputtering of glassy carbon reduces the O/C ratio to below 1% and can result in an electrochemically active surface.[122] However, Ar^+ sputtering damages the carbon microstructure, and there is no effective annealing procedure known for materials like GC and graphite. Given that sputtering generally requires an expensive vacuum system and Ar^+ beam and also leads to a disordered material, it is not recommended for routine electrochemical applications.

3.6.3. Carbon Electrode Activation

The term "activation" has been used frequently to describe procedures for increasing the reactivity of carbon electrodes, often for the purpose of detecting a specific analyte. It is more frequently encountered with carbon electrodes compared with metals, since the propensity of carbon to adsorb impurities leads to electrode surfaces with decreased activity unless great care is taken to avoid adsorption. As discussed in section 3.5, the observed electron transfer kinetics for different redox systems depend on several different surface properties, so "activation" can involve more than one mechanism in terms of its effects on the electrode surface. For "outer-sphere" redox systems such as $Ru(NH_3)_6^{3+/2+}$, the maximum electron transfer rate is observed for a clean surface, with little or no dependence on particular surface sites or functional groups (see Table 2). The $Fe(H_2O)_6^{3+/2+}$ couple, however, exhibits kinetics strongly dependent on the presence of surface oxides, particularly carbonyl groups (Table 3). Good practice dictates that one should start with a clean electrode surface before kinetic measurements or surface modification, but beyond that, "activation" may entail formation of particular active sites on the carbon surface that "activate" redox systems to varying degrees depending on their redox mechanisms.

3.6.3.1. Surface Cleaning. Many "activation" procedures are in fact cleaning steps, in many cases employed to remove surface layers resulting from handling or impure materials used for polishing. Using GC as a representative carbon electrode material, we noted in section 3.2 that "fracturing" directly in the electrolyte solution of interest exposes a pristine GC surface, and should represent the cleanest possible GC electrode. Using the $Fe(CN)_6^{3-/4-}$ system as a "surface-sensitive" benchmark, we note from Table 3 that all polishing procedures result in lower observed electron transfer rates than the fractured surface, some by 2 or more orders of magnitude. Since fracturing is not practical on a routine basis for ordinary GC electrodes, solvent/AC cleaning and ultraclean polishing are reasonably successful alternatives. With carbon fibers, cutting the fiber immediately before use or the "coarse" polishing described earlier are similar to "fracturing" in terms of their effects on the carbon surface and would be expected to yield similarly clean surfaces.[143,150]

3.6.3.2. Laser Activation. It was first reported in 1984[151] that an energetic laser pulse irradiating a carbon electrode directly in the electrolyte of interest had dramatic effects on the electron transfer rates observed for the oxidation of ascorbic acid and phenol. Since the initial report, the mechanism of the phenomenon has been explored in some detail,[51,70,96,152–155] as have electroanalytical applications in voltammetry[156–161] and amperometric detectors for liquid chromatography.[162] Laser-activated graphite, glassy carbon, and carbon fiber electrodes have been characterized with Raman, XPS, STM, and SEM to reveal changes in microstructure and surface composition.[51,69,70,73,154,163] As shown in Table 2, laser-activated GC and carbon fiber electrodes exhibit the highest $k°$ values for $Ru(NH_3)_6^{3+/2+}$ and $Fe(CN)_6^{3-/4-}$ for carbon electrodes, as well as fast kinetics for organic systems such as ascorbic acid and dopamine. The process usually involves a 7−20 ns laser pulse from a Nd:YAG (1064 nm) or nitrogen (337 nm) laser, with peak power density in the range of 10−100 MW/cm^2. The rapid thermal expansion and local heating[154] cause desorption of adsorbates and, at higher power density, can cause disruption of the carbon microstructure.[70,164] For the case of glassy carbon and carbon fiber electrodes, power densities up to 25 MW/cm^2 do not cause observable morphological changes on the carbon surface yet produce dramatic acceleration of electron transfer kinetics.[51,154] The mechanism of laser activation includes at least three effects, whose importance depends on the power density and the type of carbon electrode examined, and to a lesser extent on the laser wavelength and optical penetration depth.[8] Below 25 MW/cm^2, the thermal transient resulting from laser light absorption desorbs impurities and produces a cleaner, more reactive electrode surface. Laser irradiation above 25 MW/cm^2 can disrupt the carbon microstructure, for example, by thermal stress to the graphite planes to produce a higher density of edge planes.[69,70] In addition, the oxide coverage of the electrode may be altered during the laser pulse, particularly if dioxygen is present in the solution.[165,166]

In addition to providing major increases in electron transfer rates and electrode surface reactivity, laser activation has some practical advantages for use in electrochemical and analytical applications. It may be used in situ by directing the laser through a cell wall or window, thus obviating the need for electrode removal or cell disassembly. It is fast and repeatable, thus resulting in a "renewable" carbon electrode surface amenable to pulse voltammetry.[156,162] Electrodes deactivated by deposition of electrolysis products (i.e., "fouling") are easily reactivated, in situ. The laser beam may be used to microfabricate electrode surfaces by removal of an intentional film on the electrode surface to make microelectrode arrays.[157] Kuhr et al. used interference patterns from a 325 nm He−Cd laser to photopattern and activate glassy carbon surfaces on a micrometer scale and for photoablation of enzymes immobilized on carbon and silica surfaces.[167,168] Laser activation is applicable to microscopic or nonplanar electrodes not amenable to polishing, such as carbon fibers and microdisks.[158–161,166] While these positive aspects of laser activation have been demonstrated to be useful for many applications of carbon electrodes, the technique has not been used widely, presumably due to the requirement for a pulsed laser and the associated expense and safety concerns.

3.6.3.3. Electrochemical Pretreatment (ECP). Electrochemical oxidation or reduction in various media has long been used to "activate" carbon electrodes, and the many effects of ECP were reviewed in some detail in 1991.[3] Although most of the effects of ECP on surface structure and electrochemical activity were recognized at that time,

there has been a continuous stream of reports in recent years, including some significant new information.[108–110,160,169–175] A brief summary of ECP effects will be presented here, followed by some examples from the literature since 1991. As shown in Figure 18, polarization of a carbon electrode outside the electrochemical window yields significant current, which results from reactions both of the electrolyte and of the electrode itself. ECP is most commonly an oxidation for some period of time past the positive limit apparent in Figure 18, generally in the range of 1−2 V vs SCE. Depending on the duration of anodization, the carbon surface can be disrupted significantly, to the point of forming a surface film of "electrogenerated graphitic oxide" (EGO). This film has an O/C ratio above 0.2, contains many anionic sites, and is permeable to solvent and small molecules.[3] Carbon electrodes subjected to ECP can have dramatically different reactivity and selectivity compared with the same electrodes before ECP, particularly for charged redox systems or for those that are catalyzed by surface oxides. As shown in Table 3, the observed $k°$ for $Fe^{3+/2+}$ is much higher on an ECP-treated GC surface, due to the generation of carbonyl groups during anodization.[120] ECP has also been used for decades to impart selectivity for cationic redox systems such as dopamine over anionic interferents like ascorbate, due to electrostatic interactions with the anionic EGO film.[110]

Examples of more recent applications of ECP for carbon electrodes include oxidation of nucleotides,[160,172,175] oxygen reduction,[173] immunoassay,[174] and modification of protein adsorption.[176] A short anodization in basic solution removed polishing debris and exposed a very clean pyrolytic carbon film, as judged by scanning probe microscopy.[145,170] EGO is hydrolyzed above approximately pH 10, so a surface film does not form on carbon during anodization in basic solution. As will be described in section 4.1, anodization at elevated pH can be used to microfabricate reactive sites on carbon surfaces.[171] Passage of a high current density through carbon fibers in an electrolyte solution has an extraordinary effect on the fiber morphology, generating a very high surface area with an apparent capacitance of ~4000 $\mu F/cm^2$, more than 100 times the typical values for GC and carbon fibers.[108–110,169] A combination of cation selectivity and enhanced adsorption created strong selectivity for catechols, particularly the cationic dopamine.

For the case of diamond electrodes, electrochemical pretreatment can cause significant increases in the levels of surface oxide functional groups, with attendant effects on the electron transfer kinetics for systems that interact with the surface.[30,53] These electrochemical effects are described in more detail in section 4.2.

3.7. Summary and Generalizations

Considering sections 2 and 3 together, some generalizations are useful regarding electrochemical reactivity of carbon electrodes. First, there must be sufficient electronic states in the electrode material at energies near the $E°$ of the redox system(s) of interest. The density of electronic states is determined both by the carbon microstructure and by surface states from defects and termination. A low DOS can significantly decrease the observed electron transfer rate, as is the case with lightly doped diamond or HOPG electrodes. Second, the electron transfer and adsorption reactivity of graphitic carbon electrodes is a strong function of the surface coverage of edge relative to basal plane graphite. Edge sites are more reactive to ET, adsorption, and chemical modification, and in some cases the observed $k°$ and capacitance can be quantitatively correlated with edge plane coverage.[50,51,177,178] Third, redox systems differ dramatically in their sensitivity to the state of the carbon electrode surface, due to differences in their redox reaction mechanisms, ionic charge, etc. $Ru(NH_3)_6^{3+/2+}$, anthracene, and ferrocene are examples of nearly ideal redox systems, which are relatively insensitive to surface oxides and adsorbates, while $Fe^{3+/2+}$ and dopamine are dependent on particular surface sites that participate in an electrocatalytic mechanism. It is unwise and often incorrect to discuss "activation" of a carbon electrode without stating the redox reaction used as the indicator of electrode reactivity. Fourth, carbon materials have more variety in both bulk and surface structure than metals, and electrode preparation is particularly important for achieving reproducible electrochemical behavior. Even the most common preparation procedures, such as polishing, significantly modify the surface structure and chemistry and can have dramatic effects on reactivity, adsorption, etc.

4. Advanced Carbon Electrode Materials

As noted in the Introduction, several fundamentally novel carbon materials have come into use for electrochemistry during the last 15 years. Some of these are new manifestations of materials structurally similar to glassy carbon, such as pyrolyzed photoresist, while others are completely different allotropes of carbon, such as diamond and the fullerenes. Although there is some overlap in the classification of these recently developed materials as electrode materials, they will be subdivided into microfabricated carbon, conducting diamond, fibers and nanotubes, and carbon composites. As each electrode material is discussed, the relationships between the general properties described in sections 2 and 3 and the electrochemical behavior of the material will be considered.

4.1. Microfabricated Carbon Thin Films

The vast majority of carbon electrodes are made from bulk materials such as graphite or glassy carbon, which are shaped and packaged to expose the electrochemically active electrode surface. "Microfabricated" is used here to mean that the electrode is formed from a gas or liquid precursor, often as a thin film and occasionally in a pattern with micrometer-scale dimensions. Pyrolysis of hydrocarbons onto metal or quartz surfaces has been used fairly extensively to make carbon films of arbitrary shape, for example, as detectors for capillary electrophoresis,[179–181] and on ceramic supports.[182,183] Reactive precursors may be employed to reduce the pyrolysis temperatures and to incorporate heteroatoms or metals.[19,21,184] The properties of these materials depend strongly on their thermal history, particularly maximum preparation temperature, and the presence of metal "graphitization" catalysts such as nickel and iron. They are generally less ordered than most types of graphite but exhibit moderate electron transfer rates for both catechols and $Fe(CN)_6^{3-/4-}$.

A more recent variant of pyrolytic carbon with distinct properties for electrochemistry is pyrolyzed photoresist film (PPF),[99,149,185–190] although the process was reported for photolithography in 1985[191,192] and for microelectromechanical fabrication in 1997.[193] Many photoresists are based on a phenolic resin (e.g., "Novolac") and are available commercially (e.g., AZ4330, AZ Electronic Materials, Somerville, N.J.). These materials are designed to be spin-coated

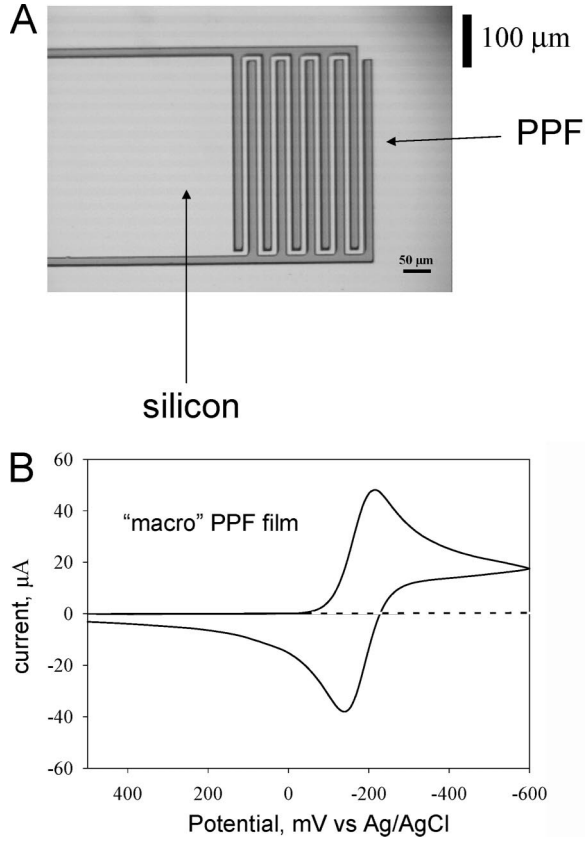

Figure 24. (A) Photomicrograph of pyrolyzed photoresist film pattern on silicon substrate and (B) voltammetry of $Ru(NH_3)_6^{3+/2+}$ (1 M KCl, 0.2 V/s) on unpatterned PPF (solid line) and on uncoated Si substrate (dashed). Reprinted with permission from ref 99. Copyright 2001 American Chemical Society.

onto silicon or quartz, then patterned if desired with standard photolithographic techniques. Pyrolysis in a reducing atmosphere, typically 5% H_2 in N_2, to maximum temperatures of 700−1100 °C removes nearly all of the heteroatoms and a significant fraction of the photoresist weight and yields quite pure sp^2 hybridized carbon. A micrograph of a PPF pattern formed lithographically on silicon is shown in Figure 24, along with a voltammogram of $Ru(NH_3)_6^{3+/2+}$ on a large area (∼5 mm^2) unpatterned PPF film. The resistivity of the photoresist decreases from $>10^{15}$ Ω·cm to $\sim10^{-2}$ Ω·cm, with the largest drop in resistance commencing at about 600 °C.[149,186] Laser pyrolysis may also be used to form patterns in the photoresist if desired.[194] Raman spectroscopy and TEM reveal that PPF formed at 1000−1100 °C is structurally similar to GC, with a resistivity of ∼0.006 Ω·cm, comparable to that of GC (∼0.005 Ω·cm).[149] AFM of the PPF surface indicates that it is very flat, with an rms roughness <0.5 nm and very few observable defects over areas larger than at least tens of micrometers. Although the flat surface implies some degree of plasticity during heat treatment, the photoresist does not flow during pyrolysis, and the lithographic pattern is preserved to a resolution below 1 μm. The PPF surface structure as investigated with scanning probe microscopy is featureless down to a resolution of ∼1 nm,[99,195−197] but its origin from a polymer implies that the surface consists of both basal and edge graphitic planes, much like GC. Finally, although PPF has a resistivity only slightly greater than GC, its usual presence as a thin film can create significant ohmic potential losses if the substrate supporting the PPF film is nonconducting.[99,149]

Although PPF is structurally and electronically similar to GC, it has several distinct properties of significant utility in electrochemical applications. The ability to photolithographically pattern PPF permits fabrication of microstructures such as interdigitated microelectrode arrays,[186,198] microcantilevers,[193] and even complex microstructures for batteries and micromechanical systems.[199] The extreme flatness of PPF is essential for applications in molecular electronics[200−202] and for investigations with scanning probe techniques such as AFM.[195,196] The PPF surface is amenable to surface modification by various routes, particularly diazonium reduction[197] and soft lithography,[203] as described in section 5.1. As noted already in Figure 11 and associated text, the surface O/C ratio of PPF is quite low, and many but not all of the surface carbons are likely to be H terminated. PPF may be formed on irregular shapes such as microelectrodes[204] and may also be made sufficiently thin to be optically transparent for spectroelectrochemistry.[58,59,89]

In terms of electrochemical reactivity for common redox systems, PPF is similar but not identical to GC. Polishing PPF would be counterproductive, so it is generally used right out of the pyrolysis oven or after solvent cleaning as described in section 3.6.1. As noted in Table 2, the $k°$ for $Ru(NH_3)_6^{3+/2+}$ is somewhat slower than that on clean GC, with at least some of the difference due to the absence of microscopic roughness on PPF. The kinetics of $Fe^{3+/2+}$ are much slower on PPF than on GC, due to the lack of surface oxides (Table 3). The lack of oxides and their associated surface dipoles makes PPF less prone to adsorption than GC, thus leading to slower electron transfer rates for organic systems that are catalyzed by adsorption, such as dopamine oxidation.[99,126] PPF may be electrochemically oxidized to increase electron transfer reactivity toward redox systems catalyzed by surface oxides.[99] To date, the majority of electrochemical applications of PPF have used relatively large areas, generally greater than a few micrometers. However, pyrolysis of polymer precursors can also be used to make the micromechanical structures noted earlier,[193,199] and block copolymer precursors can lead to carbon nanoparticles and arrays.[205,206]

Thin films of carbon formed in a vacuum have long been used for electron microscopy and to protect disk drive heads. Electron beam deposition of carbon for electrochemistry was first reported in the 1970s,[56,87] and reconsidered recently.[88] The initial objective was a carbon film sufficiently thin to be transparent for use with spectroelectrochemical techniques in transmission mode. A high-energy electron beam was focused onto graphite pellets in a $\sim10^{-6}$ Torr vacuum to generate carbon atoms and fragments, which then deposit onto a heated quartz plate. Carbon films 28 nm thick exhibited well-defined voltammograms for $Fe(CN)_6^{3-/4-}$; however the large peak separation of ∼200 mV at a scan rate of 0.01 V/s was attributed in part to significant ohmic potential error within the thin film.[87] The films had optical absorbances of 0.4−0.8 absorbance units in the range of 300−800 nm. The films were significantly less conductive when deposited onto a room temperature substrate. Electron beam deposition has become quite common for metals and refractory materials since these initial papers were published and is now readily available commercially. Blackstock et al. deposited carbon onto H-terminated heavily doped silicon at room temperature in order to reduce ohmic potential errors.[88] The carbon films were extremely flat, exhibiting an rms roughness of 0.07−0.11 nm for a 7 nm thick carbon

film on a Si substrate with a roughness of 0.06 nm. Electron transfer reactivity of carbon films formed at room temperature on silicon approached Nernstian behavior at moderate scan rates, with a $k°$ value for $Ru(NH_3)_6^{3+/2+}$ of 0.046 cm/s (Table 2). Heat treatment in 5% H_2/N_2 at 1000 °C increased the ordering of the carbon, as judged by Raman spectroscopy, and also produced changes in the voltammograms. The carbon film may be deposited through a shadow mask or a photoresist pattern, so small and complex electrodes with features down to ~1 μm may be microfabricated. Given that electron-beam deposition is expensive and cumbersome compared with many carbon electrode preparation techniques, it will likely be useful only when special properties such as a very flat surface are required.

A recent and more exotic method for carbon film formation is electron cyclotron resonance plasma sputtering.[24,132,207] The deposited carbon was also quite flat (~0.07 nm) and appeared to be amorphous, containing a significant fraction of sp^3 hybridized carbon. The material had some of the properties of boron-doped diamond, particularly stability and resistance to electrode fouling. Voltammetry of several organic and biochemical redox systems was demonstrated, including nucleotides, phenols, and NADH.[24,132] The voltammetric detection limit reported for nonylphenol was 50 nM, with a linear range of 0.125−10 μM.[207] Electron transfer rates for $Ru(NH_3)_6^{3+/2+}$ and $Fe(CN)_6^{3-/4-}$ were comparable to those observed on GC and BDD but were significantly slower for dopamine and $Fe^{3+/2+}$, as shown in Tables 2 and 3. The authors concluded that the slow rates for dopamine and $Fe^{3+/2+}$ were due to weak interactions with the carbon surface, compared with GC.[24]

4.2. Boron-Doped Diamond for Electrochemistry

The fabrication and electronic properties of BDD were discussed in section 2.1.2, and we now turn to its behavior as an electrode material. Many publications from at least five laboratories worldwide have described electrochemical applications of BDD,[36,61,63,131,208–219]and there are now several commercial suppliers of diamond electrodes for electrochemical use.[34] A comprehensive review of electrochemical applications of diamond and related materials appeared in 2004.[30] BDD electrodes have been made in a wide variety of shapes and sizes, including ultramicroelectrodes,[215,220–222] large single crystals,[131,223] nanocrystalline films,[32,208,224,225]and optically transparent electrodes.[61–63]

BDD and nanocrystalline diamond are not only structurally distinct from graphitic and fullerene electrode materials, but they also have some advantageous electrochemical properties.[225] The much greater chemical stability of BDD compared with graphitic or fullerene forms of carbon is a major advantage over the more common sp^2 hybridized carbon electrode materials. In addition to providing a long lifetime, the low chemical reactivity results in a wider electrochemical potential window and the ability to carry out normally difficult reactions such as ozone generation[217] and the oxidation of aliphatic amines.[226] The significantly weaker adsorption of most solution species on BDD makes diamond electrodes more resistant to "fouling", and they can be used after standing in ambient air for long periods without surface pretreatment. As already noted in section 2.3, diamond is sufficiently optically transparent in much of the UV−vis and infrared regions to permit spectroelectrochemistry in transmission or internal reflection modes.

Recent reports of microscopic characterization of conductivity and redox activity of both hydrogen-[208] and oxygen-terminated[227] BDD electrodes indicate that the materials are electrically heterogeneous, with both conductivity and electron transfer rates varying across the BDD surface. Conducting-tip AFM, scanning electrochemical microscopy, and cathodoluminescence permitted such heterogeneities to be observed near grain boundaries and across microcrystallite facets. Both papers noted that electron transfer reactivity for $Ru(NH_3)_6^{+3/+2}$ was observed over the entire BDD surface but that variations in conductivity and doping level caused local variations in the electron transfer rate.[208,227] While such variations are usually averaged out for BDD electrodes larger than the crystallite size of a few micrometers, the user should be aware that the materials are not as electronically homogeneous as more commonly used carbon electrodes such as glassy carbon.

The electrochemical reactivity of diamond electrodes is best considered in the context of the various classes of redox systems described in section 3.5 and summarized in Figure 19. The simplest of these is the "outer-sphere" or "surface-insensitive" group, which includes $Ru(NH_3)_6^{3+/2+}$ and $IrCl_3^{3-/4-}$. As shown in Figure 25B,C, these two couples show classical voltammetric waves on BDD, qualitatively similar to those observed on glassy carbon. The rate constant for $Ru(NH_3)_6^{3+/2+}$ is somewhat slower on BDD than on GC, but higher $k°$ values have been reported on nanocrystalline, N-doped diamond (Table 2). As noted in sections 2.2 and 3.1, most diamond materials have a lower density of electronic states than graphitic carbon, and this factor may result in somewhat slower kinetics for outer-sphere systems. However, the observation that BDD exhibits reasonably fast kinetics for redox systems with $E°$ potentials spanning a wide range of the electrochemically useful scale (Figure 15) indicates that BDD does not have significant gaps in the DOS distribution.[30] The Swain group have reported many kinetic results for BDD under standard conditions and provide a concise comparison of several common organic and inorganic redox systems.[30,53]

A second class of redox systems noted in Figure 19 is "surface-sensitive" and is much more dependent on the state of the electrode surface. In the case of diamond electrodes, the surface may be affected not only by oxides and adsorbed impurities but also by nondiamond carbon, surface termination, and grain boundaries.[30,53] An illustrative example is shown in Figure 26 for ascorbic acid oxidation on microcrystalline BDD in 0.1 M $HClO_4$. Anodization of the BDD at progressively positive potentials causes a major positive shift in the observed oxidation peak potential, and the shift may be reversed by rehydrogenation of the BDD surface. Chloride oxidation to chlorine is an electrocatalytic reaction, which is very slow on BDD due to the lack of adsorption sites. The nitrogen-incorporated amorphous tetrahedral carbon variant of diamond contains such sites, and the oxidation of chloride in 2 M HCl proceeds at a potential approximately 0.5 V lower than that on BDD.[35] In addition, the taC:N material was very stable during Cl_2 generation, despite the normally corrosive nature of chlorine evolution.

The electrochemistry of organic systems on diamond depends on the nature of surface interactions, particularly adsorption.[30] Methyl viologen voltammetry on BDD is quite similar to that on GC, since there is little or no adsorption or interaction with catalytic sites. However, dopamine oxidation is significantly slower on diamond than on GC, most likely because of weak adsorption.[53] As noted in section

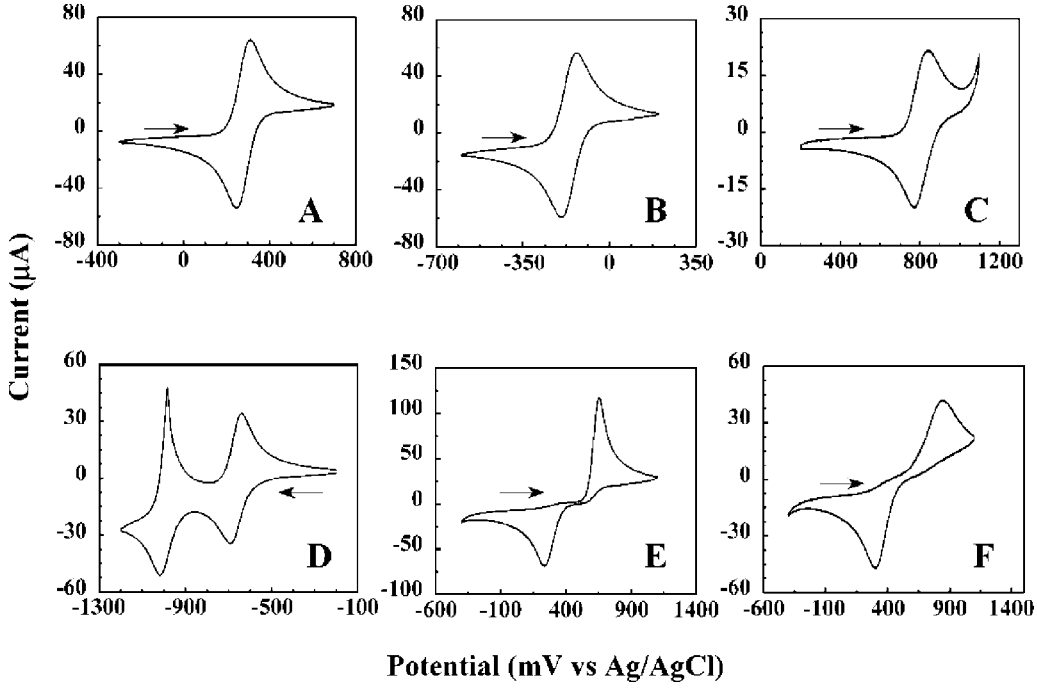

Figure 25. Voltammetry on boron-doped nanocrystalline diamond electrodes (0.2 cm^2 area, 0.1 V/s), for (A) 1.0 mM $Fe(CN)_6^{3-/4-}$, (B) 1.0 mM $Ru(NH_3)_6^{3+/2+}$, (C) 0.25 mM $IrCl_6^{2-/3-}$, (D) 0.50 mM methyl viologen in 1 M KCl, (E) 1.0 mM 4-*tert*-butylcatechol, and (F) 1.0 mM $Fe^{3+/2+}$ in 0.1 M $HClO_4$. Reprinted with permission from ref 225. Copyright 2003 American Chemical Society.

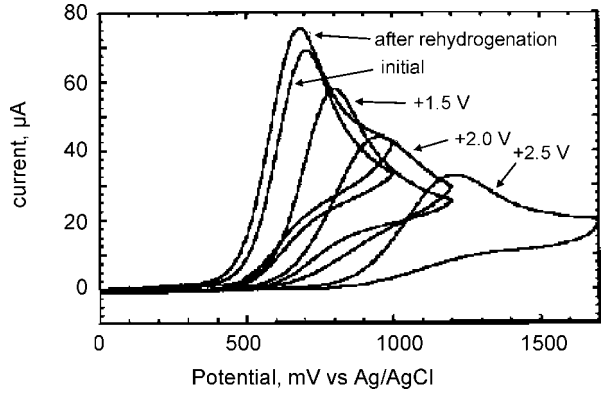

Figure 26. Effect of anodization on the voltammetry of ascorbic acid (1 mM in 0.1 M $HClO_4$) on boron-doped microcrystalline diamond. BDD surface was oxidized at the indicated potentials for 5 min before each voltammogram. "Rehydrogenation" refers to exposure to a H-atom plasma. Reprinted with permission from ref 30. Copyright 2004 Marcel Dekker.

3.4, dopamine oxidation is catalyzed by hydrogen bonding of surface carbonyls to adsorbed dopamine molecules, and diamond does not provide the necessary sites in its H-terminated form. The reported observations on diamond electrodes reinforce the conclusions of section 3.5, that is, that electrode effects on redox kinetics are strongly dependent on the nature of the electron transfer mechanism. Although diamond surfaces are comparatively inactive toward adsorption and often lack catalytic sites, there have been several examples reported of complex organic and biochemical reactions on diamond materials, including cytochrome *c*,[228] DNA-modifed diamond,[224] and glucose oxidation.[33,213,215] Additional reported analytical targets of diamond electrodes include arsenic,[214,229,230] dopamine and norepinephrine,[219,222] and polyamines.[226] Applications of diamond microelectrodes in biological media have been reviewed.[221]

In addition to the boron or nitrogen doping already discussed for diamond electrodes, several diamond composites have been studied, often to enhance the relatively weak electrocatalytic activity of diamond due to its lack of adsorption sites. Gold coating of BDD has been used for stripping voltammetry,[229,230] and Pt particles may be deposited on BDD to make dimensionally stable electrocatalytic surfaces.[231] Pt particles have also been incorporated into BDD to provide catalytic sites in a very stable conducting host.[232,233] Given the high stability of diamond as an electrode material, it seems likely that additional applications involving metal catalysts are likely. In addition, BDD may be chemically modified by several routes in common with sp^2 carbon materials, as discussed in section 5.

4.3. Fibers and Nanotubes

Carbon fibers have been used in electrochemistry since approximately the early 1980s, and their structures and properties relevant to electrochemical applications were reviewed in 1991.[3] There has been significant activity since that time due to the utility of carbon fibers for making ultramicroelectrodes and for in vivo voltammetry. Furthermore, the discovery of carbon nanotubes provided a completely new type of carbon "fiber" with distinct electrochemical properties. The discussion of carbon fibers will be divided into two sections, "conventional", meaning nonfullerene carbon fibers, and fullerene nanotubes in their single- and multiwalled manifestations.

Although carbon fibers occur with radial, "onion", and random orientations of the graphitic planes,[3,14] there does not appear to be standardization of a particular type for electrochemical applications. As with other graphitic materials, carbon fiber types differ significantly in their crystallite sizes, interplanar spacing, and disorder, but most laboratories have arrived at a useful carbon fiber source empirically. Generally, fibers used in electrochemistry are sufficiently disordered that they do not show unusual electronic properties, like HOPG or certain types of nanotubes. Fibers are encapsulated in a variety of materials, most commonly glass, often with epoxy, and then the carbon

surface is exposed by cutting the assembly.[143,150] The resulting carbon electrode exhibits one of the highest reported k° values for $Ru(NH_3)_6^{3+/2+}$ on carbon,[150] and represents a pristine surface analogous to that obtained by "fracturing" glassy carbon as discussed in section 3.6. A light polish of a glass encased carbon fiber has proven valuable for voltammetry in living organisms,[143,234] and various surface modifications have been investigated to improve analytical selectivity.[12,147,235] In some cases, a portion of the fiber walls might be exposed in addition to the fiber end to increase the electrochemically active area.[11] Carbon fibers and nanotubes may be "doped" with nitrogen or metals to promote electrocatalytic behavior.[236–239] Of particular interest is the long search for efficient electrocatalysts for oxygen reduction due to its importance to fuel cells and batteries. Incorporation of Fe, Pt, and nitrogen into carbon electrode materials provided catalytic sites for O_2 reduction to both hydrogen peroxide and water.[236,238,239]

Several examples of thin films deposited on carbon fibers have been described, with the objective of insulating all but a small fraction of the fiber in order to decrease the active electrode area. An early example is the electropolymerization of a phenolic polymer with a thickness of ~100−300 nm, after which a disk or elliptical electrode was exposed by cutting the fiber or by field emission.[160,161,240,241] A photocurable perfluoropolyether was used on both carbon and Pt fibers to make disk or conical microelectrodes, with a <10 μm thick insulating coating.[242] An important variation on electropolymerized films is deposition of "electrophoretic paint" based on poly(acrylic acid), followed by heat treatment to harden the coating.[243–247] The polymer coating shrinks slightly during heat treatment and retracts from the tip of the fiber to expose the end. Submicrometer electrode diameters were readily achieved with this approach, which was initially developed for metal electrodes.[243,244] A similar approach with an "inverted deposition" technique was used on 5 μm diameter carbon fibers that had been electrochemically etched to generate sharp conical tips.[245,246,248] Figure 27 shows well-defined voltammograms for $Fe(CN)_6^{3-/4-}$ obtained with carbon fiber electrodes with apparent radii ranging from 160 to <1 nm. These exceedingly small electrode radii were calculated from the limiting currents based on the assumption that the electrode acts as a microdisk, and that assumption appeared justified when supporting electrolyte was present.[246] However, unusual effects of both the double layer and electrode geometry have been reported for microelectrodes below ~20 nm in diameter,[244,249] so the apparent electrode radii should be considered with caution. An alternative approach that permits exposure of selected regions of the carbon fiber employs photolithographic techniques to expose particular areas on a fiber that had been coated with an electrophoretic resist. After exposure of the coated fiber to light, the electrode was "developed" with standard procedures to yield reproducible active electrode areas.[250] "Nanogap" electrode structures consisting of two carbon fiber electrodes located ~20 nm apart have been reported, starting with carbon fibers coated with electrophoretic "paint".[247]

Many of the applications of carbon fiber electrodes have been biological, because of both their small size and their activity for a variety of biochemically important materials (neurotransmitters, nucleotides, etc.). As noted in section 5, carbon fibers are subject to chemical modification by several routes to enhance reactivity or selectivity, for example, Pt-deposition,[248,251] diazonium reduction,[12] and polypyrrole

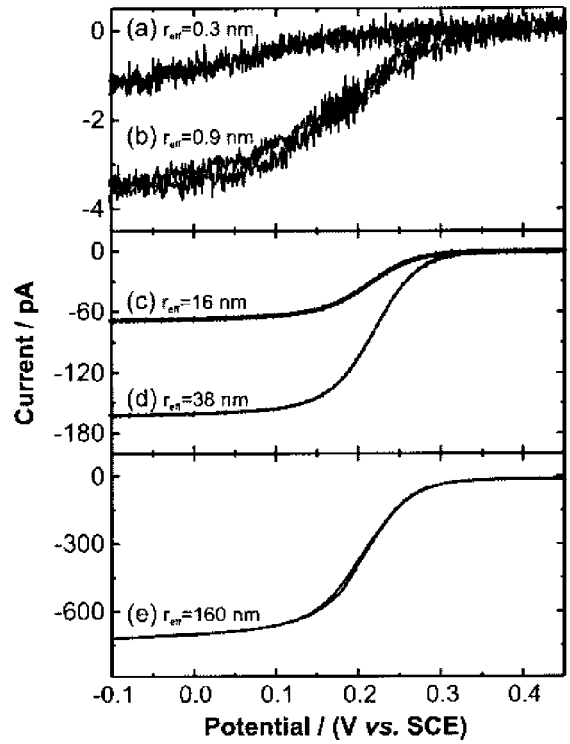

Figure 27. Steady-state cyclic voltammograms of reduction of 10 mM $Fe(CN)_6^{3-/4-}$ (0.5 M KCl, 10 mV/s) on carbon nanofiber electrodes. Indicated radius was calculated from the limiting current. Reprinted with permission from ref 246. Copyright 2002 American Chemical Society.

or Nafion coating.[147,252,253] Carbon fibers have been used to great advantage for in vivo monitoring of neurotransmitters in intact animals,[11,13,147,254–257] transmitter release and uptake by single cells,[11,13,235,258–262] and nucleotides.[160,175,263] An unusual application of carbon microelectrodes is the induction of cell−cell and cell−liposome fusion by an electric field applied at a carbon fiber.[264] In addition to bioanalytical applications, carbon fiber microelectrodes have been used for studying electrochemiluminescence, due to the high frequency response permitted by a low RC time constant, as well as the extended potential window compared with metal electrodes.[265–267]

Some generalizations about electrochemistry at "conventional" carbon fiber electrodes are available, and they are quite similar to those regarding bulk graphitic materials described in section 3.7. Most carbon fibers are sufficiently disordered that they do not display unusual electronic effects, as are observed with HOPG. The edge/basal ratio on the exposed surface determines adsorption and electrocatalytic activity, as is the case with glassy carbon and pyrolytic graphite. The potentially very small active area and total diameter of a carbon fiber electrode are of obvious importance for in vivo voltammetry and electron transfer kinetic measurements. Except for the case of carbon fibers embedded in a sturdy host such as glass or epoxy/glass, carbon fibers are not amenable to polishing, with the attendant risk of contamination or deactivation. Hence carbon fiber electrodes can be more active than bulk carbon materials in terms of electron transfer kinetics and electrocatalytic activity, if only because their freshly exposed surfaces have had less opportunity to adsorb impurities.

As discussed briefly in section 2.1.3, carbon nanotubes differ fundamentally from carbon fibers in their electronic properties and structures. A Scifinder search of the concept

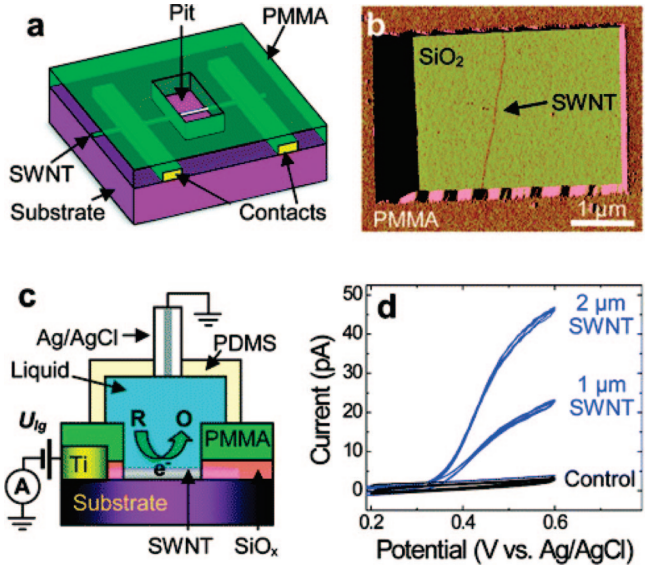

Figure 28. Apparatus (a−c) and response (d) for a metallic single-walled nanotube electrode in a solution of a ferrocene derivative in aqueous electrolyte. Reprinted with permission from ref 41. Copyright 2006 American Chemical Society.

"carbon nanotube electrochemistry" yielded more than 1700 citations, starting in 1999.[268] There is no question that nanotubes have unique conductivity and density of electronic states (Figure 2), and their small diameters and high ratio of length to diameter permit novel and unusual electrode structures. The electrochemical properties of nanotubes have been reviewed recently,[37,39] and those sources should be consulted for details and numerous references. In the context of alternative carbon electrode materials, several issues deserve special note. These include electronic properties, edge/basal ratio, oxide functional groups, and electrode kinetics. In addition to carbon nanotubes, "nanoscrolls" have been reported, which are formed by intercalation and fragmentation of graphite, followed by curling of the graphene fragment to form a "scroll".[269]

Nanotube preparations are rarely monodisperse, and most contain a difficult to separate mixture of tubes with different lengths and diameters. Multiwalled carbon nanotubes (MWNTs) are generally considered to be metallic, with any gaps or significant variations in electronic DOS averaged out in the mixture. Roughly one-third of single-walled nanotubes (SWNTs) are metallic and the remainder semiconducting, with possibly complex DOS profiles such as that shown in Figure 2. While significant effects of the DOS of SWNTs on electron transfer properties are expected,[41] they have not yet been observed experimentally. An elegant study of ferrocene voltammetry at single SWNT electrodes demonstrated that steady-state diffusion to a SWNT was observable, with the expected linear dependence of current on tube length.[40] A metallic SWNT was suspended between two titanium contacts in a PMMA "cell", which permitted exposure to electrolyte solution as shown in Figure 28.[41] A voltammogram for a 1.2 nm diameter, 2 μm long metallic SWNT is shown in Figure 29A, with a fit to Butler−Volmer kinetics, which yields a $k°$ for ferrocenylmethyl-trimethylammonium ion of 7.6 cm/s. The voltammograms for metallic and semiconducting SWNT electrodes were similar, perhaps because the ferrocene redox system is too fast to exhibit an observable dependence on electronic DOS. The authors point out that the very small nanotube diameter combined with its high aspect ratio permits fast mass transport to the

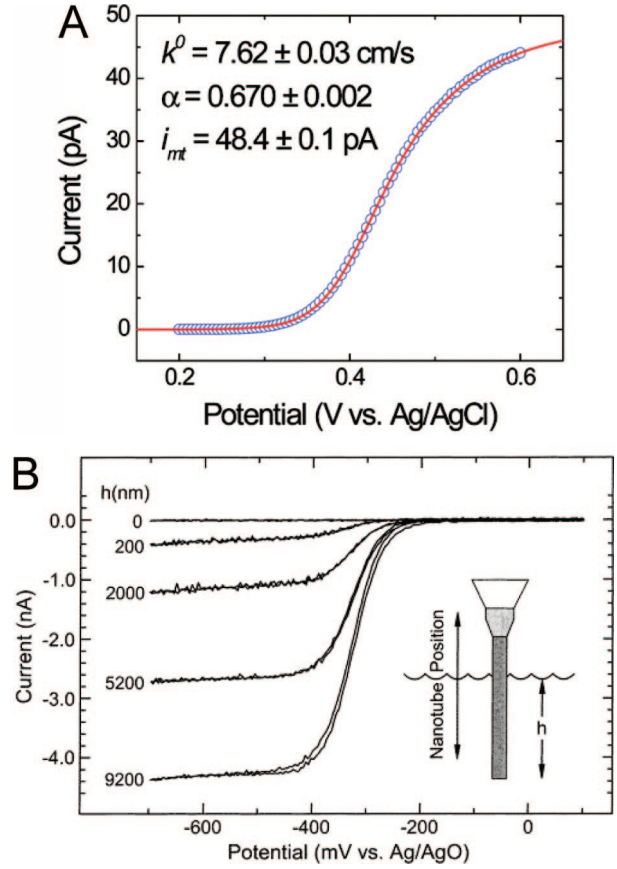

Figure 29. (A) Voltammogram from SWNT for ferrocene, with corresponding fit to Butler−Volmer kinetics[41] and (B) voltammograms at a ~100 nm diameter MWNT electrode in 5 mM $Ru(NH_3)_6^{3+/2+}$ in 0.1 M K_2SO_4 as a function of the height (h) of tube exposed to the solution.[268] Reprinted with permission from refs 41 and 268. Copyright 2006 and 1999 American Chemical Society.

electrode and correspondingly large accessible $k°$ values.[41] Although this experimental paradigm for studying electrochemistry at a SWNT is demanding, the nanotube provides a potentially valuable combination of geometry and tunable electronic properties for fundamental investigations of electron transfer kinetics.[41] Electrochemistry at a single, 150 nm MWNT was reported in 1999,[268] and a voltammogram of the reduction of $Ru(NH_3)_6^{3+/2+}$ is shown in Figure 29B. The limiting currents were proportional to the immersion depth of the MWNT, as expected, and the mounted nanotube did not appear inordinately fragile. The MWNT could be insulated with electropolymerized phenol to yield an ~150 nm diameter microdisk electrode after cutting.

The vast majority of investigations of electrochemistry at carbon nanotubes involve ensembles of many tubes, often in composites or as thin films. As already noted, such ensembles invariably contain a mixture of tubes of different diameters, and the collection of tubes is generally considered to be metallic in terms of electronic DOS. Most ensembles consist of randomly aligned and often tangled nanotubes, so the solution or matrix under study is presented with an average of "side" and "end" orientations. Nugent et al. reported apparently reversible electron transfer to $Fe(CN)_6^{3-/4-}$ at a bundle of MWNTs ranging in diameter from ~20 nm to several micrometers, and the ensemble contained non-nanotube carbon residue from the tube preparation.[270] Alignment of nanotubes in ensembles is a difficult problem,[37,39] but various methods have been employed. An interesting example is a

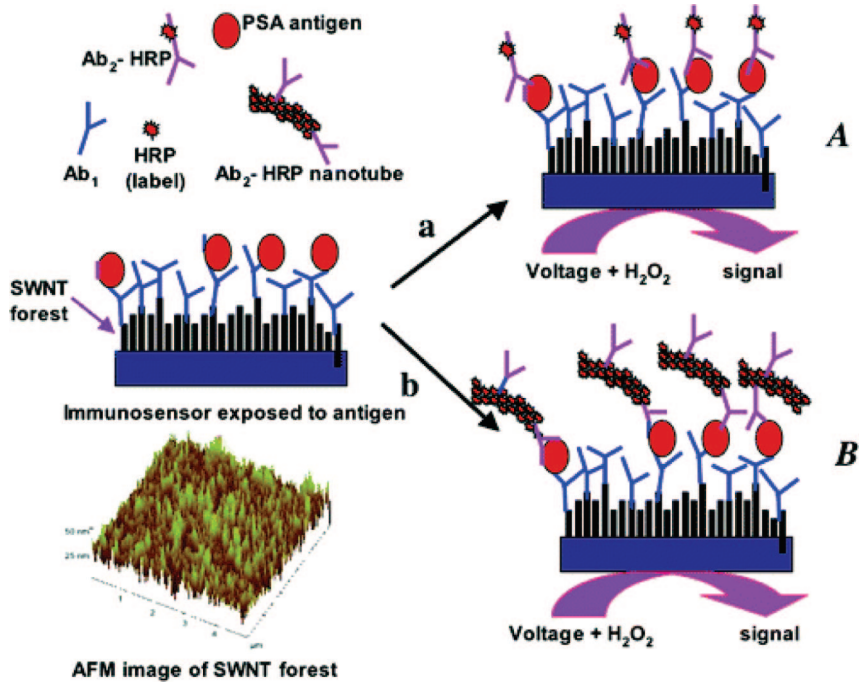

Figure 30. Construction of an antibody and horseradish peroxidase (HRP) on a "forest" of single-walled carbon nanotubes assembled onto an abraded pyrolytic graphite electrode. Reprinted with permission from ref 285. Copyright 2006 American Chemical Society.

two-dimensional network of nanotubes deposited on glass between two metallic contacts.[271–273] This arrangement permitted simultaneous monitoring of electron transfer reactivity and nanotube conductivity and also exhibited unusually high voltammetric sensitivity at the submicromolar level due to low capacitive background.[273]

SWNTs have been chemically "cut" with H_2SO_4/HNO_3, then modified to have thiol end groups so they could be assembled on a gold surface to make a nanotube array.[274] Electrochemical modification of nanotubes has been reported,[100] as has "site specific" binding of DNA and biotinylated biochemicals using photoresist techniques.[275] Arrays of nanotubes can also be "grown" on a microfabricated array of catalyst particles, then made into electrodes[276] or membranes[277] containing arrays of nanotubes suspended in either SiO_2 or polystyrene. The capacitance and electron transfer kinetics for $Fe(CN)_6^{3-/4-}$ were studied on three types of SWNT and MWNT ensembles, and it was concluded that the solution could penetrate the ensemble to access a large surface area of nanotubes and non-nanotube carbon residue.[278] The electrochemistry of $Fe(CN)_6^{3-/4-}$ was investigated on carbon nanotubes modified with Au nanoparticles, and the response was used to determine the nanotube length.[279] Nitrogen-doped CNT electrodes have been shown to exhibit electrocatalytic activity toward oxygen reduction and also to efficiently oxidize catecholamines.[236,237,280] Arrays of nanotubes have been used for studying proteins,[281] DNA and nucleotides,[282,283] and redox enzymes,[284] with the latter example exploiting the ability of a nanotube to transport electrons a long distance from the electrode surface to the redox center of the enzyme. An elegant application of SWNTs to immunoassay involved formation of a "forest" of nanotubes oriented perpendicular to the basal plane surface of abraded pyrolytic graphite, as shown in Figure 30.[285] The antibody to prostate-specific antigen (PSA) and peroxidase retained their activity when immobilized on the top of the SWNT "forest", providing greatly amplified response to PSA and a mass detection limit of 40 fg. Carbon fibers modified with MWNTs exhibited unusual reactivity for ascorbate oxidation and were used for in vivo monitoring of ascorbate in rat brain.[256] SWNT films on GC modified with ferrocene as a redox mediator exhibited selective oxidation of dopamine over ascorbate and uric acid,[286] and MWNT/chitosan films on GC permitted direct oxidation of insulin.[287] Many electrochemical studies using nanotubes involve composites with other materials, and examples are provided in section 4.4 and Table 4.

In addition to morphology and electronic properties, the defects and oxides on carbon nanotubes have important effects on electrochemical behavior. Defects can occur in the nominally "basal plane" surface of the nanotube walls, and most preparations result in unterminated tube ends, which are prone to form oxygen-containing functional groups. It has been somewhat controversial whether the behavior of nanotube electrodes is determined by special properties of the tubes themselves or by a variable level of oxides or edge defects. For example, there are reports of high electrocatalytic activity of carbon nanotubes toward the oxidation of catecholamines,[286,288,289] NADH,[102,290,291] hydrazine,[292,293] and ascorbic acid,[256,293–295] yet at least some of these effects have been attributed to the graphitic edge plane exposed at the nanotube ends.[177,178,296,297] Furthermore, nanotubes are made with Fe, Ni, or Co catalysts, which are often not completely removed in the final product. As shown in Figure 31A, the electrocatalytic oxidation of hydrazine was absent when nanotubes were prepared with very low levels of trace metals, and it was concluded that hydrazine oxidation was catalyzed by metals and not nanotubes.[292] Also shown in Figure 31C is the effect of adding MWNTs to a HOPG basal plane surface on the voltammetry of $Fe(CN)_6^{3-/4-}$. The apparently fast kinetics were attributed to a high fraction of edge sides on the nanotubes, and the sharp voltammetric peaks were ascribed to a thin layer effect in the porous ensemble.[292] The electrochemical behavior of nanotubes has also been correlated with the presence of residual iron oxides and their electrocatalytic activity.[298]

Table 4. Examples of Carbon Composite Electrodes

carbon type	host[a]	additive[b]	target analyte	reference
graphite	paraffin	enzyme, NADH	L-phenylalanine	410
graphite	mineral oil	1,2-dibromocyclohexane	vitamin B_{12}	328
graphite	mineral oil	glucose oxidase	glucose	311
graphite	mineral oil	laccase, p-hydroxybenzoate hydroxylase	NADPH	127
graphite	nujol	chitosan, ssDNA	hepatitis B virus	314
graphite	nujol	chitosan, peroxidase	rutin	313
graphite	paraffin	chitosan, sepiolite clay	aqueous ions	312
graphite	paraffin	Zr phosphate, nitro-fluorenone	NADH	411
graphite	ionic liquid		NADH, dopamine	315
graphite	ionic liquid		dopamine, ascorbate, uric acid	317
graphite	ionic liquid	$CaCO_3$, Nafion	hemoglobin	318
graphite	mineral oil	magnetic nanoparticles, laccase	hydroquinone	322
graphite	nujol, silicone oil	Pt nanoparticles	Cu^{II}	319
MWNT	nujol	Nafion, thionine	dopamine, ascorbate	288
MWNT	mineral oil	ionic liquid	$Fe(CN)_6^{3-/4-}$, $Ru(NH_3)_6^{3+/2+}$, hydroquinone	316
MWNT	mineral oil	microbes, Os polymer	glucose	412, 413
MWNT	mineral oil		NADH, AA, dopamine, H_2O_2	294
MWNT	mineral oil	Cu particles	amino acids	325
MWNT	poly(vinyl ferrocene)		glucose	326
SWNT	mineral oil		$Fe(CN)_6^{3-/4-}$, ferrocene, $Ru(NH_3)_6^{3+/2+}$	324
SWNT	redox polymer	glucose oxidase	glucose	414
SWNT	mineral oil		nucleic acids	323
GC, MWNT		chitosan	insulin	287
GC	redox hydrogel	glucose oxidase	glucose	128

[a] Pasting liquid, generally inert. [b] Catalysts, active agents, etc.

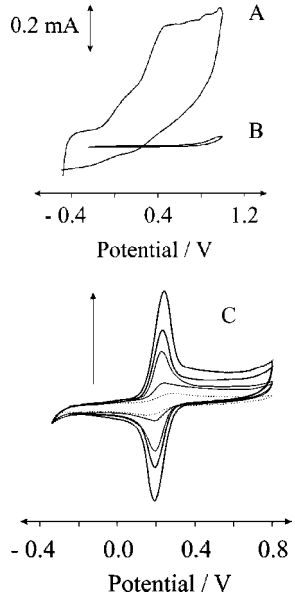

Figure 31. Voltammetry of hydrazine at MWNT preparations that contained metallic impurities (A) and were purified to remove metals (B). The arrow in panel C indicates the addition of increasing amounts of MWNTs to a solution of $Fe(CN)_6^{3-/4-}$. The dotted line is the initial response from a HOPG electrode. Reprinted with permission from ref 292. Copyright 2007 American Chemical Society.

While there is little doubt that defects can play a major role in the electrochemical behavior of nanotube electrodes, there is also evidence for intrinsic nanotube reactivity in the absence of defects. Silver and palladium may be electrodeposited onto nanotubes from solution, and the resulting metal particles are randomly and nearly continuously distributed along the length of a given nanotube.[299] If deposition occurred only at defects, then an even distribution of metal particles would not be expected. By analogy to the basal plane of HOPG, as discussed in section 3, it is possible that the "basal plane" walls of carbon nanotubes have reduced reactivity compared with a disordered surface like GC and are relatively inactive toward adsorption. But as already discussed, the reactivity differences between nanotubes and other carbon electrodes are likely to depend strongly on the redox system involved.

To summarize the preceding overview of carbon nanotube electrode behavior, it is clear that nanotubes have some distinct electrochemical properties, but they also introduce some additional variables, such as tube diameter and morphology, and often unknown levels of defects and surface oxides. In the context of the general discussion of section 3, some generalizations about nanotube electrodes are worthwhile. First, most nanotube electrodes studied to date consist of metallic tubes, although some interesting electronic effects occur in the few cases where the tubes are semiconducting. Second, nanotubes have a high aspect ratio compared with carbon particles, such that there is potentially both a high ratio of basal sites to edge sites and a long conduction path along the tube. However, some nanotube morphologies have much higher defect density than others, such as the "bamboo" nanotube compared with the SWNT. Since edge sites can be much more electrochemically active than basal sites, the observed reactivity of a single nanotube or a nanotube ensemble depends strongly on the defect density. The defect density and edge/basal ratio may be modified by "doping" with nitrogen, with observable electrochemical effects.[280] Third, nanotubes can be hydrophobic along their walls, particularly if low in defect density, and this can affect interactions with solvent or redox agents.[300,301] Fourth, the fact that nanotubes and their ensembles are not amenable to polishing has the indirect benefit of reducing surface contamination. It is possible that the long path for conductivity coupled with a significant coverage of edge plane defects is at least partially responsible for the reported high electrochemical reactivity of nanotubes. Fifth, nanotube preparations differ significantly in the synthetic route involved, and many include metal catalysts, non-nanotube carbon, or both, which are not completely removed in the finished product. Depending on the mechanism of a given redox reaction, the origin and purity of the nanotubes may be critical to the observed electrochemical response. Finally,

the relationship between nanotube structure, including morphology and defects, to electrochemical reactivity remains an important research goal, and there will likely be significant new insights into this area as nanotube electrode preparations are refined.

4.4. Carbon Composite Electrodes

Composites of graphitic carbon with a wide variety of both active and inactive materials are very common and are generally referred to as "carbon paste". The original carbon paste electrode was introduced in 1958 by Ralph N. Adams[302] and represents one of the earliest applications of carbon electrodes in the modern era. A Scifinder search yielded over 3600 articles containing the concept "carbon paste electrode" and over 100 containing "nanotube paste electrode". Electrochemical applications of carbon paste electrodes have been reviewed[303,304] and cover a wide range of objectives in electroanalysis, pharmaceuticals, biological redox processes, and mechanistic electrochemistry. Rather than attempting a comprehensive review of the many carbon composite electrode materials, we will consider here the properties that make composites popular for electrochemistry and summarize several of the more recent variants.

The now classical carbon paste electrode is made from polycrystalline graphite powder and a water-immiscible insulating organic liquid such as Nujol or hexadecane. Alternatives to organic hydrocarbons include epoxy, Nafion, and conducting polymers.[305–310] The volume fraction of graphite is high enough (typically >50%) that the graphite particles are in contact to provide a conducting pathway and sufficiently low bulk resistivity. Considering carbon composites generally, their attractiveness for electrochemistry stems from both fundamental and practical advantages over conventional solid carbon electrodes such as glassy carbon. First, the paste is readily renewed without extensive polishing, so adsorbates or electrochemical products are easily removed between runs. Second, the graphite powder has randomly exposed edge and basal plane and is usually quite electrochemically reactive. Third, the fractional area of carbon exposed to the solution is generally much smaller than the geometric area of the electrode, with the remainder occupied by the insulating "host". Since the electrode capacitance is determined nearly exclusively by the exposed graphite, the background current resulting from this capacitance is much lower than expected for a given electrode area, typically by an order of magnitude or more. Fourth, radial diffusion to the closely spaced carbon particles provides efficient mass transport of electroactive species, and the current response is based on the *geometric* area rather than the exposed graphite particle area. As a result, the observed faradaic current is proportional to the total area of the electrode, while the capacitive background (or any redox reactions of the graphite surface) is proportional to the exposed area of a few percent of the total area. The ratio of faradaic to background current is therefore much higher for a carbon composite electrode than for a solid graphite electrode of the same geometric area. Fifth, carbon paste retains the wide potential window of carbon materials compared with metals, a point of particular value in early applications to organic oxidations. Finally, a paste composition permits addition of a variety of reagents to the host material, including electrocatalysts, enzymes, and chemical recognition agents. Many of the more recent carbon composites exploit this last point in order to incorporate unusual selectivity or reactivity to the carbon composite electrode. A recent example of the merits of carbon paste is the observation that a carbon/mineral oil/enzyme composite remains active even in acidic solution, while a similar composite made with polyphenylene diamine instead of mineral oil was rapidly deactivated by acid.[311]

While carbon composites have the advantages of low background current and usually facile surface renewal, these positive points come with some costs. The host material may interfere with redox reactions and adsorption on the carbon particles, and carbon paste is generally less active for electrocatalytic reactions than glassy carbon. Not only can the host coat the graphite surface, the graphite area exposed to the solution is intentionally a small fraction of the geometric area, further decreasing the electrocatalytic current. The composite may not be stable in certain solvents, and there is a practical lower limit on the size of a composite electrode, significantly larger than most carbon fibers and much larger than nanotube electrodes.

Variations on carbon composite electrodes continue to be reported at a steady rate, with a noncomprehensive survey of examples appearing in Table 4. Composites of both powdered graphite and carbon nanotubes remain common, with a variety of hosts and additives. Chitosan is a poly-D-glucosamine derived from crustaceans and used in a variety of biomedical applications. Chitosan is polycationic at pH 7 and interacts with a variety of anionic peptides and hence is claimed to be beneficial for biosensors and immobilizing proteins in a composite electrode.[312–314] Ionic liquids such as *N*-butylpyridinium hexafluorophosphate have been incorporated into carbon composites,[315–318] as have catalytic[318–321] and magnetic[322] nanoparticles. Room-temperature ionic liquids were developed relatively recently, and carbon paste electrodes containing them have been shown to have some benefits. Figure 32 shows a comparison of a conventional graphite paste electrode with a graphite/ionic liquid paste for the voltammetry of dopamine, ascorbic acid, and uric acid.[317] There are clear differences in the apparent electrode kinetics and adsorption, which in this case permitted better resolution of the three redox systems. Composites containing single- and multiwall carbon nanotubes have been investigated with hydrocarbon,[294,323–325] ionic liquid,[316] and polymer[326] binders, and some interesting electrochemical behavior has been reported. Nanotube composites are apparently quite reactive compared with graphite composites for diverse redox analytes such as guanine, dopamine, hydroquinone, and ferricyanide.[37,316,323,324,326–328] As noted earlier, nanotube results should be viewed with some caution, due to variations in the level of edge sites and the possibility of trace metal contamination.[102,178,292] Electrical conductivity along the possibly long length of the nanotubes is an important difference compared with graphite powder and has been used to "wire" redox enzymes.[281] Nanotube composites also appear to have a large active area accessible to the solution, leading to both higher reactivity and also higher capacitance compared with conventional graphite composites.[327]

The huge commercial value of glucose sensors has driven development of "screen printed" and "ink jet printed" graphite electrodes, which in many cases are composites containing enzymes or other catalysts. A suspension of graphite powder in a volatile carrier is used to print patterns on an insulating surface, often in the form of a circular electrode and a carbon stripe as the electrode lead. Various

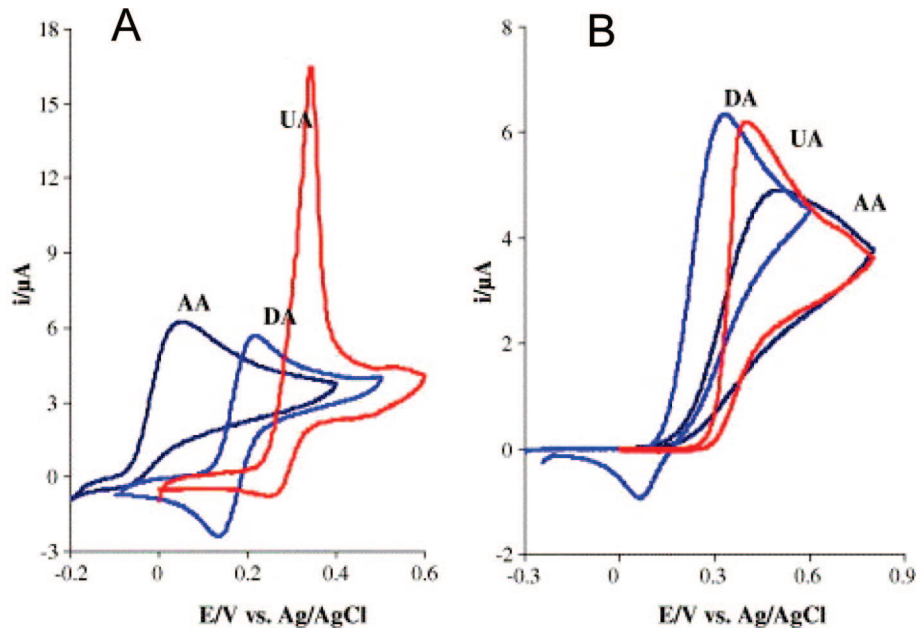

Figure 32. Cyclic voltammograms (PBS, pH 6.8, 50 mV/s scan rate) of dopamine (DA, 1.25 mM), ascorbic acid (AA, 1.25 mM), and uric acid (UA, 1.25 mM) at a composite carbon/ionic liquid (A) and conventional carbon paste (B) electrode. Reprinted with permission from ref 317. Copyright 2006 Elsevier Ltd.

reagents may be added to the printing solution, or printed separately on top of the carbon surface.[129] In commercial devices, a reference and possibly an auxiliary electrode might be printed in the same production line, resulting in automated manufacture of an electrode assembly ready for use with a drop of solution, blood, etc. Since printed electrodes may be mass produced, they are often disposable and inexpensive. Published applications of printed carbon composite electrodes include substrates for electrochemiluminescence,[329,330] monitoring tyrosine phosphorylation,[331] food analysis,[332] and immunoassay[333] and as sensors for ethanol,[334] nucleic acids,[335] and insulin.[336] It is not clear whether printed carbon electrodes differ from polycrystalline graphite in terms of the fundamental surface parameters affecting electron transfer, adsorption, and catalysis, but they have enormous practical value and are likely to dominate the commercial applications of carbon electrodes for electroanalysis.

5. Carbon Surface Modification

As already discussed in some detail, the structure and chemistry of a carbon electrode surface is vitally important to electrochemical applications, particularly those involving electrocatalysis or selectivity. Polishing, electrochemical pretreatments, and activation procedures discussed in section 3.6 could certainly be considered surface modifications, but the current section will deal with chemical reactions that lead to covalent bonds (usually) between the carbon surface and a chemical agent. Early modification procedures for carbon surfaces included adsorption of polyaromatic hydrocarbons,[337,338] bonding to surface carboxylate groups to form amide bonds,[168,339] and reactions of acid chloride reagents with surface hydroxyl groups.[107] Raman spectroscopy confirmed the reaction of surface carbonyl groups with dinitrophenylhydrazine to form a resonance Raman active adduct[106,107] and showed that the DNPH adduct was a planar molecule, oriented parallel to the graphite planes in HOPG.[340,341] A recent example of modification by physisorption involved the adsorption of pyrene modified DNA on the basal plane of HOPG.[342] Although these modifications often result in strong surface/adsorbate bonds, they are generally low in surface coverage (<10%) and often unstable toward acidic or basic media. Starting in the early 1990s, significant new approaches to surface modification were reported by several laboratories, based on radical and photochemical reactions with mainly sp^2 hybridized carbon surfaces. The most commonly used reaction was electrochemical reduction of phenyl diazonium reagents to produce a phenyl radical, which then formed a covalent bond with the carbon surface.[343] Oxidation of primary amines to a radical, which then bonded to the carbon, was reported in 1990.[344,345] As will be described below, these reactions and more recent related processes can lead to high coverage and very stable surface modifications, which have significantly broadened the utility of carbon electrodes.

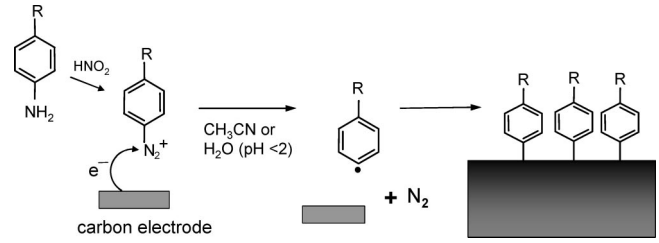

Figure 33. Modification of carbon surfaces by reduction of aryl diazonium reagents made by the reaction of an aromatic amine with nitrous acid. For details, see refs 197 and 346.

5.1. Diazonium Ion Reduction

The electrochemical reduction of phenyl diazonium ions at a carbon electrode to form a covalently modified surface was first reported by Delamar et al. in 1992[343] and was recently reviewed.[346] The process is shown schematically in Figure 33 for the case of a generic aromatic amine. The reaction of a wide range of phenyl amines with $NaNO_2$ at low temperature leads to phenyl diazonium reagents, usually isolated as a tetrafluoroborate salt. Such reagents are stable for months at low temperature, and several examples can be purchased commercially. Electrochemical reduction by one

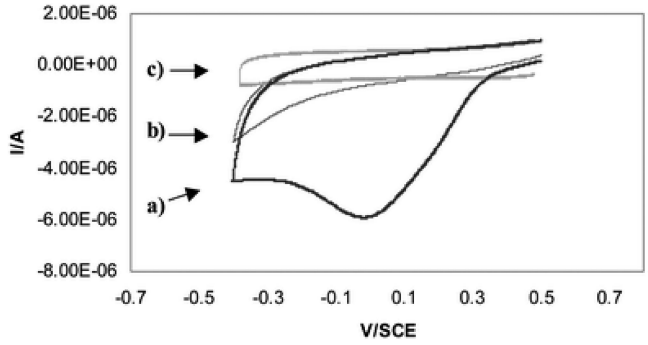

Figure 34. Voltammetric reduction of the diazonium ion $^{+}N_2C_6H_4NO_2$ in 0.1 M $TBABF_4$ in acetonitrile on a GC electrode. Curves a, b, and c are the first, second, and third scans, respectively. From ref 346 (Copyright 2005). Reproduced by permission of The Royal Society of Chemistry.

electron on carbon electrodes forms a phenyl radical and N_2; then the phenyl radical reacts with the carbon surface by coupling to an unsatisfied valence or adding to a double bond. It is likely that a short-lived neutral phenyl-N_2 species exists as an intermediate, but it rapidly and irreversibly dissociates to the much more stable N_2 and phenyl radical.[347] The fact that the reduction of aryl diazonium ions is chemically strongly irreversible provides additional driving force for radical formation, such that surface modification can occur even without an applied potential.[348,349] As shown for the case of nitrophenyl diazonium ion in Figure 34, the voltammetry of a phenyl diazonium reagent typically exhibits a broad, chemically irreversible reduction peak in the region of 0 V vs SCE, with the peak potential depending on the substituents on the phenyl ring.[346] The low reduction potential of the diazonium ion has been attributed to the strong electron-withdrawing effect of the N_2^+ group, with electron-withdrawing R-groups shifting the peak even more positive. The second and subsequent voltammetric scans generally have much smaller peak currents, because the electrode is by then covered with an organic layer, which partially inhibits further reduction. The current efficiency for surface attachment, that is, the fraction of electrogenerated phenyl radicals that bond to the surface, is generally less than 100%, with values of 56% reported for a HOPG surface and 84% for GC.

Diazonium ion reduction has several features that make it attractive for surface modification. Since the reactive radical is made electrochemically, it is generated precisely where it is most likely to react with the electrode surface. Second, uncovered regions of the electrode surface are more likely to reduce diazonium ions than modified regions, since the electron does not have to traverse an organic layer by tunneling or hopping. Thus film formation is "self-patching" with the result being relatively even surface coverage.[197] The C−C bond that is formed between the phenyl radical and the carbon surface is strong and is stable to at least 500 °C in vacuum.[347,350] The phenyl−phenyl coupling that results from diazonium modification of sp^2 carbon surfaces is symmetric and should exhibit relatively strong electronic coupling between the carbon surface and the modification layer.[140,200,202] In some cases, surface modification of carbon materials is spontaneous,[348,349,351,352] although generally yielding lower surface coverage than the electrochemical route. In addition to chemical modification of sp^2 carbon surfaces, diazonium reduction has also been used successfully on boron-doped diamond,[68] carbon nanotubes,[353–355] silicon,[349,356] GaAs,[349] coinage metals,[357–361] stainless steel,[362] and iron.[358,359] Diazonium reactions with metals vary significantly from those with carbon, and only the latter case will be discussed here in any detail.

Molecular layers formed on graphitic and diamond surfaces by diazonium reduction have been characterized by a variety of techniques, including Raman spectroscopy,[68,76,341,348,363–365] FTIR spectroscopy,[366,367] secondary ion mass spectrometry,[368] XPS,[68,200,347,363,369] ellipsometry,[349,370] and scanning probe techniques.[189,195–197,371] A common electrochemical probe of the modification layer is the reduction of a redox active substituent, notably the surface nitro group resulting from reduction of nitrophenyl diazonium ion.[363,372,373] Several of these methods have been used to determine surface coverage, with often significant variation in the apparent degree of phenyl modification and the occurrence of pinholes. The predicted coverage for a close-packed monolayer is $\sim 12 \times 10^{-10}$ mol/cm^2, based on the geometric size of a phenyl ring and minimal spacing between molecules on a flat surface.[363] Quantitative estimates of coverage are generally lower than this value, in the region of 4×10^{-10} mol/cm^2, and the discrepancy has been the subject of significant discussion.[189,372–374]

The variations in apparent coverage turned out to be an early indication of the complexity of organic films formed by diazonium reduction. Several years after the introduction of the reaction, it became apparent that multilayers were possible due to the aggressive reactions of electrogenerated radicals.[366] Since all diazonium reagents used for carbon surface modification to date are aromatic, electron tunneling through a monolayer is fairly efficient, thus permitting the generation of a second equivalent of radicals.[140,197] Alternatively, a radical generated at an unmodified carbon surface can attack an adjacent surface-bound molecule instead of the carbon surface itself. A proposed mechanism for multilayer formation is shown in Figure 35, and both SIMS[368] and FTIR[366] evidence have been presented in support of this or similar reactions. Note that the film resulting from the mechanism shown remains conjugated, although alternative mechanisms can result in termination of the chain reaction. Multilayer films as thick as 20 nm have been observed,[366] implying that the multilayer film has significant electronic conductivity.[140,197] Experience with a wide variety of diazonium reagents and carbon surfaces indicates that the tendency to form multilayers and the thickness of the modification layer depend on the nature of the surface, the particular diazonium reagent employed, and the deposition conditions, including scan rate and potential range, diazonium ion concentration, and number of deposition scans.[189,197,372]

The propensity for diazonium-generated radicals to form multilayers can be appreciated by considering the kinetics of the surface reaction. Newly electrogenerated phenyl radicals can react with the carbon surface or with each other, depending on concentration and relative reaction rates. If radical bonding to the surface is fast relative to attack of molecules already bonded to the surface, then a monolayer will form, possibly completely, before a second layer of molecules begins to form. In contrast, if the rate of radical attack on surface molecules is faster than bonding to the carbon surface, "mushrooms" will form rather than "wheat fields". On HOPG, for example, diazonium reduction resulted in nucleation of bonded molecules at edge plane defects and tall clusters of molecules were observed along edge sites by AFM.[371] Theoretical calculations predict that phenyl bonding is much stronger at graphitic edge planes than on pristine

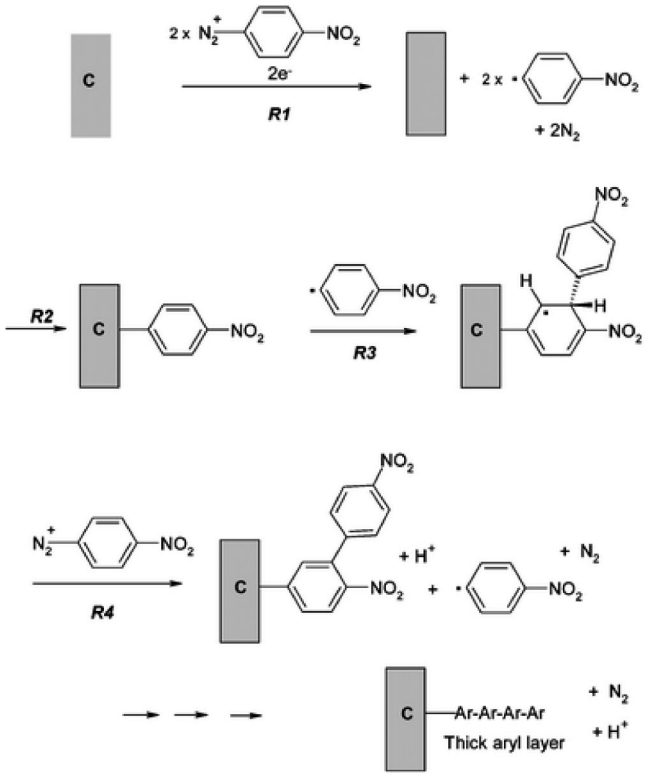

Figure 35. Proposed mechanism for the formation of multilayers during diazonium reduction at carbon electrode surfaces. From ref 346 (Copyright 2005). Reproduced by permission of The Royal Society of Chemistry.

basal plane.[375] Spatially resolved Raman spectroscopy of nitroazobenzene-modified HOPG revealed a much higher coverage of NAB molecules at defects on HOPG than on apparently defect-free basal plane.[76] Glassy carbon and PPF have a much higher density of edge plane than HOPG and therefore many more sites for radical bonding. Figure 36 shows a progression of AFM images acquired from modified PPF with scans to increasingly negative potentials in a solution of biphenyl 4-diazonium reagent.[197]

For scans from +0.4 to 0 or −0.2 V, coverage is incomplete and the variation in film thickness is large (~40%). The scan to −0.4 V shows even coverage and low roughness, while a scan to −0.6 V exhibits high points, which indicate beginning of formation of a second layer of biphenyl molecules. The squares apparent in Figure 36 are intentional "scratches" cut into the modification layer using contact mode AFM with a force gentle enough to avoid damaging the carbon surface. The depth of this scratch was determined statistically with several line profiles to provide a direct determination of film thickness. The conditions of the diazonium reduction were tuned for each molecule to produce monolayers, although the AFM thicknesses were systematically about 0.2 nm larger than that predicted for a perpendicular monolayer.[197] An FTIR investigation of molecular layers formed with the same procedure revealed an average tilt angle of ~35° relative to the surface normal.[367] Additional evidence for complete coverage of GC and PPF surfaces by monolayers resulting from diazonium reduction is the complete absence of electrochemical reactivity for the oxidation of catechols, which rely on adsorption to the carbon surface for electrocatalysis[126,140] (Figure 17A) and the ability to vapor deposit metals on top of molecular layers without contact between the metal and the carbon substrate.[200,376]

Although careful control of deposition conditions can result in monolayers from diazonium reduction, monolayers are by no means assured. If the reaction between the radical and the surface is slow, then molecule−molecule coupling reactions make multilayers possible and even likely. In order to form the 5−20 nm thick films reported for such multilayers, it must be possible for solvent and diazonium reagents to enter the film[189,203,366,374] or for the film to become electronically conductive.[140,197,377] Solvent has been observed in multilayer films, as have swelling and shrinking with changes in environment.[189] Unlike Au/thiol self-assembled monolayers, diazonium reduction is not inherently self-limiting, due to the possibility of further radical formation after deposition of initial monolayer. Fortunately, it is possible to control film thickness with suitable deposition conditions, but good practice dictates an independent verification of film thickness, for example, by AFM or ellipsometry.

The high coverage and strong surface bond resulting from diazonium modification of carbon surfaces has proven useful for a variety of applications. The surface modification may be patterned at the microscale using "soft" lithography with polydimethylsiloxane molds[203] or at the nanoscale using scanning probe lithography.[196] High coverage of the modification layer can completely inhibit electron transfer for reactions requiring adsorption to the carbon surface, such as catechol oxidation[126,140] or can significantly modify the mechanism of electrocatalytic reactions such as dioxygen reduction.[130] Modified electrodes can exhibit "conductance switching", in which the observed electron transfer rate can be increased dramatically by a redox process within the modification layer.[140] For example, the $k°$ observed for ferrocene on a GC electrode modified by reduction of biphenyl diazonium ion increased by a factor of 45 when the biphenyl layer was electrochemically reduced to a more conducting quinoid form. Carbon fiber electrodes modified with phenyl sulfonate groups by diazonium reduction show increased selectivity and sensitivity for catecholamine neurotransmitters during in vivo voltammetry,[12] while modification of GC with anthraquinone groups leads to enhanced electrocatalytic oxidation of dopamine,[126] as already noted above.

Dioxygen reduction at GC and carbon nanotube electrodes may be catalyzed significantly by bonding quinone species to the electrode surface using diazonium reduction.[173,378–380] Large biological molecules such as horseradish peroxidase may be immobilized on carbon electrodes after first reacting the protein with a phenyl diazonium reagent containing a *para* carboxylic acid group.[381] The utility of diazonium ion bonding to carbon surfaces may be broadened to a wider range of reagents by a two-step modification in which a "primer" is first attached to the surface by diazonium reduction and then a second reagent is attached to the primer, usually in a second step. Examples include attachment of epichlorohydrin to surface-bound aminophenyl groups[347] and nucleophilic substitution of surface benzyl chloride.[382]

The strong surface bond resulting from diazonium reduction on carbon is particularly important for making "molecular junctions" consisting of a layer of molecules oriented between two conductors.[200,383] A significant difficulty with making such junctions has been the deposition of a metal "top contact" on a modified electrode surface without the metal penetrating to the substrate and creating short circuits. Au/thiol monolayers are prone to this problem due to the

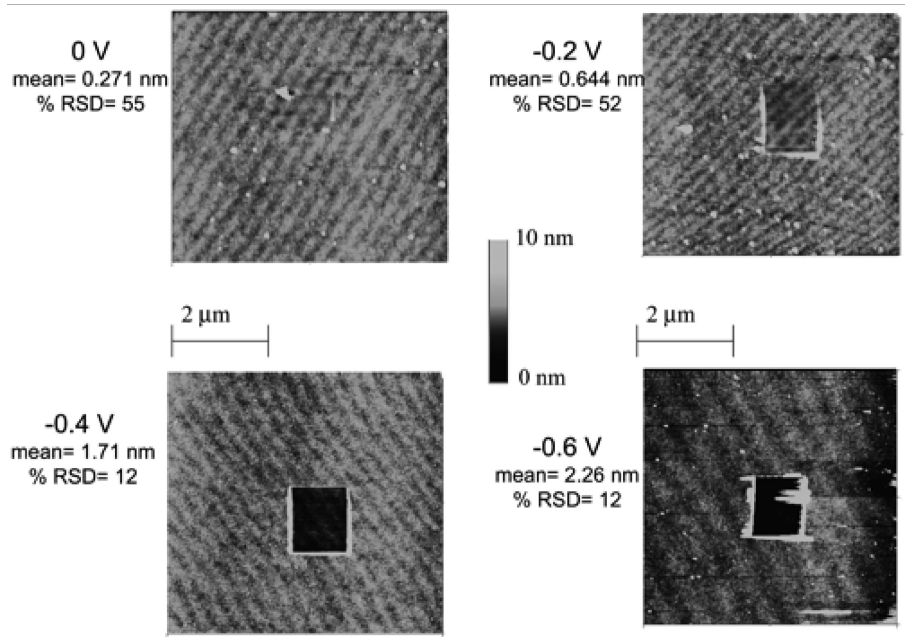

Figure 36. Tapping mode AFM images for a biphenyl-modified PPF surface following a contact mode "scratch". Single derivatization scans from +0.4 to 0, −0.2, −0.4, and −0.6 V vs Ag/Ag^+ were used to modify the PPF surface, as indicated. Also shown are the mean thickness (mean) and relative standard deviation (%RSD) determined statistically as described in the ref 197. Reprinted with permission from ref 197 Copyright 2003 American Chemical Society.

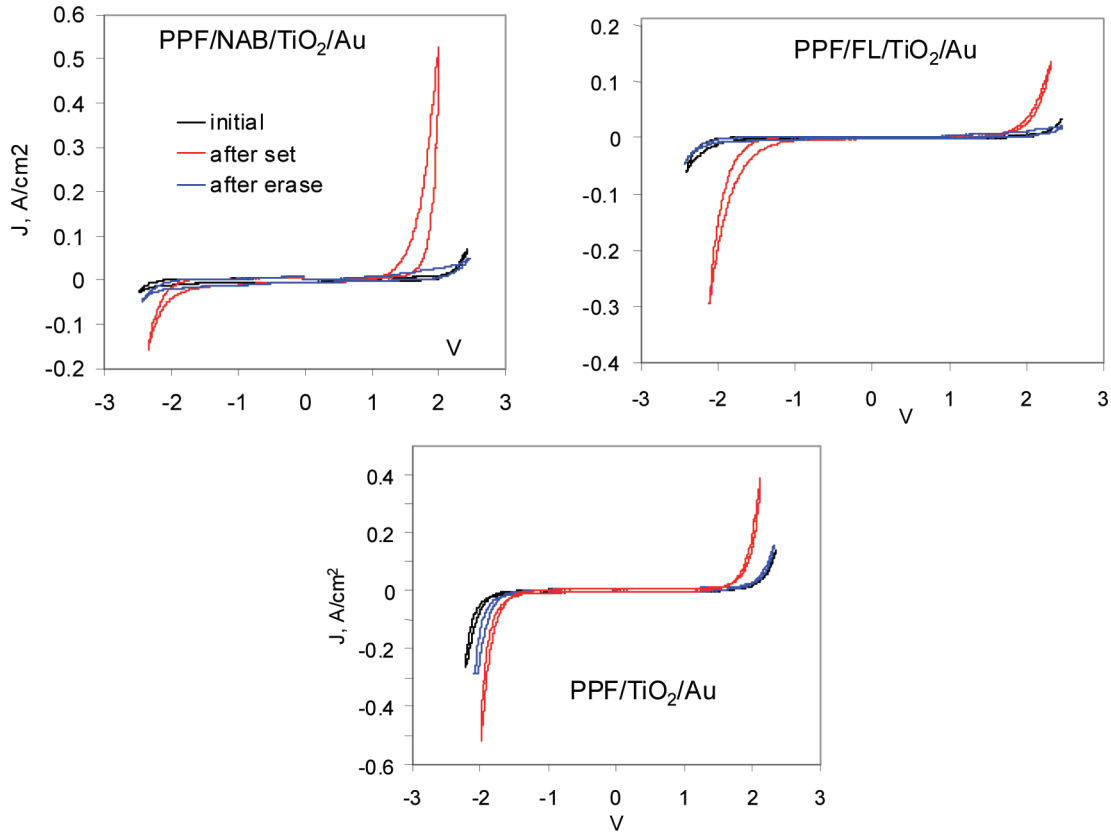

Figure 37. Current/voltage curves of molecular junctions made from nitroazobenzene (NAB) and fluorene (FL) monolayers with TiO_2 between PPF and Au conducting "contacts". Black curves are the initial scans at 1000 V/s, red are after a +3 V, 100 ms pulse (PPF relative to Au), and blue after a −3 V, 100 ms pulse. Adapted in part from ref 200 (Copyright 2006) by permission of the PCCP Owner Societies.

relatively weak surface bond and associated mobility of the monolayer.[384–386] The strong C−C bond from diazonium reduction (~4 eV compared with ~1.6 eV for Au−S) permits vapor deposition of metals or metal oxides on modified carbon surfaces without observable short circuits. An example of the behavior of a molecular junction made by vapor deposition of TiO_2 and Au onto PPF surfaces modified by diazonium reduction of fluorene and nitroazobenzene reagents is shown in Figure 37.[387] The molecular and oxide layers total 10−15 nm in thickness, and there is no intentional

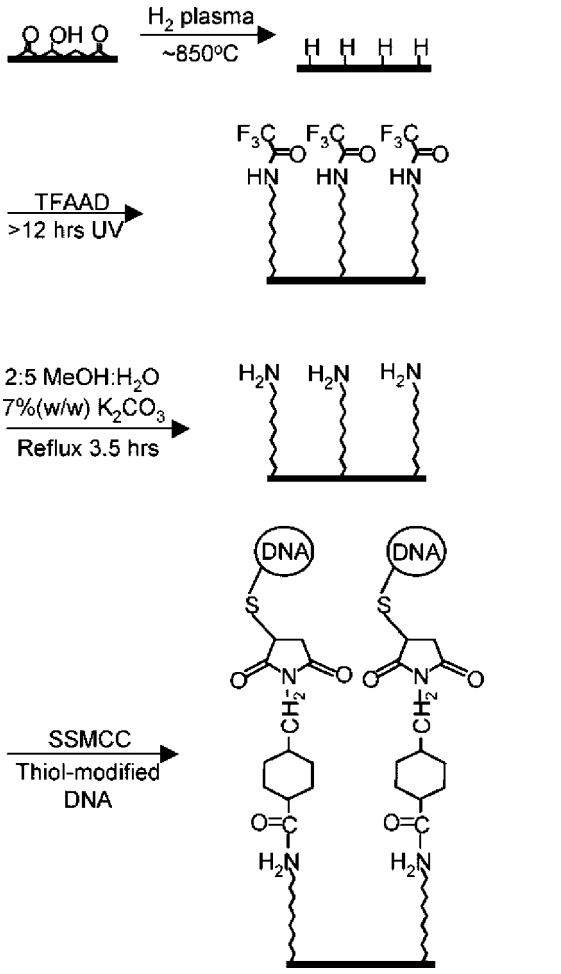

Figure 38. Photochemical route to covalent modification of diamond surfaces. TFAAD is trifluoroacetamide-protected 10-aminodec-1-ene; SSMCC is sulfosuccinimidyl-4-(*N*-maleimidomethyl) cyclohexane-1-carboxylate. Reprinted with permission from ref 397. Copyright 2003 American Chemical Society.

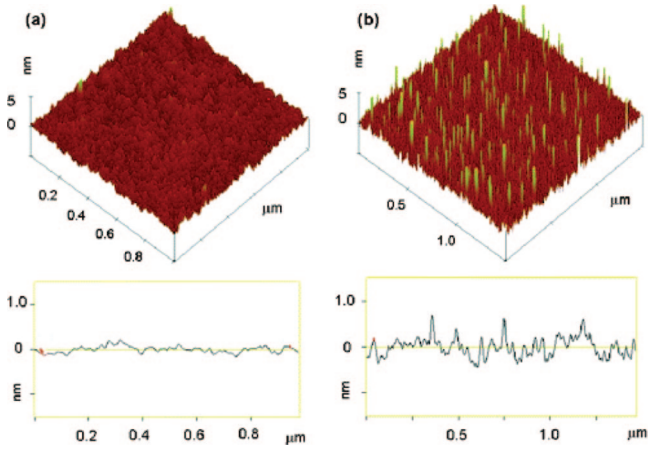

Figure 39. AFM images of PPF before (left) and after (right) UV irradiation in the presence of 1-decene, along with line profiles across the imaged surfaces. Reprinted with permission from ref 190. Copyright 2007 American Chemical Society.

solvent or electrolyte present. These molecular junctions exhibit "memory", in that they can switch between metastable low and high conductance states in response to "set" and "erase" voltage pulses. The local temperature rise of the device during metal deposition is significant, and the good thermal stability of a C−C surface bond is important to successful fabrication. The mechanisms and utility of these effects in molecular electronics have been described in some detail.[200,201,364,387]

Formation of C−C bonds between diamond surfaces and phenyl radicals generated by diazonium reduction has been reported[68] for the boron-doped diamond electrodes described in section 4.2. XPS and Raman spectroscopy of BDD modified with nitrophenyl, trifluoromethyl, and nitroazobenzene diazonium reagents revealed high coverage and stable modification layers. The modification reaction had a lower current efficiency than typically observed for graphitic carbon surfaces, presumably because 1 equiv of electrogenerated radical was required to abstract a hydrogen atom from the H-terminated BDD surface. After that, a second radical could couple with the surface radical to form the final C−C bond. Figure 4D shows a Raman spectrum of BDD before and after covalent modification of the diamond surface by reduction of nitroazobenzene diazonium ion.

Some significant variations on diazonium reduction have been reported recently, based on reactions of reactive precursors with carbon surfaces to result in a covalently bonded organic layer. These include the reduction of aryl and alkynyl iodonium salts,[388] reduction of diaryl iodonium salts,[389] and reduction of diazonium reagents that contain disulfides.[390] In the latter case, a multilayer of disulfide reagents was cleaved to yield a monolayer of a thiophenolate, thus providing a reliable route to a monolayer modification. A different example of radical mediated carbon surface modification is reduction of triaryl and alkyldiphenyl sulfonium ions, which leads to a carbon surface modified with aryl groups or with a mixture of covalently bonded alkyl and aryl groups.[391]

5.2. Thermal and Photochemical Modifications

Cycloaddition and photochemical reactions developed for modifying silicon surfaces[98] have been applied to graphitic carbon and diamond surfaces,[392–394] although the applications have not been as extensive as those of diazonium reduction. In ultrahigh vacuum (UHV), clean diamond surfaces form surface "dimers", which can react at room temperature with olefins to form C−C surface bonds. The product of the cycloaddition reaction is a four-membered ring with two C−C bonds to the diamond surface.[395] Diels−Alder type (4 + 2) cycloadditions have been reported on diamond, as well as the (2 + 2) route, again under UHV conditions.[396] A photochemical route to modification of diamond with DNA is shown in Figure 38, involving formation of a surface amine with trifluoroacetamide-protected 10-aminodec-1-ene (TFAAD) followed by coupling to DNA through a cross-linker sulfosuccinimidyl-4-(*N*-maleimidomethyl) cyclohexane-1-carboxylate (SSMCC).[397,398] A simpler modification of diamond with alkanes was achieved by UV treatment of H-terminated BDD in the presence of 1-decene, and the electrical properties of the modified surface were investigated.[399] The stability of both GC and BDD electrodes modified by covalent monolayers was found to be superior to alternative bonding schemes such as silane and Au/thiol reactions in biosensor applications due to the thermal and hydrolytic stability of the C−C bond.[224,398]

A photochemical route to bonding alkenes and alkynes to polished GC and as-prepared PPF has been reported, involving illumination of the surface in the presence of a range of alkenes and one alkyne with 254 nm light.[190] The reaction could be conducted in air without extensive electrode pretreatment. AFM images of a PPF surface before and after

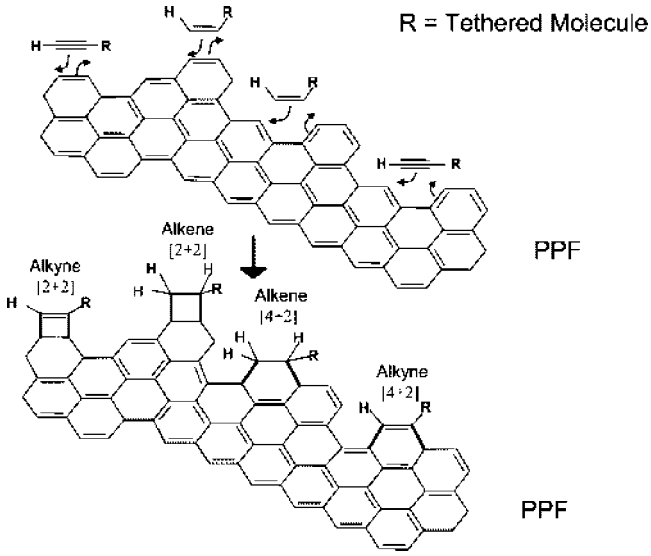

Figure 40. Mechanism proposed for thermal attachment of alkene and alkyne reagents to PPF. Reprinted with permission from ref 400. Copyright 2005 American Chemical Society.

modification are shown in Figure 39, indicating that the coverage of the surface is not complete for the conditions employed. Based on the voltammetric peak area for oxidation of a PPF surface modified similarly with ferrocene−alkyne, the coverage in that case was 16% of a densely packed monolayer. Alkene and alkyne derivatives of porphyrin and ferrocene can also be attached to graphitic carbon surfaces by heat treatment, in which a solution of the reagent reacts with a hot (175−400 °C) carbon surface in argon.[400] FTIR was used to determine that the tilt angle of the attached porphyrin center was 37°−45° relative to the surface normal. The modified surfaces were stable to sonication in tetrahydrofuran, treatment with aqueous acid or base, and extensive potential cycling in propylene carbonate electrolyte. Surface coverage was generally less than a complete monolayer, ranging from 0.2×10^{-10} to 3×10^{-10} mol/cm^2, determined voltametrically for the porphyrin modification. Although the detailed geometry of the surface bonding was not determined from the FTIR spectra due to interference from the carbon substrate, the tilt angle was statistically different for alkene compared with alkyne modification. A proposed modification scheme[400] based on Diels−Alder and (2 + 2) cycloaddition chemistry is shown in Figure 40.

5.3. Amine and Carboxylate Oxidation

Covalent bonding to graphitic carbon surfaces by oxidation of amines was reported initially in the early 1990s for carbon fiber[344] and glassy carbon electrodes[345] and has been studied in additional detail more recently.[203,361,373,401,402] Electrochemical oxidation of aliphatic primary amines yields an amine radical, which can then bond to an unsatisfied valence or double bond on the carbon electrode surface. An example is shown in Figure 41 for the oxidation of three aliphatic amines on glassy carbon in acetonitrile electrolyte.[402]

Electrolysis in a solution of a primary amine leads to complete inhibition of the voltammetric oxidation peak, while similar treatment in a secondary or tertiary amine results in only minor changes to the voltammetry. A mechanistic investigation supported by FTIR and XPS characterization of the modified carbon surfaces concluded that the reactive surface binding agent is the neutral, deprotonated amine

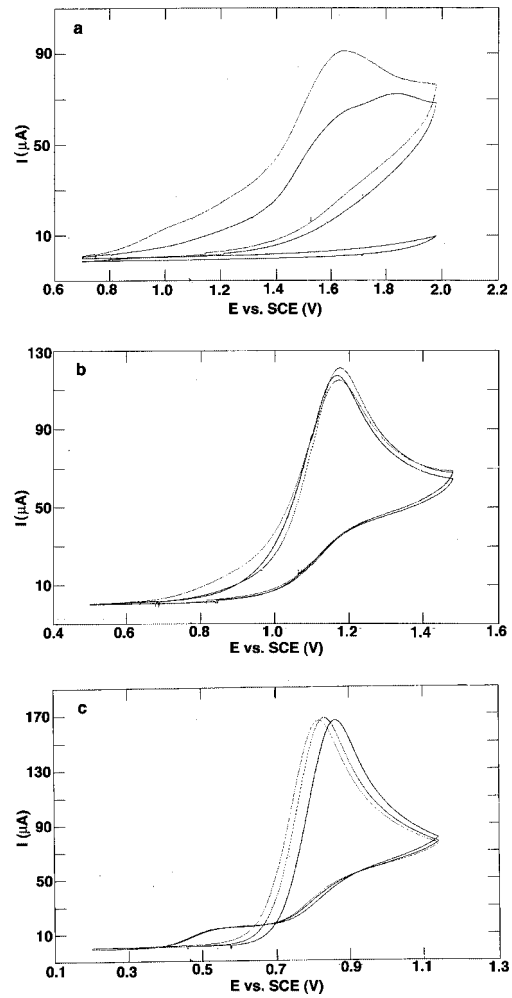

Figure 41. Cyclic voltammetry during the course of electrolytic oxidation of (a) *n*-butylamine, (b) di-*n*-butylamine, and (c) tri-*n*-butylamine in a 5.0 mM solution of the amine in acetonitirile electrolyte. Reprinted with permission from ref 402. Copyright 2004 American Chemical Society.

radical.[402] Both the earlier[345] and later[402] studies concluded that surface binding is much more efficient for primary amines than for secondary amines and that binding is essentially absent for tertiary amines. Coverage was assessed by voltammetry of surface-bound nitrophenyl groups following oxidation of nitrobenzylamine on GC to be in the range of $(3-6) \times 10^{-10}$ mol/cm^2. While this is close to that expected for monolayer coverage, there was evidence for pinholes from the electrochemical activity of modified GC surfaces.[402] Amine oxidation was also used to immobilize Au nanoparticles on carbon surfaces[361] and for detailed studies of the "blocking" properties of modification layers on carbon electrodes.[373] In a somewhat surprising recent report, spontaneous adsorption of primary amines to a GC surface was described, forming nearly monolayer coverage that resisted removal by sonication.[401] XPS and FTIR were used to observe surface bound nitrogen, and the surfaces were characterized electrochemically.[401]

A distinct modification reaction that is also mediated by a primary carbon radical is based on the oxidation of carboxylates.[374] After carboxylate oxidation and subsequent loss of CO_2, the primary radical may bond to the carbon surface. The voltammetry shown in Figure 42 illustrates the oxidation of naphthyl-methyl carboxylate at +1 to 1.1 V vs Ag^+/Ag on either GC or PPF, with the second voltammetric

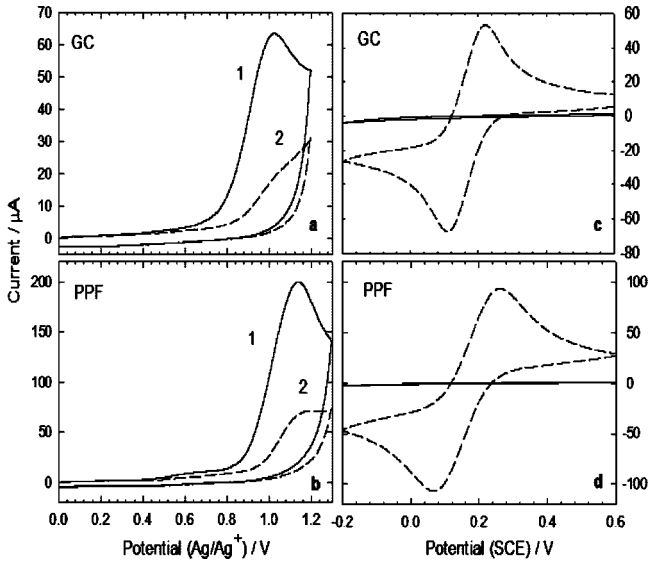

Figure 42. Cyclic voltammetry at GC (a, c) and PPF (b, d) surfaces, 0.2 V/s: (a, b) first scan (solid line) and second scan (dashed) with stirring between scans of 5.2 mM naphthylmethyl-carboxylate in 0.1 M $TBABF_4/CH_3CN$ solution; (c, d) scans of 3.1 mM $Fe(CN)_6^{3-}$ in aqueous 0.2 M KCl at bare (dashed) and naphthylmethyl-modified (solid) surfaces. Reprinted with permission from ref 374. Copyright 2005 American Chemical Society.

scan much smaller due to formation of the modification layer. The naphthyl-methyl film bonded to the surface completely inhibited electron transfer to a $Fe(CN)_6^{3-/4-}$ redox system, and it was concluded that the modification reaction formed multilayers under the conditions employed.[374]

5.4. Modification by "Click" Chemistry

A recent and potentially versatile carbon surface modification is based on "click" cycloaddition chemistry to a surface-bound azide group.[403] Cu(I)-catalyzed cycloaddition of alkynes to azides yields a stable triazole ring, and the reaction has been used in a variety of applications, including linking electroactive alkynes with azide groups in self-assembled monolayers on Au electrodes.[404–406] For graphitic carbon electrodes,[407] the azide may be covalently attached to the surface by addition of iodine azide, IN_3, across a double bond on a graphitic edge plane, as shown in Figure 43.

XPS analysis of the azide-modified PPF surface revealed the presence of a surface bound azide group (shown in Figure 43B) with a coverage of $\sim 1 \times 10^{-10}$ mol/cm^2. Reaction of the azide-modified surface with ethynylferrocene in the presence of a Cu(I) catalyst resulted in the appearance of the surface voltammetric wave for ferrocene oxidization, shown in the inset of Figure 43, as well as changes to the N_{1s} XPS bands (395−406 eV). The coverage of ferrocene determined voltametrically was less than that of a typical monolayer. The use of "click" chemistry for carbon surface modification has the attraction of using a reaction with a single reagent to bond a "primer" to the surface, followed by coupling to a possibly wide range of alkynes to yield functionalized surfaces.

6. Synopsis and Outlook

Despite at least 100 years of active use of carbon materials in electrochemistry, there is no shortage of new materials, properties, and applications. The advent of fullerenes and conducting diamond by themselves represent major new avenues for research and development of carbon electrodes, but these innovations are accompanied by microfabricated carbon films and devices, aggressive covalent surface modifications, and a variety of new carbon composites for mechanistic and analytical electrochemistry. The continued growth of applications for carbon materials in electrochemistry is assured by the properties that attracted the initial users

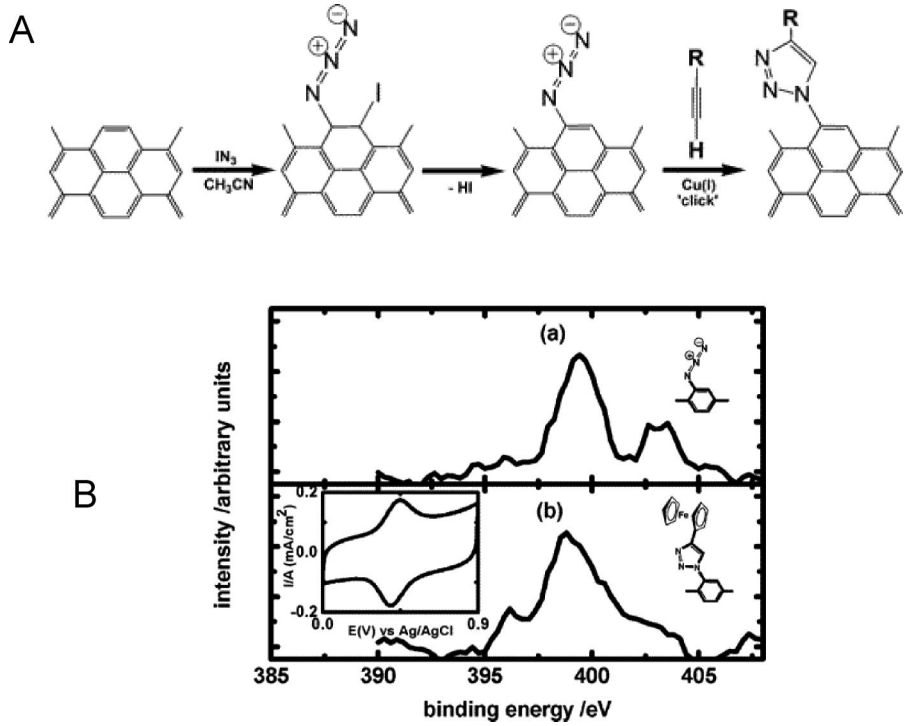

Figure 43. (A) Proposed reaction sequence for treatment of carbon surfaces with iodine azide followed by a terminal alkyne and (B) XPS spectra of a PPF surface before (a) and after (b) reaction of the azide-modified surface with a ferrocene alkyne. Inset in panel b is the surface voltammetry of the ferrocene modified surface. Reprinted with permission from ref 407. Copyright 2007 American Chemical Society.

of carbon electrodes long ago: the availability of different conducting allotropes, the strong covalent bonds within carbon materials and to a variety of surface modifiers, the good thermal and electrochemical stability, and the possibility of a wide range of carbon microstructures of varying hardness, cost, and reactivity. The obvious point that sp^2 and sp^3 hybridized carbon materials differ fundamentally from metals in their structure, reactivity, and electronic properties still deserves emphasis, because those differences enable many of the major applications of carbon materials in electrochemistry.

It is generally risky to attempt to predict future results of scientific research, but some consideration of probable upcoming developments in carbon electrochemistry is stimulated by the preceding review. Carbon nanotubes and conducting diamond both hold significant promise, the former for unusual electrode architectures enabled by nanotube conductivity and aspect ratio and the latter by the hardness and stability of diamond. Just as the dimensionally stable anode revolutionized industrial electrochemistry, the stability of diamond may find significant applications where stability is paramount. The large length to diameter ratio of carbon nanotubes, combined with their high conductivity enable new electrode architectures for "wired" composites which enhance electrical communication between a bulk conductor and an enzyme or redox-active electrode modifier. In the author's opinion, there is still work to be done on the preparation of monodisperse CNT materials and on determining and controlling the structural parameters that underlie their behavior. Applications requiring ordered arrays of CNTs with low defects will depend additionally on growth and fabrication innovations.

Another promising area for future advances in carbon electrochemistry is micro- or nanostructuring of thin films and their surfaces. With electron beam and nanoimprint lithography permitting design and microfabrication of carbon thin films at the 10−100 nm level and the variety of surface modifications discussed in section 5, there is a wealth of opportunities for nanoscale electrochemical devices based on carbon materials. These may include interdigitated arrays, nanogaps, ultramicroelectrodes, and microfluidic channels and detectors. When the dimensions of an electrode approach the nanometer scale of nanotubes and modern lithographic structures, mass transport is much more efficient, thus permitting the study of very fast electrode kinetics and enhancing the response of many electroanalytical sensors. Furthermore, when the electrode dimension approaches the double layer thickness, interesting and unusual kinetic and electrostatic effects occur. It is likely that carbon nanotubes and other nanostructured electrodes will be key players in the investigation of such phenomena. Even when the many advances in carbon materials for electrochemistry of the past ~15 years are considered, it is clear there remains plenty of "mileage" in carbon materials for both fundamental and applied research and development in electrochemistry.

7. Acknowledgments

Most of the work cited from the author's laboratory was supported by the National Science Foundation (USA), the Air Force Office of Scientific Research (USA), and ZettaCore (Denver, USA). Work performed in Canada was supported by the Natural Science and Engineering Research Council, the National Research Council, and the Alberta Ingenuity Fund.

8. References

(1) Walker, P. L.; Radovic, L. R. *Chemistry and Physics of Carbon*; Dekker: New York.
(2) Kinoshita, K. *Carbon, Electrochemical and Physicochemical Properties*; John Wiley and Sons: New York, 1988.
(3) McCreery, R. L. In *Electroanalytical Chemistry*; Bard, A. J., Ed.; Dekker, New York, 1991; Vol *17*.
(4) Leon y Leon, C. A.; Radovic, L. R. In *Chemistry and Physics of Carbon*; Thrower, P. A., Ed.; Dekker: New York, 1994; Vol *24*.
(5) Wu, J.; Pisula, W.; Mullen, K. *Chem. Rev.* **2007**, *107*, 718–747.
(6) Moore, A. In *Chemistry and Physics of Carbon*; Thrower, P. A., Ed., 1981; Vol *17*.
(7) Matthews, M. J.; Pimenta, M. A.; Dresselhaus, G.; Dresselhaus, M. S.; Endo, M. *Phys. Rev. B* **1999**, *59*, R6585–R6588.
(8) Speck, J. S.; Steinbeck, J.; Dresselhaus, G. *J. Mater. Res.* **1990**, *5*, 980–988.
(9) Al-Jishi, R.; Dresselhaus, G. *Phys. Rev. B* **1982**, *26*, 4523–4538.
(10) Wang, Y.; Alsmeyer, D. C.; McCreery, R. L. *Chem. Mater.* **1990**, *2*, 557–563.
(11) Wightman, R. M. *Science* **2006**, *311*, 1570–1574.
(12) Hermans, A.; Seipel, A. T.; Miller, C. E.; Wightman, R. M. *Langmuir* **2006**, *22*, 1964–1969.
(13) Heien, M. L. A. V.; Johnson, M. A.; Wightman, R. M. *Anal. Chem.* **2004**, *76*, 5697–5704.
(14) Dresselhaus, M. S. *Graphite Fibers and Filaments*; Springer-Verlag: New York, 1988.
(15) Jenkins, G. M.; Kawamura, K. *Polymeric Carbons, Carbon Fibre, Glass and Char*; University Press: Cambridge, England, 1976.
(16) McDermott, M. T.; McDermott, C. A.; McCreery, R. L. *Anal. Chem.* **1993**, *65*, 937.
(17) McDermott, C. A.; McCreery, R. L. *Langmuir* **1994**, *10*, 4307.
(18) Howard, H. D.; Pocard, N. L.; Alsmeyer, D.; Schueller, O. J. A.; Spontak, R. J.; Huston, M. E.; Huang, W.; McCreery, R. L.; Neenan, T.; Callstrom, M. *Chem. Mater.* **1993**, *5*, 1727.
(19) Hutton, H. D.; Huang, W.; Alsmeyer, D.; Kometani, J.; McCreery, R. L.; Neenan, T.; Callstrom, M. R. *Chem. Mater.* **1993**, *5*, 1110.
(20) Hutton, H. D.; Alsmeyer, D. C.; McCreery, R. L.; Neenan, T. X.; Callstrom, M. *Polym. Mater. Sci. Eng.* **1992**, *67*, 237.
(21) Callstrom, M.; Neenan, T.; McCreery, R. L.; Alsmeyer, D. *J. Am. Chem. Soc.* **1990**, *112*, 4954.
(22) Kim, H.-G.; Ahn, S.-H.; Kim, J.-G.; Park, S. J.; Lee, K.-R. *Thin Solid Films* **2005**, *475*, 291.
(23) Godet, C.; Conway, N. M. J.; Bouree, J. E.; Bouamra, K.; Grosman, A.; Ortega, C. *J. Appl. Phys.* **2002**, *91*, 4154–4162.
(24) Jia, J.; Kato, D.; Kurita, R.; Sato, Y.; Maruyama, K.; Suzuki, K.; Hirono, S.; Ando, T.; Niwa, O. *Anal. Chem.* **2007**, *79*, 98–105.
(25) Zhou, M.; Ding, J.; Guo, L.-p.; Shang, Q.-k. *Anal. Chem.* **2007**, *79*, 5328–5335.
(26) Li, H.-Q.; Luo, J.-Y.; Zhou, X.-F.; Yu, C.-Z.; Xia, Y.-Y. *J. Electrochem. Soc.* **2007**, *154*, A731.
(27) Raghuveer, V.; Manthiram, A. *J. Electrochem. Soc.* **2005**, *152*, A1504.
(28) Santiago, E. I.; Varanda, L. C.; Villullas, H. M. *J. Phys. Chem. C* **2007**, *111*, 3146–3151.
(29) Fang, B.; Kim, J. H.; Lee, C.; Yu, J. S. *J. Phys. Chem. C* **2008**, *112*, 639–645.
(30) Swain, G. M. In *Electroanalytical Chemistry*; Bard, A. J., Rubinstein, I., Eds.; Dekker: New York, 2004; Vol. 22.
(31) Gruen, D. M. *Annu. Rev. Mater. Sci.* **1999**, *29*, 211.
(32) Pleskov, Y.; Krotova, M.; Ralchenko, V.; Saveliev, A.; Bozhko, A. *Russ. J. Electrochem.* **2007**, *43*, 827.
(33) Zhao, W.; Xu, J.-J.; Qiu, Q.-Q.; Chen, H.-Y. *Biosens. Bioelectron.* **2006**, *22*, 649.
(34) Fischer, A. E.; Show, Y.; Swain, G. M. *Anal. Chem.* **2004**, *76*, 2553–2560.
(35) Yoo, K.; Miller, B.; Kalish, R.; Shi, X. *Electrochem. Solid-State Lett.* **1999**, *2*, 233.
(36) Lee, J.-J.; Miller, B.; Shi, X.; Kalish, R.; Wheeler, K. A. *J. Electrochem. Soc.* **2001**, *148*, C183.
(37) Wildgoose, G. G.; Banks, C. E.; Leventis, H. C.; Compton, R. G. *Electrochim. Acta* **2006**, *152*, 187–214.
(38) Valcarcel, M.; Cardenas, S.; Simonet, B. M. *Anal. Chem.* **2007**, *79*, 4788–4797.
(39) Gooding, J. J. *Electrochim. Acta* **2005**, *50*, 3049.
(40) Heller, I.; Kong, J.; Heering, H.; Williams, K.; Lemay, S. G.; Dekker, C. *Nano Lett.* **2005**, *5*, 137–142.
(41) Heller, I.; Kong, J.; Williams, K. A.; Dekker, C.; Lemay, S. G. *J. Am. Chem. Soc.* **2006**, *128*, 7353–7359.
(42) Goldsmith, B. R.; Coroneus, J. G.; Khalap, V. R.; Kane, A. A.; Weiss, G. A.; Collins, P. G. *Science* **2007**, *315*, 77–81.
(43) Kokko, K.; Ojala, E.; Mansikka, K. *Phys. Status Solidi B* **1989**, *153*, 235.

(44) Iwasita, T.; Schmickler, W. *Ber. Bunsen-Ges.* **1985**, *89*, 138–42.
(45) Royea, W. J.; Hamann, T. W.; Brunschwig, B. S.; Lewis, N. S. *J. Phys. Chem. B* **2006**, *110*, 19433–19442.
(46) Dresselhaus, M. S.; Dresselhaus, G.; Fischer, J. E. *Phys. Rev. B* **1977**, *15*, 3180.
(47) Spain, I. L. In *Chemistry and Physics of Carbon*; Thrower, P. L., Ed.; Dekker: New York, 1981; Vol *16.*
(48) Koivusaari, K. J.; Rantala, T. T.; Leppavuori, S. *Diamond Relat. Mater.* **2000**, *9*, 736.
(49) Gerischer, H.; McIntyre, R.; Scherson, D.; Storck, W. *J. Phys. Chem.* **1987**, *91*, 1930.
(50) Rice, R. J.; McCreery, R. L. *Anal. Chem.* **1989**, *61*, 1637.
(51) Rice, R. J.; Pontikos, N.; McCreery, R. L. *J. Am. Chem. Soc.* **1990**, *112*, 4617.
(52) Bard, A. J.; Faulkner, L. R. *Electrochemical Methods*; 2nd ed.; Wiley: New York, 2001.
(53) Granger, M. C.; Witek, M.; Xu, J.; Wang, J.; Hupert, M.; Hanks, A.; Koppang, M. D.; Butler, J. E.; Lucazeau, G.; Mermoux, M.; Strojek, J. W.; Swain, G. M. *Anal. Chem.* **2000**, *72*, 3793–3804.
(54) Taft, E. A.; Philipp, H. R. *Phys. Rev.* **1965**, *138*, A197–A202.
(55) Williams, M. W.; Arakawa, E. T. *J. Appl. Phys.* **1972**, *43*, 3460–3463.
(56) Mattson, J. S.; Smith, C. A. *Anal. Chem.* **1975**, *47*, 1122–1125.
(57) Anjo, D. M.; Brown, S.; Wang, L. *Anal. Chem.* **1993**, *65*, 317–319.
(58) Donner, S.; Li, H. W.; Yeung, E. S.; Porter, M. D. *Anal. Chem.* **2006**, *78*, 2816–2822.
(59) Tian, H.; Bergren, A. J.; McCreery, R. L. *Appl. Spectrosc.* **2007**, *61*, 1246–1253.
(60) Obraztsov, A. N.; Pavlovsky, I. Y.; Izumi, T.; Okushi, H.; Watanabe, H. *Appl. Phys. A: Mater. Sci. Process.* **1997**, *65*, 505.
(61) Stotter, J.; Show, Y.; Wang, S.; Swain, G. *Chem. Mater.* **2005**, *17*, 4880–4888.
(62) Stotter, J.; Zak, J.; Behler, Z.; Show, Y.; Swain, G. M. *Anal. Chem.* **2002**, *74*, 5924–5930.
(63) Martin, H. B.; Morrison, P. W. *Electrochem. Solid-State Lett.* **2001**, *4*, E17.
(64) Tuinstra, F.; Koenig, J. L. *J. Chem. Phys.* **1970**, *53*, 1126.
(65) Negri, F.; Castiglioni, C.; Tommasini, M.; Zerbi, G. *J. Phys. Chem. A* **2002**, *106*, 3306–3317.
(66) Chieu, T. C.; Dresselhaus, M. S.; Endo, M. *Phys. Rev. B* **1982**, *26*, 5867–5877.
(67) Nemanich, R. J.; Solin, S. A. *Phys. Rev. B* **1979**, *20*, 392–401.
(68) Kuo, T.-C.; McCreery, R. L.; Swain, G. M. *Electrochem. Solid State Lett.* **1999**, *2*, 288–291.
(69) Bowling, R.; Packard, R. T.; McCreery, R. L. *J. Electrochem. Soc.* **1988**, *135*, 1605.
(70) Bowling, R.; Packard, R. T.; McCreery, R. L. *J. Am. Chem. Soc.* **1989**, *111*, 1217.
(71) Bowling, R.; Packard, R. T.; McCreery, R. L. *Langmuir* **1989**, *5*, 683.
(72) Alsmeyer, Y.-W.; McCreery, R. L. *Anal. Chem.* **1991**, *63*, 1289.
(73) Alsmeyer, Y. W.; McCreery, R. L. *Langmuir* **1991**, *7*, 2370.
(74) Alsmeyer, D.; McCreery, R. L. *Anal. Chem.* **1992**, *64*, 1528.
(75) Kudin, K. N.; Ozbas, B.; Schniepp, H. C.; Prud'homme, R. K.; Aksay, I. A.; Car, R. *Nano Lett.* **2008**, *8*, 36–41.
(76) Ray, K. G.; McCreery, R. L. *Anal. Chem.* **1997**, *69*, 4680–4687.
(77) Fischer, A. E.; Lowe, M. A.; Swain, G. M. *J. Electrochem. Soc.* **2007**, *154*, K61.
(78) Dresselhaus, M. S.; Dresselhaus, G.; Jorio, A. *J. Phys. Chem. C* **2007**, *111*, 17887–17893.
(79) Heller, D. A.; Barone, P. W.; Swanson, J. P.; Mayrhofer, R. M.; Strano, M. S. *J. Phys. Chem. B* **2004**, *108*, 6905–6909.
(80) Oron-Carl, M.; Hennrich, F.; Kappes, M. M.; Lohneysen, H. v.; Krupke, R. *Nano Lett.* **2005**, *5*, 1761–1767.
(81) Kim, U. J.; Furtado, C. A.; Liu, X.; Chen, G.; Eklund, P. C. *J. Am. Chem. Soc.* **2005**, *127*, 15437–15445.
(82) Rafailov, P.; Stoll, M.; Thomsen, C. *J. Phys. Chem B* **2004**, *108*, 19241–19245.
(83) Anglaret, E.; Dragin, F.; Penicaud, A.; Martel, R. *J. Phys. Chem. B* **2006**, *110*, 3949–3954.
(84) Mattia, D.; Rossi, M. P.; Kim, B. M.; Korneva, G.; Bau, H. H.; Gogotsi, Y. *J. Phys. Chem. B* **2006**, *110*, 9850–9855.
(85) Zhang, L.; Jia, Z.; Huang, L.; O'Brien, S.; Yu, Z. *J. Phys. Chem. C* **2007**, *111*, 11240–11245.
(86) Zhou, J.; Booker, C.; Li, R.; Zhou, X.; Sham, T. K.; Sun, X.; Ding, Z. *J. Am. Chem. Soc.* **2007**, *129*, 744–745.
(87) DeAngelis, T. P.; Hurst, R. W.; Yacynych, A. M.; Mark, H. B., Jr.; Heineman, W. R.; Mattson, J. S. *Anal. Chem.* **1977**, *49*, 1395–1398.
(88) Blackstock, J. J.; Rostami, A. A.; Nowak, A. M.; McCreery, R. L.; Freeman, M.; McDermott, M. T. *Anal. Chem.* **2004**, *76*, 2544–2552.
(89) Liang, H.; Tian, H.; McCreery, R. L. *Appl. Spectrosc.* **2007**, *61*, 613.
(90) Watcharotone, S.; Dikin, D. A.; Stankovich, S.; Piner, R.; Jung, I.; Dommett, G. H. B.; Evmenenko, G.; Wu, S. E.; Chen, S. F.; Liu, C. P.; Nguyen, S. T.; Ruoff, R. S. *Nano Lett.* **2007**, *7*, 1888–1892.
(91) Sun, P.; Mirkin, M. V. *Anal. Chem.* **2006**, *78*, 6526–6534.
(92) Birkin, P. R.; Silva-Martinez, S. *Anal. Chem.* **1997**, *69*, 2055–2062.
(93) Chang, H.; Bard, A. J. *Langmuir* **1991**, *7*, 1143–1153.
(94) McDermott, M. T.; Kneten, K.; McCreery, R. L. *J. Phys. Chem.* **1992**, *96*, 3124.
(95) Kuo, T.-C.; McCreery, R. L. *Anal. Chem.* **1999**, *71*, 1553–1560.
(96) Rice, R.; Allred, C.; McCreery, R. L. *J. Electroanal. Chem.* **1989**, *263*, 163.
(97) Allred, C.; McCreery, R. L. *Anal. Chem.* **1992**, *64*, 444.
(98) Buriak, J. M. *Chem. Rev.* **2002**, *102*, 1271–1308.
(99) Ranganathan, S.; McCreery, R. L. *Anal. Chem.* **2001**, *73*, 893–900.
(100) Ye, X. R.; Chen, L. H.; Wang, C.; Aubuchon, J. F.; Chen, I. C.; Gapin, A. I.; Talbot, J. B.; Jin, S. *J. Phys. Chem. B* **2006**, *110*, 12938–12942.
(101) Osswald, S.; Flahaut, E.; Gogotsi, Y. *Chem. Mater.* **2006**, *18*, 1525–1533.
(102) Banks, C. E.; Compton, R. G. *The Analyst* **2005**, *130*, 1232–1239.
(103) Fang, H. T.; Liu, C.-G.; Liu, C.; Li, F.; Liu, M.; Cheng, H. M. *Chem. Mater.* **2004**, *16*, 5744–5750.
(104) Langley, L. A.; Villanueva, D. E.; Fairbrother, D. H. *Chem. Mater.* **2006**, *18*, 169–178.
(105) Fagan, D. T.; Kuwana, T. *Anal. Chem.* **1989**, *61*, 1017–1023.
(106) Fryling, M.; Zhao, J.; McCreery, R. L. *Anal. Chem.* **1995**, *67*, 967.
(107) Ray, K. G.; McCreery, R. L. *J. Electroanal. Chem.* **1999**, *469*, 150–158.
(108) Gotch, A. J.; Kelly, R. S.; Kuwana, T. *J. Phys. Chem. B* **2003**, *107*, 935–941.
(109) Weiss, D. J.; Kelly, R. S.; Cumaranatunge, M.; Kuwana, T. *Anal. Chem.* **1999**, *71*, 3712–3720.
(110) Kelly, R. S.; Weiss, D. J.; Chong, S. H.; Kuwana, T. *Anal. Chem.* **1999**, *71*, 413–418.
(111) Randin, J.-P.; Yeager, E. *J. Electroanal. Chem.* **1972**, *36*, 257–276.
(112) Gerischer, H. *J. Phys. Chem.* **1985**, *89*, 4249–4251.
(113) McIntyre, R.; Scherson, D.; Storck, W.; Gerischer, H. *Electrochim. Acta* **1987**, *32*, 51–53.
(114) Kneten, K.; McCreery, R. L. *Anal. Chem.* **1992**, *64*, 2518.
(115) Murray, B. J.; Newberg, J. T.; Walter, E. C.; Li, Q.; Hemminger, J. C.; Penner, R. M. *Anal. Chem.* **2005**, *77*, 5205–5214.
(116) Walter, E. C.; Murray, B. J.; Favier, F.; Kaltenpoth, G.; Grunze, M.; Penner, R. M. *J. Phys. Chem. B* **2002**, *106*, 11407–11411.
(117) Li, Q.; Olson, J. B.; Penner, R. M. *Chem. Mater.* **2004**, *16*, 3402–3405.
(118) Ta, T. C.; Kanda, V.; McDermott, M. T. *J. Phys. Chem. B* **1999**, *103*, 1295–1302.
(119) McCreery, R. L.; Cline, K. K.; McDermott, C. A.; McDermott, M. T. *Colloids Surf.* **1994**, *93*, 211.
(120) McDermott, C. A.; Kneten, K.; McCreery, R. L. *J. Electrochem. Soc.* **1993**, *140*, 2593.
(121) Chen, P.; Fryling, M.; McCreery, R. L. *Anal. Chem.* **1995**, *67*, 3115.
(122) Chen, P.; McCreery, R. L. *Anal. Chem.* **1996**, *68*, 3958.
(123) Peter, L. M.; Durr, W.; Bindra, P.; Gerischer, H. *J. Electroanal. Chem.* **1976**, *71*, 31.
(124) Huang, W.; McCreery, R. L. *J. Electroanal. Chem.* **1992**, *1*, 326.
(125) DuVall, S.; McCreery, R. L. *Anal. Chem.* **1999**, *71*, 4594–4602.
(126) DuVall, S.; McCreery, R. L. *J. Am. Chem. Soc.* **2000**, *122*, 6759–6764.
(127) Huang, T.; Warsinke, A.; Koroljova-Skorobogatko, O. V.; Makower, A.; Kuwana, T.; Scheller, F. W. *Electroanalysis* **1999**, *11*, 295–300.
(128) Mao, F.; Mano, N.; Heller, A. *J. Am. Chem. Soc.* **2003**, *125*, 4951–4957.
(129) Newman, J. D.; White, S. F.; Tothill, I. E.; Turner, A. P. F. *Anal. Chem.* **1995**, *67*, 4594–4599.
(130) Yang, H.-H.; McCreery, R. L. *J. Electrochem. Soc.* **2000**, *147*, 3420–3428.
(131) Martin, H. B.; Argoitia, A.; Angus, J. C.; Landau, U. *J. Electrochem. Soc.* **1999**, *146*, 2959.
(132) Niwa, O.; Jia, J.; Sato, Y.; Kato, D.; Kurita, R.; Maruyama, K.; Suzuki, K.; Hirono, S. *J. Am. Chem. Soc.* **2006**, *128*, 7144–7145.
(133) Devaraj, N. K.; Decreau, R. A.; Ebina, W.; Collman, J. P.; Chidsey, C. E. D. *J. Phys. Chem. B* **2006**, *110*, 15955–15962.
(134) Smalley, J. F.; Finkea, H. O.; Chidsey, C. E. D.; Linford, M. R.; Creager, S. E.; Ferraris, J. P.; Chalfant, K.; Zawodzinsk, T.; Feldberg, S. W.; Newton, M. D. *J. Am. Chem. Soc.* **2003**, *125*, 2004–2013.
(135) Finklea, H. O. In *Electroanalytical Chemistry*; Bard, A. J., Ed.; Dekker: New York, 1996; Vol *19.*
(136) French, M.; Creager, S. *Langmuir* **1998**, *14*, 2129–2133.
(137) Creager, S.; Yu, C. J.; Bamdad, C.; O'Connor, S.; MacLean, T.; Lam, E.; Chong, Y.; Olsen, G. T.; Luo, J.; Gozin, M.; Kayyem, J. F. *J. Am. Chem. Soc.* **1999**, *121*, 1059–1064.

(138) Roth, K. M.; Yasseri, A. A.; Liu, Z. M.; Dabke, R. B.; Malinovskii, V.; Schweikart, K. H.; Yu, L. H.; Tiznado, H.; Zaera, F.; Lindsey, J. S.; Kuhr, W. G.; Bocian, D. F. *J. Am. Chem. Soc.* **2003**, *125*, 505–517.
(139) Yang, H.-H.; McCreery, R. L. *Anal. Chem.* **1999**, *71*, 4081–4087.
(140) Solak, A. O.; Eichorst, L. R.; Clark, W. J.; McCreery, R. L. *Anal. Chem.* **2003**, *75*, 296–305.
(141) Kawiak, J.; Kulesza, P. J.; Galus, Z. *J. Electroanal. Chem.* **1987**, *226*, 305.
(142) McCreery, R. L.; Cline, K. K. In *Laboratory Techniques in Electroanalytical Chemistry*; Kissinger, P. T., Heineman, W. R., Eds.; Dekker: New York, 1996.
(143) Kawagoe, K. T.; Zimmerman, J. B.; Wightman, R. M. *J. Neurosci. Methods* **1993**, *48*, 225.
(144) Hu, I. F.; Karweik, D. H.; Kuwana, T. *J. Electroanal. Chem.* **1985**, *188*, 59.
(145) Kiema, G. K.; Aktay, M.; McDermott, M. T. *J. Electroanal. Chem.* **2003**, *540*, 7.
(146) Ranganathan, S.; Kuo, T.-C.; McCreery, R. L. *Anal. Chem.* **1999**, *71*, 3574–3580.
(147) Runnels, P. L.; Joseph, J. D.; Logman, M. J.; Wightman, R. M. *Anal. Chem.* **1999**, *71*, 2782–2789.
(148) Mazur, S.; Matusinovic, T.; Cammann, K. *J. Am. Chem. Soc.* **1977**, *99*, 3888–3891.
(149) Ranganathan, S.; McCreery, R. L.; Majji, S. M.; Madou, M. *J. Electrochem. Soc.* **2000**, *147*, 277–282.
(150) Hsueh, C. C.; Brajter-Toth, A. *Anal. Chem.* **1993**, *65*, 1570–1575.
(151) Hershenhart, E.; McCreery, R. L.; Knight, R. D. *Anal. Chem.* **1984**, *56*, 2256.
(152) Poon, M.; McCreery, R. L. *Anal. Chem.* **1986**, *58*, 2745.
(153) Poon, M.; McCreery, R. L. *Anal. Chem.* **1988**, *60*, 1725.
(154) Rice, R.; McCreery, R. L. *J. Electroanal. Chem.* **1991**, *310*, 127.
(155) Robinson, R. S.; Sternitzke, K. D.; McCreery, R. L. *J. Vac. Sci. Technol. B* **1991**, *9*, 960.
(156) Poon, M.; McCreery, R. L. *Anal. Chem.* **1987**, *59*, 1615.
(157) Sternitzke, K. D.; McCreery, R. L. *Anal. Chem.* **1990**, *62*, 1339.
(158) Strein, T. G.; Ewing, A. G. *Anal. Chem.* **1994**, *66*, 3864–3872.
(159) Strein, T. G.; Ewing, A. G. *Anal. Chem.* **1991**, *63*, 194–198.
(160) Chen, T. K.; Strein, T. G.; Abe, T.; Ewing, A. G. *Electroanalysis* **1994**, *6*, 746–751.
(161) Farrell; Patrick, C.; Kinley; Patrick, R.; Weiss; David, J.; Strein; Timothy, G. *Electroanalysis* **2003**, *15*, 813–820.
(162) Sternitzke, K. D.; McCreery, R. L.; Bruntlett, C.; Kissinger, P. T. *Anal. Chem.* **1989**, *61*, 1989.
(163) Treado, P. J.; Govil, A.; Morris, M. D.; Sternitzke, K. D.; McCreery, R. L. *Appl. Spectrosc.* **1990**, *44*, 1270.
(164) Braunstein, G.; Steinbeck, J.; Dresselhaus, M. S.; Dresselhaus, G.; Elman, B. S.; Venkatesan, T.; Wilkens, B.; Jacobson, D. C. *Mater. Res. Symp.* **1986**, 233–243.
(165) Jaworski, R. K.; McCreery, R. L. *J. Electrochem. Soc.* **1993**, *140*, 1360.
(166) Jaworski, R. K.; McCreery, R. L. *J. Electroanal. Chem.* **1994**, *369*, 175.
(167) Rosenwald, S. E.; Nowall, W. B.; Dontha, N.; Kuhr, W. G. *Anal. Chem.* **2000**, *72*, 4914–4920.
(168) Brooks, S. A.; Ambrose, W. P.; Kuhr, W. G. *Anal. Chem.* **1999**, *71*, 2558–2563.
(169) Kelly, R. S.; Coleman, B. D.; Huang, T.; Inkaew, P.; Kuwana, T. *Anal. Chem.* **2002**, *74*, 6364–6369.
(170) Kiema, G. K.; Fitzpatrick, G.; McDermott, M. T. *Anal. Chem.* **1999**, *71*, 4306–4312.
(171) Kiema, G. K.; Ssenyange, S.; McDermott, M. T. *J. Electrochem. Soc.* **2004**, *151*, C142.
(172) Wang, H.-S.; Ju, H.-X.; Chen, H.-Y. *Anal. Chim. Acta* **2002**, *461*, 243.
(173) Vaik, K.; Schiffrin, D. J.; Tammeveski, K. *Electrochem. Commun.* **2004**, *6*, 1.
(174) Akram, M.; Stuart; Margaret, C.; Wong; Danny, K. Y. *Electroanalysis* **2006**, *18*, 237–246.
(175) El-Nour, K. A.; Brajter-Toth, A. *The Analyst* **2003**, *128*, 1056–1061.
(176) Downard, A. J.; Roddick, A. D. *Electroanalysis* **1994**, *6*, 409–414.
(177) Moore, R. R.; Banks, C. E.; Compton, R. G. *Anal. Chem.* **2004**, *76*, 2677–2682.
(178) Banks, C. E.; Davies, T. J.; Wildgoose, G. G.; Compton, R. G. *Chem. Commun.* **2005**, 829–841.
(179) Saraceno, R. A.; Engstrom, C. E.; Rose, M.; Ewing, A. G. *Anal. Chem.* **1989**, *61*, 560–565.
(180) Kim, Y.-T.; Scarnulis, D. M.; Ewing, A. G. *Anal. Chem.* **1986**, *58*, 1782–1786.
(181) Wallingford, R. A.; Ewing, A. G. *Anal. Chem.* **1988**, *60*, 258–263.
(182) Clark, J. K.; Schilling, W. A.; Wijayawardhana, C. A.; Melaragno, P. R. *Anal. Chem.* **1994**, *66*, 3528–3532.
(183) McFadden, C. F.; Melaragno, P. R.; Davis, J. A. *Anal. Chem.* **1990**, *62*, 742–746.
(184) Pocard, N. L.; Alsmeyer, D.; McCreery, R. L.; Neenan, T.; Callstrom, M. *J. Am. Chem. Soc.* **1992**, *114*, 769.
(185) Kostecki, R.; Schnyder, B.; Alliata, D.; Song, X.; Kinoshita, K.; Kotz, R. *Thin Solid Films* **2001**, *396*, 36–43.
(186) Kostecki, R.; Song, X.; Kinoshita, K. *Electrochem. Solid-State Lett.* **1999**, *2*, 465.
(187) Fischer; David, J.; Vandaveer; Walter, R.; Ryan, I. V.; Grigsby, J.; Lunte; Susan, M. *Electroanalysis* **2005**, *17*, 1153–1159.
(188) Galobardes, F.; Wang, C.; Madou, M. *Diamond Relat. Mater.* **2006**, *15*, 1930.
(189) Brooksby, P. A.; Downard, A. J. *J. Phys. Chem. B* **2005**, *109*, 8791–8798.
(190) Yu, S. S. C.; Downard, A. J. *Langmuir* **2007**, *23*, 4662–4668.
(191) Lyons, A. M. *J. Non-Cryst. Solids* **1985**, *70*, 99.
(192) Lyons, A. M.; Hale, L. P.; Wilkins, J. C. W. *J. Vac. Sci. Technol. B* **1985**, *3*, 447.
(193) Schueller, O. J. A.; Brittain, S. T.; Marzolin, C.; Whitesides, G. M. *Chem. Mater.* **1997**, *9*, 1399–1406.
(194) Kostecki, R.; Song, X.; Kinoshita, K. *Electrochem. Solid-State Lett.* **2002**, *5*, E29.
(195) Brooksby, P. A.; Downard, A. J. *Langmuir* **2004**, *20*, 5038–5045.
(196) Brooksby, P. A.; Downard, A. J. *Langmuir* **2005**, *21*, 1672–1675.
(197) Anariba, F.; DuVall, S. H.; McCreery, R. L. *Anal. Chem.* **2003**, *75*, 3837–3844.
(198) Kostecki, R.; Song, X. Y.; Kinoshita, K. *J. Electrochem. Soc.* **2000**, *147*, 1878.
(199) Wang, C.; Madou, M. *Biosens. Bioelectron.* **2005**, *20*, 2181.
(200) McCreery, R.; Wu, J.; Kalakodimi, R. J. *Phys. Chem. Chem. Phys.* **2006**, *8*, 2572–2590.
(201) Nowak, A.; McCreery, R. *J. Am. Chem. Soc.* **2004**, *126*, 16621–16631.
(202) McCreery, R. L.; Dieringer, J.; Solak, A. O.; Snyder, B.; Nowak, A.; McGovern, W. R.; DuVall, S. *J. Am. Chem. Soc.* **2003**, *125*, 10748–10758.
(203) Downard, A. J.; Garrett, D. J.; Tan, E. S. Q. *Langmuir* **2006**, *22*, 10739–10746.
(204) Hermans, A.; Wightman, R. M. *Langmuir* **2006**, *22*, 10348–10353.
(205) Tang, C.; Qi, K.; Wooley, K. L.; Matyjaszewski, K.; Kowalewski, T. *Angew. Chem., Int. Ed.* **2004**, *43*, 2783–2787.
(206) Kowalewski, T.; Tsarevsky, N. V.; Matyjaszewski, K. *J. Am. Chem. Soc.* **2002**, *124*, 10632–10633.
(207) You, T.; Niwa, O.; Tomita, M.; Ichino, T.; Hirono, S. *J. Electrochem. Soc.* **2002**, *149*, E479.
(208) Wang, S.; Swain, G. M. *J. Phys. Chem. C* **2007**, *111*, 3986–3995.
(209) Lowe, M. A.; Fischer, A. E.; Swain, G. M. *J. Electrochem. Soc.* **2006**, *153*, B506.
(210) Farrell, J.; Martin, F. J.; Martin, H. B.; O'Grady, W. E.; Natishan, P. *J. Electrochem. Soc.* **2005**, *152*, E14.
(211) Pleskov, Y. V. *Russ. J. Electrochem.* **2002**, *38*, 1275.
(212) Pleskov, Y. V.; Evstefeeva, Y. E.; Krotova, M. D.; Varnin, V. P.; Teremetskaya, I. G. *J. Electroanal. Chem.* **2006**, *595*, 168.
(213) Ivandini, T. A.; Sato, R.; Makide, Y.; Fujishima, A.; Einaga, Y. *Diamond Relat. Mater.* **2004**, *13*, 2003.
(214) Ivandini, T. A.; Sato, R.; Makide, Y.; Fujishima, A.; Einaga, Y. *Anal. Chem.* **2006**, *78*, 6291–6298.
(215) Watanabe, T.; Ivandini, T. A.; Makide, Y.; Fujishima, A.; Einaga, Y. *Anal. Chem.* **2006**, *78*, 7857–7860.
(216) Yamaguchi, Y.; Yamanaka, Y.; Miyamoto, M.; Fujishima, A.; Honda, K. *J. Electrochem. Soc.* **2006**, *153*, J123.
(217) Arihara, K.; Terashima, C.; Fujishima, A. *J. Electrochem. Soc.* **2007**, *154*, E71.
(218) Cai, Y.; Anderson, A. B.; Angus, J. C.; Kostadinov, L. N. *J. Electrochem. Soc.* **2007**, *154*, F36.
(219) Sopchak, D.; Miller, B.; Kalish, R.; Avyigal, Y.; Shi, X. *Electroanalysis* **2002**, *14*, 473–478.
(220) Cvacka, J.; Quaiserova, V.; Park, J.; Show, Y.; Muck, A.; Swain, G. M. *Anal. Chem.* **2003**, *75*, 2678–2687.
(221) Park, J.; Show, Y.; Quaiserova, V.; Galligan, J. J.; Fink, G. D.; Swain, G. M. *J. Electroanal. Chem.* **2005**, *583*, 56.
(222) Park, J.; Galligan, J. J.; Fink, G. D.; Swain, G. M. *Anal. Chem.* **2006**, *78*, 6756–6764.
(223) Rezek, B.; Shin, D.; Nakamura, T.; Nebel, C. E. *J. Am. Chem. Soc.* **2006**, *128*, 3884–3885.
(224) Yang, W.; Auciello, O.; Butler, J. E.; Cai, W.; Carlisle, J.; Gerbi, J.; Gruen, D.; Knickerbocker, T.; Lasseter, T.; John, N.; Russell, J.; Smith, L. M.; Hamers, R. J. *Nat. Mater.* **2002**, *1*, 253–257.
(225) Show, Y.; Witek, M. A.; Sonthalia, P.; Swain, G. M. *Chem. Mater.* **2003**, *15*, 879–888.
(226) Koppang, M. D.; Witek, M.; Blau, J.; Swain, G. M. *Anal. Chem.* **1999**, *71*, 1188–1195.

(227) Wilson, N. R.; Clewes, S. L.; Newton, M. E.; Unwin, P. R.; Macpherson, J. V. *J. Phys. Chem. B* **2006**, *110*, 5639–5646.
(228) Haymond, S.; Babcock, G. T.; Swain, G. M. *J. Am. Chem. Soc.* **2002**, *124*, 10634–10635.
(229) Song, Y.; Swain, G. M. *Anal. Chem.* **2007**, *79*, 2412–2420.
(230) Song, Y.; Swain, G. M. *Anal. Chim. Acta* **2007**, *593*, 7.
(231) Bennett, J. A.; Show, Y.; Wang, S.; Swain, G. M. *J. Electrochem. Soc.* **2005**, *152*, E184.
(232) Wang, J.; Swain, G. M.; Tachibana, T.; Kobashi, K. *Electrochem. Solid-State Lett.* **2000**, *3*, 286.
(233) Wang, J.; Swain, G. M. *J. Electrochem. Soc.* **2003**, *150*, E24.
(234) Schrock, D. S.; Wipf, D. O.; Baur, J. E. *Anal. Chem.* **2007**, *79*, 4931–4941.
(235) Ewing, A. G.; Strein, T. G.; Lau, Y. Y. *Acc. Chem. Res.* **1992**, *25*, 440–447.
(236) Maldonado, S.; Stevenson, K. J. *J. Phys. Chem. B* **2005**, *109*, 4707–4716.
(237) Maldonado, S.; Morin, S.; Stevenson, K. J. *Carbon* **2006**, *44*, 1429.
(238) Vijayaraghavan, G.; Stevenson, K. J. *Langmuir* **2007**, *23*, 5279–5282.
(239) Maldonado, S.; Stevenson, K. J. *J. Phys. Chem. B* **2004**, *108*, 11375–11383.
(240) Strein, T. G.; Ewing, A. G. *Anal. Chem.* **1992**, *64*, 1368–1373.
(241) El-Giar; EmadE-Deen, M.; Wipf; David, O. *Electroanalysis* **2006**, *18*, 2281–2289.
(242) Liu, B.; Rolland, J. P.; DeSimone, J. M.; Bard, A. J. *Anal. Chem.* **2005**, *77*, 3013–3017.
(243) Slevin, C. J.; Gray, N. J.; Macpherson, J. V.; Webb, M. A.; Unwin, P. R. *Electrochem. Commun.* **1999**, *1*, 282.
(244) Conyers, J. L.; White, H. S. *Anal. Chem.* **2000**, *72*, 4441–4446.
(245) Chen, S.; Kucernak, A. *Electrochem. Commun.* **2002**, *4*, 80.
(246) Chen, S.; Kucernak, A. *J. Phys. Chem. B* **2002**, *106*, 9396–9404.
(247) Tel-Vered, R.; Walsh, D. A.; Mehrgardi, M. A.; Bard, A. J. *Anal. Chem.* **2006**, *78*, 6959–6966.
(248) Chen, S.; Kucernak, A. *J. Phys. Chem. B* **2003**, *107*, 8392–8402.
(249) Oldham, K. *Anal. Chem.* **1992**, *64*, 646–651.
(250) Lambie, B. A.; Orwar, O.; Weber, S. G. *Anal. Chem.* **2006**, *78*, 5165–5171.
(251) Wu, Z.; Chen, L.; Shen, G.; Yu, R. *Sens. Actuators, B* **2006**, *119*, 295.
(252) Pihel, K.; Walker, Q. D.; Wightman, R. M. *Anal. Chem.* **1996**, *68*, 2084–2089.
(253) Kawagoe, K. T.; Garris, P. A.; Wightman, R. M. *J. Electroanal. Chem.* **1993**, *259*, 193–207.
(254) Zimmerman, J. B.; Wightman, R. M. *Anal. Chem.* **1991**, *63*, 24–28.
(255) Peters, J. L.; Kulagina, N. V.; Hua, Y.; Michael, A. C. In *Encyclopedia of Electrochemistry*; Bard, A., Stratmann, M., Eds.; Wiley-VCH: Weinheim, Germany, 2002; Vol *9*.
(256) Zhang, M.; Liu, K.; Xiang, L.; Lin, Y.; Su, L.; Mao, L. *Anal. Chem.* **2007**, *79*, 6559–6565.
(257) Clark, R. A.; Zerby, R. A.; Ewing, A. G. In *Electroanalytical Chemistry*; Bard, A., Ed.; Dekker: New York, 1998; Vol *20.*
(258) Wang, W.; Xiong, Y.; Du, F.-Y.; Huang, W.-H.; Wu, W.-Z.; Wang, Z.-L.; Cheng, J.-K.; Yang, Y.-F. *The Analyst* **2007**, *132*, 515–518.
(259) Verchier, Y.; Lardy, B.; Nguyen, M. V. C.; Morel, F.; Arbault, S.; Amatore, C. *Biochem. Biophys. Res. Commun.* **2007**, *361*, 493.
(260) Amatore, C.; Arbault, S.; Bouret, Y.; Guille, M.; Lemaître, F.; Verchier, Y. *ChemBioChem* **2006**, *7*, 1998–2003.
(261) Troyer, K. P.; Wightman, R. M. *Anal. Chem.* **2002**, *74*, 5370–5375.
(262) Amatore, C.; Arbault, S.; Bruce, D.; Oliveira, P. d.; Erard, M.; Vuillaume, M. *Faraday Discuss.* **2000**, *116*, 319–333.
(263) El-Nour, K. A.; Brajter-Toth, A. *Electroanalysis* **2000**, *12*, 805–810.
(264) Stromberg, A.; Ryttsen, F.; Chiu, D. T.; Davidson, M.; Eriksson, P. S.; Wilson, C. F.; Orwar, O.; Zare, R. N. *Proc. Natl. Acad. Sci. U.S.A.* **2000**, *97*, 7–11.
(265) Gross, E. M.; Pastore, P.; Wightman, R. M. *J. Phys. Chem. B* **2001**, *105*, 8732–8738.
(266) Badocco, D.; Zanon, F.; Pastore, P. *Electrochim. Acta* **2006**, *51*, 6442.
(267) Maus, R. G.; Wightman, R. M. *Anal. Chem.* **2001**, *73*, 3993–3998.
(268) Campbell, J. K.; Sun, L.; Crooks, R. M. *J. Am. Chem. Soc.* **1999**, *121*, 3779–3780.
(269) Viculis, L. M.; Mack, J. J.; Kaner, R. B. *Science* **2003**, *299*, 1361.
(270) Nugent, J. M.; Santhanam, K. S. V.; Rubio, A.; Ajayan, P. M. *Nano Lett.* **2001**, *1*, 87–91.
(271) Dumitrescu, I.; Wilson, N. R.; Macpherson, J. V. *J. Phys. Chem. C* **2007**, *111*, 12944–12953.
(272) Wilson, N. R.; Guille, M.; Dumitrescu, I.; Fernandez, V. R.; Rudd, N. C.; Williams, C. G.; Unwin, P. R.; Macpherson, J. V. *Anal. Chem.* **2006**, *78*, 7006–7015.
(273) Bertoncello, P.; Edgeworth, J. P.; Macpherson, J. V.; Unwin, P. R. *J. Am. Chem. Soc.* **2007**, *129*, 10982–10983.
(274) Liu, Z.; Shen, Z.; Zhu, T.; Hou, S.; Ying, L.; Shi, Z.; Gu, Z. *Langmuir* **2000**, *16*, 3569–3573.
(275) McKnight, T. E.; Peeraphatdit, C.; Jones, S. W.; Fowlkes, J. D.; Fletcher, B. L.; Klein, K. L.; Melechko, A. V.; Doktycz, M. J.; Simpson, M. L. *Chem. Mater.* **2006**, *18*, 3203–3211.
(276) Li, J.; Ng, H. T.; Cassell, A.; Fan, W.; Chen, H.; Ye, Q.; Koehne, J.; Han, J.; Meyyappan, M. *Nano Lett.* **2003**, *3*, 597–602.
(277) Hinds, B. J.; Chopra, N.; Rantell, T.; Andrews, R.; Gavalas, V.; Bachas, L. G. *Science* **2004**, *303*, 62–65.
(278) Li, J.; Cassell, A.; Delzeit, L.; Han, J.; Meyyappan, M. *J. Phys. Chem. B* **2002**, *106*, 9299–9305.
(279) Streeter, I.; Xiao, L.; Wildgoose, G. G.; Compton, R. G. *J. Phys. Chem. C* **2008**, *112*, 1933–1937.
(280) Maldonado, S.; Morin, S.; Stevenson, K. J. *The Analyst* **2006**, *131*, 262–267.
(281) Gooding, J. J.; Wibowo, R.; Liu, J. Q.; Yang, W.; Losic, D.; Orbons, S.; Mearns, F. J.; Shapter, J. G.; Hibbert, D. B. *J. Am. Chem. Soc.* **2003**, *125*, 9006–9007.
(282) Erdem, A.; Papakonstantinou, P.; Murphy, H. *Anal. Chem.* **2006**, *78*, 6656–6659.
(283) Tuukkanen, S.; Toppari, J. J.; Kuzyk, A.; Hirviniemi, L.; Hytonen, V. P.; Ihalainen, T.; Torma, P. *Nano Lett.* **2006**, *6*, 1339–1343.
(284) Patolsky, F.; Weizmann, Y.; Willner, I. *Angew. Chem., Int. Ed.* **2004**, *43*, 2113–2117.
(285) Yu, X.; Munge, B.; Patel, V.; Jensen, G.; Bhirde, A.; Gong, J. D.; Kim, S. N.; Gillespie, J.; Gutkind, J. S.; Papadimitrakopoulos, F.; Rusling, J. F. *J. Am. Chem. Soc.* **2006**, *128*, 11199–11205.
(286) Jiao, S.; Li, M.; Wang, C.; Chen, D.; Fang, B. *Electrochim. Acta* **2007**, *52*, 5939.
(287) Zhang, M.; Mullens, C.; Gorski, W. *Anal. Chem.* **2005**, *77*, 6396–6401.
(288) Shahrokhian, S.; Zare-Mehrjardi, H. R. *Electrochim. Acta* **2007**, *52*, 6310.
(289) Pumera, M.; Merkoçi, A.; Alegret, S. *Electrophoresis* **2007**, *28*, 1274–1280.
(290) Lawrence; Nathan, S.; Deo; Randhir, P.; Wang, J. *Electroanalysis* **2005**, *17*, 65–72.
(291) Zeng, J.; Gao, X.; Wei, W.; Zhai, X.; Yin, J.; Wu, L.; Liu, X.; Liu, K.; Gong, S. *Sens. Actuators, B* **2007**, *120*, 595.
(292) Jones, C. P.; Jurkschat, K.; Crossley, A.; Compton, R. G.; Riehl, B. L.; Banks, C. E. *Langmuir* **2007**, *23*, 9501–9504.
(293) Wang, J.; Chen, G.; Chatrathi, M. P.; Musameh, M. *Anal. Chem.* **2004**, *76*, 298–302.
(294) Rivas, G. A.; Rubianes, M. D.; Pedano, M. L.; Ferreyra, N. F.; Luque, G. L.; Rodríguez, M. C.; Miscoria, S. A. *Electroanalysis* **2007**, *19*, 823–831.
(295) Punbusayakul, N.; Talapatra, S.; Ci, L.; Surareungchai, W.; Ajayan, P. M. *Electrochem. Solid-State Lett.* **2007**, *10*, F13.
(296) Banks, C. E.; Crossley, A.; Salter, C.; Wilkins, S. J.; Compton, R. G. *Angew. Chem., Int. Ed.* **2006**, *45*, 2533–2537.
(297) Banks, C. E.; Moore, R. R.; Davies, T. J.; Compton, R. G. *Chem. Commun.* **2004**, 1804–1805.
(298) Kruusma, J.; Mould, N.; Jurkschat, K.; Crossley, A.; Banks, C. E. *Electrochem. Commun.* **2007**, *9*, 2330–2333.
(299) Day, T. M.; Unwin, P. R.; Wilson, N. R.; Macpherson, J. V. *J. Am. Chem. Soc.* **2005**, *127*, 10639–10647.
(300) Kaempgen, M.; Roth, S. *Synth. Met.* **2005**, *152*, 353.
(301) Li, J.; Xu, Y.; Wei, H.; Huo, T.; Wang, E. *Anal. Chem.* **2007**, *79*, 5439–5443.
(302) Adams, R. N. *Anal. Chem.* **1958**, *30*, 1576–1576.
(303) Kalcher, K.; Kauffmann, J. M.; Wang, J.; Svancara, I.; Wytras, K.; Neuhold, C.; Yang, Z. *Electroanalysis* **1995**, *7*, 5–22.
(304) Svancara, I.; Wytras, K.; Barek, J.; Zima, J. *Crit. Rev. Anal. Chem.* **2001**, *31*, 311–345.
(305) Zhang, X.; Wang, J.; Wang, Z.; Wang, S. *Synth. Met.* **2005**, *155*, 95–99.
(306) Wu, A.; Venancio, E. C.; MacDiarmid, A. G. *Synth. Met.* **2007**, *157*, 303–310.
(307) Rusling, J. F.; Zhou, L.; Munge, B.; Yang, J.; Estavillo, C.; Schenkman, J. B. *Faraday Discuss.* **2000**, *116*, 77–87.
(308) Sebkova, S.; Navratil, T.; Kopanica, M. *Anal. Lett.* **2005**, *38*, 1747–1758.
(309) Biljana, S.; Banks; Craig, E.; Crossley, A.; Compton, R. G. *Electroanalysis* **2006**, *18*, 1757–1762.
(310) Ambrosi, A.; Castaneda, M. T.; Killard, A. J.; Smyth, M. R.; Alegret, S.; Merkoci, A. *Anal. Chem.* **2007**, *79*, 5232–5240.
(311) Wang, J.; Musameh, M.; Mo, J. W. *Anal. Chem.* **2006**, *78*, 7044–7047.
(312) Darder, M.; Lopez-Blanco, M.; Aranda, P.; Aznar, A. J.; Bravo, J.; Ruiz-Hitzky, E. *Chem. Mater.* **2006**, *18*, 1602–1610.
(313) Zwirtes de Oliveira, I. R. W.; Fernandes, S. C.; Vieira, I. C. *J. Pharm. Biomed. Anal.* **2006**, *41*, 366.
(314) Mandong, G.; Yanqing, L.; Hongxia, G.; Xiaoqin, W.; Lifang, F. *Bioelectrochemistry* **2007**, *70*, 245.

(315) Maleki, N.; Safavi, A.; Tajabadi, F. *Anal. Chem.* **2006**, *78*, 3820–3826.
(316) Kachoosangi; Roohollah, T.; Wildgoose; Gregory, G.; Compton, R. G. *Electroanalysis* **2007**, *19*, 1483–1489.
(317) Safavi, A.; Maleki, N.; Moradlou, O.; Tajabadi, F. *Anal. Biochem.* **2006**, *359*, 224.
(318) Sun, W.; Gao, R.; Jiao, K. *J. Phys. Chem. B* **2007**, *111*, 4560–4567.
(319) Yoon, J.-H.; Muthuraman, G.; Yang, J.; Shim, Y.-B.; Won, M.-S. *Electroanalysis* **2007**, *19*, 1160–1166.
(320) Nie, L.; Guo, H.; He, Q.; Chen, J.; Miao, Y. *J. Nanosci. Nanotechnol.* **2007**, *7*, 560–564.
(321) Wildgoose, G G.; Banks, C. E.; Compton, R. G. *Small* **2006**, *2*, 182–193.
(322) Zhang, Y.; Zeng, G.-M.; Tang, L.; Huang, D.-L.; Jiang, X.-Y.; Chen, Y.-N. *Biosens. Bioelectron.* **2007**, *22*, 2121.
(323) Valentini, F.; Amine, A.; Orlanducci, S.; Terranova, M. L.; Palleschi, G. *Anal. Chem.* **2003**, *75*, 5413–5421.
(324) Antiochia, R.; Lavagnini, I.; Magno, F.; Valentini, F.; Palleschi, G. *Electroanalysis* **2004**, *16*, 1451–1458.
(325) Arribas, A. S.; Bermejo, E.; Chicharro, M.; Zapardiel, A.; Luque, G. L.; Ferreyra, N. F.; Rivas, G. A. *Anal. Chim. Acta* **2006**, *577*, 183.
(326) Sljukic, B.; Banks, C. E.; Salter, C.; Crossley, A.; Compton, R. G. *The Analyst* **2006**, *131*, 670–677.
(327) Wang, J.; Kawde, A.-N.; Musameh, M. *The Analyst* **2003**, *128*, 912–916.
(328) Tomcik, P.; Banks, C. E.; Davies, T. J.; Compton, R. G. *Anal. Chem.* **2004**, *76*, 161–165.
(329) Corgier, B. P.; Marquette, C. A.; Blum, L. J. *Anal. Chim. Acta* **2005**, *538*, 1.
(330) Corgier, B. P.; Li, F.; Blum, L. J.; Marquette, C. A. *Langmuir* **2007**, *23*, 8619–8623.
(331) Kerman, K.; Vestergaard, M.; Tamiya, E. *Anal. Chem.* **2007**, *79*, 6881–6885.
(332) Prodromidis; Mamas, I.; Karayannis; Miltiades, I. *Electroanalysis* **2002**, *14*, 241–261.
(333) Crew, A.; Alford, C.; Cowell, D. C. C.; Hart, J. P. *Electrochim. Acta* **2007**, *52*, 5232.
(334) Azevedo, A. M.; Prazeres, D. M. F.; Cabral, J. M. S.; Fonseca, L. P. *Biosens. Bioelectron.* **2005**, *21*, 235.
(335) Dequaire, M.; Heller, A. *Anal. Chem.* **2002**, *74*, 4370–4377.
(336) Wang, J.; Mo, J.-W.; Erdem, A. *Electroanalysis* **2002**, *14*, 1365–1368.
(337) Jaegfeldt, H.; Kuwana, T.; Johansson, G. *J. Am. Chem. Soc.* **1983**, *105*, 1805–1814.
(338) Murray, R. W. In *Electroanalytical Chemistry*; Bard, A., Ed.; Dekker: New York, 1983; Vol *13*.
(339) Pantano, P.; K, W. *Anal. Chem.* **1993**, *65*, 623–630.
(340) Zhao, J.; McCreery, R. L. *Langmuir* **1995**, *11*, 4036.
(341) Liu, Y.-C.; McCreery, R. L. *Anal. Chem.* **1997**, *69*, 2091.
(342) Gorodetsky, A. A.; Barton, J. K. *Langmuir* **2006**, *22*, 7917–7922.
(343) Delamar, M.; Hitmi, R.; Pinson, J.; Saveant, J. M. *J. Am. Chem. Soc.* **1992**, *114*, 5883–5884.
(344) Barbier, B.; Pinson, J.; Desarmot, G.; Sanchez, M. *J. Electrochem. Soc.* **1990**, *137*, 1757.
(345) Deinhammer, R. S.; Ho, M.; Anderegg, J. W.; Porter, M. D. *Langmuir* **1994**, *10*, 1306–1313.
(346) Pinson, J.; Podvorica, F. *Chem. Soc. Rev.* **2005**, *34*, 429–439.
(347) Allongue, P.; Delamar, M.; Desbat, B.; Fagebaume, O.; Hitmi, R.; Pinson, J.; Saveant, J. M. *J. Am. Chem. Soc.* **1997**, *119*, 201–207.
(348) Itoh, T.; McCreery, R. L. *J. Am. Chem. Soc.* **2002**, *124*, 10894–10902.
(349) Stewart, M. P.; Maya, F.; Kosynkin, D. V.; Dirk, S. M.; Stapleton, J. J.; McGuiness, C. L.; Allara, D. L.; Tour, J. M. *J. Am. Chem. Soc.* **2004**, *126*, 370–378.
(350) Kuo, T.-C. Ph.D. Thesis, The Ohio State University, 1999.
(351) Price, B. K.; Hudson, J. L.; Tour, J. M. *J. Am. Chem. Soc.* **2005**, *127*, 14867–14870.
(352) Adenier, A.; Cabet-Deliry, E.; Chaussé, A.; Griveau, S.; Mercier, F.; Pinson, J.; Vautrin-Ul, C. *Chem. Mater.* **2005**, *17*, 491–501.
(353) Strano, M. S.; Dyke, C. A.; Usrey, M. L.; Barone, P. W.; Allen, M. J.; Shan, H.; Kittrell, C.; Hauge, R. H.; Tour, J. M.; Smalley, R. E. *Science* **2003**, *301*, 1519–1522.
(354) Cheng, F.; Adronov, A. *Chem. Mater.* **2006**, *18*, 5389–5391.
(355) Dyke, C. A.; Tour, J. M. *J. Am. Chem. Soc.* **2003**, *125*, 1156–1157.
(356) de Villeneuve, C. H.; Pinson, J.; Bernard, M. C.; Allongue, P. *J. Phys. Chem. B* **1997**, *101*, 2415–2420.
(357) Hurley, B. L.; McCreery, R. L. *J. Electrochem. Soc.* **2004**, *151*, B252.
(358) Bernard, M.-C.; Chausse, A.; Cabet-Deliry, E.; Chehimi, M. M.; Pinson, J.; Podvorica, F.; Vautrin-Ul, C. *Chem. Mater.* **2003**, *15*, 3450–3462.
(359) Chausse, A.; Chehimi, M. M.; Karsi, N.; Pinson, J.; Podvorica, F.; Vautrin-Ul, C. *Chem. Mater.* **2002**, *14*, 392–400.
(360) Paulik, M. G.; Brooksby, P. A.; Abell, A. D.; Downard, A. J. *J. Phys. Chem. C* **2007**, *111*, 7808–7815.
(361) Downard, A. J.; Tan, E. S. Q.; Yu, S. S. C. *New J. Chem.* **2006**, *30*, 1283–1288.
(362) Deniau, G.; Azoulay, L.; Bougerolles, L.; Palacin, S. *Chem. Mater.* **2006**, *18*, 5421–5428.
(363) Liu, Y.-C.; McCreery, R. L. *J. Am. Chem. Soc.* **1995**, *117*, 11254.
(364) Kalakodimi, R. P.; Nowak, A.; McCreery, R. L. *Chem. Mater.* **2005**, *17*, 4939–4948.
(365) Nowak, A. M.; McCreery, R. L. *Anal. Chem.* **2004**, *76*, 1089–1097.
(366) Kariuki, J. K.; McDermott, M. T. *Langmuir* **2001**, *17*, 5947–5951.
(367) Anariba, F.; Viswanathan, U.; Bocian, D. F.; McCreery, R. L. *Anal. Chem.* **2006**, *78*, 3104–3112.
(368) Combellas, C.; Kanoufi, F.; Pinson, J.; Podvorica, F. *Langmuir* **2005**, *21*, 280–286.
(369) Saby, C.; Ortiz, B.; Champagne, G. Y.; Belanger, D. *Langmuir* **1997**, *13*, 6805–6813.
(370) Rappich, J.; Merson, A.; Roodenko, K.; Dittrich, T.; Gensch, M.; Hinrichs, K.; Shapira, Y. *J. Phys. Chem. B* **2006**, *110*, 1332–1337.
(371) Kariuki, J. K.; McDermott, M. T. *Langmuir* **1999**, *15*, 6534–6540.
(372) Downard, A. J. *Langmuir* **2000**, *16*, 9680–9682.
(373) Cruickshank, A. C.; Tan, E. S. Q.; Brooksby, P. A.; Downard, A. J. *Electrochem. Commun.* **2007**, *9*, 1456.
(374) Brooksby, P. A.; Downard, A. J.; Yu, S. S. C. *Langmuir* **2005**, *21*, 11304–11311.
(375) Jiang, D. e.; Sumpter, B. G.; Dai, S. *J. Phys. Chem. B* **2006**, *110*, 23628–23632.
(376) Anariba, F.; Steach, J.; McCreery, R. *J. Phys. Chem B* **2005**, *109*, 11163–11172.
(377) McCreery, R. *Electrochem. Soc. Interface* **2004**, *13*, 46–51.
(378) Vaik, K.; Sarapuu, A.; Tammeveski, K.; Mirkhalaf, F.; Schiffrin, D. J. *J. Electroanal. Chem.* **2004**, *564*, 159.
(379) Mirkhalaf, F.; Tammeveski, K.; Schiffrin, D. J. *Phys. Chem. Chem. Phys.* **2004**, *6*, 1321–1327.
(380) Alexeyeva, N.; Laaksonen, T.; Kontturi, K.; Mirkhalaf, F.; Schiffrin, D. J.; Tammeveski, K. *Electrochem. Commun.* **2006**, *8*, 1475.
(381) Polsky, R.; Harper, J. C.; Dirk, S. M.; Arango, D. C.; Wheeler, D. R.; Brozik, S. M. *Langmuir* **2007**, *23*, 364–366.
(382) Holm, A. H.; Moller, R.; Vase, K. H.; Dong, M.; Norrman, K.; Besenbacher, F.; Pedersen, S. U.; Daasbjerg, K. *New J. Chem.* **2005**, *29*, 659–666.
(383) McCreery, R. *Chem. Mater.* **2004**, *16*, 4477–4496.
(384) Fisher, G. L.; Hooper, A.; Opila, R. L.; Jung, D. R.; Allara, D. L.; Winograd, N. *J. Electron Spectrosc. Relat. Phenom.* **1999**, *98*−*99*, 139–148.
(385) Fisher, G. L.; Hooper, A. E.; Opila, R. L.; Jung, D. R.; Allara, D. L.; Winograd, N. *J. Phys. Chem. B* **2000**, *104*, 3267–3273.
(386) Haynie, B. C.; Walker, A. V.; Tighe, T. B.; Allara, D. L.; Winograd, N. *Appl. Surf. Sci.* **2003**, *203*−*204*, 433–436.
(387) Wu, J.; Mobley, K.; McCreery, R. *J. Chem. Phys.* **2007**, *126*, 24704.
(388) Vase, K. H.; Holm, A. H.; Pedersen, S. U.; Daasbjerg, K. *Langmuir* **2005**, *21*, 8085–8089.
(389) Vase, K. H.; Holm, A. H.; Norrman, K.; Pedersen, S. U.; Daasbjerg, K. *Langmuir* **2007**, *23*, 3786–3793.
(390) Nielsen, L. T.; Vase, K. H.; Dong, M.; Besenbacher, F.; Pedersen, S. U.; Daasbjerg, K. *J. Am. Chem. Soc.* **2007**, *129*, 1888–1889.
(391) Vase, K. H.; Holm, A. H.; Norrman, K.; Pedersen, S. U.; Daasbjerg, K. *Langmuir* **2008**, *24*, 182–188.
(392) Buriak, J. M. *Angew. Chem., Int. Ed.* **2001**, *40*, 532–534.
(393) Hamers, R. J.; Coulter, S. K.; Ellison, M. D.; Hovis, J. S.; Padowitz, D. F.; Schwartz, M. P.; Greenlief, C. M.; Russell, J. N., Jr. *Acc. Chem. Res.* **2000**, *33*, 617–624.
(394) Nichols, B. M.; Metz, K. M.; Tse, K. Y.; Butler, J. E.; Russell, J. N.; Hamers, R. J. *J. Phys. Chem. B* **2006**, *110*, 16535–16543.
(395) Hovis, J. S.; Coulter, S. K.; Hamers, R. J.; D'Evelyn, M. P.; Russell, J. N.; Butler, J. E. *J. Am. Chem. Soc.* **2000**, *122*, 732–733.
(396) Wang, G. T.; Bent, S. F.; Russell, J. N.; Butler, J. E.; D'Evelyn, M. P. *J. Am. Chem. Soc.* **2000**, *122*, 744–745.
(397) Knickerbocker, T.; Strother, T.; Schwartz, M. P.; Russell, J. N., Jr.; Butler, J.; Smith, L. M.; Hamers, R. J. *Langmuir.* **2003**, *19*, 1938–1942.
(398) Lasseter, T.; Clare, B.; Abbott, N.; Hamers, R. J. *J. Am. Chem. Soc.* **2004**, *126*, 10220–10221.
(399) Tse, K.-Y.; Nichols, B. M.; Yang, W.; Butler, J. E.; Russell, J. N., Jr.; Hamers, R. J. *J. Phys. Chem. B* **2005**, *109*, 8523–8532.
(400) Ssenyange, S.; Anariba, F.; Bocian, D. F.; McCreery, R. L. *Langmuir* **2005**, *21*, 11105–11112.
(401) Gallardo, I.; Pinson, J.; Vila, N. *J. Phys. Chem. B* **2006**, *110*, 19521–19529.
(402) Adenier, A.; Chehimi, M. M.; Gallardo, I.; Pinson, J.; Vila, N. *Langmuir* **2004**, *20*, 8243–8253.
(403) Tornoe, C. W.; Christensen, C.; Meldal, M. *J. Org. Chem.* **2002**, *67*, 3057–3064.

(404) Devaraj, N. K.; Dinolfo, P. H.; Chidsey, C. E. D.; Collman, J. P. *J. Am. Chem. Soc.* **2006**, *128*, 1794–1795.
(405) Collman, J. P.; Devaraj, N. K.; Eberspacher, T. P. A.; Chidsey, C. E. D. *Langmuir* **2006**, *22*, 2457–2464.
(406) Collman, J. P.; Devaraj, N. K.; Chidsey, C. E. D. *Langmuir* **2004**, *20*, 1051–1053.
(407) Devadoss, A.; Chidsey, C. E. D. *J. Am. Chem. Soc.* **2007**, *129*, 5370–5371.
(408) Beriet, C.; Pletcher, D. *J. Electroanal. Chem.* **1994**, *375*, 213.
(409) Fagan, D. T.; Hu, I.; Kuwana, T. *Anal. Chem.* **1985**, *57*, 2759–63.
(410) Huang, T.; Warsinke, A.; Kuwana, T.; Scheller, F. W. *Anal. Chem.* **1998**, *70*, 991–997.
(411) Munteanu, F. D.; Mano, N.; Kuhn, A.; Gorton, L. *J. Electroanal. Chem.* **2004**, *564*, 167.
(412) Timur, S.; Anik, U.; Odaci, D.; Gorton, L. *Electrochem. Commun.* **2007**, *9*, 1810.
(413) Antiochia, R.; Gorton, L. *Biosens. Bioelectron.* **2007**, *22*, 2611.
(414) Joshi, P. P.; Merchant, S. A.; Wang, Y.; Schmidtke, D. W. *Anal. Chem.* **2005**, *77*, 3183–3188.

CR068076M

SUPERINTENDENCIA DE INDUSTRIA Y COMERCIO
CONSULTA DE DOCUMENTOS

Microbial Reduction and Precipitation of Vanadium by *Shewanella oneidensis*

W. Carpentier, K. Sandra, I. De Smet, A. Brigé, L. De Smet and J. Van Beeumen
***Appl. Environ. Microbiol.* 2003, 69(6):3636. DOI: 10.1128/AEM.69.6.3636-3639.2003.**

APPLIED AND ENVIRONMENTAL MICROBIOLOGY, June 2003, p. 3636–3639 Vol. 69, No. 6
0099-2240/03/$08.00+0 DOI: 10.1128/AEM.69.6.3636–3639.2003

Microbial Reduction and Precipitation of Vanadium by *Shewanella oneidensis*

W. Carpentier,[1] K. Sandra,[1] I. De Smet,[2] A. Brigé,[1] L. De Smet,[1] and J. Van Beeumen[1]*

Laboratory for Protein Biochemistry and Protein Engineering[1] and Department of Plant Systems Biology, Flanders Interuniversity Institute for Biotechnology,[2] Ghent University, B-9000 Ghent, Belgium

Received 9 September 2002/Accepted 24 February 2003

Shewanella oneidensis **couples anaerobic oxidation of lactate, formate, and pyruvate to the reduction of vanadium pentoxide (V^V). The bacterium reduces V^V (vanadate ion) to V^{IV} (vanadyl ion) in an anaerobic atmosphere. The resulting vanadyl ion precipitates as a V^{IV}-containing solid.**

Vanadium is a transition metal which, at neutral pH, can exist in two oxidation states, V^{IV} (vanadyl ion, cationic species VO^{2+}), and V^V (vanadate ion, anionic species, $H_2VO_4^-$) (10, 11).

The environmental chemistry of vanadium is complex. Vanadium is an abundant element that has proven to be a valuable resource for different industrial applications such as vanadium alloys, oxidation catalysis in sulfuric acid manufacturing and automobile catalytic converters, photographic development, textile dyeing, and ceramic coloring. A number of bacteria are able to reduce metal compounds, most commonly iron and manganese, through anaerobic reduction. Some organisms are known to be able to reduce other metals such as arsenic, mercury, selenium, uranium, technetium, chromium, molybdenum, gold, silver, and copper (4, 8, 13). The microbial reduction of vanadate has also been reported (1, 14). To date, two *Pseudomonas* strains have been described to be capable of reducing vanadium (5, 15). In this study we demonstrate that the gram-negative facultative anaerobic nonfermenting bacterium *Shewanella oneidensis* (6) can also reduce vanadium V^V.

Vanadium uptake on solid media. Colonies of *S. oneidensis* were grown on Luria-Bertani 1% agar plates containing 5 mM vanadate at 28°C for 48 h. Plates were then exposed to hydrogen sulfide in a sealed container. Upon formation of metal sulfide, plates were examined for changes in the regions surrounding or inside bacterial colonies. A halo could be seen indicating possible sequestration of the metal. Darkening of the cells indicated accumulation or possible reduction of the metal (data not shown).

Vanadate detection. To facilitate the detection and quantification of the reduction of vanadate to V^{IV}, a vanadate detection assay was designed, based on a detection assay for chromium described by Sandel (12). Vanadate was thereby detected on the basis of its reaction with diphenylcarbazide (DPC) in acid. The assay solution was made by addition of 1% (wt/vol) DPC in acetone to an equal volume of 2 M H_2SO_4. A volume of 500 μl of diluted sample was added to the same volume of assay solution. Absorbance was measured at 320 nm after 15 min. A standard curve was made with vanadium pentoxide dilutions. Vanadyl ions do not react in this assay.

Anaerobic vanadium reduction. *S. oneidensis* was grown aerobically on a rotary shaker (150 rpm) at 28°C in LB medium containing 2 or 10 mM V_2O_5 and anaerobically with a Coy anaerobic chamber (Coy Laboratories, Grass Lake, Mich.) in phosphate-buffered defined medium (7) containing 10 mM lactate as the electron donor and 2 or 10 mM V_2O_5 as the electron acceptor. An increase in lag phase could be detected in cultures grown with 10 mM but not with 2 mM V_2O_5 compared to cultures grown aerobically in pure LB medium or anaerobically in defined medium with fumaric acid as the electron acceptor (data not shown).

The color of the anaerobic cultures eventually became blue if vanadate was used, indicating the formation of the blue vanadyl ion. The formation of reduced vanadyl ion was confirmed by capillary electrophoresis. A capillary electrophoretic method was used for simultaneous detection of vanadate and vanadyl ion, essentially as described earlier (3), with a P/ACE 2100 (Beckman Instruments, Fullerton, Calif.) and a 50-μm fused silica capillary (Polymicro Technologies, Phoenix, Ariz.). The sample was diluted 50 times in assay solution and introduced by a 15-s hydrodynamic injection. Both the $[P(V^VMo_{11})O_{40}]^{4-}$ and the $[P(V^{IV}Mo_{11})O_{40}]^{5-}$ complex were detected at 214 nm, confirming the presence of reduced vanadyl ion. For this experiment, 50 ml of an aerobically grown late-exponential-phase culture (2×10^8 cells/ml) was centrifuged, and cells were washed and resuspended in an equal volume of anaerobic bicarbonate buffer containing 5 mM V_2O_5 and 2 or 10 mM lactic acid. Vanadate reduction and vanadyl formation were monitored over time (Fig. 1). The results show the initial reduction of vanadate ion to vanadyl ion and subsequently the decrease in amount of vanadyl ion by reductive precipitation. The precipitation of vanadyl ion is in accordance with the low solubility of the ion at neutral pH (9).

Vanadate accumulation. To determine the accumulation of vanadate by the cells, a culture was grown aerobically on a rotary shaker (200 rpm) at 28°C in LB medium containing 2 or 10 mM V_2O_5. No significant reduction or precipitation was detected. The cultures had a density of 1.5×10^7 cells/ml and 1×10^7 cells/ml, respectively. Cells were harvested at 4,000

* Corresponding author. Mailing address: Laboratory for Protein Biochemistry and Protein Engineering, Ghent University, 9000 Ghent, Belgium. Phone: 32 9 264 5109. Fax: 32 9 264 5338. E-mail: jozef.vanbeeumen@rug.ac.be.

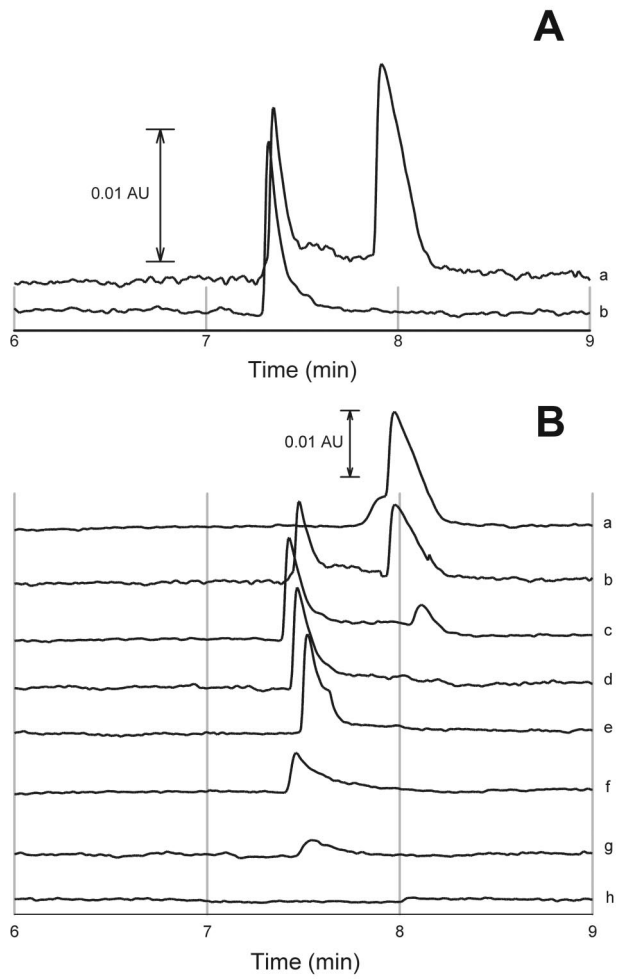

FIG. 1. Electrophoretic determination of vanadium(V) and vanadium(IV). (A) Reference sample with 10 mM V^V (right peak) and 10 mM V^{IV} (left peak) (a) and analysis of precipitate composition (b). (B) Vanadium speciation during anaerobic reduction at different times: 0 min (a), 30 min (b), 45 min (c), 60 min (d), 90 min (e), 150 min (f), 1 day (g), and 1 week (h).

rpm for 15 min, washed and resuspended in Tris-EDTA buffer, and lysed by sonication. The vanadate concentration was determined with the DPC assay. Of the total vanadate initially present in the medium, 2% (standard error of the mean 6%) or 9% (standard error of the mean 5%) was detected in the cells grown with 2 and 10 mM V_2O_5, respectively.

Effect of different buffers. The effect of different buffers on anaerobic vanadium reduction was tested. Previous to all anaerobic experiments, sterile solutions were placed overnight in an anaerobic glove box (Coy Laboratories). Cultures were grown aerobically on a rotary shaker (150 rpm) at 28°C in LB medium to the late exponential growth phase (2×10^8 cells/ml) before being washed in appropriate buffer in anaerobic conditions and resuspended in equal volumes of either 20 mM Na_2HPO_4, pH 7, 20 mM Tris, pH 7, 20 mM HEPES, pH 7, or 20 mM $NaHCO_3$, pH 7, containing 10 mM lactic acid and 5 mM V_2O_5. Vanadate reduction was monitored over time with the DPC assay. The buffer affected both the initial rate of reduction and the overall extent of reduction. Phosphate was revealed to be the most inhibitory, followed by Tris and HEPES. Carbonate-buffered solutions supported the highest reduction rates (Fig. 2).

Effect of different electron donors. To examine the effect of different carbon sources and electron donor compounds on vanadate reduction, formic, pyruvic, citric, and fumaric acids were tested in addition to lactate. In each experiment, 50 ml of aerobically grown late-exponential-phase cultures (2×10^8 cells/ml) were centrifuged; the cells were washed, weighed, and resuspended in equal volumes of anaerobic bicarbonate buffer containing 5 mM V_2O_5 and 10 mM lactic, formic, pyruvic, fumaric, or citric acid. Vanadate reduction rates were monitored over time. While only a limited reduction of vanadate was measured in cultures containing fumaric and citric acid compared to cultures containing no electron donor, the cultures containing formic, lactic, and pyruvic acid significantly reduced vanadate (Fig. 3). Citric and fumaric acid cannot be used as electron donors by the organism and hence they do not support vanadate reduction.

Vanadium reduction is a biochemical process. Proof was found to eliminate the possibility that vanadate reduction was the result of a chemical or spontaneous process catalyzed by a biological component or product of the cell. In each experiment, 50 ml of an overnight-grown culture (2×10^8 cells/ml) was centrifuged; the cells were washed, weighed, and resuspended in equal volumes of anaerobic bicarbonate buffer containing 10 mM lactate and 5 mM V_2O_5. To demonstrate that the reduction is a biological process, one set of cells was heat killed prior to inoculation. Over a period of 5 h, no reduction in vanadate concentration could be measured. The reference culture had an initial reduction rate of 12.4 mmol of V^V per h per g of cells (wet weight). By heat killing the cells and subsequently assaying their vanadate reduction, we demonstrated

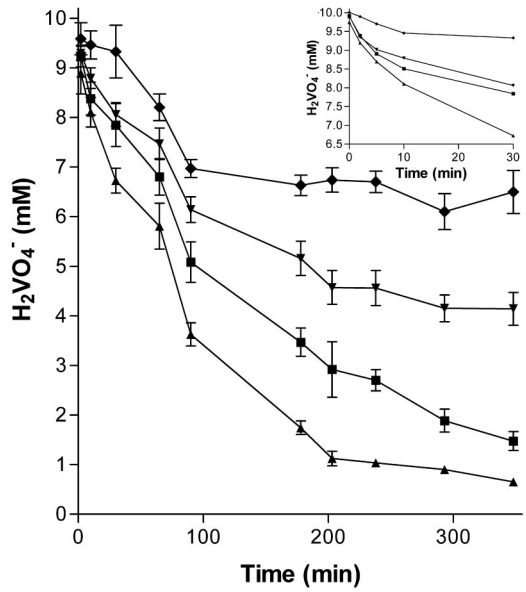

FIG. 2. Change in vanadate concentrations over time in the nongrowth mode for anaerobic cultures containing 5 mM V_2O_5 and 10 mM lactic acid in phosphate (◆), Tris (▼), HEPES (■), or carbonate (▲) buffer.

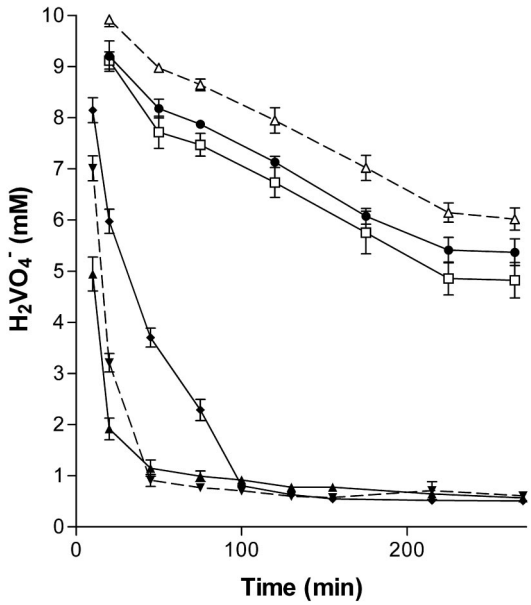

FIG. 3. Change in vanadate concentrations over time in the non-growth mode of cultures containing 5 mM V_2O_5 and 10 mM formic (▲), lactic (▼), pyruvic (◆), fumaric (●), or citric (□) acid. The control experiment contained 5 mM V_2O_5 (△).

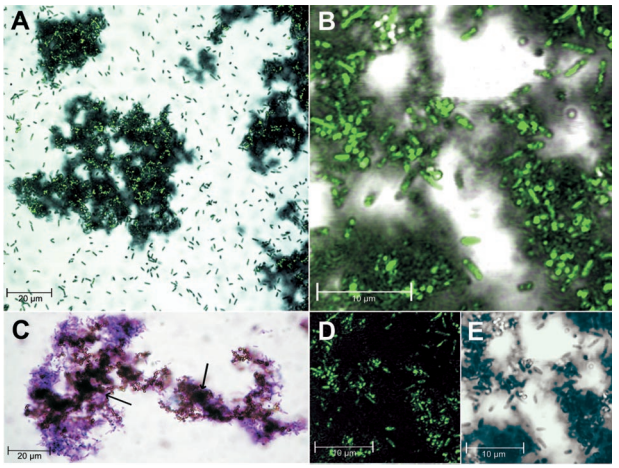

FIG. 4. Microscopic analysis of vanadium granules and bacterial localization. (A) Confocal microscopic image of a colonized granule (central) with autofluorescence of *S. oneidensis* superimposed in green (HeNe laser excitation at 543 nm). (B) Enlarged image of A, central part of the granule (split view in D and E indicating the association of autofluorescence with the presence of bacterial cells). (C) Differential interference contrast image of crystal violet-stained cells (purple) on vanadium granules (brown, indicated by arrows). (D) Confocal autofluorescence image. (E) Differential interference contrast image showing a perfect overlap with D.

that this reduction required intact and metabolically active *S. oneidensis* cells.

To assess whether vanadate reduction requires de novo protein synthesis, the ribosome inhibitor tetracycline was added at a final concentration of 5 μg/ml. This concentration is known to completely inhibit growth but does not affect cell viability. In the experiment, 50 ml of an overnight-grown culture was centrifuged; the cells were washed and resuspended in equal volumes of anaerobic bicarbonate buffer containing 5 μg of tetracycline per ml. After 5 min of incubation, 10 mM lactate and 5 mM V_2O_5 were added. Vanadate concentration was monitored over time with the DPC assay. No significant decrease in the reduction rate could be measured, indicating that the activity does not depend on the induction of specific proteins (results not shown). The vanadate reduction pathway thus seems to be constitutively present in the bacterium.

Vanadium-containing granular precipitate. In the course of the experiments with anaerobic vanadate-reducing cultures, a significant formation of precipitate was detected. In an attempt to rule out precipitation of a compound from the medium, different media were tested. Growth on vanadate in Luria Bertani broth, carbonate buffer, HEPES buffer, Tris buffer, and, to a limited extent, phosphate buffer resulted in a vanadate-containing precipitate. The granules were revealed to be insoluble at neutral pH, insoluble in 10 N NaOH, and soluble in 2 M H_2SO_4. V^V is known to be soluble in basic and acidic solutions (2), while V^{IV} is soluble in acid solutions and is not oxidized to V^V below pH 2 (9). The sediment was washed three times with water. The pellet was solubilized in 2 M H_2SO_4. The sample was centrifuged to remove cell debris and subsequently analyzed by capillary electrophoresis. Only V^{IV} and no vanadate could be detected (Fig. 1A).

Further examination of the precipitate revealed large granules with a diameter of up to 100 μm after 5 days of growth. Precipitate formed by cultures grown with 10 mM lactic acid and 5 mM V_2O_5 was examined with differential interference contrast (DIC) microscopy at a magnification factor of 320× (Leica DMLB, Wetzlar, Germany). Microscopic examination combined with crystal violet staining showed that the granules were completely colonized with *S. oneidensis* (Fig. 4C). By confocal microscopy with a combination of DIC and HeNe laser excitation at 543 nm (Zeiss Axiovert 100 M; Carl Zeiss), an autofluorescence of the bacteria was detected (Fig. 4D and E), which allowed us to unambiguously localize the bacterium in the granule matrix. Only a small number of motile free-living cells were seen compared to the dense accumulations of sessile cells contained in the granule matrix (Fig. 4A and B).

In summary, we present evidence for a dissimilatory vanadate reduction process in *S. oneidensis*. The bacterium is able to reduce V^V (vanadate ion) to V^{IV} (vanadyl ion) under anaerobic conditions. We evaluated different electron donor compounds for their ability to sustain vanadium pentoxide reduction and showed that significant reduction can be attained with formic, lactic, and pyruvic acids under these conditions. A small but measurable accumulation of vanadium pentoxide was present inside the bacterial cells. Anaerobic reduction resulted in a granular precipitate containing predominantly V^{IV} (vanadyl ion), which was revealed to be completely colonized by sessile *S. oneidensis.* Further studies will focus on identification and isolation of the components of the vanadate reduction pathway.

This work was supported by the Institute for the Promotion and Innovation of Science and Technology in Flanders (IWT) through STWW research grant 174IWT20.

REFERENCES

1. **Bautista, E. M., and M. Alexande.** 1972. Reduction of inorganic compounds by soil microorganisms. Soil Sci. Soc. Am. J. **36:**918–920.
2. **Greenwood, N. N., and A. Earnshaw.** 1984. Chemistry of the elements, Pergamon Press, Oxford, p. 1147–1148.
3. **Kitazumi, I., Y. Nakashima, and S. Himeno.** 2001. Simultaneous electrophoretic determination of vanadium(V) and vanadium(IV) based on the complex formation with a Mo(VI)-P(V) reagent. J. Chromatogr. A **21:**123–129.
4. **Lovley, D. R.** 1993. Dissimilatory metal reduction. Annu. Rev. Microbiol. **47:**263–290.
5. **Lyalikova, N. N., and N. A. Yurkova.** 1992. Role of microorganisms in vanadium concentration and dispersion. Geomicrob. J. **10:**15–26.
6. **Myers, C. R., and K. H. Nealson.** 1988. Bacterial manganese reduction and growth with manganese oxide as the sole electron acceptor. Science **240:** 1319–1321.
7. **Myers, C. R., and K. H. Nealson.** 1990. Respiration-linked proton translocation coupled to anaerobic reduction of manganese(IV) and iron(III) in *Shewanella putrefaciens* MR-1. J. Bacteriol. **172:**6232–6238.
8. **Niggemyer, A., S., S. Spring, E. Stackebrandt, and R. F. Rosenzweig.** 2001. Isolation and characterization of a novel As(V)-reducing bacterium: implications for arsenic mobilization and the genus *Desulfitobacterium*. Appl. Environ. Microbiol. **67:**5568–5580.
9. **Patel, B., S. J. Haswell, and R. Grzeskowiak.** 1989. Flow-injection flame atomic-absorption spectrometry system for the pre-concentration of vanadium(V) and characterization of vanadium(IV) and vanadium(V) species. J. Anal. Atom. Spectrom. **4:**195–198.
10. **Rehder, D.** 1991. The bioorganic chemistry of vanadium. Angew. Chem. **30:**148–167.
11. **Rehder, D.** 1992. Structure and function of vanadium compounds in living organisms. Biometals **5:**3–12.
12. **Sandell, E. B.** 1959. Colorimetric determination of traces of metals, 3rd ed., p. 82. Interscience Publishers, New York, N.Y.
13. **von Canstein, H., Y. Li, K. N. Timmis, W.-D. Deckwer, and L. Wagner-Döbler.** 1999. Removal of mercury from chloralkali electrolysis wastewater by a mercury-resistant *Pseudomonas putida* strain. Appl. Environ. Microbiol. **65:**5279–5284.
14. **Yurkova, N. A., and N. N. Lyalikova.** 1990. New vanadate-reducing facultative chemolithotrophic bacteria. Microbiology **59:**672–677.
15. **Yurkova, N. A., and N. N. Lyalikova.** 1993. Oxidation of molecular-hydrogen and carbon-monoxide by facultatively chemolithotrophic vanadate-reducing bacteria. Microbiology **62:**367–370.

Electrochemical Remediation and Stabilization of Contaminated Sediments

A Final Report Submitted to

The NOAA/UNH Cooperative Institute for Coastal and Estuarine Environmental Technology (CICEET)

Submitted by

Dr. Kevin Gardner
Civil Engineering Department
University of New Hampshire
Durham, NH 03824

December 8, 2005

This project was funded by a grant from NOAA/UNH Cooperative Institute for Coastal and Estuarine Environmental Technology, NOAA Grant Number NA17OZ2507

I. TABLE OF CONTENTS

II. LIST OF FIGURES

III. LIST OF TABLES

1. ABSTRACT

A promising contaminated sediment treatment and management technology that uses a low voltage, direct current to degrade organics, remove metals and salts, and dewater sediments was investigated at the University of New Hampshire in conjunction with visiting scholars from the Technical Institute of Denmark and the Institution of Higher Education in Engineering (Nantes, France). One reason this treatment option shows such potential, other than its prospect to address three different treatments, is because it can be applied to sediments in-situ (most likely in confined disposal cells) and ex-situ (such as at a facility that prepares sediment for beneficial uses), and because of it's cost-effectiveness to run the treatment at low electrical current (<50 mA). The three foci of the project investigated at the bench-scale were to determine the effectiveness of electrochemical remediation on the removal of metals and salts, on the degradation or removal of organics (specifically polyaromatic hydrocarbons [PAHs]), and on stabilization of sediments via dewatering. In several 3-4 week laboratory experiments, selected metals plus chloride were mobilized in the electric field and accumulated in the area of the electrolytes, as was theoretically proposed. Initial investigations of the degradation of PAHs proved promising for naphthalene and acenaphthalene, and a more comprehensive month-long bench scale experiments offered more comprehensive results. After 30 days of electrokinetic remediation at a current 20-30 mA, approximately 20% of total PAHs were degraded, and a discrete investigation of the individual PAH compounds concluded that they tend to migrate towards the anode along with the natural organic carbon. Electroosmotic flow was witnessed in the batch experiments visually and in measuring the water content, indicating successful dewatering of the sediments.

KEYWORDS: sediment, electrochemical remediation, polyaromatic hydrocarbons, metals, dewatering

2. INTRODUCTION

Contaminated sediments in rivers, harbors, and estuaries act as continuous sources of contaminants to riverine, estuarine, and coastal ecosystems. Although much of this contamination is diffuse and unrealistic to remediate, in cases where concentrated "hotspots" exist, including some 100 Superfund sites (ie., upper Hudson River, New Bedford Harbor, Housatonic River), remediation of sediments in place may be effective. Further, there is a growing crisis in treating those contaminated sediments removed from navigational dredging activities. Historically, material from navigational dredging was disposed of at open ocean disposal sites, but increasing restrictions to protect benthic biology and ecology have eliminated this option for all but the cleanest sediments. Typically, these sediments contain a wide range of contamination, including heavy metals, polyaromatic hydrocarbons (PAHs), polychlorinated biphenyls (PCBs), and other persistent organics.

There are two primary methods that are being used to currently try to solve this problem. One is using contaminated sediments at upland sites as inexpensive fill material at Superfund and Brownfields sites to reclaim or redevelop the land (regulated state-to-state). The major consideration in this method is the cost in stabilizing the sediment (dewatering, additives to increase strength) and the cost to decontaminate (including major salts such as chloride). Of note, the technology considered in this research project is effective in both dewatering and chloride removal.

The second material handling method is to place contaminated sediment in Confined Aquatic Disposal (CAD) cells, typically in harbors, estuarine, or near-shore areas. A CAD cell is a pit dug in the sediment which is then refilled with contaminated dredged material and capped, typically with clean sand, although reactive barriers are emerging as well. CAD cells are cost-effective and do achieve some degree of isolation and minimization of exposed contamination. A number of problems with CAD cells exist, however, which may have significant ramifications for the long-term health of our coastal and estuarine systems. Sand caps have a high permeability, which is well understood that due to diffusion, the flux of contaminants can be significant. Release of many contaminants from CAD cells has been measured to reach tons per year (Shine, 2000).

CAD cells do offer a distinct geometrical configuration of contaminated sediments that may be amenable to certain types of in-situ remediation techniques, similar to those used on contaminated terrestrial soils. Confined disposal facilities (CDFs) offer a similarly convenient configuration for treatment of dredged sediments, without the confounding effects of being submerged. There is one type of treatment that is uniquely suited for these types of contaminated sediment storage: electrochemical remediation (Acar, 1992; 1993).

2.1 Electrochemical Remediation Theory

Electrochemical remediation involves the application of a low density direct current to a pair of positive (anode) and negative (cathode) electrodes placed in the soil to mobilize contaminants in the form of charged species. The contaminants within the electric field are transported to the anode or to the cathode where they are removed by one of the following methods: electrodialysis into electrolyte solutions, adsorption onto the electrode, precipitation or co-precipitation at the electrode, pumping next to the electrode, complexing with ion exchange resins, or capturing in permeable reactive barriers.

In the United States and Europe, there is a patent for ElectroChemical Remediation Technologies (ECRTs), which consist of two types. ElectroChemcial GeoOxidation (ECGO) uses a low voltage, low amperage DC/AC current to induce a polarization field within the sediment. The sediment acts as a capacitor, discharging and charging electricity resulting in redox reactions, which cause desorption of the contaminants from the sediments and mineralization of the organics to their inorganic constituents (e.g., carbon dioxide and water). Empirical evidence indicates that reaction rates are inversely proportional to grain size, such that ECRTs remediate faster in finer-grained material typically found at sediment sites. The second method of removal, Induced Complexation (IC), significantly enhances the mobilization of metals and radio nuclides in a sediment matrix through redox reactions that desorb the contaminants from the sediment and create ionic metal complexes (Doering, 2000).

Electrochemical remediation was originally developed for remediation of heavy metal polluted soil (Hansen et al., 1997; Ottosen et al., 1997). The electrokinetic phenomena in porous media are based on the relative motion between a charged surface and the bulk solution at its interface. The formation of an electric double layer at the charged surface of clay particles explains the processes mobilizing the charged particles via three phenomena: electromigration, electroosmosis, and electrophoresis. These processes force the aqueous phase and ions to desorb from the sediment surface and migrate through the electric field either towards the anode or the cathodes, depending on the speciation.

Electromigration is the movement of ions and ionic complexes in a soil solution due to an applied electric field. The ions move towards the electrode of opposite charge: anions towards the anode and cations towards the cathode. Electromigration is the most important transport mechanism aiding electrochemical remediation (Lageman et al., 1989) and is dependent on tortuosity, porosity, and the charge of the ion (Acar, 1993).

Electroosmosis is the movement of water in a porous media in an applied electric field. Soil particles are negatively charged, which creates a diffuse double layer of water and dissolved cations around the soil particles. When an electric field is applied, the cations will migrate in the direction of the cathode along with the water molecules. Whereas values of hydraulic conductivity can vary many orders of magnitude for different soil types, the electroosmotic conductivity lie in a narrow range of $1x10^{-9}$ to $1x10^{-8}$. Thus, an electric field is a much more effective force driving the fluid through fine grained soils of low hydraulic conductivity than a hydraulic gradient (Akram, 1999). Furthermore, electroosmosis is independent of the pore size distribution or the presence of macro-

pores. The effect of the electroosmosis process to the total mass transport varies according to soil type, water content, types of ion species, and pore fluid concentration of ions (Acar, 1993).

The final phenomenon affecting electrochemical remediation is electrophoresis. Electrophoresis is the transport of particles in an applied electric field and includes all charged particles (e.g. colloids, clay particles, organic particles) (Acar, 1993). Figure 1 below shows a visual observation of both electroosmosis and electrophoresis.

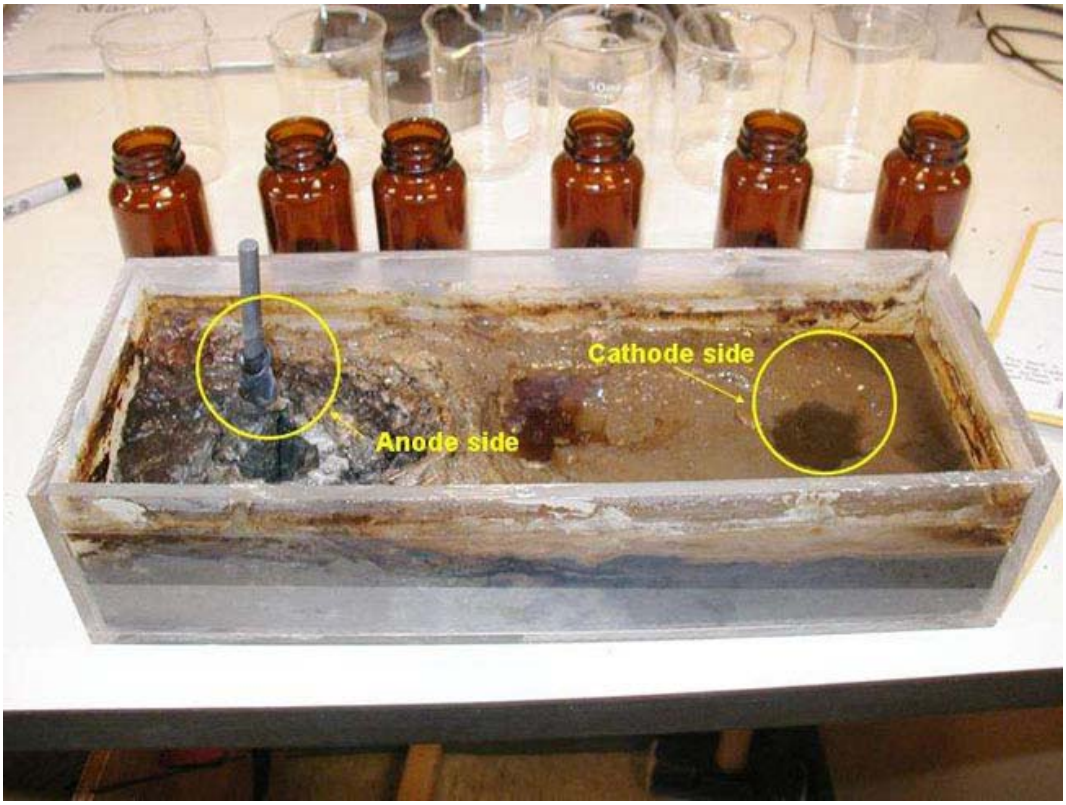

Figure 1: Visual observation of electroosmosis and electrophoresis, the movement of soil and water particles under an applied electric field (anode on left, cathode removed from right).

Since only released ions in the pore water are transported in the electric field during electrochemical remediation, the precipitated and adsorbed metals in the sediment must be converted to mobile ionic forms before they can be removed. Mobilization is enhanced in an electrochemical reactor by pH changes in the sediment during the treatment. Water splitting at the anode occurs via the following reactions (Equations 1 and 2) and results in an acidic front that moves from the anode to the cathode (Ottosen, 2000).

(1) Cathode: $4\ H_2O + 4\ e^- \rightarrow 2\ H_2(g) + 4\ OH^-$

(2) Anode: $2\ H_2O \rightarrow O_2(g) + 4\ H^+ + 4\ e^-$

Theoretically, in an electrochemical reactor, equal amounts of current are carried by anions and cations in solution. Closer to the electrodes, the concentration of anions and cations decreases compared to the bulk concentration. When the concentration reaches zero, the limiting current density has been reached. Operation at current densities higher than the limiting current results in the water splitting phenomenon (formation of H+ and OH-). The limiting current is lower at the anode than at the cathode, thus an acidic front is formed desorbing metals and transporting them with water and soil particles towards the cathode. For metals of concern that are not mobile at low pH (e.g. As or Cr (VI)), surfactants and complexing agents have been used to assist in the migration (Ottensen, 1998). Surfactants have also been used to assist transport of organic contaminants in electrochemical remediation (Elektorowicz, 2001).

2.2 Developments in Electrochemical Remediation

The first electrochemical remediation experiments were performed in soil at the Technical University of Denmark. In their PhD theses, Ottosen (1995) described the development of the experimental cell and first electrodialytic remediation experiments and Hansen (1995) tested the suitability and advantages of different ion exchange membranes for use in the electrodialytic cell (Note that the difference between electrokinetic and electrodialytic experiments are that the former applies current directly to the soil with electrodes in the soil and the latter uses an ion exchange membrane and separate electrolyte solution compartments). From 1995 to 2000, three more PhD studies were completed on electrodialytic soil remediation: Jespersen (1996) built the first pilot and full scale plants and Ribeiro (1998) and Kliem (2000) studied the changes in soil characteristics by different analytical methods during and after electrodialytic remediation.

Together with developing the soil remediation technique, the electrodialytic remediation process was also used to remediate other porous materials, such as fly ash (Pedersen, 2002), impregnated wood waste (Ribeiro, 2000) and waste water sludge (Jakobsen, 2004). Pedersen introduced the stirred electrodialytic treatment cell in her PhD thesis to combat problems of high electrical resistance and hardening of the material. Christensen (2004) used oxalic and phosphoric acid as a desorbing agent to remove Cu, Cr, and As from impregnated wood waste, in the laboratory, bench, and pilot scale. This was the first time large scale experiments were made for other materials other than soil.

There is definite potential for remediating harbor sediments as well by the electrodialytic method (Nyostrom, 2004). Dredged sediment is often too contaminated to be dumped at sea. Sediment consists of many similar components as soil: clay, silt, organic matter, oxides, and carbonates. Therefore, the expectations for the remediation of sediment were based on the past experiences from the electrodialytic remediation of soil. The greatest difference is in the effect of salinity on remediation success, because heavy metals can form uncharged complexes with chloride, thus not being mobile in an electric field.

Grande and Gent (2002) conducted an electrokinetic field scale in-situ experiment in a 2000 m^2 waste lagoon located in a tidal marsh in the United States. The saline sediment was remediated for both heavy metals and chlorinated solvents (PCEs). The field experiment lasted 96 weeks and showed that the heavy metals moved towards the cathode. In 77.5% of the area the chromium level was reduced to under background level (<109 mg/kg) and in 78.8% of the area the cadmium level was reduced to under background level (<3.1 mg/kg). Degradation of up to 99.0% of PCEs was also experienced. The current density had to be lowered during the remediation because of formation of Cl_2 (g) at the anodes. The chloride gas reacted with dissolved organic carbon in the system and formed trihalomethanes, especially chloroform. Air sparging at the anodes and replacement of the electrolytes were used to reduce the production of chloride gas.

Roulier et al. (2000) studied the feasibility of electrokinetic soil remediation in horizontal Lasagna™ cells and described some problems related to the installation and operation of horizontal electrodes. A hydraulic fracturing process (adapted from oil field practice), where a horizontal layer of porous electrode material (e.g. graphite) can be installed, was suggested as a suitable installation method. No major problems were anticipated installing electrodes this way, but in an initial assessment some problems maintaining flow of liquids and electrical current in the electrode layers seemed to occur. Good hydraulic as well as electrical conductivity in the electrode material are critical to the success of the electrochemical process. Evolved gases at the electrodes must be removed continuously to maintain satisfactory electrical conductivity. In a vertical electrode design, the gases can bubble out and do not cause problems, but in horizontal electrodes the gases do not vent readily but may displace water, thereby reducing the contact between the electrodes, leading to decreased electrical conductivity. It was claimed that the use of horizontal Lasagna cells only beneath the water table would reduce the problems with water flow in electrode fractions that exhibit reduced transmissibility due to evolution of H_2 and O_2 from electrolysis of water.

The United States Army Corps of Engineers is mandated by Congress to maintain navigation on the Nation's 40,234 km (25,000 miles) of waterways and 400 ports, and dredging is a significant part of the maintenance activities. As such, the Corps has a keen interest in new contaminated dredged material management tools and techniques. However, even though the Corps' Environmental Laboratory has participated in a pilot program on electrokinetic remediation of terrestrial soils (USACE, 2000), it seems little attention has been given to electrokinetic remediation of sediments. In May 2000, the Corps' Dredging Operations and Environmental Research (DOER) program co-sponsored a workshop on innovative sediment decontamination technology that featured a review of a bench scale and field scale demonstration of electrokinetic remediation in Europe (Francingues, 2000). It stated that processing costs would be \$33/yd^3 for volumes greater than 100,000 yd^3, which compares well with the other technologies reviewed, however, the capital costs were not provided. This remediation method also compared favorably in that it can be performed *in-situ* or *ex-situ*, creates a limited waste stream, and has beneficial use options for creating manufactured soil.

2.3 Advantages and Disadvantages of Electrochemical Remediation

Electrokinetics may be an appropriate remediation technique in sediment remediation because:

- There are currently no other viable *in-situ* methods for treating inorganic and organic compounds in porous media simultaneously.
- Ionic contaminants are absorbed to sediment particles and are often not available for removal by the simple flushing action of water. The pH shift produced by the electrolysis of the water effectively desorbs contaminating ions.
- In clayey sediments, hydraulic flow through pores can be extremely limited. Electrokinetic remediation is an effective method of inducing movement of water, ions, and colloids through fine-grained sediment.
- The process is competitive in cost and remediation effectiveness to other methods currently in use.

However, electrochemical remediation does have associated limitations, such as:

- The electrokinetic process is limited by the solubility of the contaminant and the desorption of contaminants from the soil matrix. Heavy metals in metallic states are difficult to dissolve and separate from soil samples. Organic compounds may be tightly bound to natural organic matter. The process is also not efficient when the target ion concentration is low and non-target ion concentration is high.
- Acidic conditions and corrosion of the anode may create difficulties in *in-situ* efforts.
- Precipitation of species close to the electrode is an impediment to the process. Heavy metals can prematurely precipitate close to the cathode at their hydroxide solubility value.

3. OBJECTIVES

The initial objective of the proposal written to CICEET was not met: to build upon a successful bench-scale demonstration of the low voltage, direct current technology in the PI's laboratory by testing the treatment of sediments at the pilot scale. Rather, the researchers further developed theoretical proof on the bench-scale that electrochemical remediation can be used to reduce the amount of inorganic and organic contamination, as well as dewater sediments in an *in situ* and *ex situ* application.

The initial graduate student chosen to participate on this project as the research assistant left at the end of two semesters due to health constraints. The project sat dormant for several months until a doctoral student from the Technical Institute of Denmark brought her expertise of electrochemical remediation to the University of New Hampshire. In the summer of 2004, a visiting student from Institution of Higher Education in Engineering (Nantes, France) performed several more bench-scale tests. Lastly, a research staff in the Environmental Research Group was requested to complete the project by continuing

work in the laboratory, authoring a journal article, and submitting this final report to CICEET.

- The graduate student determined the electrokinetic setup to be used for the batch experiments at UNH. Testing of Cocheco River sediments showed promise for using the technique to mobilize naphthalene in sediment.
- Gunvor Nystrom from Denmark investigated the leachability of metals from elecrodialytically treated sediments versus those untreated and a control that was batch extracted with distilled water. Her work was recently submitted to Environmental Engineering Science Journal in a paper entitled "Leaching Properties of harbor sediment before and after EDR", which awaits peer review.
- The student from France, Raphael Grand, studied the affect of using an assisting agent, acetic acid, to aid in desorbing metals for better migration during electrokinetic remediation.
- Lastly, the research staff at UNH, Deana Aulisio, performed bench-scale tests on Cocheco River sediments at a short and long time scale to evaluate a comprehensive list of parameters including pH, water content, organic carbon content, chloride, metals, and PAH compounds.

4. METHODS

4.1 Physical and Chemical Laboratory Methods

A baseline description of the untreated sediment properties is necessary in determining the effectiveness of treatment. Characterization falls into two categories, chemical and geotechnical/physical. Chemical analyses included metals, PAHs, salt (Cl^-), and pH. Physical parameters included water content and organic carbon content.

Two methods of metals digestion were applied to experiments to determine total and available metals. Sediment samples were prepared for metals analysis using the Nordtest Dutch Availability Method, Nordtest Envir 003, adapted by research scholars visiting UNH from Netherlands, including Anne Pedersen and Gunvor Nystrom. On-Site Inductively Coupled Plasma Atomic Emission Spectroscopy (ICP-AES) was used to analyze metals concentrations in the extracts. Duplicate samples were sent to Eastern Analytical, Inc. (EAI) of Concord, NH for a more rigorous digestion procedure, USEPA Method 3051 Microwave Digestion. ICP-AES was also the means of chemical analysis at the laboratory. Results using Microwave-assisted extraction are considered totals and those from the Nordtest method are considered available metals, which is more pertinent for regulatory considerations and risk determinations.

PAHs in sediments were extracted using ultrasonication and USEPA Method 3550B, which uses methylene chloride and acetone as the extracting solvents, and 2-fluorobiphenyl or o-terphenyl as surrogates to evaluate percent recovery. The concentrations of PAHs in the extracts were measured on a gas chromatograph-mass spectrometer (GCMS) at UNH using SW-846 USEPA Method 8100. Deuterated PAH compounds were used as an internal standard with an internal calibration to calculate analyte concentrations.

Chloride content was measured in samples that were muffled at 360ºC for 2 hours. These samples were added to de-ionized water at a liquid to solid (L/S) ratio of 5 g to 25 mL. After stirring for 24 hours, samples were filtered and the filtrate was measured using a Cl^- selective combination electrode.

pH was measured in a similar manner, however samples were dried at 105ºC instead of using the muffle furnace, the L/S ratio was 5 g to 100 mL, and samples were stirred for only 1 hour before measuring with a pH probe.

Water contents were determined by massing the wet sample and then drying completely at 105ºC. The dry mass was recorded and the percent water content was determined by the following equation:

(3) $WC(\%) = (M_W - M_D)/M_W$;

Where:

WC = water content

M_W = mass wet

M_D = mass dry

The organic carbon content was determined by massing the dried sample and then heating it in a muffle furnace at 360ºC for 2 hours. The difference between the initial mass and the mass after burning off organics is the amount of organic carbon in the sample.

4.2 Experimental Sediments

Sediment obtained from New York Harbor was used for the preliminary testing outlined in the proposal to CICEET. One of the experimental sediments (used by Nystrom), which was contaminated with heavy metals, originated from Haakonsvern Harbor, Bergen, Norway. The harbor sediment was dredged by NCC Norway with a specific dredging device for removing only the finer (< 5 μm), more polluted material. Three more contaminated sediments collected from industrialized rivers in the United States were also subjected to electrochemical remediation in this research: the Gowanus Creek Canal located in north-western Brooklyn, New York; Newtown Creek, the waterway that serves as the border between Brooklyn and Queens; and Cocheco River located in Dover, NH. These river sediments are contaminated with pollution of all kinds, including oils, sewage, PCBs, PAHs, and heavy metals.

4.1 Experimental Design

A schematic of electrodialytic remediation, used primarily by researchers from the Technical Institute of Denmark is shown in Figure 2. In this case, sediment is placed in a central cell and electrolyte solutions are circulated in outer cells. The electrolyte solution and the sediment are separated by permeable ion exchange membranes. pH can be monitored in the electrolyte compartments and adjusted to ideal conditions. The sediment slurry in the center can be stirred to achieve better removals. This experimental

setup is much more controlled than an electrokinetic setup, shown in Figure 3. In the electrokinetic setup, the electrodes are placed directly in the sediment. Contaminants migrate towards the electrodes and will plate out on the electrode or precipitate near the electrode. This setup is more applicable to an *in situ* situation; however pH shifts cannot be controlled.

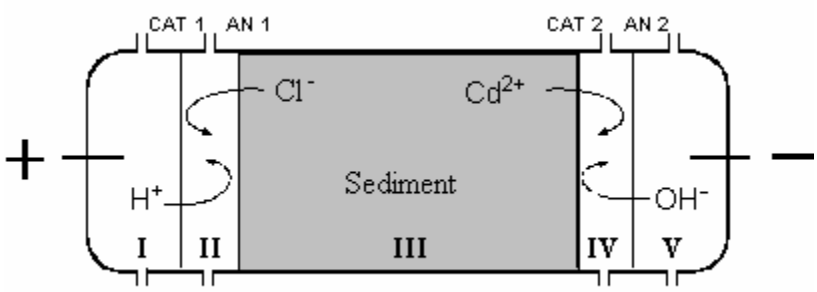

Figure 2: The principle of electrodialytic remediation, where contaminants migrate through the sediment and accumulate in electrolyte solutions. CAT = cation exchange membrane;, AN = anion exchange membrane.

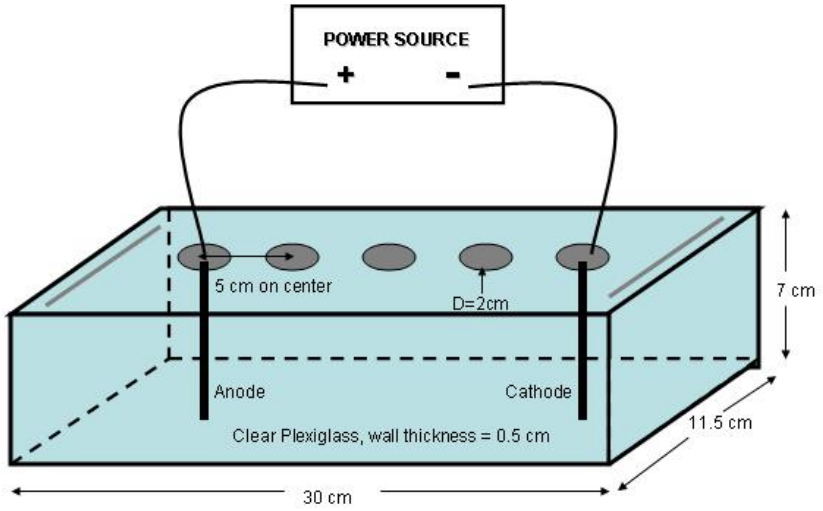

Figure 3: The principle of electrokinetic remediation, where the electrodes are placed directly into the sediment and contaminants migrate to an electrode and form precipitates

The following Table 1 delineates several electrochemical bench-scale tests run by different researchers using the experimental sediments described in Section 4.2. All experiments are referenced and/or described in detail in the Results section of this report.

Table 1: Experimental Parameters for Several Different Sediments and Conditions

Sediment	Experiment Name	Treatment *	Current (mA)	Duration (weeks)	Desorbing agent	L/S or initial WC %	Mass of sediment (g dry)
Haakonsvern	2 HCl-Haak	EDR	30	2	0.6 M HCl	4.0	100
Haakonsvern	2 DW-Haak	EDR	50	2	Distilled water	4.0	100
Haakonsvern	4 DW-Haak	EDR	50	4	Distilled water	4.0	100
Gowanus	Gow	EDR	50	2	Distilled water	5.0	100
Newtown	New	EDR	50	2	Distilled water	3.8	100
Cocheco	Expt 1-Coch	EKR	40	3	Distilled water	72	-
Cocheco	Expt 2-Coch	EKR	40	2	Acetic Acid	74	-
Cocheco	HCST-Coch	EKR	40	2	Distilled water	69	450
Cocheco	HCLT-Coch	EKR	40	4	Distilled water	70	450
Cocheco	R1 – Coch	EKR	10-20	4	Distilled water	74	450
Cocheco	R2 – Coch	EKR	30	5	Distilled water	74	450

* EDR = electrodialytic remediation, EKR = electrokinetic remediation

5.0 RESULTS

5.1 Preliminary Testing

The initial graduate student working on this project performed bench scale experiments to investigate the effects of electrokinetic remediation on chloride removal, dewatering, and PAH migration. Chloride from marine sediments is a significant concern and can limit the beneficial use options for sediment material. Furthermore, its conservative behavior means it is extremely mobile in an electric field, which makes it a good tracer for monitoring the effectiveness of remediation. Figure 4 shows a one-way ANOVA and t-test of chloride content after the electrochemical treatment of the sediment for 24 hours. The results show that the chloride is effectively removed from all three sections of the sediment reactor, and is likely being evolved as chloride gas from the anode by the following reaction:

$$(3) \qquad 2\,Cl^- \rightarrow Cl_2(g) + 2e^-$$

Results from preliminary experiments in which direct current was applied to PAH contaminated sediments from the Cocheco River in Dover, NH are shown in Figure 5. The concentrations of naphthalene before and after remediation clearly show migration of the contaminant towards the anode under an applied electric field.

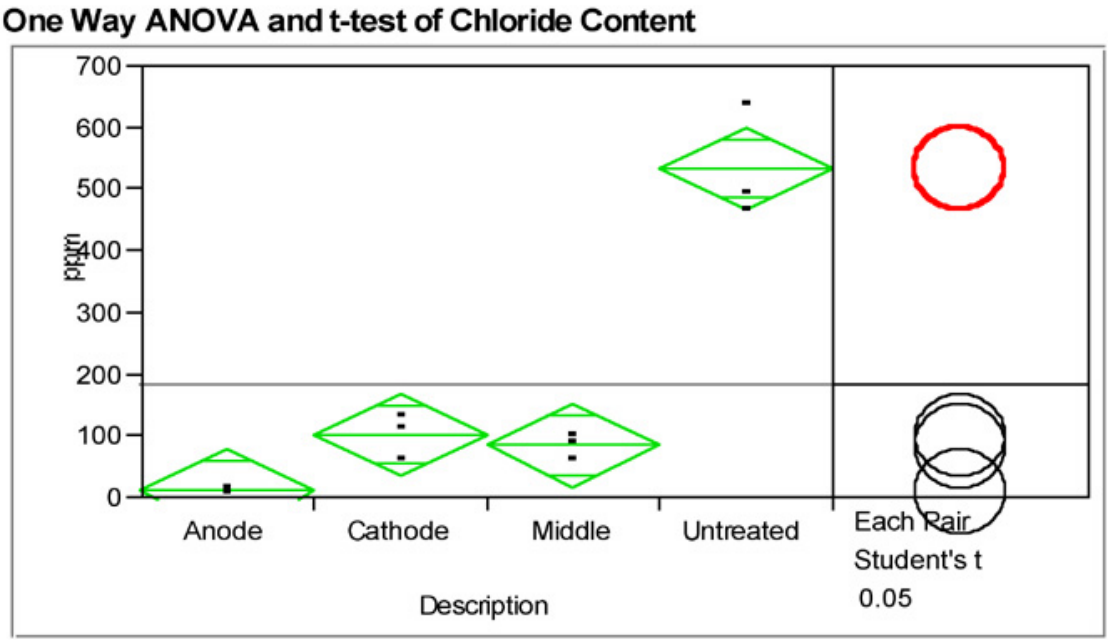

Figure 4: Chloride concentrations and t-test of sediment subjected to electrochemical treatment for 24 hours.

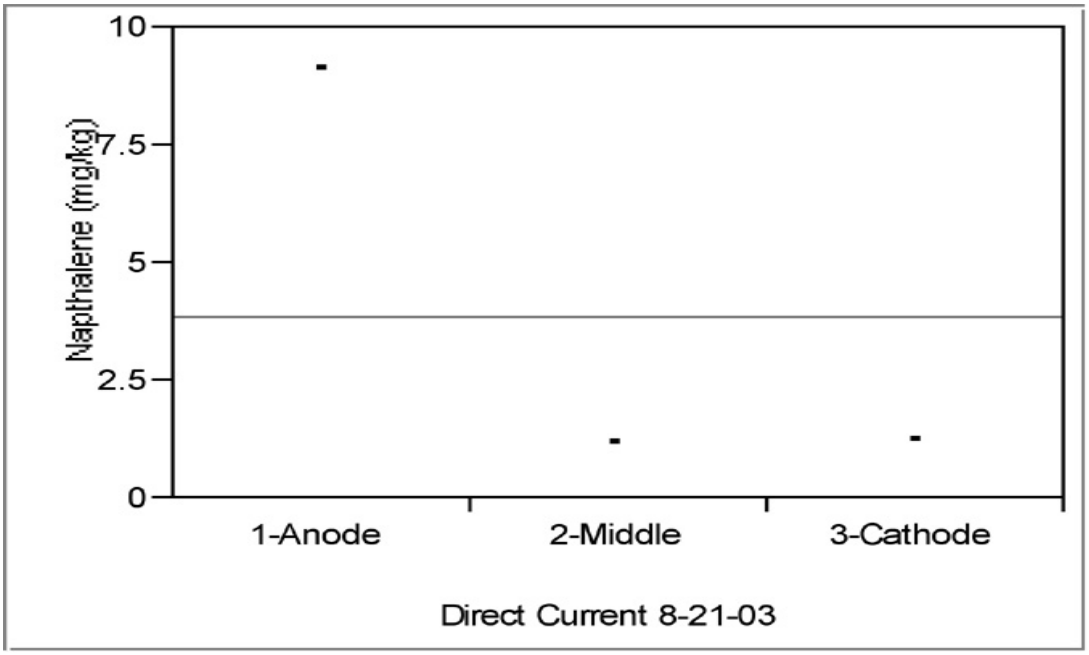

Figure 5: Migration of naphthalene in sediment subjected to electrokinetic remediation for 24 hours.

5.2 Electrokinetic Remediation of Cocheco River Sediments – Bench-scale Testing

At the University of New Hampshire, several electrokinetic experiments were performed with Cocheco River sediments, which are contaminated with PAHs and heavy metals. The work presented here further elucidates the prospect of using electrochemical remediation on sediments, however, was left incomplete by not testing the method at the pilot scale.

The visiting scholar from France witnessed differences in metal migration when acetic acid was used as an assisting agent. The results are presented in Figure 6. There are different results for the two different experiments. The major trends witnessed are reported in Table 2.

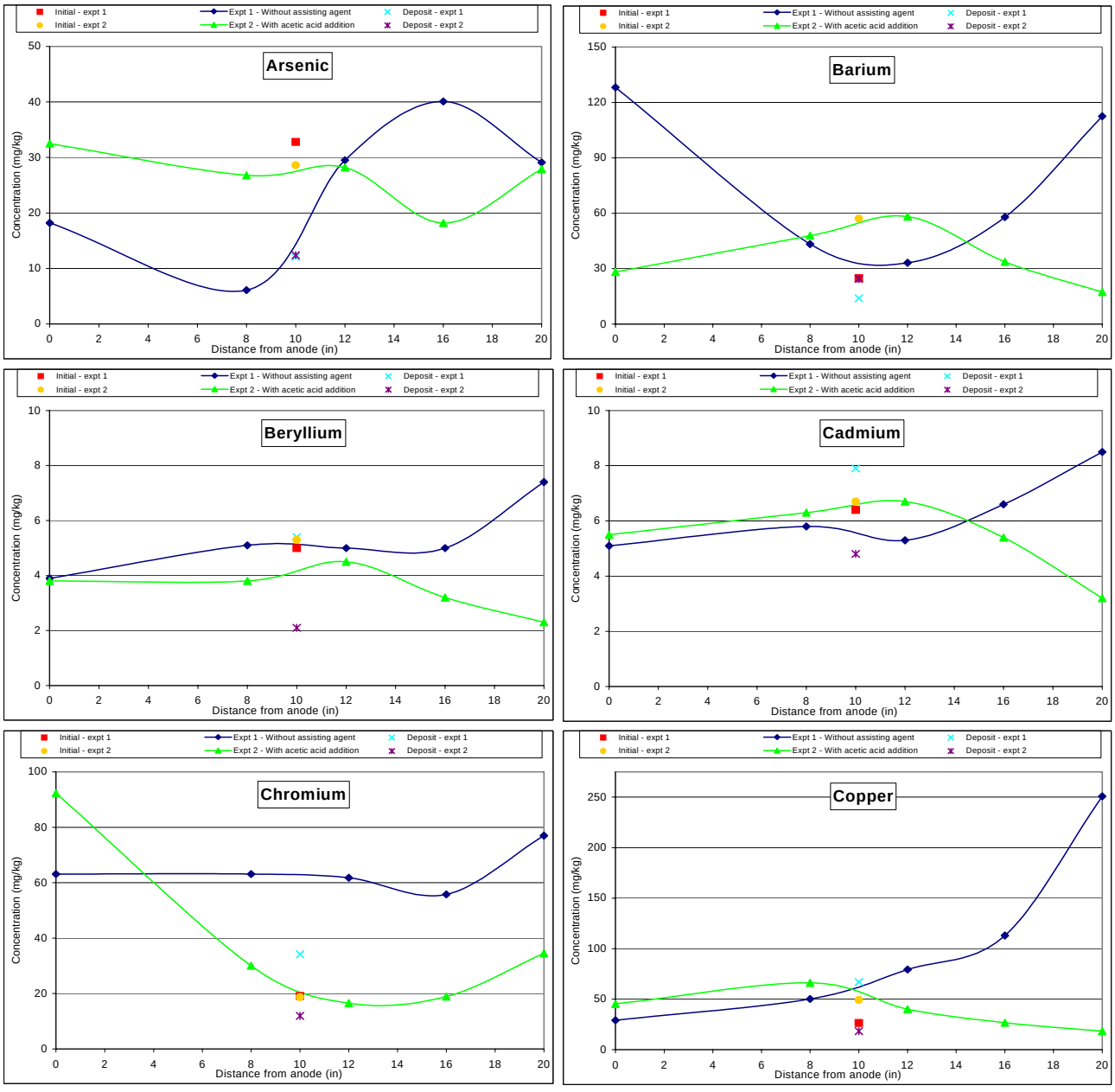

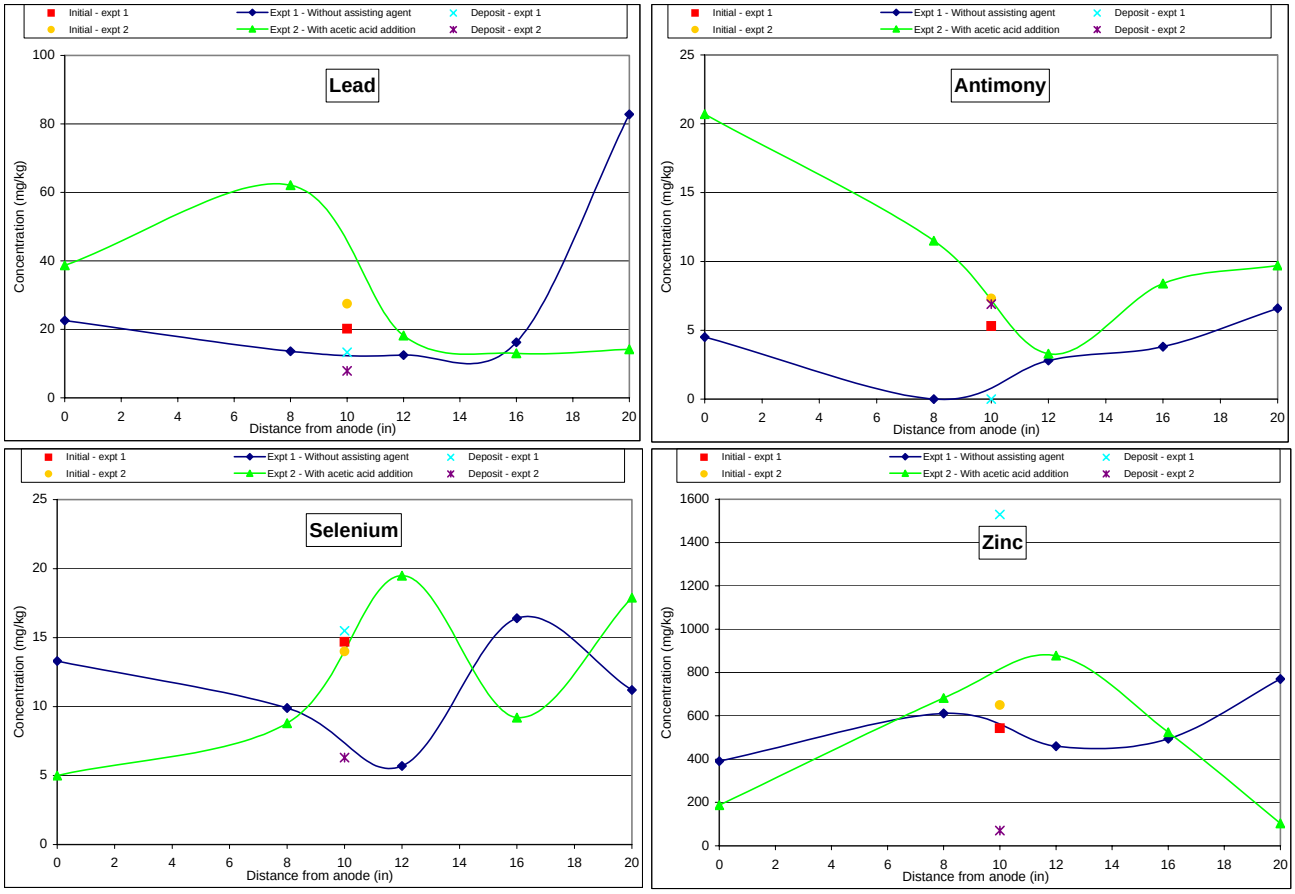

Figure 6: Comparing results of electrochemical experiments using the assisting agent, acetic acid, to mobilize metals.

Table 2: Major trends observed in Figure 6

Expt 1 - Without assisting agent	
Movement to the cathode side:	As, Ba, Be, Cd, Cr, Cu, Pb, Sb, Se, Zn
Movement to the anode side:	Ba (moved in both directions)
Expt 2 - With acetic acid addition	
Movement to the cathode side:	Se
Movement to the anode side:	As, Be, Cd, Cr, Cu, Pb, Sb
Unable to determine:	Ba, Zn

As expected from the first experiment, using only distilled water to solubilize the metals, most constituents migrated towards the cathode and became more available in the acidic side of the reactor. The addition of acetic acid produced opposite results, where metals appeared to have greater availability near the anode side. Since the pH shift was similar for both experiments, it is possible to conclude that complexes were formed with the heavy metals. Essentially, the most appropriate data would include a comparison of the total metals versus the available metals in order to determine the viability of an electrokinetic treatment scheme. This type of data is presented in section 5.2 below.

Two bench-scale experiments (HCST and HCLT) were conducted with Cocheco River sediments under a direct current of 40 mA for 15 and 33 days. Voltage was measured using the Dr. DAQ data collection system employed in previous experiments. Sediment samples were measured pre- and post-remediation for several constituents, including water content, pH, chloride, and organic carbon. Nine metals of concern and the suite of 16 PAH compounds are the contaminants of concern in the sediment; they were investigated to determine removal efficiency of electrochemical remediation.

The two reactors (30x11.5x7.5 cm) were arranged in series, each containing approximately 1500 g of wet sediment and 500 mL of additional overlying tap water. A graphite steel electrode was inserted 5 cm from each end and connected with alligator clips to the outside power source. The clips are also connected, in series, to the Dr. Daq data collector. Figure 7 shows photographs of the laboratory setup.

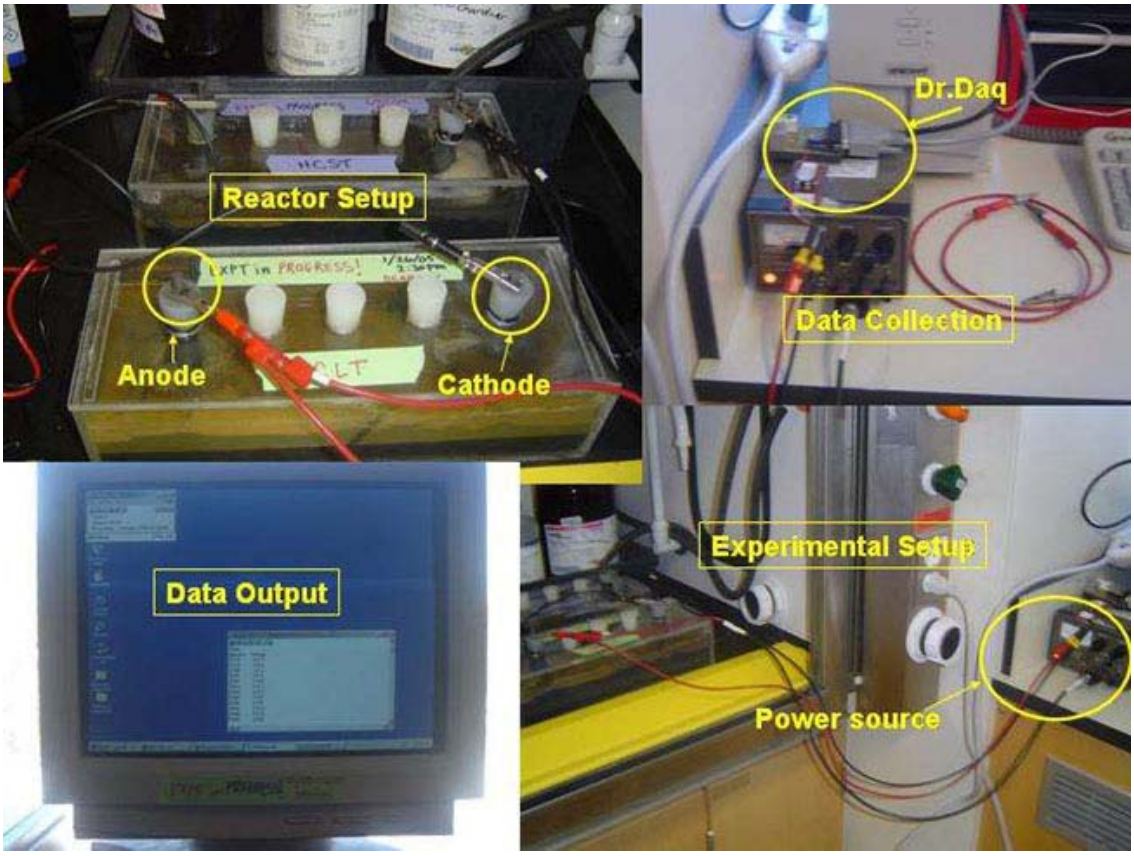

Figure 7: Bench-scale setup of electrokinetic experiments.

During the experiment, adequate water content was maintained to allow migration of the contaminants until the final days when dewatering was permitted to gain shear strength of the sediment. Figure 8 displays the dewatering of sediments during electrokinetic remediation. Significant voltage increase corresponds to a decrease in the electrical conductivity of the medium essentially reflecting a decrease in water content. Additional

water was added to continue solubilizing metals, and the re-wetting and drying phenomenon can be seen on the graph below.

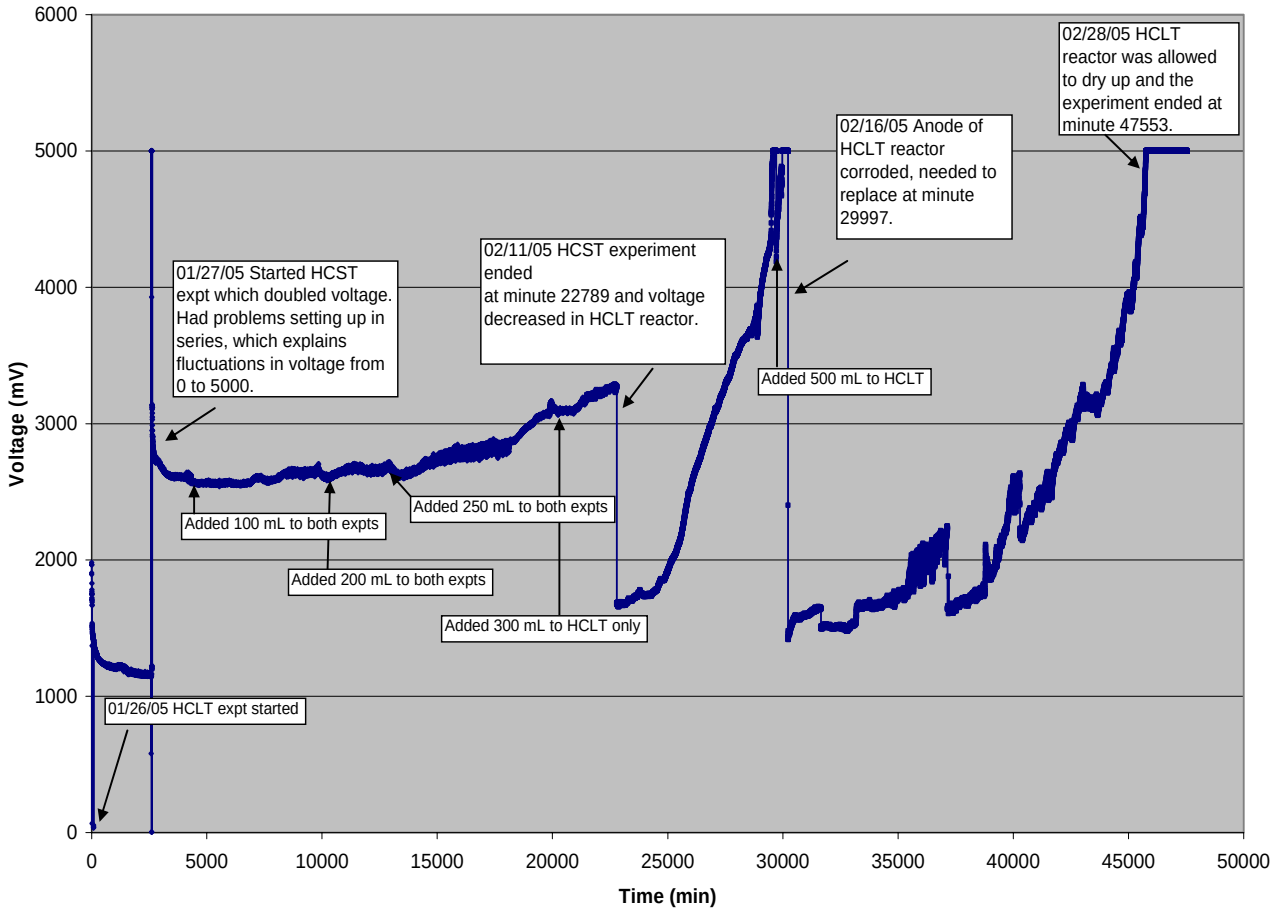

Figure 8: Voltage measurements taken during electrokinetic experimentation over time. Water was added to continue effective remediation of sediments.

Figure 9 shows the solids content of the sediment before remediation, after 15 days (dewatering not allowed at end), and after 33 days (dewatering allowed at end). Note that 5 samples (slices) and one duplicate were collected from each reactor. The theory of electroosmotic flow and electromigration of solutes are responsible for the migration of contaminants from one electrode to another. Electroosmotic flow moves from the anode to the cathode, so that the sediment near the anode is drier.

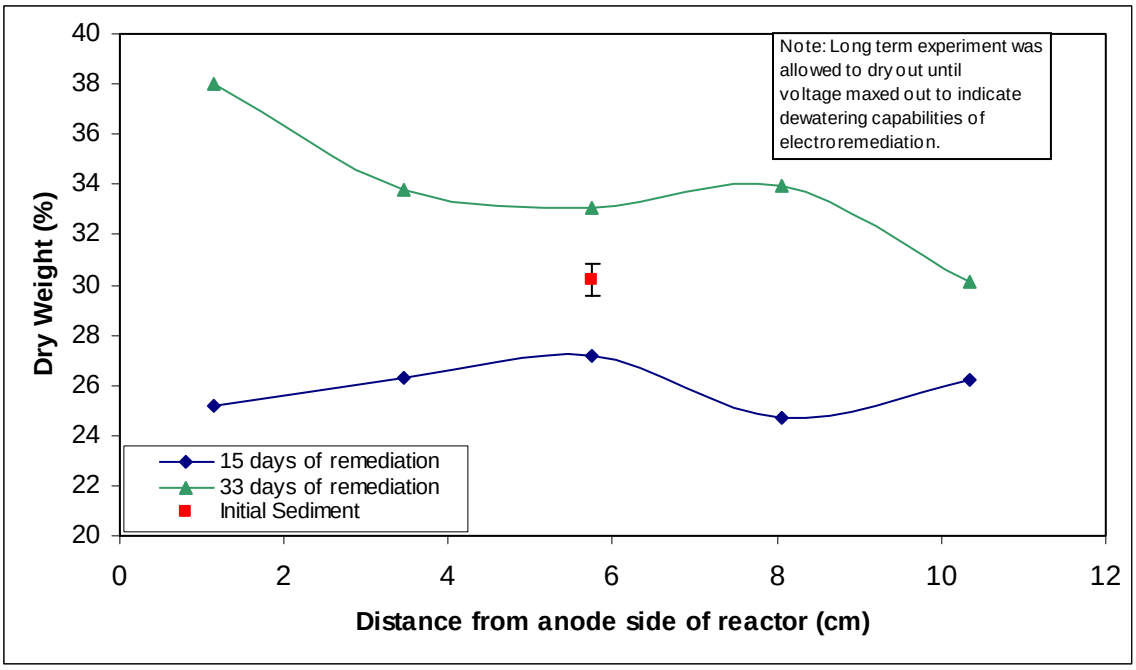

Figure 9: Dry Weight percentage of short and long term experiment.

The pH front within the reactor is also responsible for migration of contaminants. At low pH (near the anode), metals will dissolve and transport with the electroosmotic flow of water. Figure 10 shows the results, which span from a pH of 3 at the anode to above 10 at the cathode.

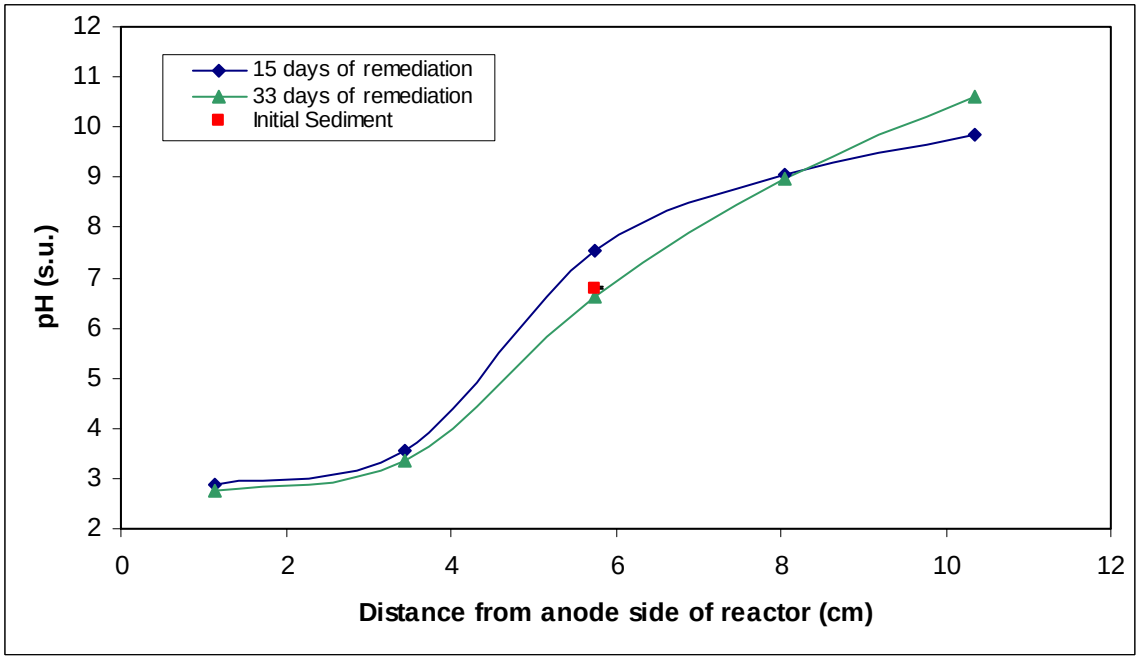

Figure 10: pH gradient in sediment after electrokinetic remediation.

Because organic contaminants tend to sorb to organic carbon found in sediments, organic carbon percentage was an important parameter to measure (Figure 11). Organic carbon tends to increase closer to the anode. PAH concentrations will then theoretically increase at the anode as well.

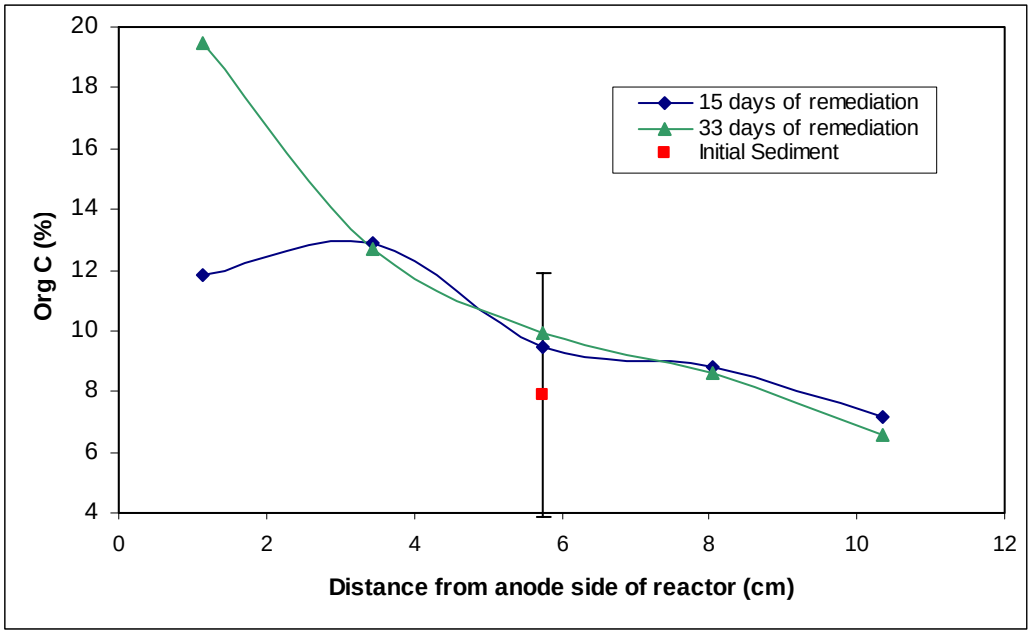

Figure 11: Organic Carbon Content in short and long term experiments.

Each of the five sampled sections was analyzed for total chloride with a chloride probe and mV meter. The results show clearly that chloride is effectively reduced from all sections of the sediment after 33 days except that at the cathode, particularly after dewatering (Figure 12).

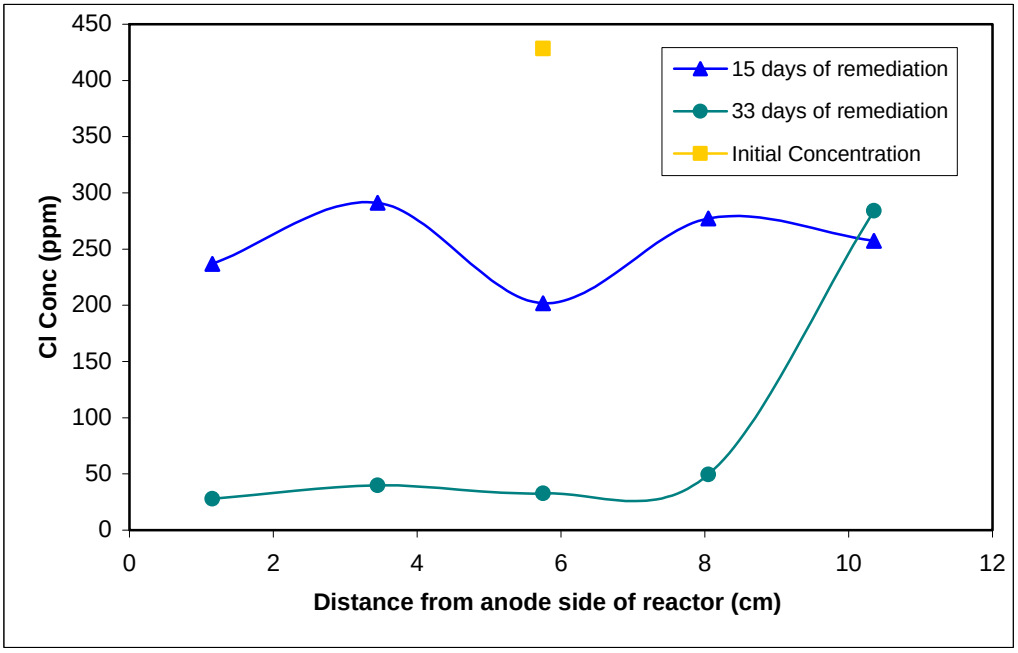

Figure 12: Chloride removal from short and long term experiments.

Figure 13 shows the leached results of arsenic, calcium, cadmium, chromium, copper, iron, lead, and zinc after electrokinetic remediation. Available metals concentrations at the cathode were less after 33 days of remediation than after 15 days, except in the case of cadmium and calcium. Another interesting result is that after the 33-day experiment, cadmium, chromium, copper and lead had an increase in concentration at the anode, which seems to be an anomaly in that sample or simply that a percentage of the metals did not migrate towards the cathode in that reactor but became more available after longer treatment time. Where the initial concentrations are lower than the post-remediation concentrations, this indicates that the metal became more available after treatment. Also, metals will become more available in acidic soil, so stabilization of the treated sediment may result in lower availability and should be considered before reuse.

Interpretation of these results is difficult in an electrokinetic experiment because of the physical and chemical gradients that form across the reactor, like pH and organic carbon content. These gradients may have an effect on the availability tests performed to leach the metals, for example, organic carbon content of the sample may affect the amount of metal that leaches at pH 4. In an electrodialytic cell, however, sediments are more homogenous and the gradients are not as explicit. Furthermore, metals migrate outside of the sediment compartment in electrodialytic remediation, but remain in the sediment pore water or as precipitates in an electrokinetic reactor, making calculations of percent removals ambiguous.

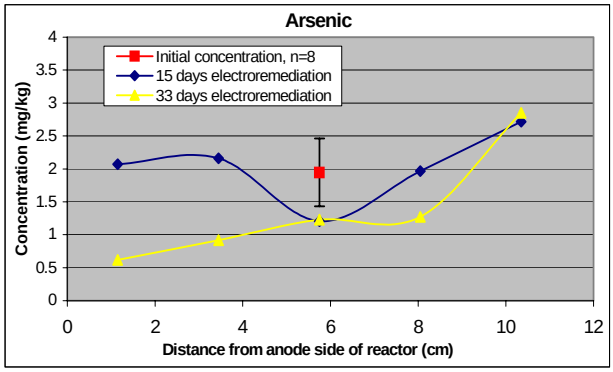

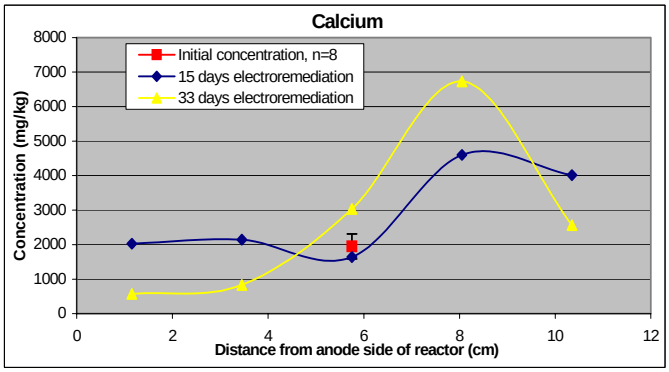

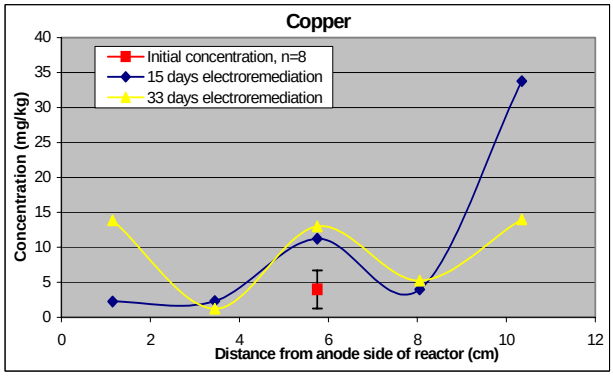

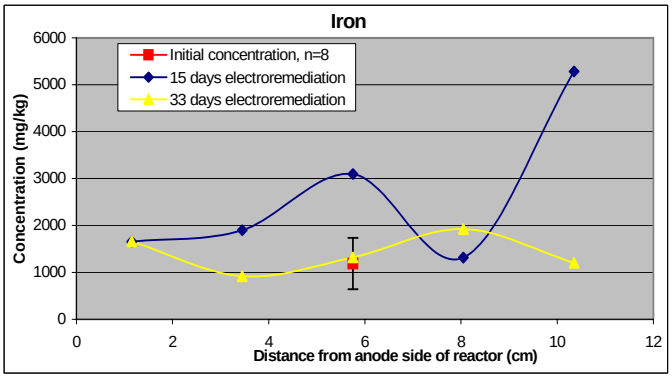

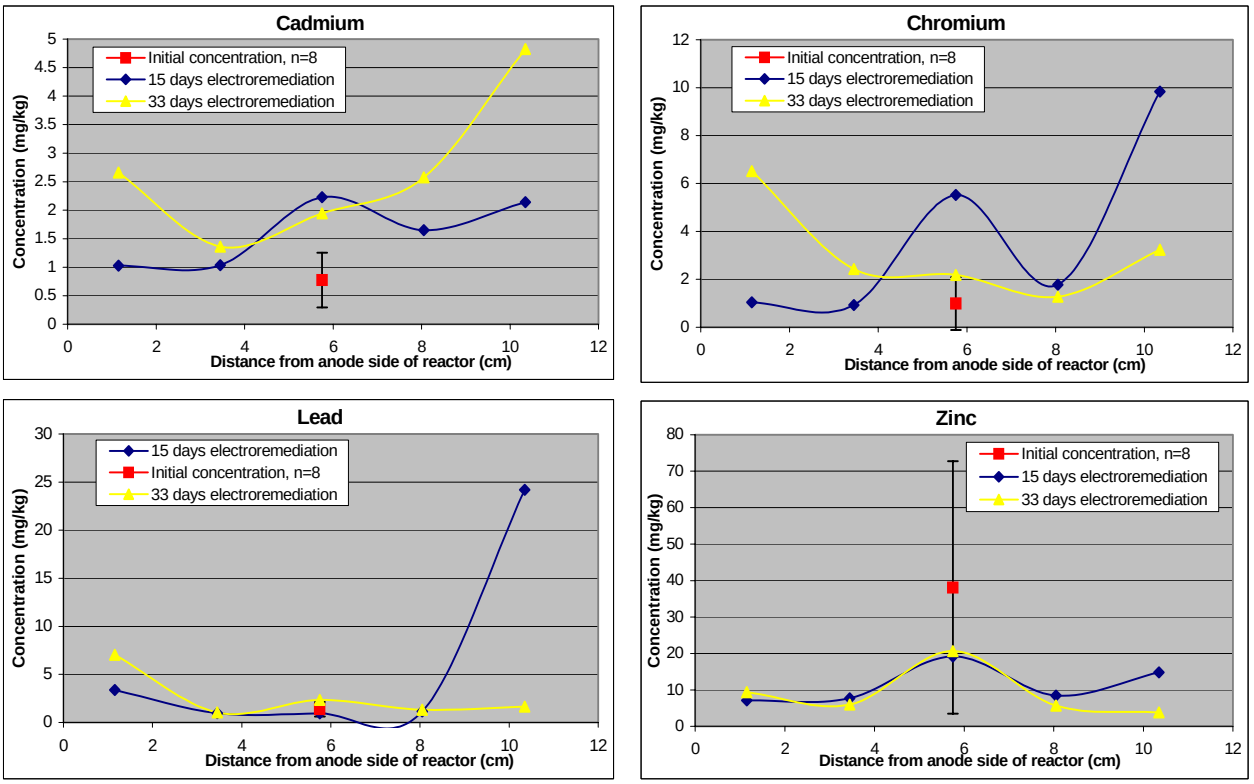

Figure 13: Metals results of slices taken from a reactor of electrochemically remediated sediment. Most metals migrate toward the cathode at 10 cm.

The last set of data is for PAH migration in the sediments. Total PAH migration is shown for experiments R1 and R2 in Figure 14. On average, the electrokinetic experiment only removed approximately 20% and 21%, respectively of total PAHs in the sediment after approximately 30 days. PAHs seemed to move towards both ends of the reactor in the first experiment and primarily to the anode in the second experiment, which is what is predicted due to the migration of organic carbon content observed in experiments HCST and HCLT.

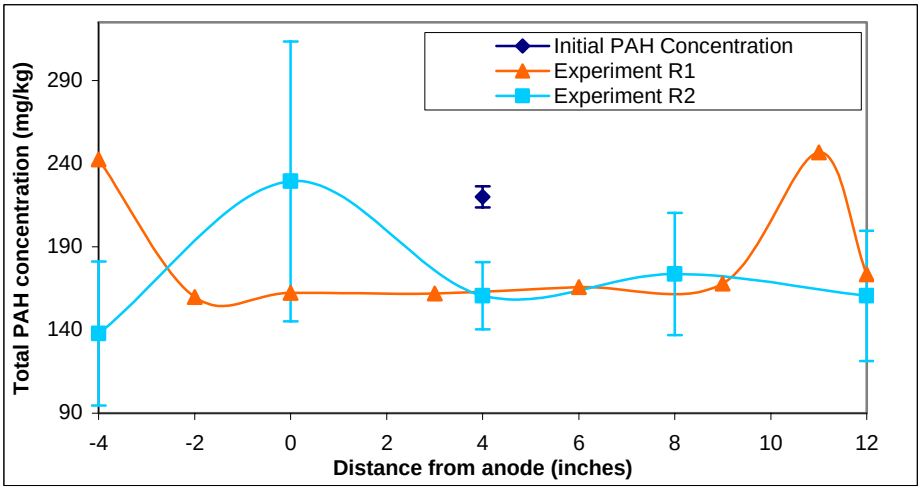

Figure 14: Analysis of PAH concentrations in electrokinetically treated sediments.

An analysis of the migration of individual PAH compounds is even more valuable to investigate, and is shown in Figure 15. In this case, using three duplicate samples, the highest concentration for most of the compounds interestingly occurs precisely at the anode.

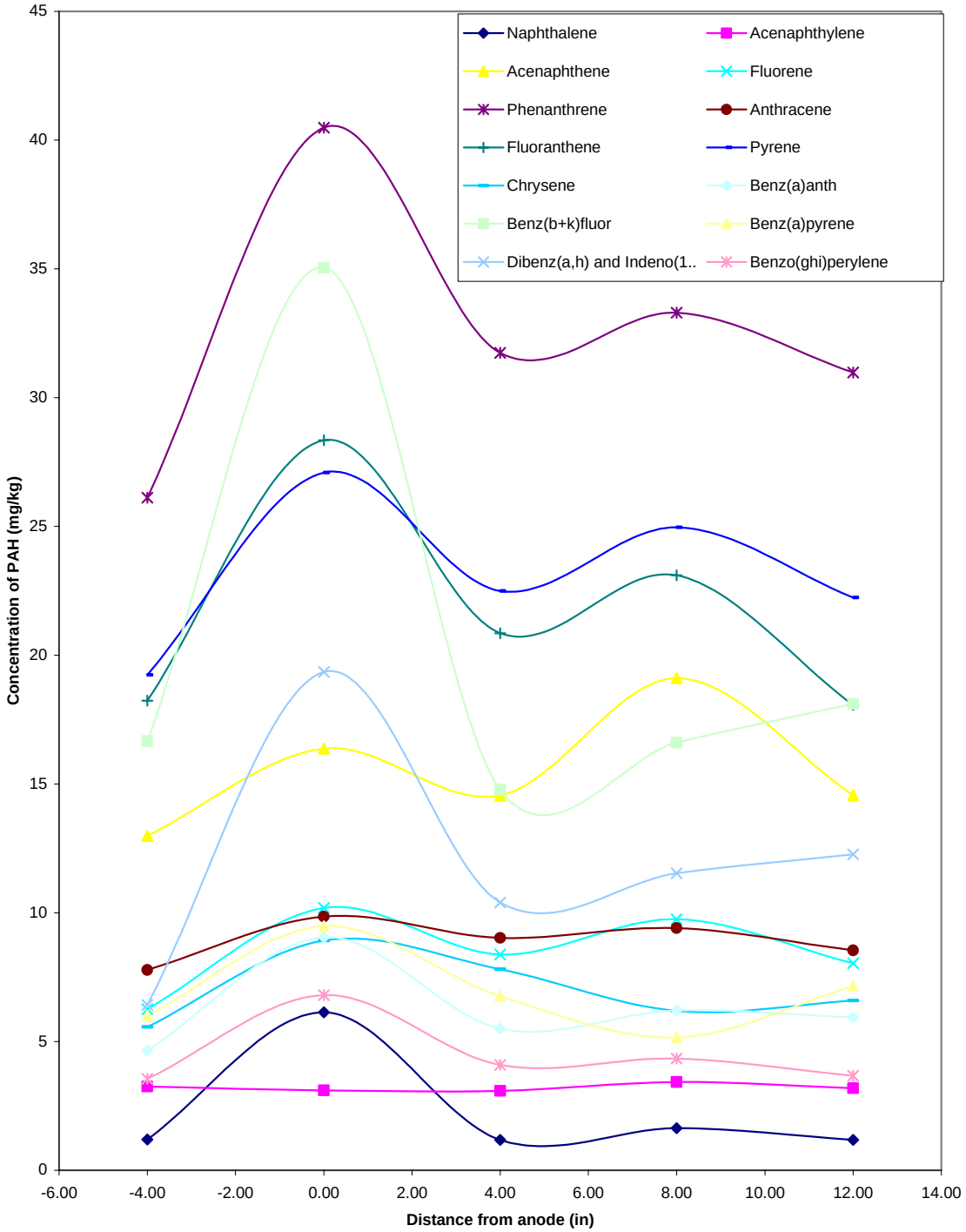

Figure 15: Analysis of individual PAH compounds in electrokinetically-treated sediment.

5.2 Continuing work from DTU

Electrodialytic remediation was used to extract heavy metals from sediment by a visiting scholar obtaining her PhD from the Technical Institute of Denmark. A paper of this work, entitled "Leaching Properties of Estuarine Harbor Sediment Before and After EDR" has been submitted to Environmental Engineering Science Journal and currently awaits peer review. Contaminated harbor sediment from two locations in the U.S. and one in Norway were subjected to electrodialytic remediation, and these were compared to controls that were not electrochemically treated. pH-static leaching, water extractions, and an availability test were used to evaluate changes in leaching properties of the treated and control sediments.

Electrodialytic treatment of contaminated Haakonsvern Harbor sediment effectively removed up to 96% and an average of 57% of the total heavy metals, Cu, Zn, Pb, Cd, Fe, Al, Ni, As, and Ti. A controlled batch experiment run without electrical current and adjusted to a pH of 3.0 with hydrochloric acid removed an average of only 36% of the total heavy metals. Treatment of more highly contaminated sediments from Newtown Creek and Gowanus Canal in the U.S. resulted in average metal removal of 89% (Cu, Zn, Pb, Cd only) and 79% (Cu, Zn, Pb only), respectively.

Changes in leaching behavior were witnessed in pH – static leaching experiments when contaminated Haakonsvern Harbor sediment was electrodialytically treated (Figure 16). Treatment of the sediment increased leaching of K, Pb, Cu, Ti, Cd, As, Al, and Fe, even though the total concentrations in the treated sediments were lower than in the untreated sediment for all elements. Thus, the elements were still available in the sediments after treatment, and environmental leaching was not reduced by the treatment. Increased remediation time from 2 to 4 weeks resulted in higher removals of total elements, but with similar leached concentrations of available elements, probably due to continuous changes in speciation and dissolution during electrodialytic remediation. At alkaline pH values, there was an increase in leaching of several heavy metals in the treated sediments compared to the untreated, which could cause problems if the sediment was reused in construction material with natural high pH (e.g., concrete). The water solubility of elements at their natural pH, in the untreated sediments, or achieved pH, in the treated sediments, was solubility and pH controlled. Results from the pH – static leaching showed lowest leaching of elements in the treated sediments at pH 6, and therefore stabilization, by increasing pH after treatment, could be used prior to reuse/disposal.

Comparing the availability of the elements before and after treatment (Figure 17), greater concentrations of Cu, Pb, Fe, Al, and Ti were measured in the treated sediment than in the untreated. Increased availability of some elements following EDR treatment is a concern that could be addressed by longer remediation time or adjusting the pH of the sediment prior to reuse. For all other elements of concern, including Zn, Cd, Ni, and As, the availability after treatment went down, demonstrating that electrodialytic remediation of contaminated sediments was effective in decreasing the availability of certain heavy metals.

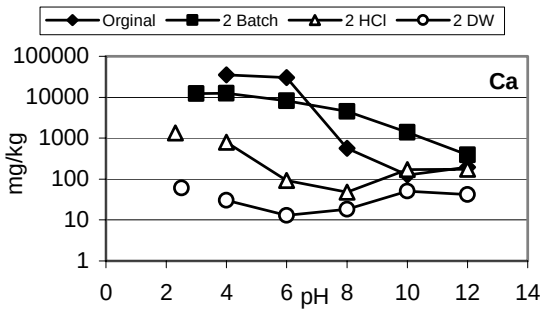
Orginal
2 Batch
2 HCl
2 DW
Ca
mg/kg
100000
10000
1000
100
10
1
0 2 4 6 pH 8 10 12 14

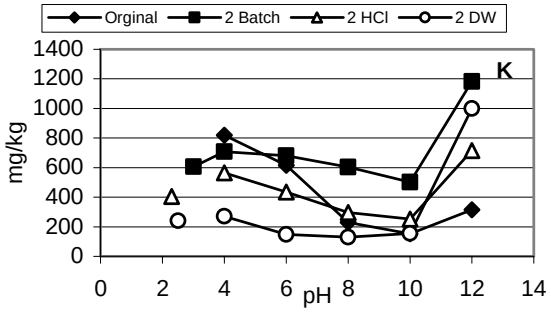
Orginal
2 Batch
2 HCl
2 DW
K
mg/kg
1400
1200
1000
800
600
400
200
0
0 2 4 6 pH 8 10 12 14

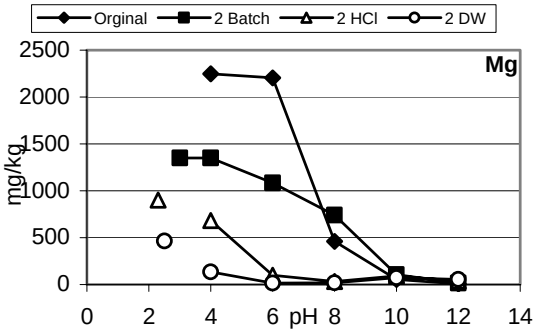
Orginal
2 Batch
2 HCl
2 DW
Mg
mg/kg
2500
2000
1500
1000
500
0
0 2 4 6 pH 8 10 12 14

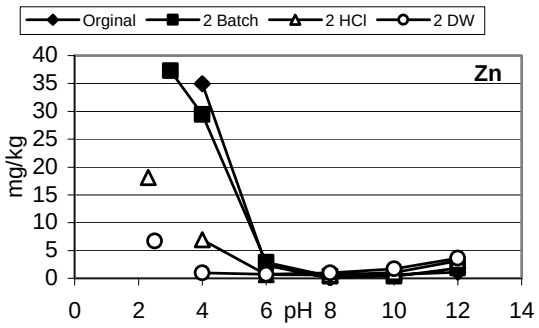
Orginal
2 Batch
2 HCl
2 DW
Zn
mg/kg
40
35
30
25
20
15
10
5
0
0 2 4 6 pH 8 10 12 14

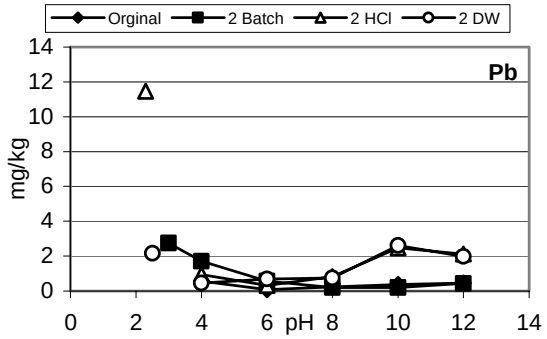
Orginal
2 Batch
2 HCl
2 DW
Pb
mg/kg
14
12
10
8
6
4
2
0
0 2 4 6 pH 8 10 12 14

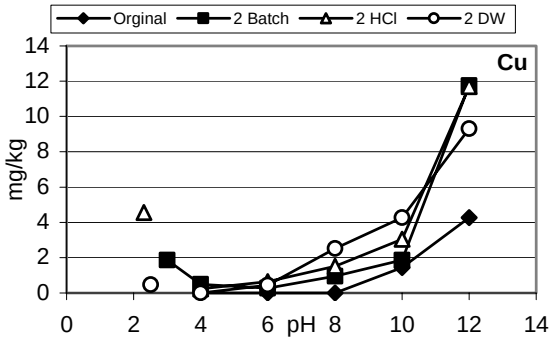
Orginal
2 Batch
2 HCl
2 DW
Cu
mg/kg
14
12
10
8
6
4
2
0
0 2 4 6 pH 8 10 12 14

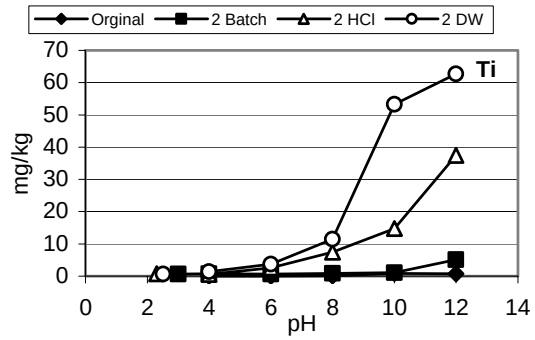
Orginal
2 Batch
2 HCl
2 DW
Ti
mg/kg
70
60
50
40
30
20
10
0
0 2 4 6 pH 8 10 12 14

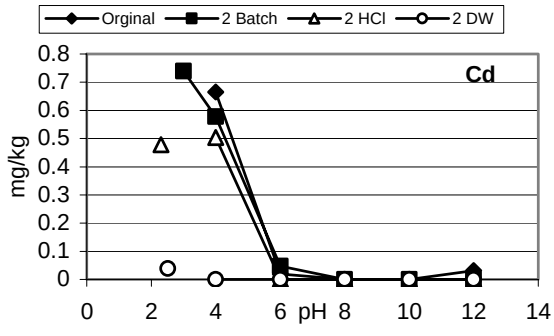
Orginal
2 Batch
2 HCl
2 DW
Cd
mg/kg
0.8
0.7
0.6
0.5
0.4
0.3
0.2
0.1
0
0 2 4 6 pH 8 10 12 14

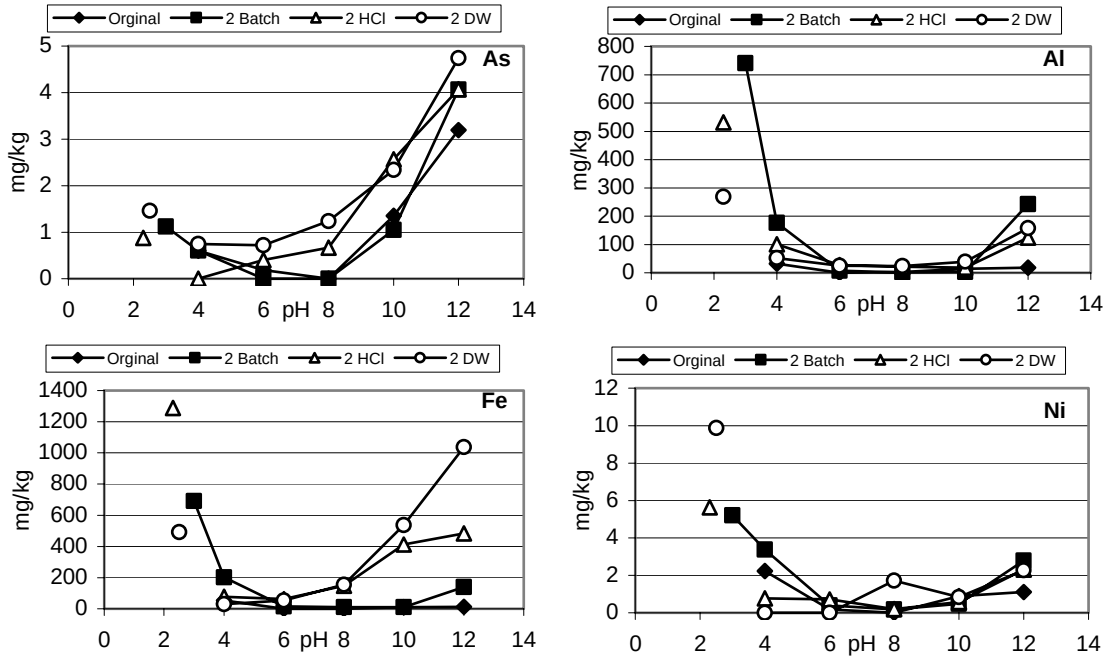

Figure 16: pH – static leaching at several pH for the untreated (original), control (batch) and treated (HCl and DW) Haakonsvern sediments

**Isolated marks represent the leachability in water at the respective, post-treatment pH of each sediment sample.*

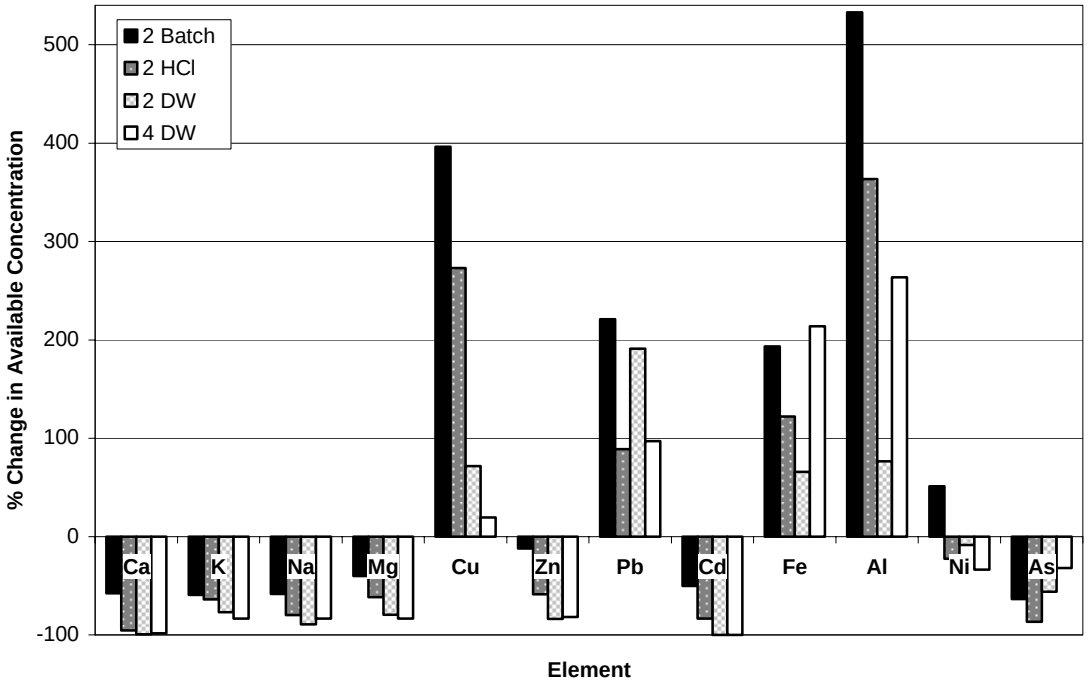

Figure 17: Percent change in availability compared to the untreated Haakonsvern sediment

6. DISCUSSION

Large amounts of sediments are dredged around the world to maintain navigational depths or improve water quality. Ocean dumping or land application are two means to dispose of uncontaminated or slightly contaminated dredged sediments. Sediments can be contaminated with heavy metals, PAHs, PCBs, and other anthropogenic compounds. Disposal of contaminated sediments in confined disposal facilities (CDFs) on land or confined aquatic disposal (CAD) cells at sea are the most common options for handling contaminated dredged sediments. The use of CDFs and CAD cells are simply a means of buying time, because they are not effective solutions to the problem of contaminated sediments.

The alternatives to disposal of contaminated sediments are reuse and treatment. Reuse of sediments depends on the sediment properties, such as strength, oxide content, or contaminant concentrations. Contaminant removal methods, such as those developed for soil, can be applied to sediments, but are still limited by inadequate research at the laboratory scale. Reuse and treatment are not widespread in use, mainly because of increased cost compared to disposal.

Electrochemical remediation is one type of treatment that can be cost-effective because it is performed with a low, direct current between two electrodes. It is a developing technology because it is intended to separate and extract heavy metals and organic contaminants from saturated or unsaturated soils and sediments, as well as stabilizing the media via dewatering. The results obtained from this study indicate that there is potential to use electrochemical remediation to achieve those three treatment goals in sediments in both an *in-situ* or *ex-situ* application.

In this study several chemical and physical parameters were investigated to determine the effectiveness of electrochemical remediation. Several bench-scale studies, and a thorough literature review of past research, indicate success for the mobilization of metals in sediments when subjected to an applied electric field. Comparing past work using electrodialytic experiments (Nystrom, 2004) to the current study using electrokinetic experiments, the electrodialytic setup produced more effective results due to the use of electrolyte solution compartments that attract the metal complexes rather than expecting the metals to plate directly to an electrode to be removed. However, the electrodialytic method can only be applied to *ex-situ* sediments, where the electrokinetic method is accomplished by placing electrodes directly into *in-situ* sediment.

Although there is a great deal of research on using assisting agents in the literature; such as anionic, cationic, and non-ionic surfactants, ethylenediaminetetraacetic acid (EDTA), and ammonium citrate (Kaya, 2005; Giannis; 2005; Pedersen, 2005); results here showed that the use of the assisting agents acetic acid and hydrochloric acid did not produce a significant increase in metal removal percentages. The experiments performed using acetic acid actually reversed the direction of migration for most metallic complexes and ions towards the anode rather than the cathode, which was the case in the distilled water experiments; however, did not increase removal. HCl was evaluated in the EDR

experiment of the Haakonsvern harbor sediments as a desorbing agent to increase removal. HCl dissolves carbonates in the sediment, lowers the pH and releases heavy metals. Chlorocomplexes can be formed to further enhance metal solubility (Nystrom et al., 2004). The potential for chlorocomplexation by HCl did not increase the metal removal compared to using distilled water in these experiments. HCl increases the ionic strength of the solution, which influences the electrical conductivity and current efficiency. H^+ and Cl^- are more mobile in the electric field than divalent ions; and thus, the current efficiency for heavy metal ions is reduced (Acar and Alshawabkeh, 1993). When using HCl, the sediment was acidified immediately, which did not seem to influence the removal efficiency compared to using distilled water, where acidification took place during the course of the experiment. These results suggest low influence of using HCl as a desorbing agent on the solubility of heavy metals, because it did not contribute to greater elemental removals following EDR treatment.

Probably the most significant conclusion to come of this research was that the availability was found to increase for certain metals after treatment of the sediments. In pH dependent leaching tests, element leaching from the sediment was generally pH–dependent, both before and after treatment, and the results also suggested that greater liquid-to-solid ratios (L/S) increase elemental solubility. Acidification of the sediments caused by treatment resulted in higher water dissolution of elements at the sediments achieved pH, compared to the untreated sediment. Significant fractions of total concentrations were removed during treatment (typically 35-95%); however, the total availability of metals in the treated sediment samples increased for Cu, Pb, Fe, and Al (for which total concentrations decreased by up to 56%, 64%, 47%, and 90%, respectively). All other elements of concern were less available after treatment. This research highlights the importance of understanding contaminant speciation and availability, as total metals concentrations, in this particular case, do not relate to estimates of the environmental and ecological availability of metals.

Organic carbon content was measured in the post-treated sediments of an electrokinetic experiment. These results showed that organic carbon content was higher near the anode, demonstrating the electrophoresis phenomena in which negatively charged, natural organic matter will migrate towards the anode. Since organic pollutants, such as PAHs, sorb strongly to natural organic matter, it would be assumed that the PAHs will also travel towards the anode. Several papers suggest that black soot carbon found in sediments is actually the strongest organic sorbent for PAHs and PCBs (Lohmann, 2005; Bucheli, 2003; Gustafsson, 1997). The measurement of the soot carbon fraction of the sediments was measured in the post-treated sediments also; however, did not produce the expected results that indicate migration of soot carbon to the anode. Soot carbon fractions were variable throughout the reactor. Most importantly, however, data collected for PAH migration in electrokinetic experiments showed that most PAH compounds did migrate to the location of the anode and total PAHs were decreased by 20% in one month at a low current of 10-20 mA.

7. TECHNOLOGY TRANSFER AND MANAGEMENT APPLICATION

The lack of cost-effective solutions to the contaminated sediment/dredged material issue has the potential to have significant effects on many coastal environments by putting significant economic and political pressure on the existing legislation; therefore, it is essential that innovative and more cost-effective approaches be developed to treat contaminated sediments. This project investigated a technology that could be extremely cost-effective, particularly if used in conjunction with the beneficial use of sediment post-treatment.

Navigational dredging can be viewed as a means of cleaning up a diffuse, non-point source of contaminants to the coastal environment, however, proper management of the sediment must occur for the dredging to have this fortuitous benefit. Proper management will not be maintainable without cost-effective and sustainable management alternatives.

Future work in order to bring this project to the full scale includes testing at the pilot scale, which was left unfinished in this work, to evaluate removal efficiency and large scale remediation potential. Remediation costs must be estimated and reuse options should be recommended for the remediated sediments.

8. ACHIEVEMENT AND DISSEMINATION

Some very compelling experimental data resulted from research conducted by the visiting scholars from Denmark supported by this project. The following journal articles report the outcomes:

Pedersen A.J., K.H. Gardner. (2003). "Characterization of municipal solid waste incineration fly ash before and after electrodialytic treatment," *Journal De Physique IV* 107: 1029-1032.

Pedersen, A.J., K.H. Gardner (2003). "Electrochemical Remediation of Dredged material for Beneficial Use," *In* Beneficial Use of Recycled Materials in Transportation Applications, T.T.Eighmy Eds., Air and Waste Management Association Press, 389-399.

Nystrom, G.M., K.H. Gardner, and D.A. Aulisio. (under review). Leaching characteristics of estuarine harbor sediments before and after EDR. Environmental Engineering Science.

Anne Pedersen completed her PhD thesis in 2002 at the Technical Institute of Denmark on the Electrodialytic Removal of Heavy Metals from Fly Ashes. Gunvor Marie Nystrom completed her PhD thesis in 2004 at the Technical Institute of Denmark on the Electrodialytic removal of heavy metals from contaminated harbor sediments.

9. REFERENCES

Acar, Y.B. (1992). "Electrokinetic Cleanups," Civil Engineering, 62, 58-60.

Acar, Y.B., and A.N. Alshawabkeh. (1993). "Principles of Electrokinetic Remediation." Environmental Science and Technology. 27(13), 2638-47.

Akram, N., N. Alshawabkeh, A. T. Yeung, M.R. Bricka. (1999). Practical aspects of in-situ electrokinetic extraction. Journal of Environmental Engineering, 27-35.

Bucheli, Thomas D. and O. Gustafsson. (2003). Soot sorption of non-ortho and ortho substituted PCBs. Chemosphere, 53:515-22.

Christensen, I.V. (2004). Electrodialytic Remediation of CCA-Treated Waste Wood. Department of Civil Engineering, Technical University of Denmark. PhD Thesis.

Doering, Falk; Niels Doering; Joe L. Iovenitti; Donald G. Hill; and William A. McIlvride (2000). Electrochemical Remediation Technologies for Soil, Sediment and Ground Water. The Annual International Conference on Soils, Sediment, and Water. University of Massachusetts, Amherst.

Elektorowicz, M. and J. Lin. (2001). Removal of PAH using Electrokinetic Transport of Biosurfactants in Clayey Soil, 3rd Symposium on Electrokinetic Remediation. April 18-20. Karlsruhe Univeristy, Germany.

Francingues, N.R. and D.W. Thompson. (2000). "Innovative dredged sediment decontamination and treatment technologies," DOER Technical Notes Collection (ERDC TN-DOER-T2), U.S. Army Engineer Research and Development Center, Vicksburg, MS.

Giannis, Apostolos; E. Gidarakos. (2005). Washing enhanced electrokinetic remediation for removal cadmium from real contaminated soil. Journal of Hazardous Materials, B123: 165-175.

Grande S. and Gent D. (2002). Electrokinetic remediation of contaminated sediments. In: Remediation and Beneficial Reuse of Contaminated Sediments. Conference Proceedings. Edited by Hinchee, R.E., A. Porta, and M. Pellei. Battelle Press, Columbia Richland. 205-212.

Gustafsson, Orjan; F. Haghseta; C. Chan; J. Macfarlane; and P.M. Gschwend. (1997). Quantification of the dilute sedimentary soot phase: implications for PAH speciation and bioavailability. Environmental Science and Technology, 31: 203-9.

Hansen, H.K. (1995). Practical and theoretical aspects concerning the use of ion exchange membranes and resins in electrokinetic soil remediation. Department of Physical Chemistry and Department of Geology and Geotechnical Engineering, Technical University of Denmark, PhD thesis.

Hansen, H.K. et al. (1997). Electrodialytic Remediation of Soils polluted with Cu, Cr, Hg, Pb and Zn. Journal of Chemical Technology and Biotechnology. 70(1), 67-73.

Jakobsen, M.R., J. Fritt-Rasmussen, S. Nielsen, L.M. Ottosen. (2004). Electrodialytic removal of cadmium from wastewater sludge. Journal of Hazardous Materials. 106B: 127-132.

Jespersen R.D. (1996). Elektrokinetisk jordrensning. Department of Geology and Geotechnical Engineering and Department of Chemistry, Technical University of Denmark and A/S Bioteknisk Jordrens. PhD thesis (in Danish).

Kaya, Abidin; Y. Yukselen. (2005). Zeta potential of soils with surfactants and its relevance to electrokinetic remediation. Journal of Hazardous Materials, B120: 119-26.

Kliem B.K. (2000). Bonding of heavy metals in soil. Department of Geology and Geotechnical Engineering and Department of Chemistry, Technical University of Denmark. PhD Thesis.

Lageman R., W. Pool, G. Seffinga. (1989). Electro-Reclamation: Theory and Practice. Chemistry and Industry (18), 585-590.

Lohmann, R.; J.K. Macfarlane, and P.M. Gschwend. (2005). Importance of Black Carbon to Sorption of Native PAHs, PCBs, and PCDDs in Boston and New York Harbor Sediments. Environmental Science and Technology, 39: 141-48.

Nystrom, G. M. (2004). Electrodialytic removal of heavy metals from contaminated harbour sediments. Department of Civil Engineering, Technical University of Denmark, PhD thesis.

Ottosen, L.M. (1995). Electrokinetic soil remediation. Application to soil polluted from wood preservation. Department of Geology and Geotechnical Engineering and Department of Physical Chemistry, Technical University of Denmark, PhD thesis.

Ottonsen, L.M., H.K. Hansen, S. Laursen, A. Villumsen. (1997) Electrodialytic Remediation of Soil Polluted with Copper from Wood Preservation Industry. Environmental Science and Technology. 31, 1711-15.

Ottensen, L.M., H.K. Hansen, L. Hansen, B.K. Kliem, G. Bech-Nielsen, B. Pettersen, A. Villumsen. (1998). Electrodialytic soil remediation – improved conditions and

acceleration of the process by addition of desorbing agents to the soil. Contaminated Soil '98, Thomas Telford, London, 471-8.

Ottosen, L.M.; H.K. Hansen; C. Hansen. (2000). Water splitting at ion exchange membranes and potential differences in soil during electrodialytic remediation. Journal of Applied Electrochemistry. 30, 1199-1207.

Pedersen, A.J. (2002). Electrodialytic Removal of Heavy Metals from Fly Ashes. Department of Civil Engineering, Technical University of Denmark. PhD Thesis.

Pedersen, A.J.; L.M. Ottosen; A. Villumsen. (2005). Electrodialytic removal of heavy metals from municipal solid waste incineration fly ash using ammonium citrate as assisting agent. Journal of Hazardous Materials, B122: 103-9.

Ribeiro A.B. (1998). Use of electrodialytic remediation technique for removal of selected heavy metals and metalloids from soils. Department of Geology and Geotechnical Engineering and Department of Physical Chemistry. Technical University of Denmark. PhD Thesis.

Roulier, M.; Kemper, M.; Al-Abed, S.; Murdoch, L.; Cluxton, P.; Chen, J.; Davis-Hoover, W. (2000). Feasibility of electrokinetic soil remediation in horizontal Lasagna™ cells. Journal of Hazardous Materials. B77: 161 – 176.

Shine, J. (2000). "The Use of Confined Aquatic Disposal (CAD) Cells to Manage Contaminated Sediments in Ports and Harbors: Chemical Migration." Presented at the *Conference on Dredged Material Management: Options and Environmental Considerations*. Dec 3-6, MIT, Cambridge, MA.